Wheel/Rail Interface Optimisation

Wheel/Rail Interface Optimisation

Proefschrift

ter verkrijging van de graad van doctor
aan de Technische Universiteit Delft,
op gezag van de Rector Magnificus prof.dr.ir. J.T. Fokkema
voorzitter van het College voor Promoties,
in het openbaar te verdedigen op dinsdaag 3 juni 2008 om 10:00 uur

door Ivan Yevhenovich SHEVTSOV

mechanical engineer - researcher, Dnipropetrovsk State University
geboren te Dnipropetrovsk, Oekraine

Dit proefschrift is goedgekeurd door de promotor:
Prof.dr.ir. C. Esveld

Samenstelling promotiecommissie:

Rector Magnificus, voorzitter
Prof.dr.ir. C. Esveld, Technische Universiteit Delft, promotor
Dr. V.L. Markine, Technische Universiteit Delft
Prof.Dr.Ing. I.A. Hansen, Technische Universiteit Delft
Prof. R. Lundén, Chalmers University of Technology, Sweden
Prof. E. Hohnecker, University of Karlsruhe, Germany
Prof. R. Dwyer-Joyce, University of Sheffield, UK
Prof. V.V. Toropov, University of Leeds, UK
Prof.dr.ir. G. Lodewijks, Technische Universiteit Delft, reservelid

Published and distributed by:

I.Y. Shevtsov
E-mail: rail-citg@tudelft.nl

Section of Road and Railway Engineering
Faculty of Civil Engineering and Geosciences
Delft University of Technology
P.O. Box 5048
2600 GA Delft
The Netherlands

ISBN 978-90-8570-303-7

Keywords: wheel/rail profiles, railway vehicle, dynamic simulations, optimisation

Printed in The Netherlands

I dedicate this work to my family, who patiently awaited its completion.

Acknowledgements

It is with sincere gratitude that I acknowledge those who have encouraged and supported me in myriad ways during my PhD research studies and my life in The Netherlands.

This dissertation was completed under the supervision of Professor dr.ir. Coenraad Esveld, head of the Railway Engineering Section of Delft University of Technology. His guidance and insight has been both invaluable and inspiring, and I thank him for his time and assistance, and for the opportunity afforded me in pursuing the dissertation.

This project was carried out under the direct supervision of Assistant Professor Dr. Valeri Markine. I thank him for his time, help, and patience. Also, his help in my acclimation to life in Delft has been invaluable.

Special gratitude is reserved for Professor Victor Fedorovich Ushkalov of the Institute of Technical Mechanics, Dnepropetrovsk, Ukraine. Professor Ushkalov introduced me to world of railway vehicle dynamics and wheel/rail contact and he provided the impulse and the opportunity to come to The Netherlands in the first place.

I would like to heartily thank Prof.dr.ir. A.D. de Pater[†] and Prof.dr.ir. P. Meijers for their supervision, support and care during my very first year at TU Delft.

Many colleagues from Road and Railway Engineering Group of Delft University of Technology also helped me in the successful completion of this work. It is impossible to name all of them; however, I specifically acknowledge the head of the department, Prof.dr.ir. A.A.A. Molenaar, secretaries J. Barnhoorn and S. van den Bos, Z. Li, S. Jovanovich, A. de Man, P. Joksimovich, A. Miradi, J. Moraal, and J.-W. Bientjes. Many thanks go to my PhD student colleagues, among them, railway PhD students X. Zhao, M. Molodova, O. Arias Cuevas, and last but not least, my roommate M.J.M.M. Steenbergen.

During the first few years of this work, I received significant support from P. Scheepmaker, and M. Elsinga from HTM, The Hague.

Special words of gratitude are reserved for Gert Liefting and all the members of his group at Lloyd's Register Rail Europe (formerly NedTrain Consulting) for their professional fascination and experience in railway vehicle–track dynamics, which I was happy to share with them.

Special thanks to Kees Wijbrandts and Theo Kruse from ProRail for allowing me to finish my PhD thesis, and for patiently accepting my need to prepare for its defence.

I am grateful to my former and present colleagues for their direct and indirect support, and for creating a pleasant and stimulating work environment.

Further thanks to Anton and Gerke Spruijt and their family, as well as to Nelleke Fontein for their help in introducing me to Dutch life.

I thank all the researchers whose articles I read and used in the preparation of this manuscript. Much of the work in this project is based on previous theoretical and numerical work, and my thanks go out to all those who have contributed to the advancement of nonlinear dynamics, contact mechanics, railway vehicle dynamics, wheel/rail contact, and numerical optimisation, without which this work would have been impossible.

I thank the members of the Examination Committee for their attention to this thesis.

I am grateful to all my and my family friends in Delft and Rijswijk for their direct and indirect support.

I would like to express my gratitude to all my big family, brothers, sisters, aunts, grandparents and parents-in-law, for providing me inspiration for my work.

I am deeply indebted to my parents for their continuous support and encouragement.

Finally, I thank my wife, Olga, for her patience, support and encouragement; she never tired of my stories about ‘my wheels’ during these many years. My children, Fedor and Maria, are a continuing source of my inspiration.

Ivan Y. Shevtsov

Delft, 20.04.2008.

Contents

1 Introduction

Rail transportation remains the most cost effective method for moving passengers or freight between two locations connected by land. This is due to the low energy loss of metal on metal contact between wheels and rail. In recent years the problem of the wheel/rail contact has become very important for railway transport. Increasing axle loads in heavy-haul freight cars, the presence of tight curves and light vehicles in tram and fast transit systems, and the high speeds of vehicles on high-speed lines present differing requirements with respect to wheel/rail interface. However, these differing requirements are all oriented toward same targets – increased durability, reduction of maintenance costs, and increased safety. To address such complex requirements, a combination of knowledge from various disciplines of the mechanical, mathematical, and physical sciences is required.

This study seeks to solve the problem of wheel/rail interface optimisation on the basis of the accumulated knowledge of many railway scientists, and application of this knowledge toward a relatively simple but powerful procedure for the design of the wheel (or rail) profile. This chapter formulates a problem statement and a number of research questions. Section 1.1 explains changes that have taken place in the field of railway wheel–rail interaction, as well as the existing problems of railway transport associated with wheel/rail contact. Section 1.2 describes the various approaches toward the design of wheel/rail profiles that were developed and used over the past 20 to 30 years. Section 1.3 introduces the research objectives that result from the above described wheel/rail contact problems, and discusses the research questions and strategies. Finally, Section 1.4 provides a summary of the research and an outline of the succeeding chapters.

1.1 Wheel/rail interface development

A transport system consisting of a vehicle moving along a prepared track that provides guidance and support for the vehicle has been known for more than 400 years. As with many mechanical systems, it has developed over the course of centuries and is still developing. ‘Wagonways’ were developed in Germany in the 1550s, and the use of these tracks, consisting of wooden (usually edged) rails for horse-drawn wagons, spread across Europe. At first confined to mines, they were in use in Britain for surface transport by the early 1600s. The Wollaton Wagonway is the earliest, proven, surface railway. It is recorded as running from Strelley to Wollaton near Nottingham and was completed in 1604. Other early wagonways are recorded at Broseley in Shropshire from 1605 onwards. Such railways existed in a number of areas, and in most cases their function was to facilitate the transport of coal from the pits to a stair on a riverbank, from where it could continue by water. Because rails were smoother than roads, a greater quantity could be carried, and without damage to highways.

In the late 1760s, the Coalbrookdale Company began to fix plates of cast iron to the wooden rails. These (and earlier railways) had flanged wheels as on modern railways, but Coalbrookdale introduced another system, in which unflanged wheels ran on L-shaped metal plates; these became known as plateways. John Curr, a Sheffield colliery manager, invented this flanged rail, though the exact date of this is disputed. William Jessop, a civil engineer, used this (or a similar design) on a scheme at Loughborough, Leicestershire in 1789. On July 26, 1803, Jessop opened the Surrey Iron Railway in south London – arguably, the world’s first public railway, albeit a horse-drawn one. However, it was not until 1825 that the success

of the Stockton and Darlington Railway proved that railways could be made as useful to the general shipping public as to the colliery owner. At the outset, this 'road' was regarded as only a special sort of toll-road upon which any carrier might transport goods or passengers in his own vehicles, but experience showed that it was necessary for the railway company to transport the goods as well.

James Watt, a Scottish inventor and mechanical engineer, was responsible for improvements to the steam engine that caused this device to see wider use, encouraging wider experimentation; but Watt's engines were stationary engines, not locomotives. The first steam locomotive was built by Richard Trevithick, an English engineer, in 1804. This machine used high pressure steam to drive the engine. His locomotive had no name, and was used at the Penydarren ironworks at Merthyr Tydfil in South Wales. However, this locomotive was not financially viable, because the engine was too heavy for the track and kept breaking down.

In 1813, George Stephenson persuaded the manager of the colliery where he worked to allow him to build a steam-powered machine. He built the Blucher, the first successful flanged-wheel adhesion locomotive. The flanges enabled the trains to run on top of the rails rather than in sunken tracks. This greatly simplified construction of switches and rails, and opened the path to the modern railway.

The conventional railway wheelset, which consists of two wheels mounted on a common axle, has a long history and evolved empirically. In the early days of the railways, speeds were low, and the design objectives were the reduction of rolling resistance and solving problems of strength and wear. The flanges were positioned on the inside, the outside, or even on both sides of the wheels. Flange positioning was debated all the way through the 1820s. Wheels were normally fixed to the axle, although freely rotating wheels were sometimes used in order to reduce friction in curves. From the beginning, the play allowed between wheel flange and rail was minimal.

Coning was introduced partly to reduce the rubbing of the flange against the rail, and partly to ease the motion of the vehicle around curves. It is not known when coning of the wheel tread was first introduced. It would be natural to provide a smooth curve uniting the flange with the wheel tread, and wear of the tread would contribute to this. Moreover, by the time wheels were made of cast iron, taper had already become normal foundry practice. Beginning in the early 1830s, flangeway clearance was opened up to reduce the lateral forces between wheel and rail such that, in current practice, typically 7 to 10 mm of lateral displacement is allowed before flange contact. The standard wheelset with flanged wheels rolling on a track is shown in Figure 1.1.

Wheel/rail interface advances in tandem with the development of the railways. First, cylindrical free-rotating wheels running on flanged rails were replaced by rigidly mounted on-axle conical wheels with flanges (see Figure 1.2). This design was successfully used until the 1970s, when increased axle load, travel speed, and maintenance demands placed new requirements on wheel/rail interface. Extensive research on in-service wheel and rail profiles reveals that worn profiles have curvilinear shapes, in contrast to the quasi-linear shape of the conical wheel. It was discovered that the worn shape of the wheel is more stable, i.e., less changes with the mileage and wear. Another advantage of the worn shape was that it is already ground-in to the existing rail; therefore, the initial high wear rate typical of new wheels was significantly reduced. Ever since, many railways have adopted the curvilinear wheel profiles as a standard.

Figure 1.1: The steel wheel rolling on a steel rail is the basis of almost all railway systems.

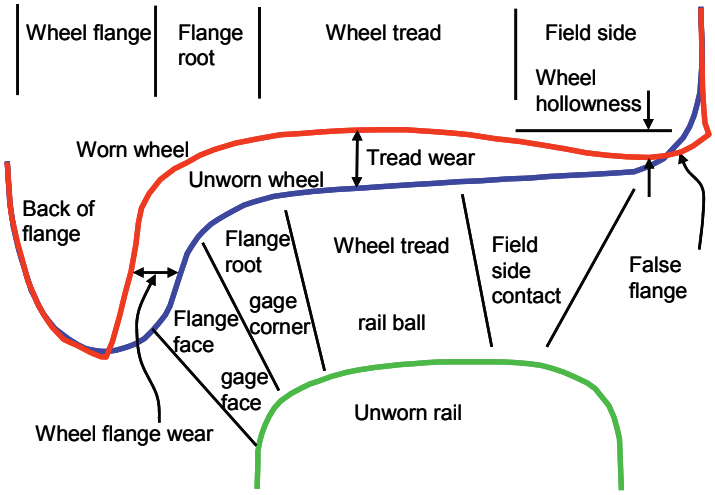

Figure 1.2: Worn and unworn wheels with unworn rail.

Although great progress has been made in railway transportation systems of all kinds (inter-city transport, mass transit systems, and heavy haul), some wheel/rail interface problems persist and, moreover, new problems continue to emerge. Below is a list and description of the current problems in railway transport associated with wheel/rail contact, as summarised by Kalousek [2002] at the 5th International Conference on Contact Mechanics and Wear of Rail/Wheel Systems:

- Safety (derailment due to wheel climb or broken rail);
- Economic (excessive wear, rolling contact fatigue);
- Environmental (noise and poor ride quality).

Safety problems. Derailments from broken rail or wheels, and wheel climb derailments represent the most serious safety hazards. Although many factors contribute to wheel climb, contact angle and the magnitude of friction coefficient are the most important. Yet, both friction coefficient, and the contact angle between the worn wheel-flange and the gauge of the worn rail are difficult to control in practice.

Around the world, rolling contact fatigue (RCF) cracks, or deep-seated shells, constitute a major cause of broken rail. These defects can initiate a transverse defect that may be difficult to detect during their early stages of growth, because the horizontal cracks shield the

transverse crack from ultrasonic detection. Railways with excessive grinding intervals do not keep-up with the need to remove these types of defects. Similarly, grinding is absolutely essential to control RCF defects (known as squats or dark spots) that are prevalent in lines carrying passenger and high-speed traffic. Loss of adhesion or electrical contact between the wheel and rail is another source of concern.

Economic problems. Wear is a problem that is well understood and that can be solved; however, it can occur unexpectedly on new lines. There, measures must be taken to control it. On wheels, the most common problem is flange wear. Substantial metal removal from the wheel tread is required to restore the thickness of the flange. Wear, therefore, now requires as much or more attention than it did 100 years ago.

RCF is first manifested by numerous micro-cracks and, if left untreated, results in the development of flaking or spalling, with cracks growing to a depth of 5 mm or more. This is a very costly problem. Both rails and wheels are affected. It was initially thought to be a problem associated only with heavy haul lines. Now, it is known that equally deep RCF cracks can develop on the wheels of passenger trains, and on many curves carrying passenger or high-speed traffic. With anticipated axle loads increasing in Europe, India and North America, it seems that RCF problems will never disappear. More and more railway companies use grinding to control RCF defects and corrugations on the rail. Grinding contributes to the attrition of metal from the crown, and actually represents just another form of wear. It is a great economic challenge for railway companies to grind off RCF and other rail surface damage without wasting valuable, undamaged metal.

Environmental problems. Railways and mass transit systems represent one of the most air-pollution benign modes of transportation. However, two problems remain: noise and poor ride quality. Although not all railway systems are affected, those that are may require a great deal of ingenuity to achieve a satisfactory solution. Noise originates from rough wheel and rail surfaces, corrugation-induced vibrations, or stick-slip–induced squeal. Each mass transit system seems to have unique mechanisms of corrugation formation, and in some systems the wheels may also corrugate. Corrugated wheels produce noise at frequencies dependent on train-speed. As the train accelerates and decelerates between stations, the sound produced is reminiscent of dog howling.

Although the lateral dynamic instability known as hunting is now well understood, it remains a common problem on many mass transit and heavy haul systems, as the conformal wear of wheel to rail often results in hunting.

These safety, economic, and environmental problems can be greatly reduced or brought under control through modification and optimisation of wheel/rail interface. Magel [1991] points to four key technologies essential for optimising wheel/rail interface. Optimising wheel/rail interface requires a focus on the following four areas: **contact mechanics, wheel/rail dynamics, metallurgy,** and **friction management**. Changes to wheel and rail materials are comparatively expensive and time consuming, since new material must not be only developed (a challenge in itself), but any new material must also pass regulatory muster with regard to all required legislative standards. Railways are quite conservative with regard to the introduction of new materials for wheels and rails, due to safety concerns. New materials must be carefully tested to prove their ability to function without failure under required conditions for a period of 10–20 years in the case of rails, and for 2–3 years for wheels. Wheel/rail friction management (lubrication) is also a very powerful method for reduction of wheel/rail wear (especially on sharp curves), train rolling resistance, and the occurrence of wheel/rail rolling contact fatigue. However, use of lubrication requires careful monitoring, because contamination of rail or wheel with sand or dust in combination with lubrication can

lead to increased wear. Excessive lubrication can lead to increased RCF occurrence, due to liquid (lubricant) entrapment in the cracks. Metallurgy and friction management will not be considered in this work on wheel/rail interface optimisation. Extensive research and practical implementation already have been carried out in these two fields (see Proceedings of Contact Mechanics Conferences and Iwnicki [2006]). In this thesis, the research will focus mainly on contact mechanics, and wheel/rail dynamics problems. Strategies of wheel profile design will be discussed in Section 1.3, after an overview, in Section 1.2, of the current state-of-the-art in the design of wheel/rail profiles.

1.2 Works on design of wheel/rail profiles

Wheel/rail contact physically occupies an area the size of a small coin, and such contact transfers the load from a vehicle ranging from 3.5 t (28 t lightweight passenger coach) to 17.5 t (heavy freight car of 140 t) per wheel. The material in and around the contact area is therefore highly stressed. High rates of wear might be expected from such contact but, because the load is applied and removed many times during the passage of each train, there is the added possibility of fatigue of the rail surface. (Further details on these loads and their effects on steel rails and wheels are presented in the relevant chapters below). The ideal material, which would have zero wear and suffer zero fatigue, and which would nevertheless be economically viable, is yet to be found.

The selection of railway wheel and rail profiles is a challenge that has faced engineers since the dawn of the railway age. From the first cylindrical wheels running on flat plates, wheels were made conical to produce better guidance, and flanges were added for safety. Modern wheels often have complex profiles based on the shape of worn wheels in an attempt to increase their life. Rails also now have complex profiles with different radii on the rail head, where the wheel tread makes contact, and on the corner, where the flange contacts.

A high level of wheelset conicity allows good curving behaviour even in the tightest curve, without flange contact. This can however, lead to a relatively low critical speed and possibly dangerous hunting instability. A low level of wheelset conicity on the other hand, allows stable operation at high speeds, but flangeway clearance will quickly be used up in curves, resulting in flange contact and possible flange climb derailment. Flange angle and root radius are also variables that can have a significant effect on the potential for derailment. In addition to vehicle behaviour, engineers must consider stresses on both the wheel and rail. These have a major influence on the development of RCF, which can have expensive and sometimes dangerous consequences.

Typically, wheel and rail profiles were designed using a trial and error approach. The choice of wheel and rail cross-sectional shapes was based mainly on designer intuition and experience, as well as measurement data. During the last several decades, a number of efforts have been made to use numerical methods in the wheel and rail design process.

One of the ways in which railways have traditionally maintained the shape of the rail is through rail profile grinding. Over the years, researchers, railways, and rail grinding contractors have developed a series of patterns that are used to impose a specific profile upon the rail. These profiles have been characterized as ‘one-point’ and ‘two-point’ contact profiles. Optimisation of the rail grinding process, and the factors affecting the selection of the one- or two-point contact profiles is described by Magel [1999]. This work is extended in Magel and Kalousek [2002]. A quasi-static curving program (called PUMMEL) is used by Magel and Kalousek [2002] to quantify the performance of rail profiles when loaded using a large number of measured new and worn wheels.

Grohmann and Schoech [2002] describe a long-term experiment launched by the German Railways (Deutsche Bahn) to specify a target profile with appropriate grinding tolerances to limit or even prevent head check development. Optimal rail maintenance policy can be developed to balance wear and surface fatigue through grinding. The objective is to maximize rail service life, and to consequently optimise the life cycle costs of rails.

Design of the rail head profiles for the Tokaido Shinkansen line in Japan is described in Sato [1990]. To improve rail conditions on this line, studies of worn rail profiles and rail damage were carried out, and the causes of damage assessed. Then, the abrasion of rail corners on tangent track was studied. Through the study of contact points between wheel and rail, the fact that the lateral movement of bogies is accelerated by tilting of the rail was made clear. On the basis of these findings, new measures, such as limiting the displacement of contact points between wheel and rail, cutting off neighbouring parts of the running fringe, having the rail head side conform to the tyre profile, and cutting off the gauge corner on curves with larger radius, and on tangent track, were proposed, and a new rail profile with full use of grinding was designed.

It has been common practice to use heavy rail on heavy haul railways to reduce rail defects and track deterioration. The clear advantages of using heavy rail on high-speed railways are discussed in Sato [1996]. Since future railways should guarantee the dynamic stability of rolling stock and be free of rail defects, it is appropriate to consider modifying the wheel running band formed by rail grinding. A new 75 kg rail profile with full use of grinding was proposed. This profile was developed based on experience with rail profile design in Japan. Mathematical equations were used to model the profile, instead of drawings. An historical review of wheel and rail profile development on the Shinkansen line can be found in Sato [2005].

Smallwood et al. [1990] have been using optimisation techniques to minimize rail contact stresses. A modification to the transverse rail profile has been proposed which should result in reduction in contact stress. Contact stresses between wheel and rail are believed to be influential in the initiation and growth of RCF cracks, particularly on the high rails of curves on high speed lines. Theoretical methods have been used to investigate the effect of profile changes on contact stress and conicity. The predicted contact stresses for the modified profile are up to 50% lower than those for an unworn standard British Railways (BR) profile, while the conicity remains within an acceptable range. The metal removal required to achieve this profile appears practical using the latest generation of more aggressive grinding trains.

Since 1970, the ORE C116 committee has endeavoured to determine a standard European profile adapted for wear (see Casini and Tacci [1996]). However, rail type, track gauge, and rail inclination differ among European railway networks; therefore, it is difficult to arrive at a standard profile adapted for wear. An attempt to create a standard profile was made with the ORE S1002 wheel profile. The ORE S1002 profile was calculated on the basis of the DB II profile, by transforming the three arcs of the wheel into a higher degree polynomial curve. The difference in the coordinates is very small, and the two profiles may be considered equivalent. The ORE S1002 wheel profile is adapted for wear for rails inclined at 1:40.

Smith and Kalousek [1990] developed a numerical procedure for design of a wheel profile, described by a series of arcs. Although the procedure was specifically developed for steered axle vehicles, some important aspects of this work may be applied to conventional systems as well. Casini and Tacci [1996] also use a series of arcs to develop a new wheel profile adapted for the Italian network. The process of designing a new wheel profile for North American railways is described by Leary et al. [1990], wherein alternative profiles are derived through two techniques: an average worn wheel profile, and profiles based on expansions of rail

shapes. Both methods provide good base designs for candidate profiles. However, the initial wheel shapes produced were modified to suit the specific concerns of the task involved. This was done through careful computer analysis of the dynamic and contact stress characteristics of each wheel. One procedure for design of a wheel profile using a numerical optimisation technique is proposed in Shen et al. [2003], wherein the contact angle function is used for the design of railway wheel profiles. Using the inverse method for known contact angles and rail profile, a corresponding wheel profile was found. Persson and Iwnicki [2004] and later Novales et al. [2006] use a direct optimisation procedure based on a genetic algorithm for design of a wheel profile for railway vehicles. Two existing wheel profiles were chosen as parents, and genes were formed to represent these profiles. These genes were mated to produce offspring genes then reconstructed into profiles that had random combinations of the properties of the parents. Each of the offspring profiles were evaluated by running a computer simulation of the behaviour of a vehicle fitted with these wheel profiles and calculating a penalty index. The inverted penalty index was used as the fitness value in the genetic algorithm. This method was used to produce optimised wheel profiles for two typical vehicles, one with a relatively soft primary suspension, and the other with a relatively stiff primary suspension.

A recent project to design a wheel profile to reduce RCF on rails is described by Magel and Kalousek [2004]. They suggest that creepage can be controlled and manipulated to minimize contact fatigue. Although creep forces are dramatically influenced by a range of operational conditions that include traction and braking demands, friction coefficient and suspension characteristics, the focus of the research was on wheel and rail profiles. Through quasi-static and dynamic modelling it was shown that a modified wheel profile, by reducing both normal contact stress and traction, can play a significant role in mitigating RCF.

Research on wheel/rail contact problems on Russian Railways is described by Zakharov and Zharov [2000] and Zakharov and Goryacheva [2003]. Serious problems of wheel and rail profile design arise particularly when combined freight and passenger traffic exists on the line or this task should be solved on a big railway network scale. Profile selection policies and real practices applied on Russian Railways are described by Zakharov et al. [2006].

In some cases, wheel/rail interface optimisation cannot be performed merely through the modification of wheel and/or rail profiles. In Guidelines to Best Practices for Heavy Haul Railway Operation (Harris et al. [2001]), it is recommended that a systems approach be applied to optimising wheel/rail performance. A complex modernization of the conventional three-piece bogie 18-100 type used for freight cars in Ukraine (as well as other countries of the former USSR) has been suggested by the Institute of Technical Mechanics of the National Academy of Sciences of Ukraine. To reduce wheel flange wear, a non-linear ‘one-point’ contact type wheel profile was developed. This profile was implemented on an upgraded freight bogie. This modernization includes the utilization of A. Stucki roller-assisted, constant-contact side bearings, polyurethane pads for the friction wedges, and bolster wedge pockets. Running tests over three years (about 190000 km) have shown that this modernization resulted in an increase of the critical velocity of empty cars by 30–40 km/h, decrease in wheel flange wear by a factor of two, along with other benefits (see Ushkalov et al. [2002]). Ukrainian Railways is now performing the above described modernization on several hundred freight cars.

1.3 Research questions and strategy

The main objective of the present research is to develop a procedure for the design of an optimised railway wheel profile. This procedure should be computationally inexpensive and

flexible with regard to rolling stock type. In general, the design of a new wheel will be focused on five main problems in wheel/rail contact:

- Wear of contact surfaces;
- Rolling contact fatigue;
- Stability on a straight track;
- Stability on passing curves (minimisation of *Y/Q* and track forces);
- Safety requirements.

These problems maintain a complex relationship with each other. For example, decreasing wear can lead to RCF problems, and increasing conicity to pass curves with larger rolling radius can lead to decreased critical speed of the vehicle, and vice versa. Depending on the type of railway system, one of these five problems may be more pronounced; however, they all are present in the wheel/rail interface, and should be considered together.

Obviously, an optimum profile is a compromise between stability, curving, wear, and RCF. Magel and Kalousek [2002] formulated criteria for optimal wheel/rail contact. Optimised wheel and rail profiles from the aspect of contact mechanics should satisfy the following criteria:

- Avoid contact stresses greater than three times the strength of material in shear;
- Avoid closely conformal contact;
- Design appropriate steering capability;
- Ensure effective conicity that is within the conicity window of the truck;
- Arrange for as many contact points across the wheel tread as possible.

In the past, such a compromise would have been achieved by manually modifying the wheel shape to find satisfactory contact characteristics in relation to a given rail. However, this design approach is quite time consuming and expensive. Therefore, it would be advantageous to develop and use numerical methods for the design of the wheel and rail profiles.

The kinematic properties of wheel–rail contact, such as rolling radius, contact angle and wheelset roll angle vary as the wheelset moves laterally, relative to the rails. The nature of the functional dependence between these geometrically constrained variables and the wheelset lateral position is defined by the cross-sectional shape of wheel and rail. By studying the geometric characteristics of the contact between wheel and rail, it is possible to judge the dynamic behaviour of the wheelset, as well as dynamic properties (like stability) of the vehicle. The wheel and rail cross-sectional shapes define not only the kinematic and dynamic properties of the wheelset, but also such physical properties as contact stress, creep, and wear.

An important characteristic of contact between wheel and rail is the rolling radius of the wheel at the contact point. Consequently, the difference between the rolling radius of the right and the left wheel (rolling radius difference or RRD) as a function of the lateral displacement of a wheelset is one of the main characteristics of wheel/rail contact that defines the behaviour of a wheelset on a track. For more information about RRD function, see Chapter 2 and Chapter 4.

The rolling radii of the left and right wheels are present in the equations of wheelset motion (see Dukkipati [2000]). Therefore, the RRD function is important for the dynamic behaviour of a wheelset. From another viewpoint, the RRD function is defined by the wheel and rail cross-sectional profiles. Track and wheelset geometric parameters of course influence the RRD function as well, but they are considered to be given.

But if the shape of the RRD function is defined by the wheel and rail profiles, then the opposite is also valid; that is, the RRD function can define the shape of the wheel or rail

profile. In computational modelling of railway vehicle, modification of the RRD function can change dynamic behaviour of the wheelset helping to achieve the required performance. This modified RRD function virtually corresponds to a new combination of wheel/rail profiles. For a given rail profile, one may solve the inverse problem in order to find a wheel profile to match the modified RRD function. The inverse problem can be solved using an optimisation method. This idea was used as a strategic concept in the creation of the procedure for wheel profile design.

In the wheel profile design procedure, the optimisation searches for an optimum wheel profile by minimizing the difference between target (desired) and actual RRD functions. To solve the minimization problem, an optimisation procedure based on Multipoint Approximations based on Response Surface fitting (MARS method) was used. Different constraints can be applied in the optimisation procedure to reflect safety, construction, and other requirements for the designed profile.

Static analysis of geometric wheel/rail contact is used as a first step in the design of appropriate profiles. Analysis of railway vehicle dynamics is needed to verify that the designed profiles will perform well under given vehicle and track conditions. Limited track tests should also be conducted, if possible, to confirm the analysis results.

The complete procedure of wheel and rail profile design is described in Chapter 6. Several application cases of the wheel profile design procedure are described in Chapter 7.

1.4 Summary and chapter outline

The particular chosen aspect of wheel/rail interface optimisation determines the range of problems to be studied in this thesis. First, geometric contact between wheel and rail must be investigated. Then contact mechanics must describe the physics of rolling contact between wheel and rail. Next, railway vehicle dynamics should be considered with the help of ADAMS/Rail multi-body dynamic simulation software. Finally a numerical optimisation method should be used for the design of the wheel profile.

In the present research, three main railway systems are considered, tram, metro, and railway. Tram systems are characterised by the presence of many sharp curves and the comparably low speed of the tram vehicles. Mainly, flange wear is the greatest concern for the tram operators. Metro lines are characterised by larger radius curves and higher speeds in comparison with tram systems. Therefore, together with wear of the wheel profile, the problem of vehicle stability arises. Conventional railways are characterised by high speed and large radius curves. Wear and stability of vehicles have been of great concern for railway engineers since before the 21st century. However, with the development of new types of rolling stock, and the introduction of curvilinear profiles, new problems arise. At the present time, RCF is the largest problem for railways. As can be seen, these three systems present different requirements for wheel/rail contact, and require different solutions in wheel design.

Freight rolling stock is not considered in the present research. There are several reasons for this. First, a main criterion for freight vehicles is interoperability. For this reason, the wheel profile of the freight wagon should be uniform, unless the vehicle is operated on a closed line. Second, the variety of freight vehicles is probably as great as the variety of passenger vehicles. Third, requirements for freight vehicles are significantly different compared to passenger rolling stock (axle load is greater, and travel speed is lower for freight vehicles). Therefore, freight rolling stock constitutes a distinct field of research, requiring separate investigation.

In this dissertation, research questions will be answered individually in the following chapters. Chapter 2 describes solution technique for geometric contact between track and wheelset, and

the method used in this research. Chapter 3 describes the present state of the science in rolling contact between wheel and rail from a physical point of view. Chapter 4 presents basic information about the modelling of railway vehicles using ADAMS/Rail software. The numerical optimisation method is described in Chapter 5. Chapter 6 presents the design procedure for wheel and rail profiles. Next, the methods of wheel profile design for three case studies are described in Chapter 7. Chapter 8 finalises the thesis with conclusions and recommendations for further research in the field of wheel/rail interface.

2 Geometric contact between track and wheelset

In this chapter, the kinematics of a railway wheelset moving on a track are described. A short introduction is given in Section 2.1. Starting from a simplified wheelset with conical wheels, the kinematics of the wheelset on straight and curved tracks is introduced in Section 2.2. Next, methods for determining contact locus between a real wheel and rail profiles are described in Section 2.3. Examples of geometric contact between different wheel/rail profile combinations are presented in Section 2.4. Section 2.5 concludes the chapter with a discussion.

2.1 Introduction

The conventional railway wheelset consists of two wheels rigidly mounted on a common axle. Normally, wheels have a coned or profiled tread with a flange on the inside edge. The tread cone angle is about 2º, while the flange cone angle is about 70º. The wheelset rests on two rails fixed to the sleepers (ties) or other support (e.g., embedded rail). A typical wheelset on rails is shown in Figure 2.1. A wheelset runs on rails normally inclined (canted) at 1 in 40 (1 in 20), see Figure 2.2. The gap between the flange of the wheel and the gauge side of the rail is such that it allows 4–7 mm lateral wheelset displacement before flange contact occurs.

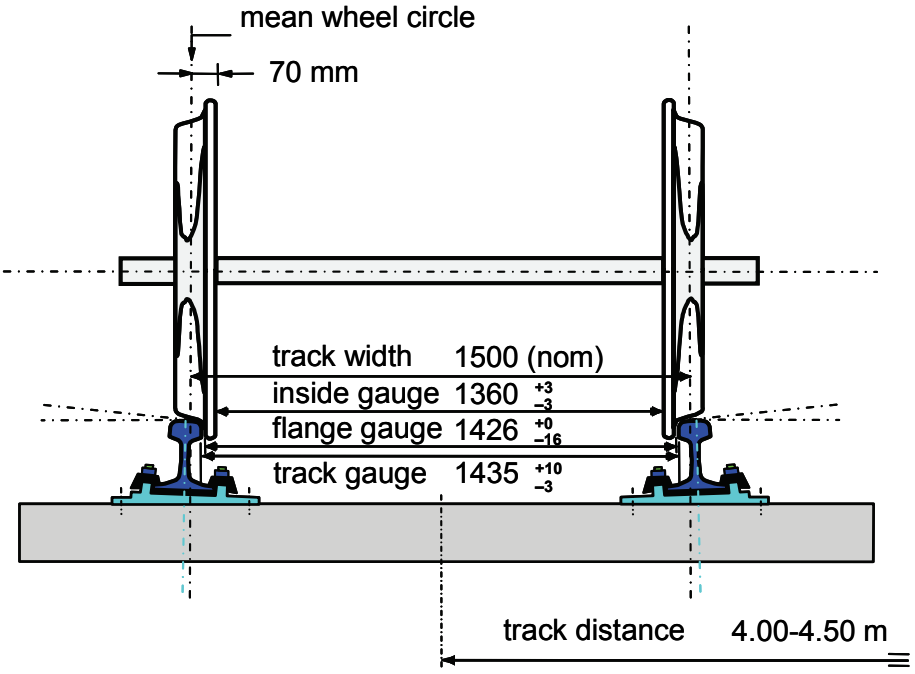

Figure 2.1: The wheelset–track system.

The shapes of wheel/rail surfaces (tread, flange root and flange of the wheel, rail head, gauge corner, and gauge face of the rail, as shown in Figure 1.2) are important to vehicle stability, wheel/rail interaction forces, contact stresses, and wear characteristics. Vehicle dynamic response, wheel/rail contact forces and positions, and track dynamic response can be derived from vehicle/track dynamic simulation. Normally, vehicle and track dynamics models are considered separately, due to complicity of the models, and limitations on computer recourses. Vehicle and track dynamics systems interact via wheel/rail interface, using output from one model as input for another, and vice-versa. For example, track irregularities can be use as an

input for wheel/rail contact, causing disturbances in contact forces, which in turn will be used as an input for the vehicle model. To determine forces in wheel/rail contact, values of creepage and spin are required, which can be obtained from analysis of geometric contact between wheelset and track. In the following sections, the kinematics of a simplified wheelset are briefly introduced, followed by a discussion of the problems of real wheel/rail contact.

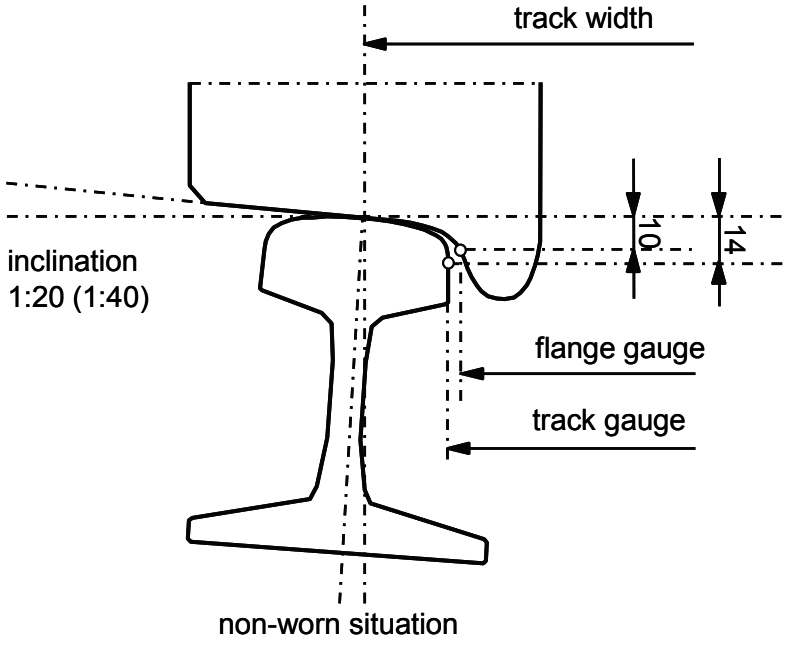

Figure 2.2: Definition of track and flange gauge.

2.2 Basics of wheelset and track interaction

2.2.1 Kinematics of a wheelset on straight track

First, consider the motion of an unrestrained single wheelset as it rolls along perfectly aligned straight track. For small displacements, the flanges do not come into play and therefore the coning of the wheels dominates the motion (see Figure 2.3). The coned wheels are rigidly attached to a solid axle. If the track is considered to be rigid, then the railway wheelset has two main degrees of freedom:

- the lateral displacement y, and
- the yaw angle ψ.

If, as the wheelset is rolling along the track, it is displaced slightly to one side, the wheel on one side is running on a larger radius and the wheel on the other side is running on a smaller radius. If pure rolling is maintained, the wheelset would move back into the centre of the track, and a steering action would be realized with the aid of coning. However, it will be found that following such a disturbance, the wheelset overshoots the centre of the track and traces out a more or less sinusoidal path as it proceeds down the track. This motion is referred to as kinematic oscillation. It was first described by George Stephenson in his 'Observations on Edge and Tram Railways', 19 May 1821 (as in Dendy Marshall [1938] according to Wickens [1999]):

It must be understood the form of edge railway wheels are conical that is the outer is rather less than the inner diameter about 3/16 of an inch. Then from a small irregularity of the railway the wheels may be thrown a little to the right or a little to the left, when the former happens the right wheel will expose a larger and the left one a smaller diameter to the bearing surface of the rail which will cause the latter to lose ground of the former but at

the same time in moving forward it gradually exposes a greater diameter to the rail while the right one on the contrary is gradually exposing a lesser which will cause it to lose ground of the left one but will regain it on its progress as has been described alternately gaining and losing ground of each other which will cause the wheels to proceed in an oscillatory but easy motion on the rails.

This is a very clear description of what is now called the kinematic oscillation, as shown in Figure 2.3.

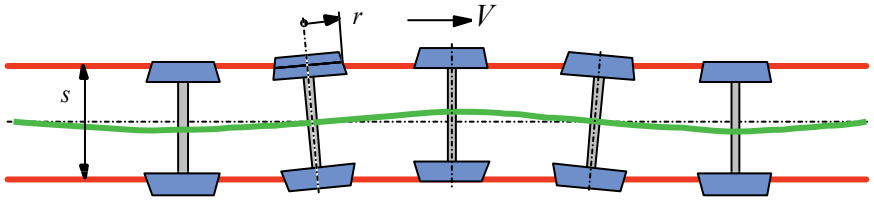

Figure 2.3: The kinematic oscillation of a wheelset.

Kinematic oscillation was first analysed mathematically for the case of purely coned wheels by Klingel in 1883, who showed that the frequency of oscillation is proportional to speed and to the square root of the cone angle. Klingel's description of wheelset oscillation assumes that pure rolling is maintained throughout the motion of the wheelset. In reality, this is not so because of the phenomenon of creep, first described in the present application by Carter in 1916, see Wickens [2003].

2.2.1.1 Klingel theory

In 1883, Klingel formulated the first mathematical analysis of the kinematic oscillation of the conical wheelset. Freely rolling wheelsets perform a sinusoidal motion, as shown in Figure 2.3. Klingel derived the relationship between the wavelength L_k and the wheelset conicity γ, wheel radius r, and the lateral distance between contact points s as

$$L_k = 2\pi\sqrt{\frac{rs}{2\gamma}}. \tag{2.1}$$

Thus with Klingel, the linear, purely kinematic motion of a single wheelset is solved. Klingel's formula shows that as the speed is increased, so is the frequency of kinematic oscillation. Any further aspects of the dynamic behaviour of railway vehicles must be deduced from a consideration of the acting forces this had to wait for Carter's much later (1916) contribution to the subject. If V represents vehicle speed, the time domain frequency of the Klingel movement is

$$f = \frac{V}{L_k}. \tag{2.2}$$

The Klingel movement is dependent only on track and wheelset geometric characteristics, and represents a global effect of wheel–rail interaction. If the frequency f is close to one of the natural frequencies of the wheelset, the periodic movement could cause the vehicle instability. The lateral accelerations on the wheelset due to Klingel movement are described by the ratio V/L_k:

$$\ddot{y}_{\max} = 4\pi^2 y_0 \left(\frac{V}{L_k}\right)^2, \tag{2.3}$$

where y_0 is the amplitude of wheelset lateral displacement. At the same speed, a lower conicity γ produces a movement with greater wavelength, but with lower lateral acceleration.

Lateral oscillations caused by coning have been experienced since the early days of the railways. One solution to the oscillation problem that has been proposed from time to time, even in modern times, is to fit wheels with cylindrical treads. However, in this case, if the wheels are rigidly mounted on the axle, very slight errors in parallelism would induce large lateral displacements that would be limited by flange contact. Thus, a wheelset with cylindrical treads tends to run in continuous flange contact.

Wheelset stability can be provided by the proper choice of the longitudinal stiffness of the primary suspension of the bogie. This subject was first solved in its entirety by Wickens [1965 a,b], and is discussed in Section 4.3.

2.2.1.2 Rolling radius difference

Let us continue with a simplified wheelset with a conical wheel profile. When the conical wheel runs on the circular rail without flange contact, there is only one contact point between the wheel and rail profiles, as shown in Figure 2.4. On the wheel profile, this point identifies the rolling radius. In the central position of the wheelset, due to the symmetry of the wheelset/track system, the rolling radii r and r_1, r_2 for the right and left wheels are equal, $r_1 = r_2 = r$. If the wheelset centre is displaced for quantity Δy, then the rolling radii due to conicity of the wheels will be different for the right and left wheels, creating rolling radii difference (RRD) $\Delta r = r_1 - r_2$. An instantaneous difference between the rolling radius of the right and the left wheel can be defined as a function of lateral displacement y of a wheelset with respect to its central position (Figure 2.4), according to:

$$\Delta r(y) \equiv r_1(y) - r_2(y) . \tag{2.4}$$

Some examples of rolling radius difference functions (also known as a '$y - \Delta r$' curve) for purely conical, and worn profiles, are given in Figure 2.5. Due to wear, a wheel profile changes (see Figure 1.2), and consequently so does its RRD function. As is evident, RRD function is dependent on wheel and rail shape; it is also included in the equations of wheelset motion, and therefore is a very important parameter for wheelset dynamics.

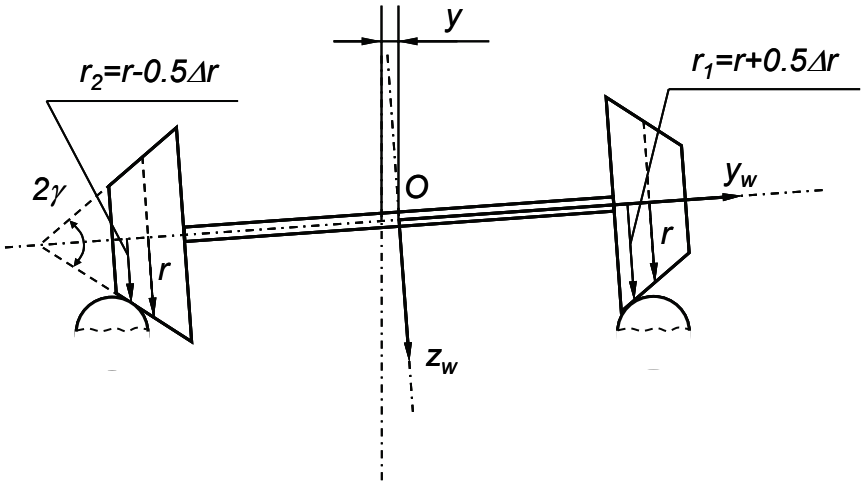

Figure 2.4: Rolling radius (r_1 and r_2) corresponding to wheelset displacement y, wheels are conical, γ is wheel conicity.

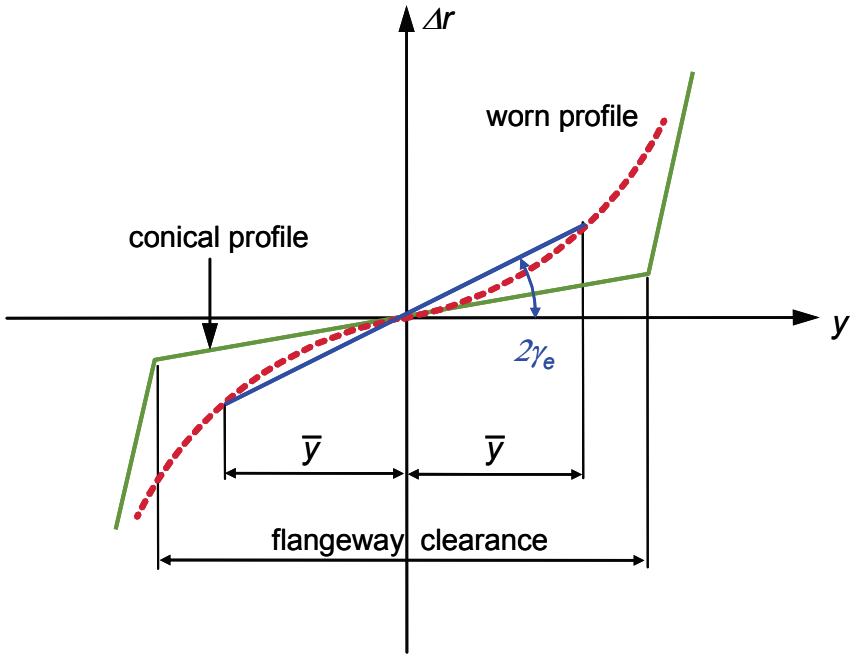

Figure 2.5: Rolling radius difference functions (‘ $y - \Delta r$ ’ curves).

2.2.1.3 Equivalent conicity

In the previous section, we saw that Klingel movement is one effect related to wheel–rail interaction; this movement is periodic. Its wavelength is independent from of vehicle speed and is a function of the angle γ of the conical wheel profile. So, wheel conicity γ provides information about wheel–rail interaction (also see Section 2.2.2):

- a high conicity value is suitable to counteract the centrifugal effects on curved track, but it generates a periodic movement on straight sections that can reduce riding comfort;
- low conicity increases the ride quality, but on curved track it can cause the contact between the rail gauge and the wheel flange, producing excessive wear for both rail and wheel.

On a modern wheelset, the real wheel profile is not conical, but it has a curvilinear shape that matches the rail head profile, as shown in Figure 2.6.

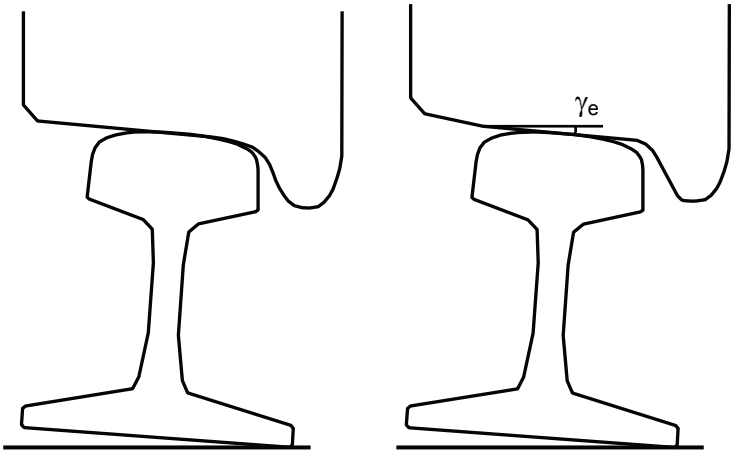

Figure 2.6: Real (left) and conical (right) wheel profiles on the rails.

To characterize wheel–rail interaction for a wheelset with real wheel profiles, a parameter, "equivalent conicity", is introduced. To identify the equivalent conicity, characteristics of the real wheelset/track pair are replaced with an "equivalent wheelset" with conical wheel tread surface. This replacement is valid for only one value of the wheelset lateral displacement.

Let us assume a lateral shift of the wheelset for quantity y from the central position. This shift is schematically shown in Figure 2.4. The shift translates the contact points on the wheel profiles, leading to differences in the rolling radii $\Delta r = r_1 - r_2$, see (2.1). Conicity γ of the wheel tread can then be expressed as a function of wheelset rolling radii difference and wheelset lateral displacement:

$$\gamma = \frac{r_1 - r_2}{2y} = \frac{\Delta r}{2y}. \tag{2.5}$$

The equivalent conicity γ_e is determined for a certain lateral displacement $y = \overline{y}$. For the conical wheel profile $\Delta r(y)$ is a linear function, and the conicity $\gamma_e = \gamma$ is constant and independent from the displacement y.

The equivalent conicity provides a quantitative measure of the influence of wheel/rail interaction on running quality. The threshold values for the equivalent conicity are defined in the UIC 518 fiche (UIC CODE 518 [2003]). The higher the vehicle speed, the lower should be the conicity of the wheel/rail pair to provide the required critical speed. The equivalent conicity must be lower than 0.5 to ensure vehicle stability, though it must be higher than 0.1 to generate the appropriate restoring forces. For real-world wheelsets, equivalent conicity is maintained in the range of 0.2–0.3.

2.2.2 Kinematics of a wheelset on curved track

The action of a wheelset with coned wheels in a curve was understood intuitively early in the development of railways. For example, in 1829 Ross Winans took out a patent that stressed the importance of the axles taking up a radial position on curves, a fundamental objective of running gear designers ever since. Redtenbacher (see Iwnicki [2006]) provided the first theoretical analysis on this matter in 1855. Consider a conical wheelset on curved track of radius R, as shown in Figure 2.7. A simple geometric relationship between the outward movement of wheelset y, the radius of the curve R, the wheel radius r, the distance between the contact points $2b$ and the conicity γ of the wheels can be derived in order to obtain pure rolling:

$$\frac{r + \Delta r}{r - \Delta r} = \frac{R + b}{R - b}. \tag{2.6}$$

Therefore, the required rolling radii difference in wheelset for passing a curve without slippage can be calculated according to the formula

$$\Delta r = \frac{2br}{R}. \tag{2.7}$$

Taking into account formula (2.5), the relationship between lateral displacement y of the wheelset and curve radius R can be derived as follows:

$$y = \frac{rb}{\gamma R}. \tag{2.8}$$

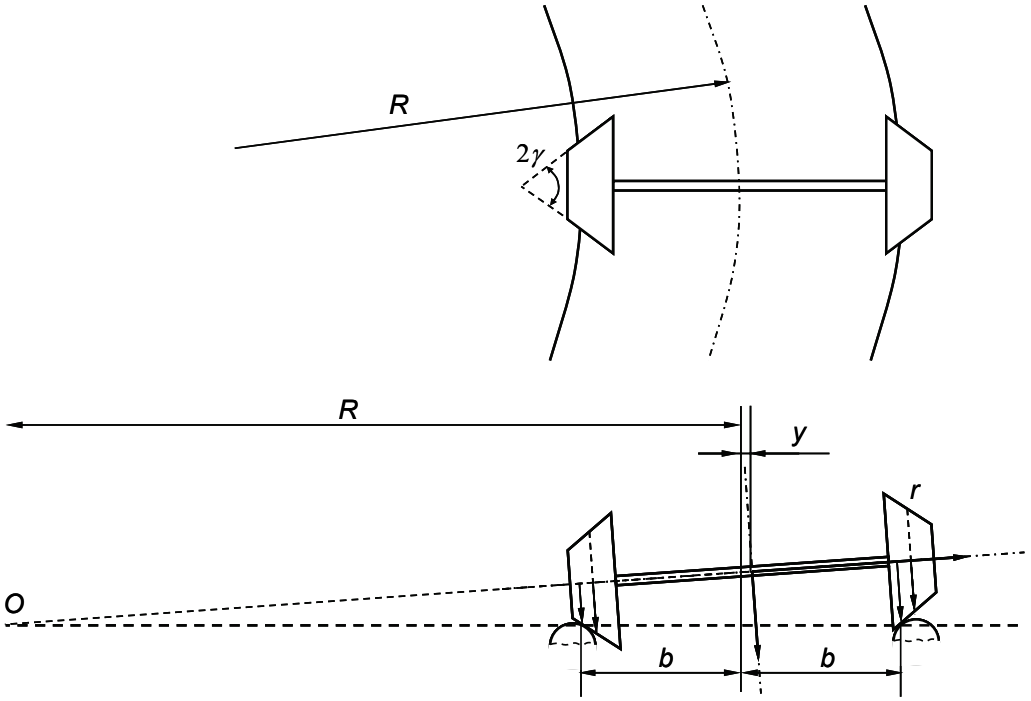

Figure 2.7: Rolling of a coned wheelset in a curve.

The application of Redtenbacher's formula shows that a wheelset will be able to move outwards to achieve pure rolling only if either the radius of curvature or the flangeway clearance is sufficiently large. Otherwise, a realistic consideration of curving requires analysis of the forces acting between the vehicle and the track.

Let us consider equation (2.7) assuming that flangeway clearance is sufficient, and that the distance between the contact points $2b$ is equal to track width $2b = s = 1.5\,m$. The required values of the RRD for passing curve with radius R without slippage are presented in Table 2.1 (wheel radius r is presented in brackets).

Table 2.1: Required RRD (Δr) for curves with radius R.

R, m	Δr, mm (r=0.331 m)	Δr, mm (r=0.390 m)	Δr, mm (r=0.460 m)	Δr, mm (r=0.500 m)
3000	0.166	0.195	0.230	0.250
2000	0.248	0.293	0.345	0.375
1500	0.331	0.390	0.460	0.500
1000	0.4965	0.585	0.690	0.750
500	0.993	1.170	1.380	1.500
300	1.655	1.950	2.300	2.500
150	3.310	3.900	4.600	5.000
100	4.965	5.850	6.900	7.500
50	9.930	11.700	13.800	15.000
30	16.550	19.500	23.000	25.000
25	19.860	23.400	27.600	30.000
18	27.583	32.500	38.333	41.666

From equation (2.7) and Table 2.1, it is clear that the wheels with smaller radius require smaller RRD to pass curve in comparison with wheels of larger radius. Due to the fact that

tram tracks feature great numbers of the sharp curves, tram vehicles use wheels with smaller radius to be able to produce the required RRD within given wheel/rail profile combinations.

2.3 Geometric contact between track and wheelset

The calculation of wheel/rail contact locus and of wheel/rail geometric contact parameters is a well know problem, and a number of solution methods have been developed. Starting from the Klingel theory, where cone was rolling over knife edge, researchers began to focus on the real shapes of wheel and rail (Wikens [1965a], Cooperrider et al. [1976]). In this thesis, two theories will be described:

- so-called first-order theory set forth by de Pater [1988, 1995, 1997, and 1999] (also see PhD thesis by Yang [1993]) and
- the theory set forth in Wang [1984], which is described in a PhD thesis by Li [2002].

De Pater [1997] applied a first-order theory to a stylised vehicle consisting of a single wheelset and a car body moving along a curved track. Wheel and rail profiles were presented as arcs of different radiuses. On the basis of this model, a number of problems from railway practice have already been investigated; however, in several cases (for example, derailment investigation) the model is too restricted. Later, de Pater [1999] considered the behaviour of a simplified railway vehicle with a number of wheelsets. Arrus, de Pater and Meyers [2002] extended this first order theory to the case of non-linear wheel and rail profiles with possible double-point contact. Unfortunately, this theory can be used only for relatively smooth (new) wheel and rail profiles. For non-smooth (measured, worn) profiles, the theory developed by Wang [1984] should be used.

Wang [1984] (according to Li [2002]) developed his theory based on a very simple assumption – the wheelset lifted over the track, then shifted in the lateral position, and by rotating the wheelset can be find the equal minimal distance between wheel and rail profiles for the left and right sides. The location of this minimal distance reveals the location of the contact point on the wheel and rail profiles. In this way, the contact locus for any kind of wheel and rail profile can be found easily.

The theories of de Pater and Wang are strictly two-dimensional. Three-dimensional approaches have been developed and implemented by Duffek [1982], Arnold and Frischmuth [1998], Li [2002], and other researchers. These three-dimensional approaches have been implemented for the calculation of the wear of wheels and rails; such approaches are necessary for such calculations. For analysis of the properties of geometric wheel/rail contact, the two-dimensional approach is sufficient.

For purposes of investigation of geometric wheel/rail contact, it is assumed that the track and the wheelsets are rigid. In most cases, wheel and rail profiles are symmetric; the profile of the left-hand rail is the mirror image of that of the right-hand rail, and the same holds for wheel profiles. However, in some cases left and right wheel and rail profiles are non-symmetrical. For example, measured worn profiles or high (outer) and low (inner) rail profiles in curves can have different shapes. These cases will be discusses in the parts of this thesis that correspond to this topic.

2.3.1 Analytical model

A single wheelset is here considered as a rigid body, and so presents a mechanical system with six degrees of freedom. As the wheelset moves along a track, usually each wheel contacts the rail at one point such that the system has two constraints, four independent

coordinates and two dependent coordinates. Referring to de Pater [1999], we choose the displacement of the wheelset centre in the direction perpendicular to the track plane, and the wheelset rotation about the longitudinal axis through its centre (the rolling angle) as dependent coordinates. Then, we find the constraint relations between the dependent and the independent coordinates, and we enunciate how the coordinates of the contact points, the conicity angles, and the radii of curvature in these points may be calculated.

We introduce two global coordinate systems, the frame (o^*,x^*,y^*,z^*), the origin o^* of which coincides with the wheelset centre, whereas the axis o^*y^* coincides with the lateral symmetry axis of the wheelset, and secondly, the track reference frame (o,x,y,z), which moves with velocity V along the track, and has its origin at the wheelset centre in the central position. In this position, the frames coincide. The x-coordinate is chosen in longitudinal direction, the y-coordinate in lateral direction, parallel to the track plane with the positive direction to the right-hand side, and the z-coordinate is normal to the track and downwards.

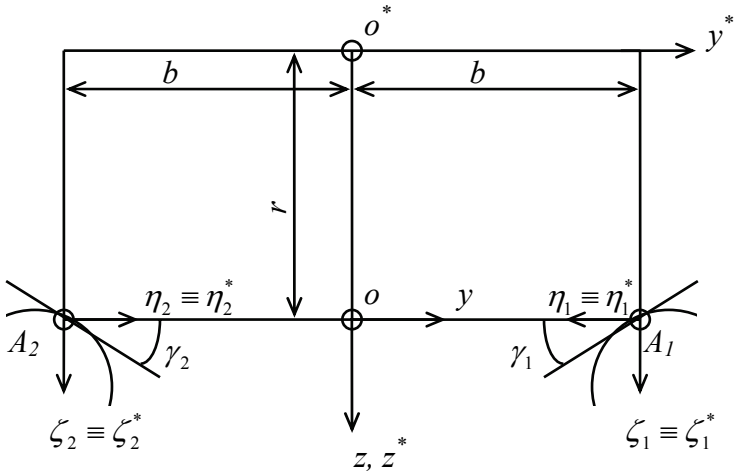

Figure 2.8: The contact points and the local coordinate systems for the central position of the wheels.

The contact points on the rails are indicated by A_j, and those on the wheelset by A_j^*. We call x_j, y_j, z_j the coordinates of A_j and x_j^*, y_j^*, z_j^* the coordinates of A_j^*. A contact point on the wheel is always indicated by the index j = 1 (right) or j = 2 (left), see Figure 2.8. Furthermore we introduce the local systems of coordinates ξ,η,ζ and ξ^*,η^*,ζ^* according to the relations:

$$\left.\begin{aligned} x_j &= \xi_j, \quad y_j = \pm(\mathrm{b} - \eta_j), \quad z_j = w_j + \zeta_j, \\ x_j^* &= \xi_j^*, \quad y_j^* = \pm(\mathrm{b} - \eta_{ij}^*), \quad z_{ij}^* = r + \zeta_{ij}^* \end{aligned}\right\} \text{ (j=1,2),} \tag{2.9}$$

where b is the half-distance between the contact points in the central position for a standard track gauge and r is the nominal wheel radius; in the notation $\pm$ or $\mp$, the upper sign refers to a right-hand contact point and the lower sign to a left-hand contact point. Then, we may describe the rail and wheel profiles by means of the functions $\zeta = f(\eta)$ and $\zeta^* = f^*(\eta^*)$, giving at the contact points

$$\zeta_j = f(\eta_j) \text{ and } \zeta_j^* = f^*(\eta_j^*) \text{ for j = 1,2} \tag{2.10}$$

Their derivatives are associated with the conicity angles γ and γ^*:

$$\frac{d\zeta_j}{d\eta_j} = tg\gamma_j, \quad \frac{d\zeta_j^*}{d\eta_j^*} = tg\gamma_j^* \text{ (j=1, 2).} \tag{2.11}$$

By imposing that the contact points on the rail and on the wheel, and the directions of the normal vectors to the two profiles at the contact points coincide, we derive the following relations (de Pater [1995a]):

$$\left.\begin{aligned} r\varphi \mp (\eta_j - \eta_j^*) &= v - v_j, \\ w \pm b\varphi - (\zeta_j - \zeta_j^*) &= w_j, \\ \pm\varphi + \gamma_j - \gamma_j^* &= \pm\varphi_j \end{aligned}\right\} \text{(j=1, 2),} \tag{2.12}$$

where v and w are the displacements of the wheelset centre in the y - and z - direction, respectively, and φ is the rolling angle of the wheelset. The remaining unknowns, namely the longitudinal coordinates of the contact points, are expressed in terms of the independent coordinates u and ψ:

$$\xi_j = u \mp (b - rtg\gamma_j)\psi, \quad \xi_j^* = \pm r\psi tg\gamma_j, \tag{2.13}$$

where u is the longitudinal displacement of the wheelset centre and ψ is the yaw angle. From (2.11) we calculate the radii of curvature in the contact points:

$$r_{yj} = (\kappa_{yj})^{-1} = \left(\frac{d^2\zeta_j}{d\eta_j^{\,2}}\cos^3\gamma_j\right)^{-1}, \quad r_{yj}^* = (k_{yj}^*)^{-1} = \left(\frac{d^2\zeta_j^*}{d\eta_j^{*2}}\cos^3\gamma_j^*\right)^{-1}. \tag{2.14}$$

Altogether, for single-point contact we have at our disposal the 14 non-linear equations (2.11), (2.12), and (2.13) in order to express the 14 unknowns $w, \varphi, \eta_j, \eta_j^*, \zeta_j, \zeta_j^*, \gamma_j$ *and* γ_j^* in terms of the lateral displacement of the wheelset v. The usual method to solve this system of equations in the case of single-point contact gives rise to difficulties when the profile combination also admits double-point contact. De Pater [1995b] finds a mathematical procedure to solve the equations for the case of double-point contact; it is based on a method indicated by Seydel [1988].

In order to avoid the problem of double solutions for the geometric output quantities at the double-point contact, this method does not use as the independent variable the lateral displacement of the wheelset, but rather the arc-length of the profiles, and follows their coupling when somewhere penetration (which has no physical meaning) arises.

Figure 2.9 shows the rolling angle φ of the wheelset for the profile combination UIC60 1:40 S1002, as a function of the lateral displacement of the wheelset v obtained by this method. In Figure 2.10 a qualitative explanation of wheel/rail contact is given. In the curve shown in Figure 2.9, there are two turning points, C and D, whereas in the point $B \equiv E$ there is contact in two points (double-point contact); the lateral displacement of the centre of the wheelset decreases rather than increases between points C and D, when the contact point moves continuously along the rail and wheel profile (see Figure 2.10). However, on sections BC, CD, DE, the wheel penetrates into the rail, which is physically impossible; this means that these sections have no physical meaning, and that they must be left out of consideration. At the point $B \equiv E$, the contact point jumps from one position to another.

Because of the assumed symmetry conditions, the results for the left-hand contact point (j=2) can be obtained from those related to the right hand contact point by means of changing the sign of the independent variable v:

$\gamma_2(v) = \gamma_1(-v)$, $\eta_2(v) = \eta_1(-v)$, and so on. (2.15)

Arnold and Frischmuth [1998] propose a regularization method for non-smooth dynamic systems, where the non-smoothness may occur due to the double-point contact situations between rigid rails and rigid wheels. They refer to the applied model as a quasi-elastic contact model, because the corrections can be limited to the order of the elastic deformations. For example, a simple smoothing procedure by solving the geometric contact problem for a number of discrete and equidistant points, and fitting polynomials between these points can be used. In this way double-point contact conditions are transformed to single-point contact situations.

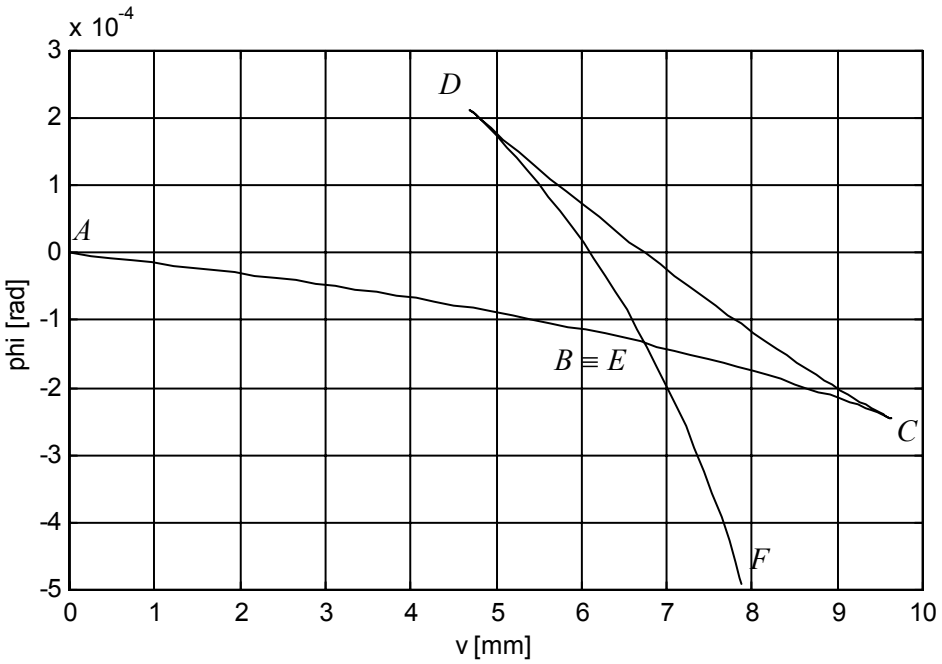

Figure 2.9: Relation between lateral displacement v and roll angle φ.

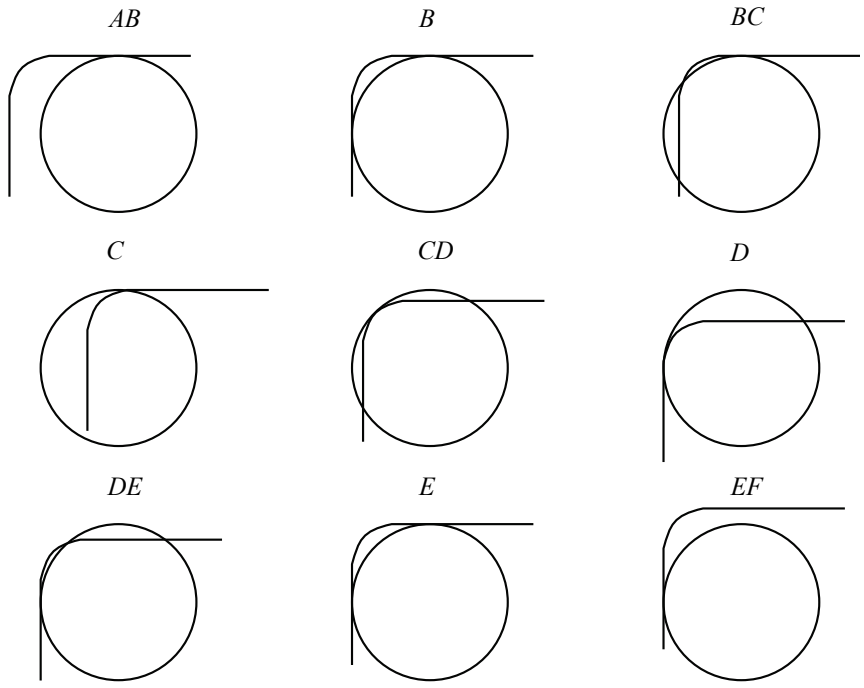

Figure 2.10: Qualitative explanation of rail-wheel contact.

2.3.2 Semi-analytical model

In this chapter, we consider the problem of calculation of wheel contact locus. The semi-analytic model is used for calculation of wheel/rail contact geometry parameters; this model is described in the PhD thesis of Li [2002], and is based on the work of Wang [1984].

Let us assume that the wheelset and the rails are rigid. Due to track constraints, a wheelset has two degrees of freedom (DOF). We do not include wheelset longitudinal displacement and rolling along the track, since these have nothing to do with the wheel/rail geometric constraint problem. Usually, lateral displacement of the wheelset, and wheelset rotation about the vertical axis passing its centre (yaw angle), are taken as the generalized coordinates. This is the so-called 3-D wheel/rail geometric contact problem.

If we do not consider wheelset yaw angle, the number of DOFs is reduced to one, and the problem becomes planar. The wheel/rail geometric parameters become the only functions of the lateral displacement of the wheelset centre.

As mentioned in Section 2.3.1, both the left and right wheel-rail contacts must meet the following conditions:

1. the vertical wheel-rail distance must be zero at contact points, and greater than zero at non-contact points;
2. at a contact point, the normals of the wheel and rail surfaces coincide.

These two conditions are equivalent. The first condition is employed in this thesis, and the second one is used for validation.

Put the wheel profiles $\zeta_j^* = f^*(\eta_j^*)$ in the coordinate system $o^* y^* z^*$ and the rail profiles $\zeta_j = f(\eta_j)$ in the coordinate system oyz, as shown on Figure 2.11. The position of the rails is indicated by dashed lines. For convenience, shift the rails over a distance z_{rs}, downwards (solid lines in Figure 2.11). The above contact point condition now becomes that the minimal vertical distances at the contact points between the left wheel and rail and between the right wheel and rail are equal. The contact points are sought for according to this condition.

Calculate the left and right vertical wheel-rail distances, and find their respective minima $\Delta z_{\min 1}$ and $\Delta z_{\min 2}$, and also store their locations $y_{\min 1}$ and $y_{\min 2}$ as the possible contact points. This process is referred to as search.

If the two points are indeed the left and right contact points, then

$$\Delta z_{\min 1} = \Delta z_{\min 2}. \tag{2.16}$$

If $\Delta z_{\min 1} \neq \Delta z_{\min 2}$, the condition is violated, and the roll angle must be adjusted.

Suppose $\Delta z_{\min 1} > \Delta z_{\min 2}$, then the wheelset must be rotated anti-clockwise over an angle

$$\Delta\varphi = \frac{\Delta z_{\min 1} - \Delta z_{\min 2}}{y_{\min 2} - y_{\min 1}}. \tag{2.17}$$

After the rotation, the search is repeated, to check with the new wheelset orientation, whether the minimal left and right wheel-rail vertical distances are equal. Actually here 'equal' is in the sense of a small tolerance ε. In other words the termination criterion for the iteration is

$$\left|\Delta z_{\min 1} - \Delta z_{\min 2}\right| < \varepsilon. \tag{2.18}$$

$\varepsilon = 10^{-3} \sim 10^{-4}$ mm is small enough for engineering calculation.

The locations where the minimal vertical wheel–rail distances on both sides are found in the last iteration are the contact points, and the roll angle is

$$\varphi = \varphi_0 + \sum_{i=1}^{k} \Delta\varphi_i \,, \tag{2.19}$$

where k is the number of iterations and φ_0 is the initial roll angle.

The other wheel-rail contact geometry parameters can now be calculated in the same way as was discussed in Section 2.3.1.

Figure 2.12 shows the flow chart of the search for the wheel/rail contact locus.

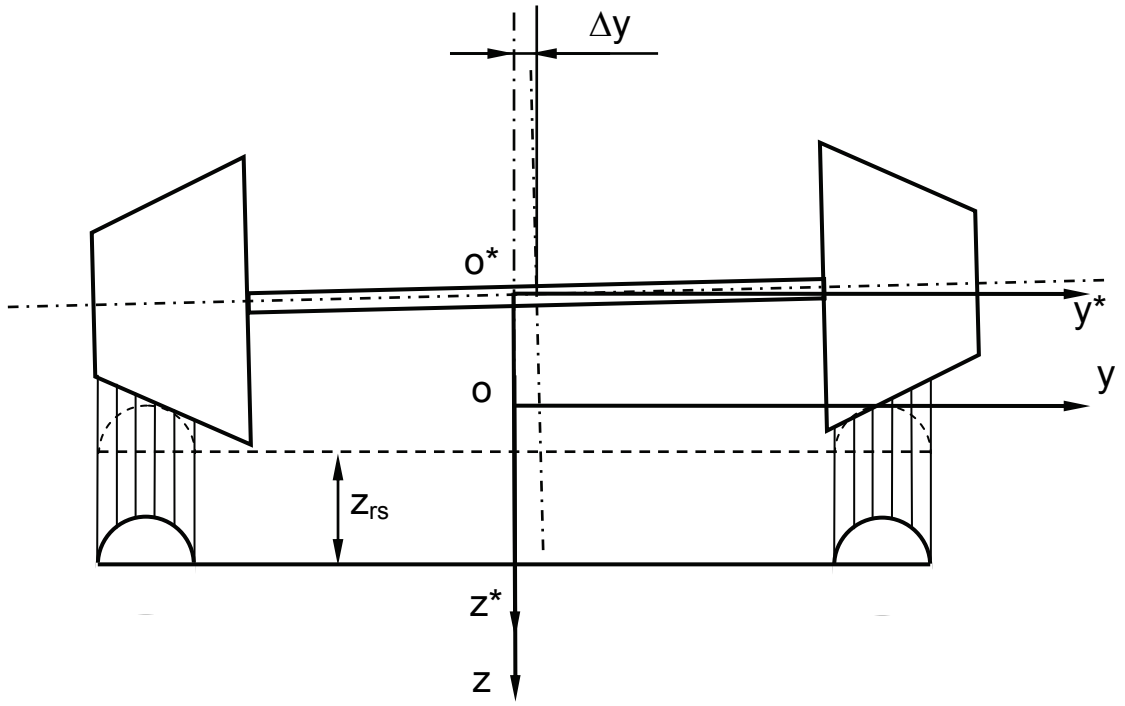

Figure 2.11: Wheelset and track coordinate systems.

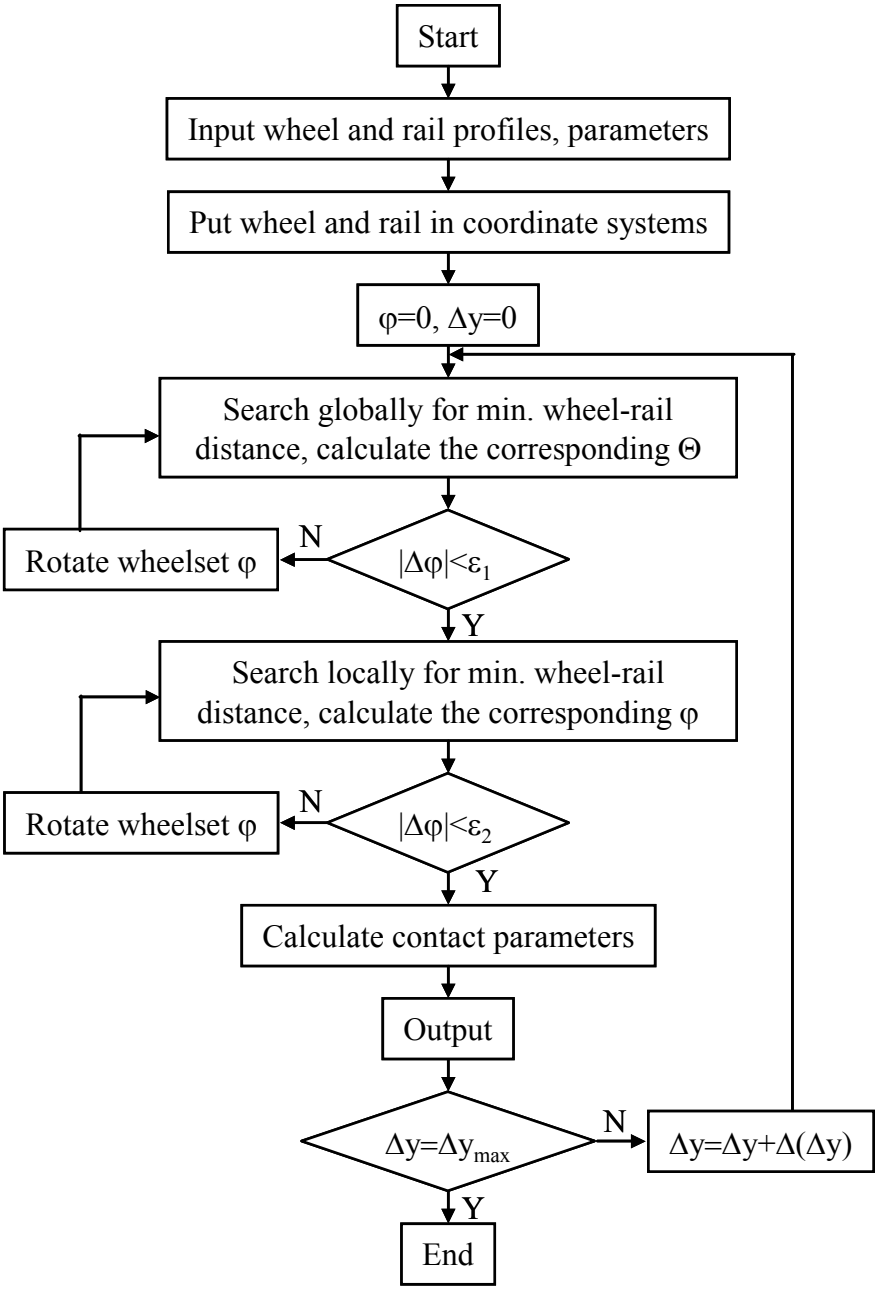

Figure 2.12: Flow chart of the search for wheel/rail contact locus.

2.3.3 Program for calculation of geometric contact

On the basis of the theory of the calculation of the wheel–rail contact locus, described in the previous sections, a computer program for calculation of wheel/rail contact locus and its parameters is created. The program is written in computer language MATLAB.

When we consider real profiles, we deal with measured data, which is represented by the lateral and vertical coordinates of the points along the wheel and rail profiles in their local coordinate systems. In the program, the points of the wheel and rail profiles are connected by piecewise cubic Hermite interpolating polynomial.

In the files pfr_uic60.mat, pfw_s1002.mat and others, we dispose of the data for the vertical and lateral coordinates of the rail and wheel profiles saved in the binary form; then we find results for the following real profiles:

rail:

UIC60 1:40 (pfr_uic60.mat),

UIC60 1:20 (pfr_uic6020.mat),

wheel:

S1002 (pfw_s1002.mat),

Conical wheel (pfw_st.mat).

Profiles can be created from the text file, which consists of two columns with vertical and lateral coordinates of the desired profile. Examples of these coordinates can be found in file xys1002.txt. The user has the option to choose between existing profiles from the database or a new profile described by coordinates. Profiles from the database are ready for calculation after loading. For new profiles, the file with coordinates must be loaded into the program; coordinates must be processed and saved as a binary file with the name pfw_"file name of data file".mat, for example pfw_xys1002.mat. This profile will then be available in the database menu. Simultaneously, the plot of the profile appears on the screen.

Users can view the wheel or rail profile itself and its geometric properties, such as first derivative, conicity angle, and curvature, as functions of the lateral coordinate of the profile. In Figure 2.13 and Figure 2.14 the geometric properties of the rail profile UIC 60 with inclination 1:40 and wheel profile S1002 are presented correspondently. Note that in the local coordinate system of the right-hand rail, the y axis points to the field side of the track, and the z axis has its positive sense upwards; the same holds for the local coordinate system of the right-hand wheel. It is different from the local system used in the program and is introduced only for user convenience.

For all the possible profile combinations, the distance between the inside surface of the wheels is equal to 1360 mm, the track gauge is equal to the default value 1435 mm, and the wheel radius is equal to 500 mm. These values are defined in the file scinit.m and can be varied by the user.

In order to find the points of the rail used to measure the track gauge, we consider the top level of the rails, then determine the points of the rail profile that are 14 mm below that level on the side of the centre of the track; the track gauge is defined as the distance between these two points (see Figure 2.2). The default value of 14 mm can be changed by the user if necessary. In file scgauge2.m the value of hgauge must be set to the required value.

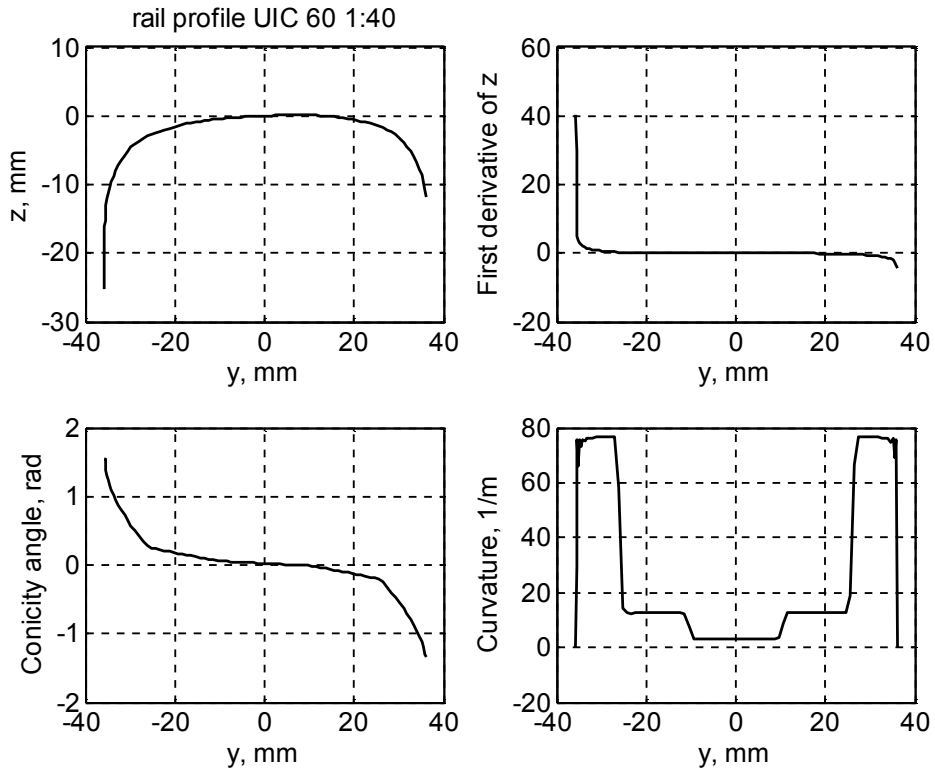

Figure 2.13: Parameters of rail profile UIC 60 with inclination 1:40.

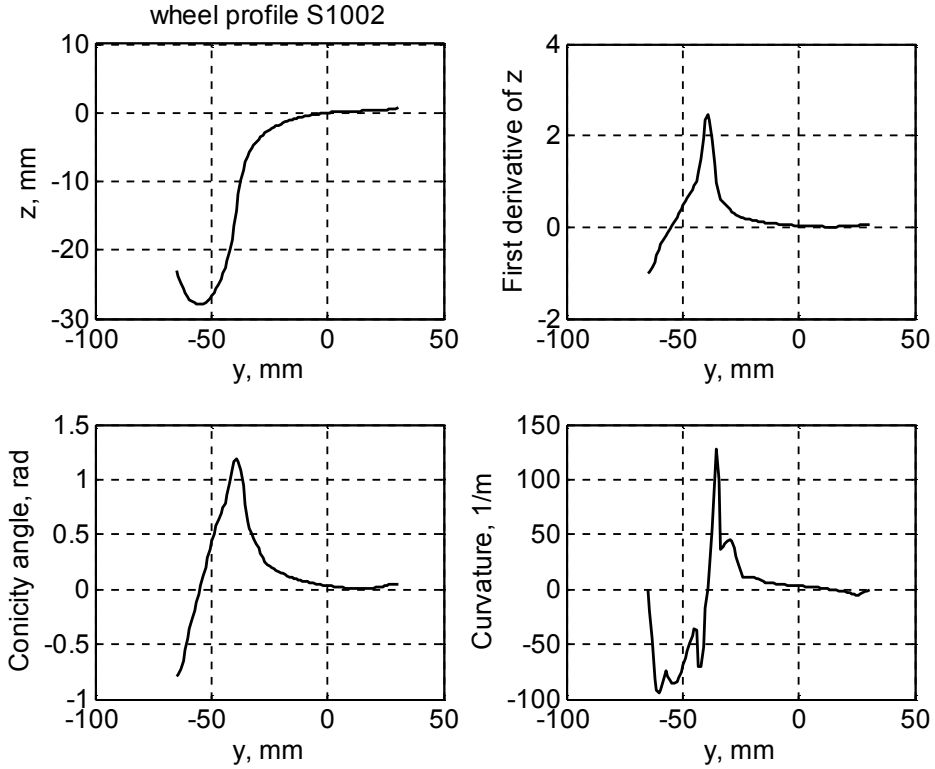

Figure 2.14: Parameters of wheel profile S1002.

In the MATLAB program called main_frame.m, in function "Calculate_Callback", we make use of the mathematical methods described in the Section 2.3.2 to solve for the geometric contact problem. For scaling purposes, we introduce the quantity $y_{\max}$, which represents the largest value of the lateral displacement in the calculations. When a user chooses menu "Calculate", he/she will be prompted for the value $y_{\max}$. By default, this value is equal to 30 mm, which is usually enough to obtain top flange contact. After the calculation is performed, results are saved in a file with the name mg_"wheelname"_"railname".txt. Users may load any existing results file to view the geometric contact parameters; corresponding wheel and rail profiles are loaded automatically.

After the calculation is performed, or the results file is loaded, it is possible to view the results of calculations in several modes. Users can choose "Static view" or "Dynamic view"; these are described below.

In "Static view" there are two modes: "Short static view" and "Full static view". Results from "Full static view" are presented in Figure 2.15a-d. In "Short static view" only Figure 2.15a and Figure 2.15d are shown. In Figure 2.15a-c the diagrams of

a) φ (wheelset roll angle), w (wheelset vertical displacement), $\gamma_1 - \gamma_2$ (contact angle difference), $\zeta_1^* - \zeta_2^*$ (rolling radii difference);

b) η_1 (y rail), η_1^* (y wheel), ζ_1 (z rail), ζ_1^* (z wheel); and

c) $\kappa_{y1} = 1/r_{y1}$ (rail curvature), $\kappa_{y1}^* = 1/r_{y1}^*$ (wheel curvature), γ_1 (rail contact angle) and γ_1^* (wheel contact angle)

are shown as functions of v, in the case of wheel profile S1002 combined with rail profile UIC60 inclined 1:40. In Figure 2.15d the function of lateral wheelset displacement as a function of wheel and rail lateral coordinates is shown, respectively, above the wheel and rail profiles. Choosing the value of the lateral wheelset displacement and making a vertical projection on the profile plot, one can find the position of the contact point on the profile. Please, pay attention, that z-values are plotted with negative value to show graphs in convenient perception.

An example of "Dynamic view" is presented in Figure 2.16 for the case of 6 mm of lateral displacement of the wheelset. Users can employ the slider or enter the value of the lateral displacement of the wheelset to view the position of the contact points on the left and right wheels and rails. Corresponding values of the rolling radii difference are shown below the profiles plots.

Using the program prof_cont2.m, users can view the location of contact points between wheel and rail for various calculated values of lateral displacement. Examples of contact between wheel S1002 and rail UIC 60 with inclination 1:40 are presented in Figure 2.17. The lines between the wheel and the rail profiles connect the corresponding contact points, and the values of corresponding lateral displacements of the wheelset are shown above the wheel profile. The wheel profile is lifted over the rail on 10 mm. The rail profile is arranged in its real position, the coordinate system used in this figure is the wheelset coordinate system (see Figure 2.11) with the origin in the centre of the wheelset when it placed in the neutral position. Please, pay attention, that z-values are plotted with negative value to show graphs in convenient perception.

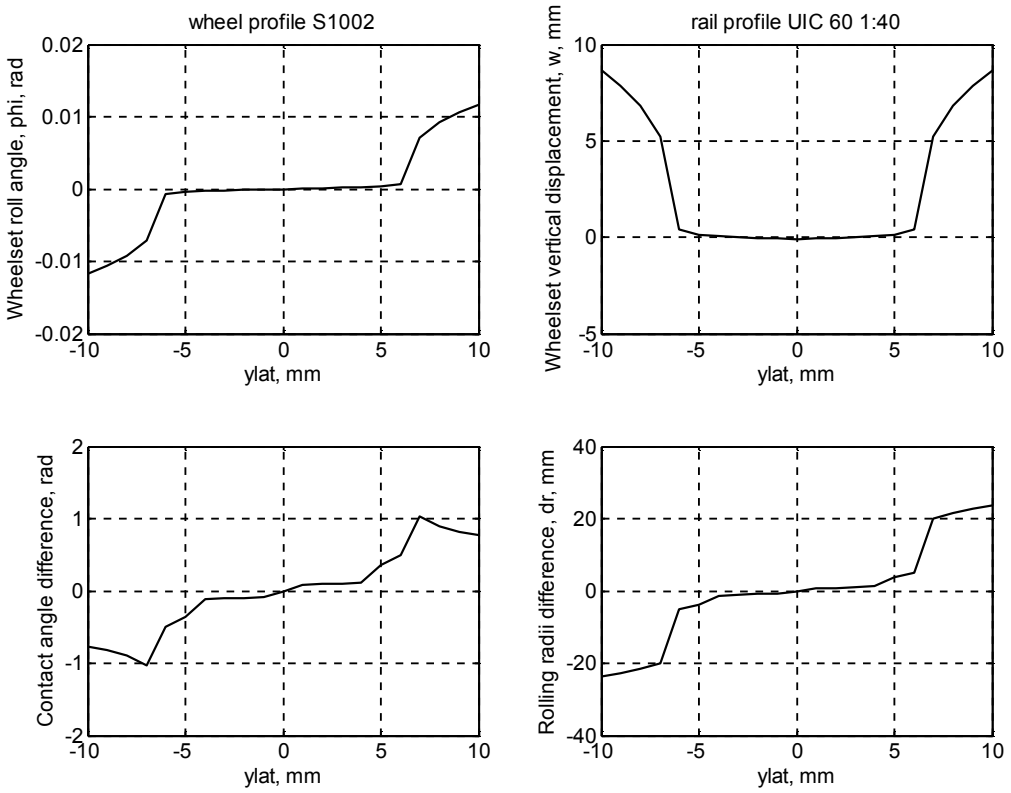

Figure 2.15a: Geometric contact characteristics for the combination of UIC60 1:40 and S1002.

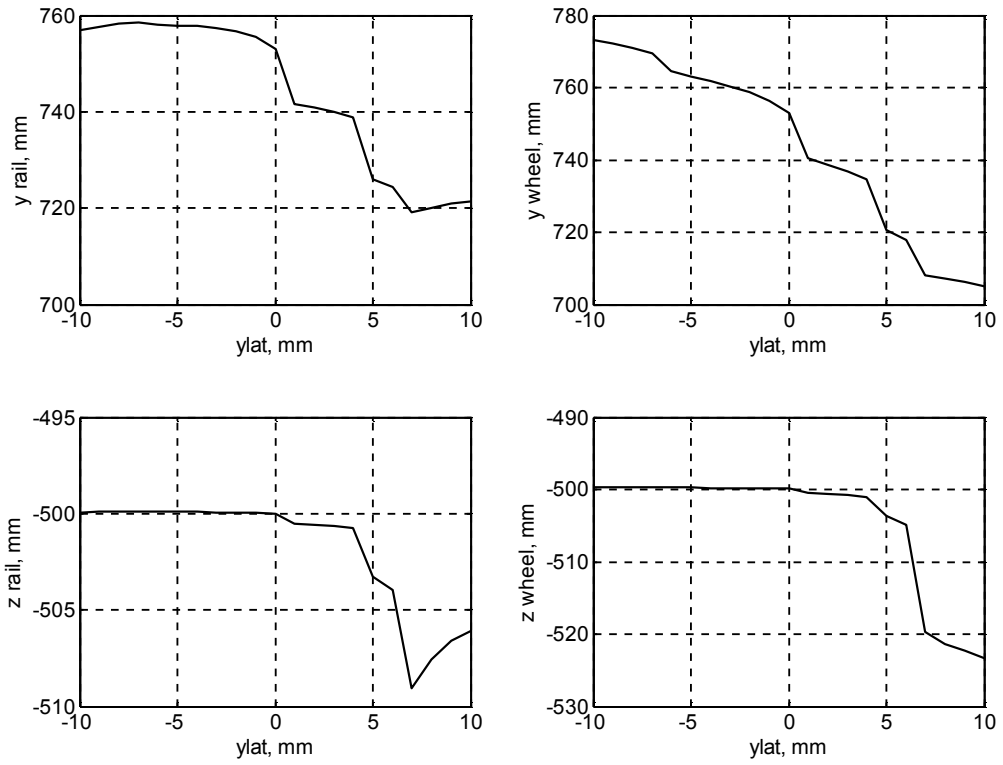

Figure 2.15b: Geometric contact characteristics for the combination of UIC60 1:40 and S1002.

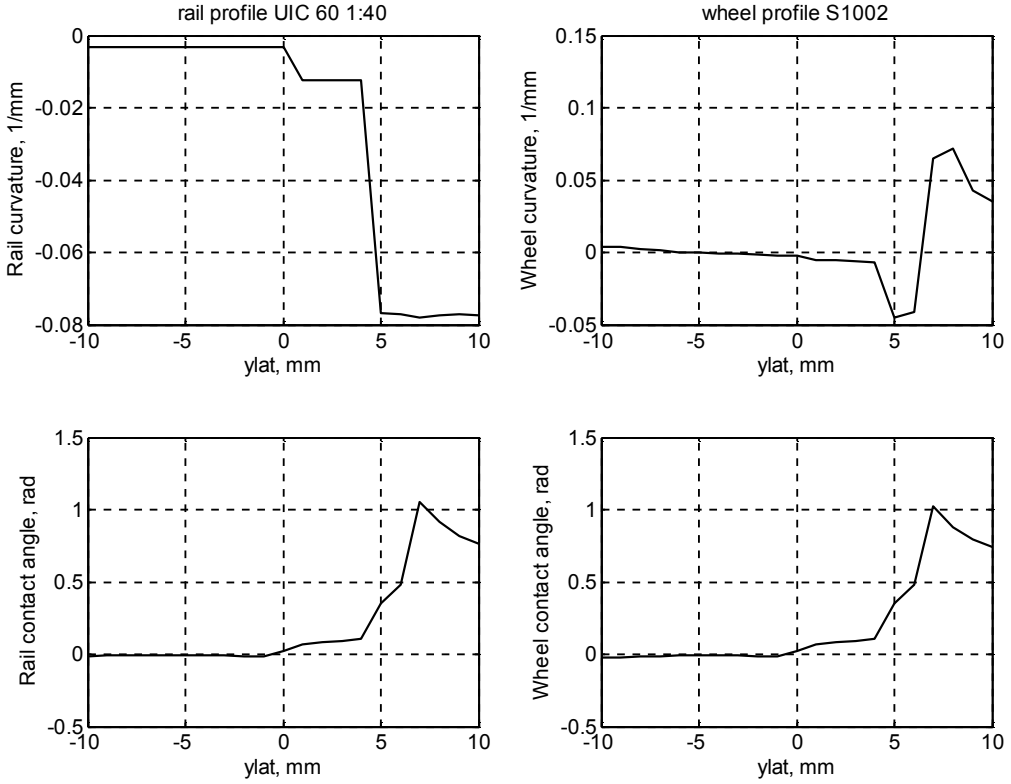

Figure 2.15c: Geometric contact characteristics for the combination of UIC60 1:40 and S1002.

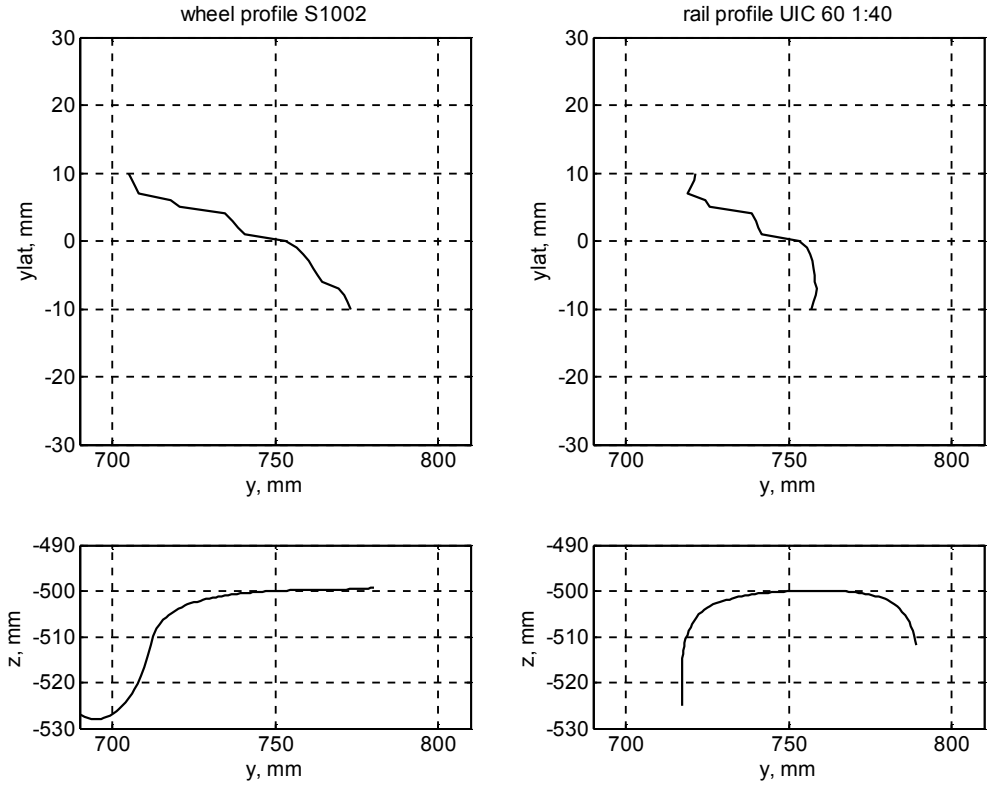

Figure 2.15d: Geometric contact characteristics for the combination of UIC60 1:40 and S1002.

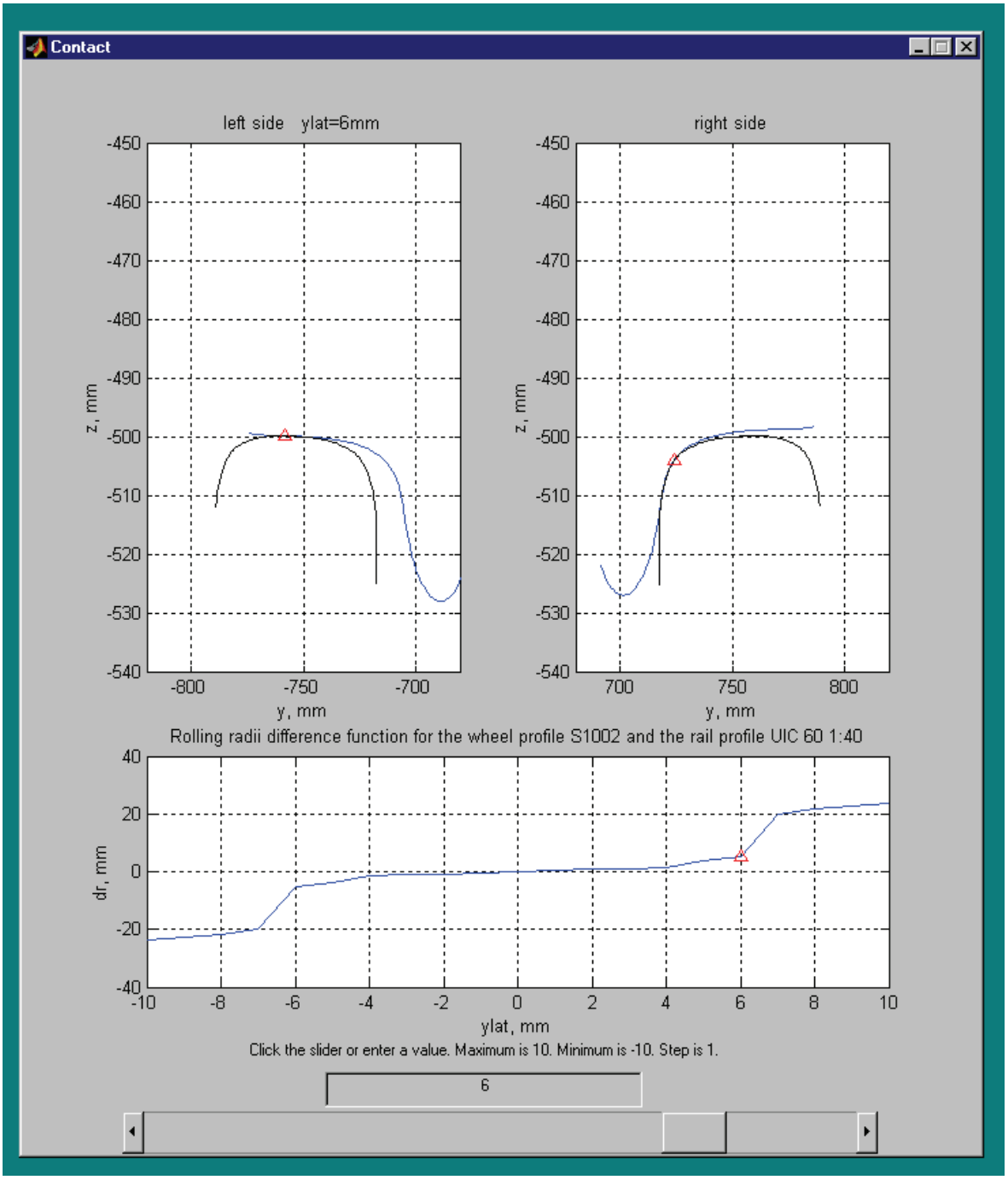

Figure 2.16: Example of "Dynamic view" of the contact between S1002 wheel and UIC 60 rail with inclination 1:40.

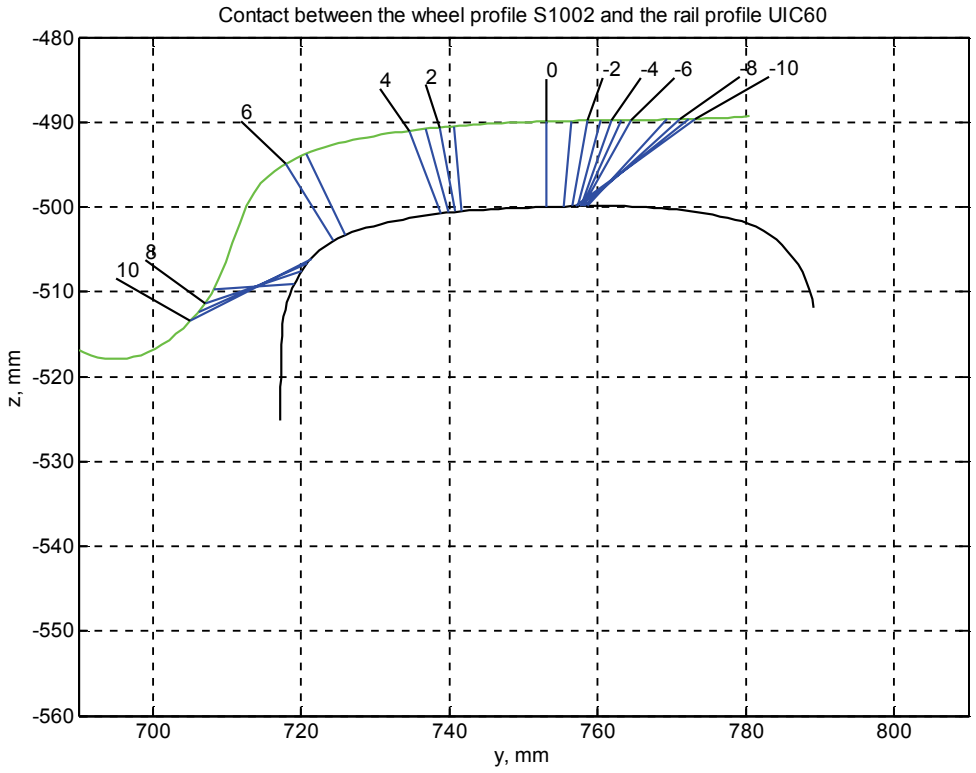

Figure 2.17: Position of the contact points on wheel S1002 and rail UIC 60 with inclination 1:40.

2.4 Analysis of geometric wheel/rail contact

In general, analysis of wheel/rail contact is performed to study the effects of wheel/rail interaction on vehicle performance or wheel/rail wear. Depending on the objectives, the analysis can be geometric, static, or dynamic.

Geometric analysis concerns only wheel and rail shapes and their relative positions, without regard to the vehicle or its motion. The results from geometric analysis are parameters of wheel/rail contact constraints. Static analysis gives normal contact stress under a specified loading condition. Dynamic assessment is usually performed using vehicle simulation software, which provides detailed information on vehicle dynamics and wheel/rail interaction, including normal forces, tangential forces, creepages, displacements, velocities, accelerations, and other dynamic parameters for wheel and rail contact patches. Contact parameters resulting from dynamic assessment are related not only to wheel/rail shapes and relative positions, but are also influenced by speed, vehicle/bogie characteristics, and track geometry.

In geometric wheel/rail contact software, any possible combination of wheel and rail profile contact situations can be analysed for many wheelsets against a measured pair of rails, or many rails against a measured pair of wheels. This method provides a comprehensive view of wheel/rail contact at a system level. For example, thousands of wheels with different profiles (due to different levels of wear or resulting from different truck performance) could contact a section of rail at different positions and, therefore, could produce different contact patterns and different levels of contact stress. The performance of the majority of wheel/rail pairs is therefore the focus of the assessment.

The distribution of contact parameters can be used to predict likely vehicle performance, wheel/rail wear, and contact fatigue. For example, consider a group of measured wheels

contacting a pair of rails measured on a curve. If the rails are judged to have unsuitable profiles due to resulting high contact stress and undesirable contact patterns, then appropriate action can be taken. If only a small number of wheels display unwanted wheel/rail interaction, then it might be best to remove such wheels from service. Alternatively, if many wheels cause problems, then it might be best to re-profile the rail by grinding.

2.4.1 Overview of wheel/rail contact types

2.4.1.1 Types of wheel and rail profiles

As mentioned in Section 1.1, at the present time, railways commonly use curvilinear wheel profiles as the standard wheel profile. However, until several decades ago, a conical wheel profile was widely used. In Figure 2.18, the unworn curvilinear S1002 wheel profile, and the unworn conical wheel profile are shown. Both profiles are aligned to cross the horizontal axis at the coordinate 70 mm (wheel tape line). It is clearly seen that the shapes of these two profiles are significantly different at the tread and flange root areas. Conical profiles have a straight tread, whereas the tread of the S1002 wheel profile has variable curvature. The radius of flange root of the conical profile is smaller in comparison to the radius of flange root of the S1002 wheel profile. Remarkably, flanges on the S1002 and conical profiles have the same shape. This is explained by the fact that wheel flange must provide sufficient safety against derailment (also see Section 4.5.2, where the phenomenon of derailment is described). Safety requirements are the same for different wheel profiles, which leads to the same flange shape.

Wheel profiles can differ on many parameters, depending on the requirements imposed by the rolling stock on which they are used. For example, tram wheels usually have shorter flange height, thinner flange width, and shorter wheel tread.

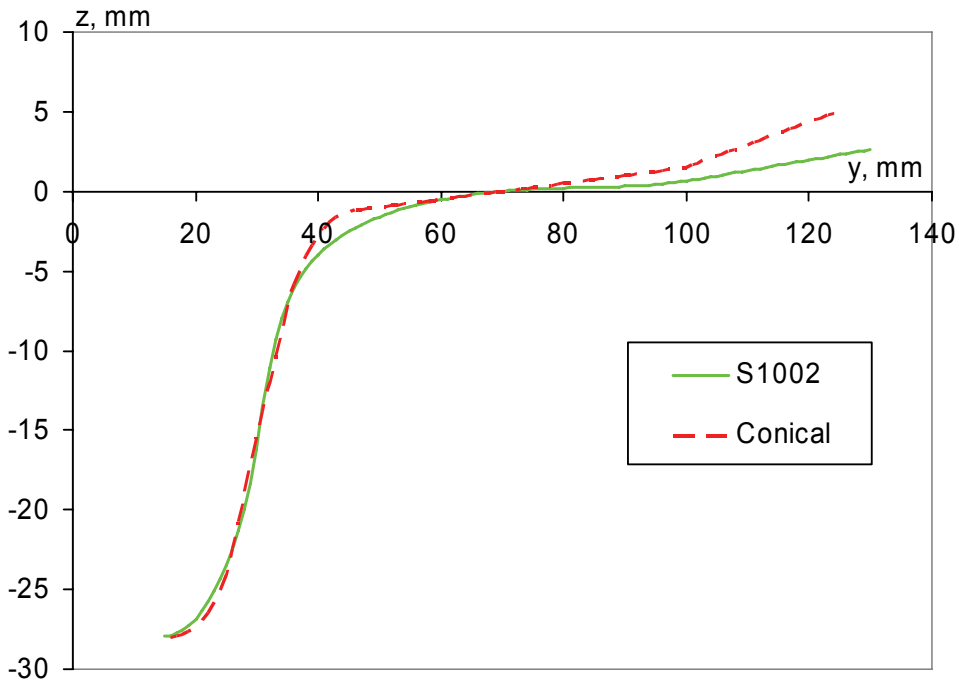

Figure 2.18: S1002 and Conical wheel profiles.

While the number of standard wheel profiles is limited to one or two profiles per railway company or network, the number of the standard rail profiles is usually larger. This is a consequence of the use of rails of different weight per meter for the different types of lines.

The sizes of the rail heads differ in accordance with the weight of the rails and consequently rail profiles are different. Also, inclination of the rails plays a significant role in the actual shape of the rail profile. For example, currently Dutch railways use the UIC54 rail profile inclined 1:40, while previously the NP46 rail with a cant of 1:20 was used in this rail network. These profiles are shown in Figure 2.19. It should be noted that the UIC54 rail is shown with an inclination of 1:40, whereas NP46 rail is shown inclined 1:20. There is a significant difference between these two profiles (Figure 2.19a), which becomes noticeable when the top of the rails is shown zoomed in, as in Figure 2.19b. This difference, mainly the result of the differing rail inclinations, can be responsible for substantial changes in wheel/rail contact, and consequently in differing wear and rolling contact fatigue behaviour for wheels and rails.

In addition to the rail types used on a main line, many tram or light rail companies widely use grooved rails, where wheel flange contact can occur not only on the field side of the wheel flange, but also on the inner side of the wheel flange. Contact with a grooved rail, together with wheel/rail contact in switches and crossings, presents additional complication in the analysis of contact between wheel and rail.

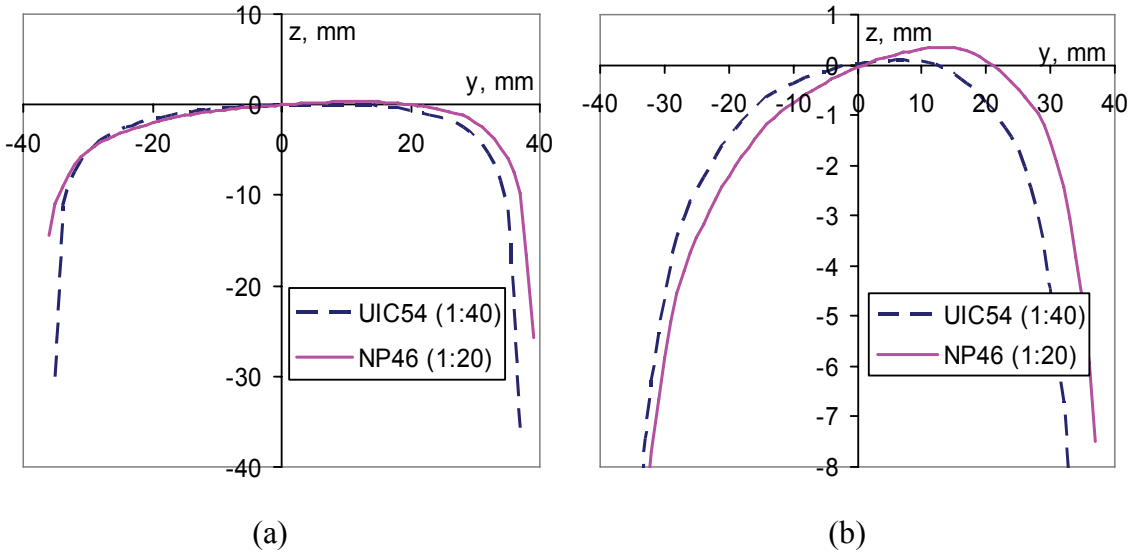

(a) (b)

Figure 2.19: Comparison of the rails: UIC54 inclined 1:40 and NP46 inclined 1:20. a) not zoomed; b) zoomed in.

2.4.1.2 Types of wheel/rail contact

As shown in Figure 2.20, in the general case for unworn wheel and rail profiles, four types of wheel/rail contact can take place:

1. wheel tread–rail head contact,
2. wheel flange root–rail gauge corner,
3. wheel flange–rail gauge corner, and
4. wheel field part of the tread–rail field side.

The first type of contact occurs mainly on straight track and in large radius curves; the second type of contact occurs in curves, and the thrird type of contact (flange contact) occurs only in sharp curves, or when the wheel attempts to roll over the rail head. The fourth type of contact occurs when the wheelset is shifting toward the one side of the track rail, introducing flange root or flange contact of the wheel on that side, simultaneously the wheel on the opposite side will experience contact on the field side of the tread.

One or two contact points can exist between wheel and rail along with conformal contact. Let us consider contact between wheel flange root and rail gauge corner, as shown in Figure 2.21. If the wheel flange root radius is larger than the gauge corner radius of the rail, then single point contact between wheel and rail will occur. If the radii of the circular arcs of the flange root and the gauge corner are identical, then conformal flange root–gauge corner contact can occur. In the case where wheel flange root radius is smaller than rail gauge root radius, double point contact will occur. In general, the same is valid for the wheel tread and rail head curvatures, i.e., to achieve a single point contact between wheel tread and rail head, the curvature of the rail head must be larger than the curvature of the wheel tread.

Single-point, double-point, and conformal types of wheel/rail contact have significant influence on rolling contact behaviour. Depending on the targets and requirements in wheel and rail profile design, one or another type of contact can be either desirable or unwanted. This will be discussed in detail in Chapter 6.

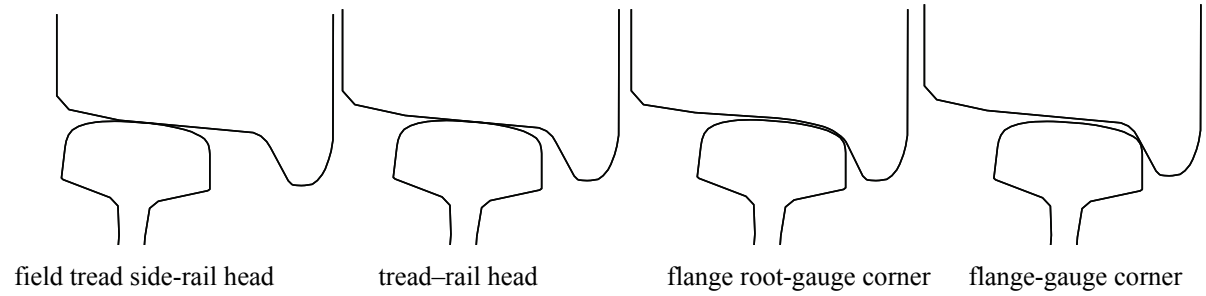

Figure 2.20: Types of contact between wheel and rail profiles.

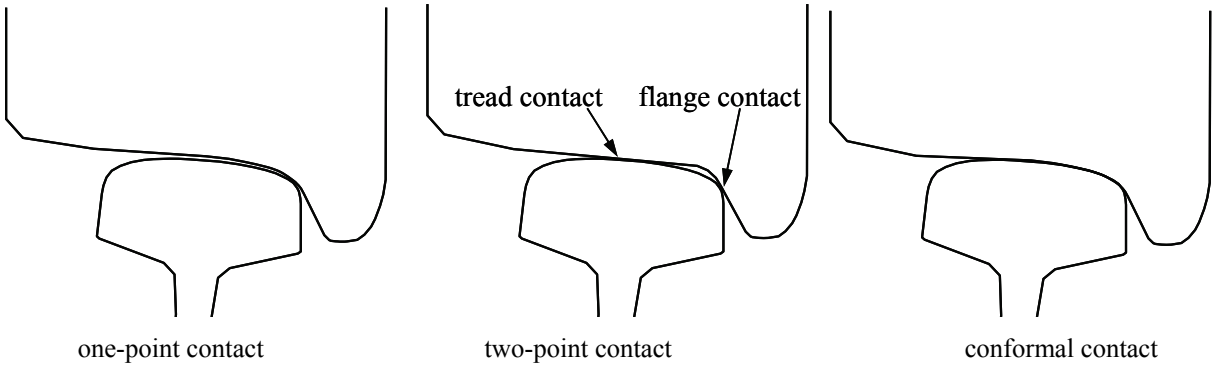

Figure 2.21: One and two point contact between wheel flange root and rail gauge corner.

2.4.2 Properties of geometric wheel/rail contact

As shown in Section 2.3.3, analysis of geometric wheel/rail contact can provide researchers with a number of parameters describing wheel/rail interface. In the present section, focus is made on the rolling radii difference function, and its relation with wheel and rail profiles.

2.4.2.1 Three main parts of RRD function and their relation to wheel/rail contact

Wheel and rail contact can be roughly divided into three parts corresponding to track curvature:

- Straight track: Contact occurs between the central region of the rail head and wheel tread for both sides

- Large radius curves: Contact occurs between tread and flange root parts of the wheel and gauge side of the rail head. Wheel flange contact is rare. On the opposite side of the track, contact is moving to the field side of the wheel and rail
- Small radius curves: Contact occurs between the wheel flange root and flange, and the gauge corner of the rail. On the opposite side of the track, the field side of the wheel contacts with the field side of the rail.

To illustrate this, the wheel/rail contact points of a new (unworn) wheel profile S1002 with an unworn UIC54 rail inclined 1:40 are shown in Figure 2.22. In this figure the lines between the wheel and rail profiles connect the corresponding contact points, which were calculated for each 0.5 mm of lateral wheelset displacement. Lateral wheelset displacements are shown above the wheel profile. The coordinate system in this figure is the wheelset coordinate system $y_w O z_w$ (see Figure 2.11), with the origin in the centre of the wheelset in neutral position. It should be noted that in this figure the wheel is shifted 10 mm vertically. Please, pay attention, that z -values are plotted with negative value to show graphs in convenient perception.

The rolling radii difference versus lateral displacement of the wheelset for S1002 wheel and UIC54 rail profiles is shown in Figure 2.23. By comparing Figure 2.22 and Figure 2.23, one can find direct correlation between a discontinuity (a jump) in the position of the contact point between wheel and rail after 6, 4, and -0.5 mm of lateral displacement, see Figure 2.22. These discontinuities can be found directly in the rolling radii difference function. For 4 mm of lateral displacement, one can see a sharp increase in RRD, and for 6 mm of lateral displacement, the increase in RRD is even sharper. For the jump of contact point after -0.5 mm of lateral displacement, the changes in the RRD function are less visible, due to smaller changes; however, one can find variation in the tangent to the RRD function around ± 0.5 mm of lateral displacement.

The wheel/rail combination S1002-UIC54 clearly indicates four areas of the contact. Starting from the field side, one can see contact between wheel tread and rail head top part. Such contact occurs when the wheelset is moving toward the opposite rail. Next, contact between wheel tread (closer to the flange root side) and the rail central region occurs for 0-4 mm of lateral displacement. This typically corresponds to the motion of a wheelset on a straight track, and in large radius curves (in this particular case curves larger than R=500 m, see Table 2.1 for r=0.460 m). Further, for 4.5–6 mm of lateral displacement, contact occurs between the wheel flange root and the rail gauge corner parts, corresponding to wheel/rail contact in smaller radius curves (smaller than R=500 m). Finally, for displacements larger than 6 mm, contact between wheel flange and rail gauge occurs.

The RRD function can provide significant information about wheel/rail contact properties. Undoubtedly, its shape and behaviour are dependent on wheel radius, track and wheelset inner gauges and, of course, on wheel and rail shapes. A brief description of the dependence of the RRD function on the shape of the wheel profile is provided in the next section.

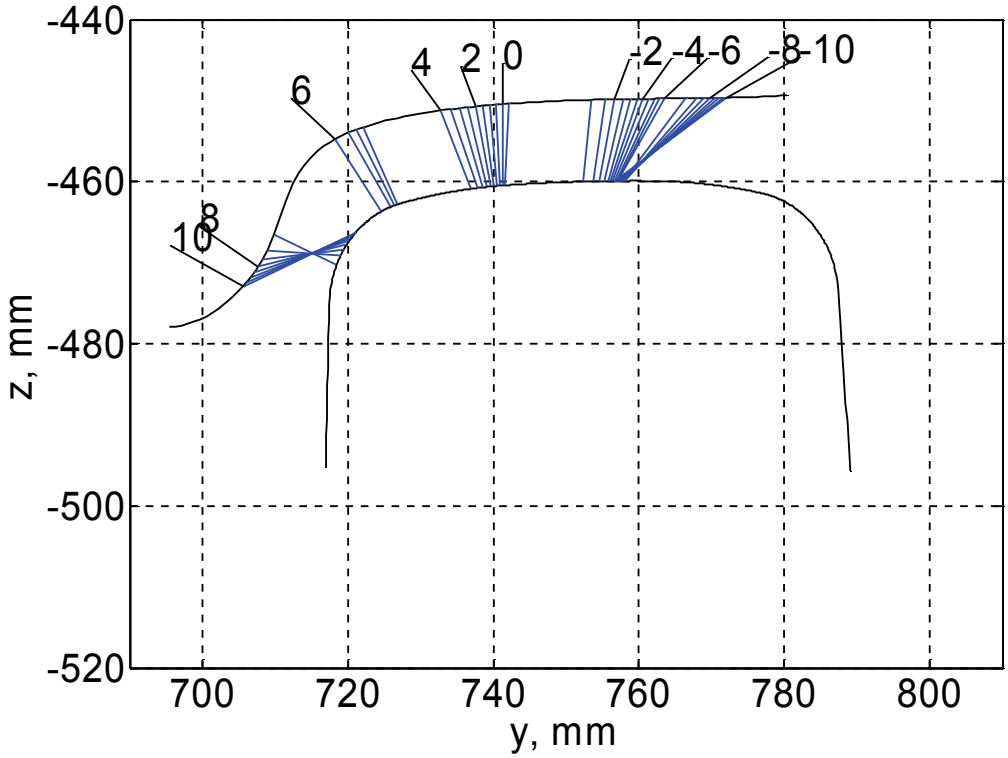

Figure 2.22: Contact points of S1002 wheel on UIC54 (1:40) rail.

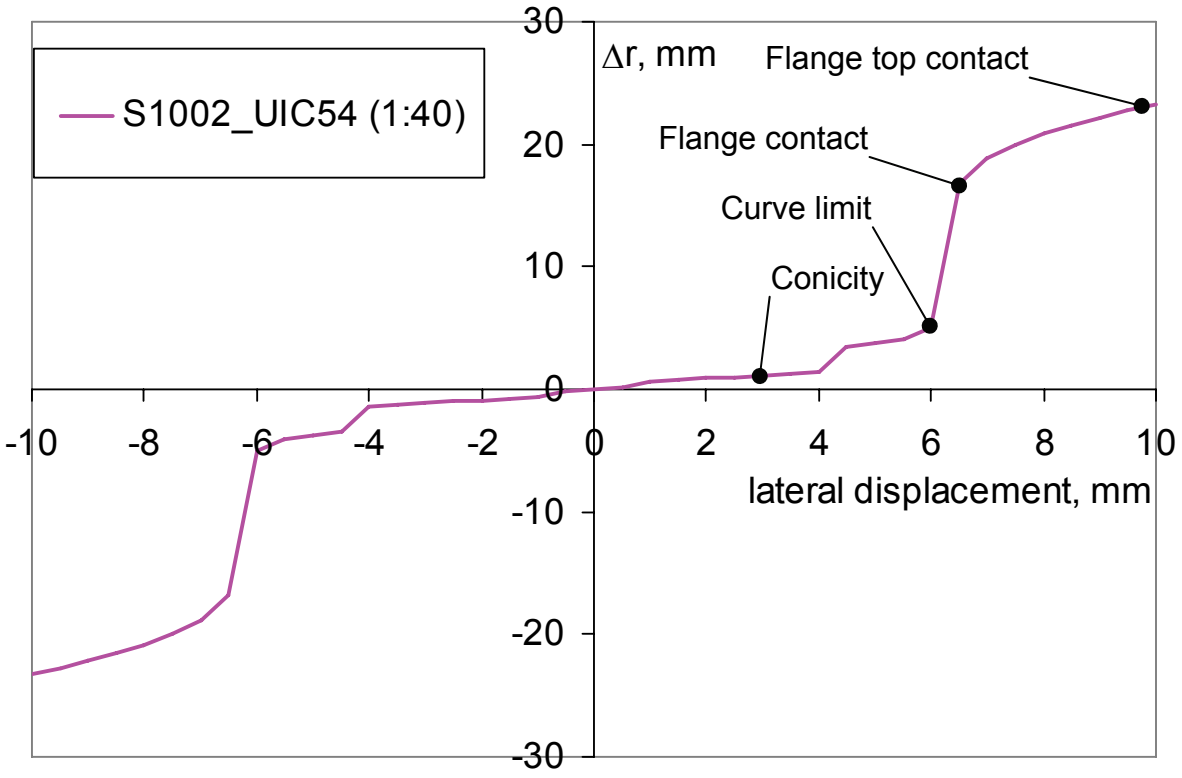

Figure 2.23: RRD function of S1002 wheel on UIC54 (1:40) rail.

2.4.2.2 Dependence of RRD function properties on wheel profile

Let us consider geometric contact of Conical and S1002 wheel profiles (see Figure 2.18) with UIC54 (1:40) and NP46 (1:20) rail profiles (see Figure 2.19). The wheel/rail contact points for the Conical wheel profile with the UIC54 and NP46 rails, respectively, are shown in Figure 2.24a and Figure 2.24b. The wheel/rail contact points for S1002 wheel profile with UIC54 and NP46 rails, respectively, are shown in Figure 2.25a and Figure 2.25b. Contact behaviour of the conical wheel profile is similar on both rails. Wheel tread–top rail contact exists up to 5 mm of wheelset lateral displacement. After 5 mm of lateral displacement, the contact point jumps to the wheel flange–rail gauge corner. This produces a clear double-point contact situation between wheel tread–rail head and wheel flange–rail gauge corner typical for conical wheel profiles, as shown in Figure 2.26. By comparing Figure 2.25a and Figure 2.25b corresponding to the S1002 wheel profile, one can observe a discontinuity (a large jump) in the position of the contact point on the NP46 rail around 6 mm of lateral displacement. This displacement typically corresponds to the motion of a wheelset on a curved track. However, as shown in Figure 2.27b, the S1002 wheel profile on NP46 rail during curve negotiation produces conformal contact, rather than double point contact. Both double point and conformal contact situations can produce a high wear rate. On the other hand the wheel/rail combination S1002/UIC54 has more uniformly distributed contact points on a straight track and in curves, as shown in Figure 2.25a. This wheel/rail combination produces a single contact point between flange root–rail gauge corner, as shown in Figure 2.27a. As a result, the wear rate of the S1002 wheels on the UIC54 rails is much lower. However, as will be shown later, such contact can lead to RCF problems.

As was mentioned earlier, rolling radius difference plays an important role in vehicle dynamics and is therefore investigated next. The RRD functions of the Conical and S1002 wheel profiles on, respectively, the UIC54 and NP46 rails are shown in Figure 2.28. This figure reveals that the Conical wheel profile has practically the same RRD function on both rail profiles. This is one of the significant properties of the conical profiles – equivalent conicity of the wheelset does not vary with lateral displacement of the wheels. The S1002/UIC54 wheel/rail combination has much higher inclination of RRD function compared to the S1002/NP46 combination (and the Conical profile as well), which means that the corresponding equivalent conicity (2.4) is higher for the UIC54 than for the NP46 rail. The higher conicity allows a vehicle to pass curves at the required RRD. However, due to stiff primary suspension, a hunting problem does not occur with the S1002/UIC54 wheel/rail profile combination at the operational speed.

As can be seen from Figure 2.28, both wheel and rail profiles define the shape of the RRD function. They are responsible for the absence or presence of the jumps of contact points and consequently for the absence or presence of sharp bends in the corresponding RRD function. Also wheel and rail profiles define tangent (or equivalent conicity) of the RRD function. For non-linear wheel profiles, conicity can be influenced by other parameters. These other parameters, namely wheel radius, track gauge, and wheelset inner gauge, define the distortion of the RRD function. Decrease or increase in wheel radius is responsible for corresponding stretching or shrinking of the RRD function in the vertical direction. Increase in track gauge (and/or decrease of wheelset inner gauge) leads to stretching of the RRD function in the lateral direction. And vice versa, decrease of the track gauge (and/or increase of the wheelset inner gauge) leads to shrinking of the RRD function in the lateral direction. Examples of these phenomena are examined in the reports of Esveld, Markine and Shevtsov [2003, 2005].

Nevertheless, even though the conical wheel is an obsolete, it has some important properties. For example, its equivalent conicity is independent of track or wheelset gauges (within

wheelset lateral free play limits). This means that vehicles with such wheels are less prone to instability problems due to narrower track gauge. Curvilinear profiles are more sensitive to track gauge variation, and therefore require smaller tolerances for track gauge variation. In the author's opinion, this is one of the reasons why conical wheel profiles have only recently been replaced by curvilinear profiles.

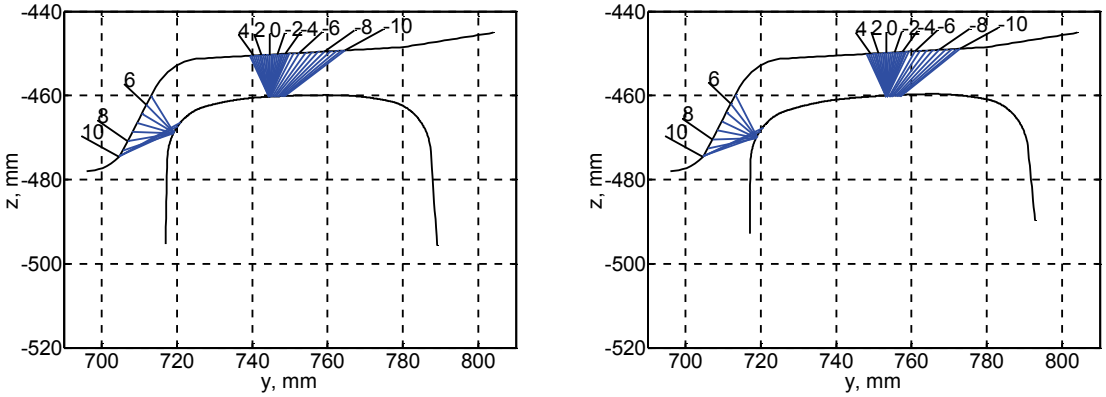

(a) (b)

Figure 2.24: Contact points of Conical wheel on UIC54 (1:40) rail (a) and NP46 (1:20) rail (b).

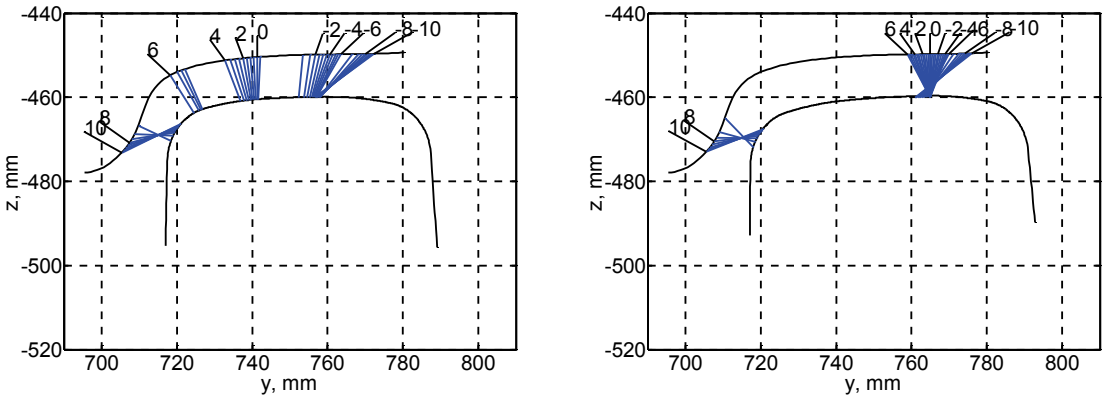

(a) (b)

Figure 2.25: Contact points of S1002 wheel on UIC54 (1:40) rail (a) and NP46 (1:20) rail (b).

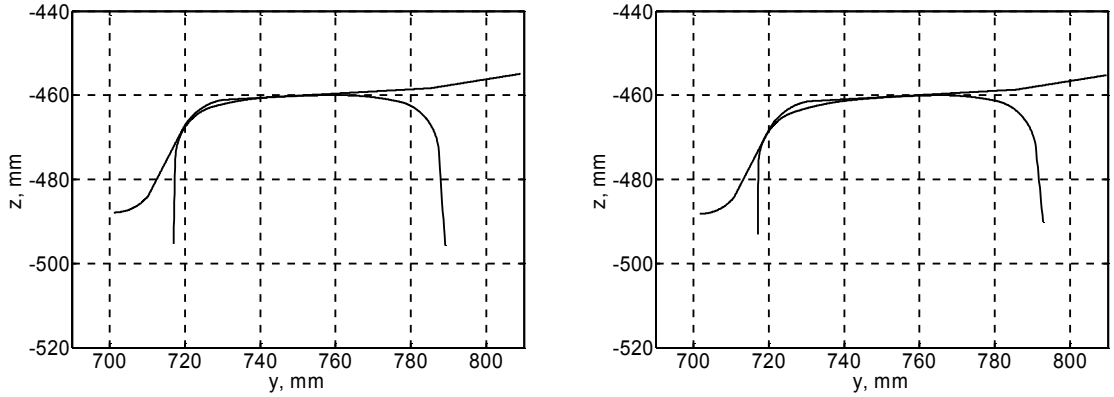

(a) (b)

Figure 2.26: Double point contact of Conical wheel on UIC54 (1:40) rail (a) and on NP46 (1:20) rail (b). Wheelset has positive lateral displacement.

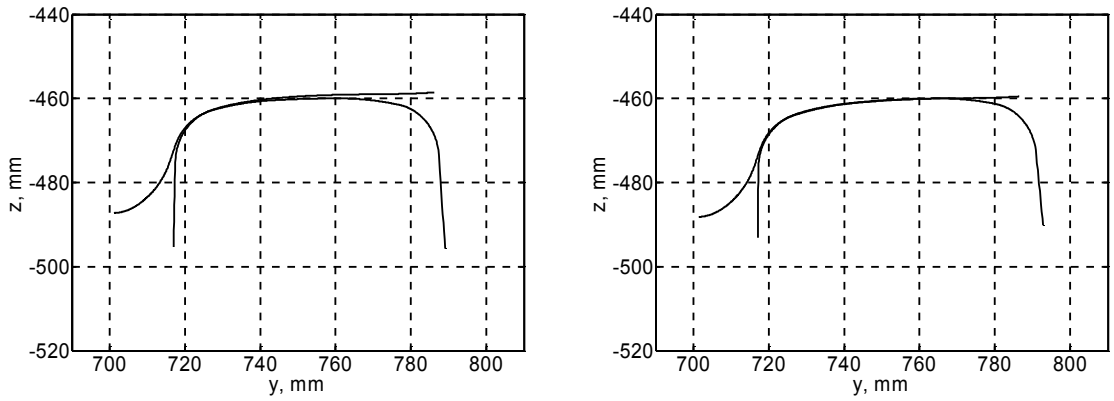

Figure 2.27: Single point contact of S1002 wheel on UIC54 (1:40) rail (a) and conformal contact of S1002 wheel on NP46 (1:20) rail (b). Wheelset has positive lateral displacement.

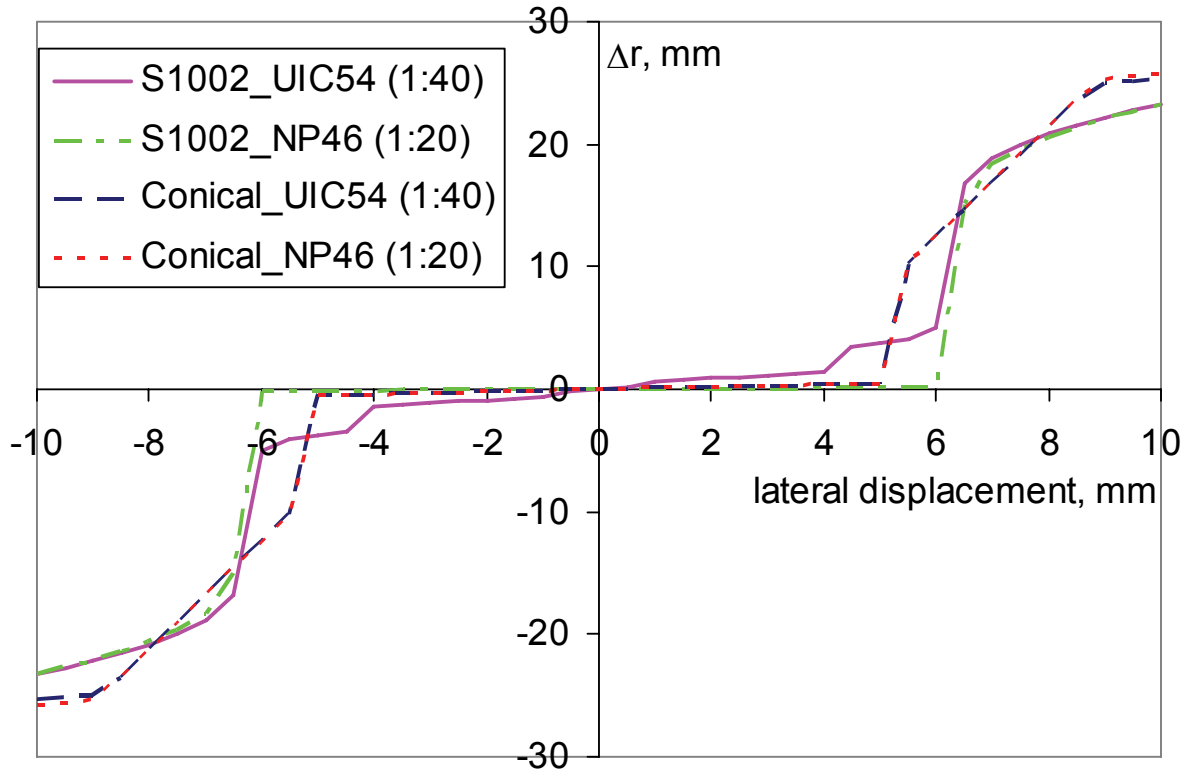

Figure 2.28: RRD functions of S1002 and Conical wheels on NP46 (1:20) and UIC54 (1:40) rails.

From analysis of the RRD function, one can obtain important information about wheel/rail contact. For example, for 3 mm of lateral displacement of the wheelset, the rolling radii difference is equal 1.122, therefore, using formula (2.4), the equivalent conicity of the wheelset is 0.1869, as shown in Table 2.2. Data on equivalent conicity will be used further during the design of a new wheel profile.

One should be aware of the difference between equivalent conicity and the real conicity in wheel/rail contact. The geometric parameters of S1002 and Conical wheel profiles on UIC 54 (1:40) and NP46 (1:20) rails are presented in Table 2.2. The initial conicity of the wheel profiles is calculated at the initial contact point (zero lateral displacement of wheelset). The equivalent conicity of wheel profile is calculated for 3 mm of the lateral displacement.

Obviously, the initial conicity of the Conical profile is equal to its equivalent conicity. However, the initial conicity of the non-conical profile S1002 is not the same as the equivalent conicity.

Table 2.2: Properties of wheel profiles.

Profile	Initial conicity	Equivalent conicity (measured for 3 mm of lateral displacement of wheelset)
S1002/UIC 54 (1:40)	0.0681	0.1869
S1002/NP 46 (1:20)	0.0090	0.0096
Conical/UIC 54 (1:40)	0.05	0.0528
Conical/NP 46 (1:20)	0.05	0.0525

2.5 Implementation and discussion

This chapter introduces the basics of wheel/rail interaction. The two theories for finding the locus of geometric contact between wheel and rail are presented and discussed. A computer program created on the basis of these theories is described, and results of calculations are shown and discussed.

Qualitative and quantitative description of wheel/rail interaction given by the rolling radii difference function and equivalent conicity, as well as distribution of contact points along wheel and rail profiles will be used in the design procedure of the wheel (and/or rail) profile.

In this chapter both wheel and rail profiles are assumed to be symmetric, such that the profile of the left-hand side is the mirror image of that of the right-hand side. This assumption is perfectly valid in the case of the unworn profiles. Theory can be easily extended to the case where profiles are not symmetric, for example, for the case of worn wheel (rail) profiles, or curved track with differing rail profiles for the upper and lower rail. The influence of the different left- and right-wheel and rail profiles, as well as different left- and right-wheel radiuses on geometric contact properties and vehicle dynamics are examined in the reports of Esveld, Markine and Shevtsov [2003, 2005].

At the present time, several geometric contact computer programs are able to consider three-dimensional contact problems where the contact situation is influenced not only by lateral displacement, but also by the yaw angle. However, in the present research, the contact program deals with two-dimensional or plane contact problems, where the contact point and the describing functions depend only on lateral displacement. This is necessary to reduce the number of influencing parameters during the design of the wheel and rail profiles.

3 Basics of rolling contact mechanics

The basics of contact mechanics applied to wheel/rail contact are described in this chapter. First, an introduction is given in Section 3.1. Then the rolling contact theory is summarized in Section 3.2, explaining the principles of creep and contact forces calculation. Section 3.3 explains methods of wheel/rail contact modelling in multi-body software ADAMS/Rail, which is used in the thesis for modelling railway vehicle dynamics. Shakedown, wear law, and fatigue problems in wheel/rail contact are described in Sections 3.4, 3.5, and 3.6, respectively. Section 3.7 concludes with a discussion.

3.1 Introduction

The problem of wheel/rail rolling contact is still a subject of intensive research. With the increasing capacity of modern computers, the focus has turned to three-dimensional models for the numerical simulation, including additional effects such as temperature development and its influence on creep. Nevertheless, empirical models or simplified two-dimensional representations of wheel/rail contact are necessary for efficient simulation of railway vehicle dynamics.

In the last 20 years, two state-of-the-art articles devoted to this problem were published. These are Elkins [1991], and Knothe et al. [2001]. Elkins [1991] provides an overview of the methods and techniques used until 1991 for the prediction of wheel–rail interaction. Since then, numerous developments have occurred, although some important questions, like the prediction of wear or rolling contact fatigue, have still not been answered precisely. The recent and important state-of-the-art paper by Knothe et al. [2001] describes advanced methods of contact mechanics applicable to wheel–rail and tyre–road contact. The paper gives a detailed description of the historical development and the new features of applicable theories and computer codes.

According to the simplest theory of contact, a rolling wheel and the rail are rigid, and contact is governed by Coulomb's law of friction. In this theory, the circumferential velocity of the wheel, and the translational velocity of the wheel over the rail are equal unless the tangential force is saturated. Since contact takes place at a single point, the forces transmitted are concentrated forces. However, as soon as one wishes to consider frictional losses in the driving wheel of the locomotive, vehicle dynamics, strength and fatigue calculations, or wear phenomena, this simple hypothesis becomes too crude. Indeed, in vehicle dynamics the low velocities that actually occur in wheel–rail contact are important; in strength and fatigue calculations, one cannot have concentrated forces; and in friction and wear calculations, the slip-force product is essential. For these applications, one needs a more refined theory, which may be called the continuum theory of rolling contact. In this chapter, various significant theories devised for this type of rolling contact will be briefly described.

There are various methods for the computation of wheel–rail forces in railway vehicle dynamics. The best known methods can be divided into four groups:

- exact theory by Kalker (implemented in programme CONTACT);
- simplified theory by Kalker (implemented in programme FASTSIM);
- look-up tables;
- simplified formulae and saturation functions.

Carter [1926] was the first to study creep in railway wheels, and he looked to the earlier work of Reynolds in belt drives. Carter approximated the wheel by a thick cylinder, and the rail by an infinite half space, and he examined creepage only in the longitudinal direction. He assumed without proof that the area of adhesion was at the leading edge of the contact patch. Johnson [1958] extended the theory to the three-dimensional case of the two rolling spheres in contact, including consideration of lateral and longitudinal slip.

The relationship between creepage and creep force has been studied thoroughly by Kalker [1967, 1982, 1990]. The exact theory that Kalker implemented using the computer programme CONTACT (see Kalker [1990]) usually is not used in dynamic simulations because of its very long calculation time.

The simplified theory used in Kalker's programme FASTSIM (see Kalker [1982]) is much faster than the exact theory, but the calculation time is still relatively long for on-line computations in complicated multi-body systems. FASTSIM is used in the railway vehicle dynamics simulation tools ADAMS/Rail, MEDYNA, SIMPACK, and GENSYS, among others.

Another possibility for computer simulation consists of the use of look-up tables with saved pre-calculated values of contact parameters (contact path dimensions) vs. lateral displacement and yaw angle of the wheelset (ADAMS/Rail, VAMPIRE). Because of the limited data in the look-up tables, there are differences with respect to the exact theory as well. Large tables are more exact, but searching in such large tables consumes more calculation time.

Searching for faster methods, some authors found approximations based on the saturation functions (e.g., Vermeulen and Johnson [1964], Shen, Hedrick and Elkins [1983]). The calculation time using these approximations is short, but there are significant differences with respect to the exact theory, especially in the presence of spin. Simple approximations are often used as fast and less exact alternatives to standard methods (e.g., in SYMPACK, MEDYNA, VAMPIRE).

Kik et al. [1981, 1983] developed a wheel–rail contact element for the analysis of multi-body systems. These authors produced both a successive and a simultaneous iteration method for the iteration of the compatibility and equilibrium equations. The successive method is applicable for rigid rails and wheels in single-point contact; the simultaneous method is suitable for elastic rails and wheels in multi-point contact. In Kik et al. [1983], an application of the successive method on the determination of the steady state motion in a circular curve is given. The wheel–rail contact element is implemented in ADAMS/Rail to model wheel/rail contact; this element will be described in Section 3.3 in more detail.

A fast method for the computation of wheel–rail forces developed by Polach [1992, 1999] yields a good compromise between calculation time and the required accuracy. In spite of the simplifications used, spin is taken into consideration. Due to short calculation time, this method can be used as a substitute for Kalker's programme FASTSIM to save computation time, or to substitute for approximation functions to improve accuracy.

In the next section, the basics of wheel–rail rolling contact theory are described in detail, yielding the possibility of understanding the principles of calculation of creep and contact forces in wheel/rail contact.

3.2 Rolling contact theory

The wheel and the rail interface through a small contact patch. The centre of this contact patch is the application point of normal F_z and tangential forces (traction and braking F_x, guiding

or parasite F_y forces). Knowledge of these forces is necessary to determine the general wheelset equilibrium and its dynamic behaviour.

In order to determine the above described behaviour and forces, first several contact parameters must be determined: the contact surface, the pressure, and the tangential forces. This determination is generally separated into two steps:

1. the normal problem (Hertz theory), and

2. the tangential problem (Kalker's theory).

A short description of these two theories is presented below.

3.2.1 Contact geometry

In this section, the so-called Hertzian contact is considered. The wheel and the rail are two non-conforming surfaces that are brought toward each other until they come into contact and touch each other at one point. A plane called the contact plane is placed at the contact point and is tangent to both bodies. A coordinate system is placed at the contact point, with the z axis normal to the contact plane, and the y and x axes oriented in the direction of the main curvatures of the two contacting surfaces. We introduce the main radii of curvature of the contacting surfaces and we call R_{rx}, R_{ry}, R_{wx}, and R_{wy} the radii of curvature of the rail, and the radii of curvature of the wheel, respectively. The surface of each body in an area around the contact point is expressed in its own contact system in quadratic form:

$$z_w = \frac{1}{2R_{wx}} x_w^2 + \frac{1}{2R_{wy}} y_w^2, \tag{3.1}$$

$$z_r = \frac{1}{2R_{rx}} x_r^2 + \frac{1}{2R_{ry}} y_r^2. \tag{3.2}$$

The distance between the two bodies is given by the sum of the two distances. Simplifying the geometry, the distance between the two surfaces is given by:

$$d = z_w - z_r = Ax_r^2 + By_r^2 = \frac{1}{2R_x} x_r^2 + \frac{1}{2R_y} y_r^2, \tag{3.3}$$

where A and B are the principal relative curvatures, defined as follows:

$$A = \frac{1}{2}\left(\frac{1}{R_{wx}} + \frac{1}{R_{rx}}\right), \quad B = \frac{1}{2}\left(\frac{1}{R_{wy}} + \frac{1}{R_{ry}}\right). \tag{3.4}$$

3.2.2 Creepage and spin creepage

The concept of creepage has been studied in the field of railway vehicle dynamics for many years and is well understood. De Pater [1962] and Johnson [1958 a,b] analysed the motion of the wheel with respect to the rail when both are considered as rigid. That is, they sought for the generalization of Carter's notion of creepage. It was pointed out by Kalker that this motion is a rigid body motion in the plane of contact, i.e., the common tangential plane of wheel and rail, and that the velocity corresponding to this motion is a translation and a rotation about the common normal at the centre of the contact area, which is taken as the z axis. In general, the wheel and rail surfaces can be pressed against each other, tangentially displaced and rotated.

The following relative motions can be defined:

- A displacement parallel to the z axes given by δ. Such displacement is called compression if $\delta < 0$, and loss of contact if $\delta > 0$.
- Two tangential velocities along x and y axes called rolling velocity: $V_{roll,x} = -\frac{1}{2}\left(V_{w,x} + V_{r,x}\right)$ and $V_{roll,y} = -\frac{1}{2}\left(V_{w,y} + V_{r,y}\right)$, where V_w is translational velocity, and V_r is circumferential velocity. The total velocity is given by $V_{roll} = \left(V_{roll,x}^2 + V_{roll,y}^2\right)^{1/2}$. The x-velocity contains the rolling velocity of the vehicle, to which is added some perturbing motions, while the y-velocity contains only perturbations. We can assume that the x component is much larger than the y, i.e., $V_{roll} \simeq V_{roll,x}$.
- Two displacements along the x and y axes whose velocities are $V_{w,x}$, $V_{w,y}$, $V_{r,x}$, $V_{r,y}$. The differences, $V_x = V_{w,x} - V_{r,x}$ and $V_y = V_{w,y} - V_{r,y}$, are called creep velocity. The creep velocity divided by the rolling velocity is called correspondingly longitudinal ξ, and lateral η creepage:

$$\xi = \frac{V_x}{V_{roll}} = \frac{V_{w,x} - V_{r,x}}{V_{roll}}, \tag{3.5}$$

and

$$\eta = \frac{V_y}{V_{roll}} = \frac{V_{w,y} - V_{r,y}}{V_{roll}}. \tag{3.6}$$

- Two rotations around the x and y axes whose angular velocities are $\Omega_{w,x}$, $\Omega_{w,y}$, $\Omega_{r,x}$, and $\Omega_{r,y}$. The differences $\Omega_x = \Omega_{w,x} - \Omega_{r,x}$, and $\Omega_y = \Omega_{w,y} - \Omega_{r,y}$ are called rolling.
- One rotation around the z axis whose angular velocity is $\Omega_{w,z}$, $\Omega_{r,z}$. The difference $\Omega_z = \Omega_{w,z} - \Omega_{r,z}$ is called spin. The spin, divided by the rolling velocity is called spin creepage:

$$\phi = \frac{\Omega_z}{V_{roll}} = \frac{\Omega_{w,z} - \Omega_{r,z}}{V_{roll}} \tag{3.7}$$

We illustrate creepage in Figure 3.1. Consider a wheelset on a track (Figure 3.1 (a)). The wheel makes a yaw angle ψ with the rail; ψ has angular velocity $\dot{\psi}$. The wheelset moves with lateral velocity $\dot{y}$, translational velocity V_w, and circumferential velocity V_r. The angular velocity of the wheelset is Ω.

Longitudinal creepage arises *inter alia* through the difference in effective rolling radii of the wheels, left and right, due to conicity, through accelerating or braking couples and, very importantly, through the rotation $\dot{\psi}$ of the yaw angle ψ, by which the left wheel moves with a different velocity over the rail than the right wheel.

V_w and V_r make an angle ψ with one another, see Figure 3.1. Hence the difference velocity $V_w - V_r$ has a component in the y direction that leads to lateral creepage; $\dot{y}$ of course, also gives rise to lateral creepage.

Spin creepage, or spin for short, consists of two parts. The first results from the velocity of the yaw angle $\dot{\psi}$; the second is a consequence of conicity. Spin creepage due to conicity is called camber in the automotive industry, and is illustrated in Figure 3.1 (b). We observe that the angular velocity of the wheelset Ω is not parallel to the contact plane, owing to conicity. Indeed, there is a component of rotation $\Omega_z = |\Omega| \sin\gamma$ about the z axis. Division by $V \simeq |\Omega| R_{wx}$ yields the camber spin $\sin\gamma / R_{wx}$. The total spin is

$$\phi = -\frac{\dot{\psi}}{V} + \frac{\sin\gamma}{R_{wx}}. \tag{3.8}$$

When creepages and spin creepage are known, we can calculate the contact forces.

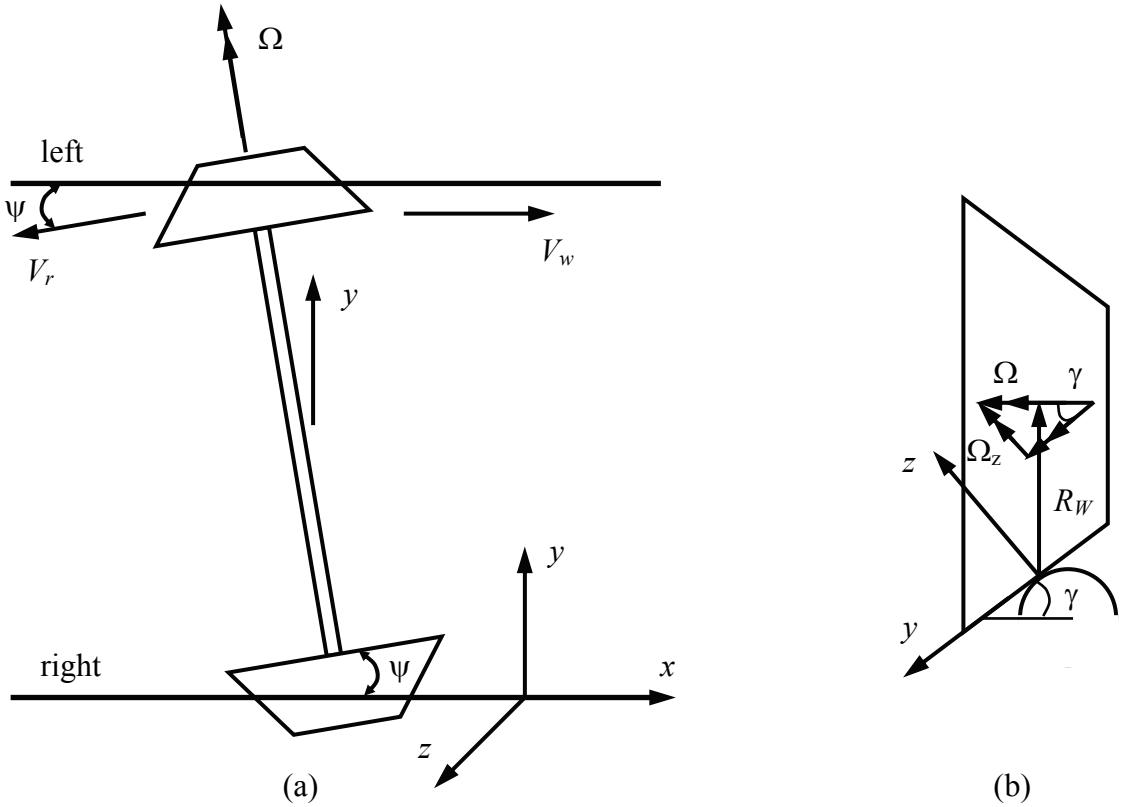

Figure 3.1: The creepages: (a) a wheelset on a track; (b) illustration of camber spin. (Taken from Kalker [1991].)

3.2.3 Normal contact force

A surface stress field is present in the contact surface. This field can be integrated to provide contact forces and moments:

- a normal force F_z called compression force;
- two tangential forces F_x and F_y called creep or sliding forces;
- two tangential moments M_x and M_y called rolling friction moment, which are in most problems sufficiently small to be ignored, as they are in the present work;

- one vertical moment M_z called the spin moment.

In this section, determination of the normal force is described, while in the next Section 3.2.4, the tangential forces are determined.

Around 1956, de Pater and Johnson established that the Hertz solution could be used to predict the shape and size of the contact area, and the normal pressure carried by it. In the creep law theory, it is shown that the normal pressure distribution in the contact area is independent of the tangential pressure distribution when the materials of the two contacting bodies have the same elastic constants, as is the case in railway engineering. It turns out that the contact area is elliptical in form, with semiaxes a and b in the rolling and lateral directions respectively. The ratio of the axis, a/b, depends only on the curvature of wheel and rail. The size of contact depends on the normal force F_z, but is independent of tangential forces F_x and F_y.

Hertz analytically solved the normal problem assuming that the contact surface is elliptical in shape. The normal stress field in the elliptical contact surface area is semi-ellipsoidal:

$$p(x,y) = p_0(1-(x/a)^2-(y/b)^2)^{1/2}. \tag{3.9}$$

The maximum value of the contact stress p_0, occurs at the centre of the ellipse. By integrating this pressure in the contact surface, the normal force F_z is obtained:

$$F_z = \frac{2}{3} p_0 \pi a b. \tag{3.10}$$

If R_x and R_y are longitudinal and lateral relative radii of curvature respectively, then to find the size of the contact ellipse, the next formula can be used:

$$\frac{A}{B} = \frac{R_x}{R_y} = \frac{(a/b)^2 \mathbf{E}(e) - \mathbf{K}(e)}{\mathbf{K}(e) - \mathbf{E}(e)}, \tag{3.11a}$$

$$\sqrt{AB} = \frac{1}{2}\sqrt{\frac{1}{R_x R_y}} = \frac{p_0}{G}\frac{b}{a^2 e^2}\sqrt{\left((a/b)^2 \mathbf{E}(e) - \mathbf{K}(e)\right)\left(\mathbf{K}(e) - \mathbf{E}(e)\right)}, \tag{3.11b}$$

in which the factors $\mathbf{K}(e)$ and $\mathbf{E}(e)$ are the complete elliptic integrals of the first and second kind. For railway application, these integrals can be used in tabulated form (see Kalker [1990]). The parameter e represents the eccentricity of the contact ellipse $e = \sqrt{1-(b/a)^2}$ and G is the combined modulus of rigidity of the wheel and the rail:

$$\frac{1}{G} = \left(\frac{1-\nu_w^2}{E_w} + \frac{1-\nu_r^2}{E_r}\right), \tag{3.12}$$

where E_w and E_r are the Youngs modules, and ν_w and ν_r are the Poissons ratios of the wheel and the rail, and which are equal in the case of steel wheel and steel rail.

Johnson [1985] shows that the ratio (b/a) varies between the following two bounds

$$(b/a) \in \left[1, \left(\frac{R_x}{R_y} \right)^{-\frac{2}{3}} \right]. \tag{3.13}$$

Equation (3.11) can be solved with the bisection method using the two bounds given above. An equivalent radius is defined:

$$R_e = (R_x R_y)^{1/2}. \tag{3.14}$$

The values of the semi-elliptical radii are given by

$$a = m\left(\frac{3\pi F_n}{4G(A+B)} \right)^{\frac{1}{3}}, \qquad b = n\left(\frac{3\pi F_n}{4G(A+B)} \right)^{\frac{1}{3}}. \tag{3.15}$$

The coefficients m and n in equations (3.15) are given by Hertz (see Kalker [1990]).

The total deformation of two contacting bodies is given as:

$$\delta = \frac{p_0 b}{G} \mathbf{K}(e). \tag{3.16}$$

Once the ratio of the elliptical radii is calculated, the normal force is given by:

$$F_z = K_H \delta^{\frac{3}{2}} = \delta^{\frac{3}{2}} \left(\frac{9}{16 R_e G^2} \right)^{-\frac{1}{2}} F_2^{-\frac{3}{2}}, \tag{3.17}$$

where K_H is Hertzian spring stiffness and in which factors F_2 and F_1 are given by:

$$F_2 = \frac{2}{\pi} \sqrt{\frac{b}{a}} F_1^{-1} \mathbf{K}(e), \tag{3.18}$$

$$F_1^3 = \frac{4}{\pi e^2} \left(\frac{b}{a} \right)^{\frac{3}{2}} \left[\left(\left(\frac{b}{a} \right)^2 \mathbf{E}(e) - \mathbf{K}(e) \right) \left(\mathbf{K}(e) - \mathbf{E}(e) \right) \right]^{\frac{1}{2}}. \tag{3.19}$$

In the next section computation of the tangential forces is described.

3.2.4 Tangential contact forces

The normal force calculation is described in Section 3.2.3. In this section, computation of the tangential forces in wheel/rail contact is considered. As shown in Kalker [1967] (pp. 136-143), the normal force, two tangential forces, and a spin moment are calculated as functions of the known variables: the a/b ratio, the two creepages, and the spin creepage. At small values of creepage, the relationship can be considered to be linear, and linear coefficients can be used in the calculation of the creep forces. However, at larger values of creepage, for example during flange contact, the relationship becomes highly non-linear, and the creep force approaches a limiting value determined by normal force and the coefficient of friction in the contact area.

According to the Kalker linear theory (see Kalker [1979, 1990]), the longitudinal F_x and lateral F_y components of the creep force, and the spin creep moment M_z that develop in the wheel-rail contact region are expressed as:

$$\begin{bmatrix} F_x \\ F_y \\ M_z \end{bmatrix} = -G\,ab \begin{bmatrix} c_{11} & 0 & 0 \\ 0 & c_{22} & \sqrt{ab}\,c_{23} \\ 0 & -\sqrt{ab}\,c_{23} & ab\,c_{33} \end{bmatrix} \begin{bmatrix} \xi \\ \eta \\ \phi \end{bmatrix}, \tag{3.20}$$

where G is the combined shear modulus of rigidity of wheel and rail materials (3.18) and a and b are the semi-axes of the contact ellipse, which depend on the material properties of wheel and rail, and on the normal contact force. The parameters c_{ij} are the Kalker creepage and spin coefficients, and can be obtained from Kalker [1979, 1990], and the quantities ξ, η, and ϕ represent the longitudinal, lateral, and spin creepages at the contact point, respectively. For sufficiently small values of creep and spin, the linear theory of Kalker is adequate to determine the creep forces. For larger values, this formulation is not appropriate since it does not include the saturation effect of the friction forces, i.e., it does not assure that $F_{lat} \le \mu N$.

The complete Kalker theory is implemented in the computer program CONTACT (see Kalker [1990]). However, to speedup the calculations, one of the programs based on the Kalker simplified theory can be used, for example FASTSIM (Kalker [1982]). Also, a simpler method based on the cubic saturation theory of Johnson and Vermeulen can be used, as well as the non-linear method of Polach [1999].

FASTSIM program uses an approximate, and faster, approach than the complete theory. If the flexibility in the contact area is isotropic, then (Wikens [2003]):

$$u_x = f\sigma_x, \quad u_y = f\sigma_y, \tag{3.21}$$

where u_x and u_y are relative displacements in the plane of the contact area, and σ_x and σ_y are tangential tractions. The area of adhesion is then calculated as

$$\frac{\partial \sigma_x}{\partial x} = \frac{\gamma_1}{f} - \frac{\omega_3 y}{f}, \tag{3.22}$$

$$\frac{\partial \sigma_y}{\partial x} = \frac{\gamma_2}{f} + \frac{\omega_3 x}{f}. \tag{3.23}$$

These equations are approximated by

$$\frac{\partial \sigma_x}{\partial x} = \frac{\gamma_1}{f_1} - \frac{\omega_3 y}{f_3}, \tag{3.24}$$

$$\frac{\partial \sigma_y}{\partial x} = \frac{\gamma_2}{f_2} + \frac{\omega_3 x}{f_3}, \tag{3.25}$$

where f_1, f_2, and f_3 are determined so as to obtain results that agree with a linear theory for small creepages. This leads to

$$f_1 = \frac{8a}{3c_{11}G}, \quad f_2 = \frac{8a}{3c_{22}G}, \quad f_3 = \frac{\pi a\sqrt{a/b}}{4c_{23}G}, \tag{3.26}$$

Now equations (3.24) and (3.25) can be integrated.

Kalker [1983] has extended the simplified theory of rolling contact to cover the non-Herzian contact case, which can occur particularly in the case of worn wheels and rails. In the case of

two-point contact, the complex non-Hertzian contact patches can be approximated by one or more elliptic patches.

3.3 Contact model in ADAMS/Rail

The wheel-rail element implemented in ADAMS/Rail is based on the work of Kik et al. [1981] on modelling of a wheel-rail interconnection element. The more detailed description of the wheel-rail elements can be found in the ADAMS/Rail manual (for example, see ADAMS/Rail [2005]). Through the years, the description of the element has evolved from the use of constraints together with flexibility and contact patches based on curvature in the contact point, to a model where normal force is computed due to flexibility of the contacting bodies and contact patches due to deformation.

This wheel-rail element always describes the kinematics of one wheel relative to one rail. Three types of contact description are derived from this wheel-rail element. These derived elements differ in the way they handle kinematics:

- a linearized element with kinematics described by conicity, contact angle and roll angle parameter;
- an element that uses pre-calculated nonlinear kinematic functions as input;
- an element that uses wheel and rail profile as input.

To model a wheelset, it is necessary to use two wheel–rail elements: one for wheel–rail contact on the left side, and one on the right side. A body describing wheelset has a wheel or wheelset defining wheel–rail interconnection element between the body itself and the track or rails. Theoretically, for non-linear types of wheel-rail element, it is possible to model the contact between one wheel and two rails using two interconnection elements on the same wheel. For example, a guiding rail contacting an inner flange.

Within a vehicle model, this description of the wheel–rail contact enables the use of different wheel–rail element types at the same time. Also, it is possible to change wheel–rail elements along the track by switching the type of element:

- The quasi-linear element type allows examination of the influence of conicity, contact angle, and roll angle parameters by defining them independently of a given wheel and rail profile. This type of analysis can be used to study the stability of a vehicle.
- The element type with a pre-calculated kinematic table is based on the kinematics of given profiles for wheel and rail, but approximates the contact patch by an ellipse, uses a constant value for contact patch stiffness, and models only one contact patch inside one interconnection.
- The wheel–rail interconnection element, where profiles are used within the interconnection, is the most general element. It models non-elliptical contact patches and contact stiffness according to the Boussinesq formulation (see Kik and Piotrowski [1996]). It does not restrict the number of contact patches in one interconnection.

Modelling of rail irregularities is treated in the wheel–rail element as foot point input u. Due to rail irregularities, the relative position of the wheel with respect to the rail changes. The relative velocity does not change. Errors in roundness of wheels, either due to geometric errors or flexible modes, can be introduced as an increment ΔR to the distance to the rotational centre of the wheel.

In the present research, the most general case of wheel/rail contact will be used. This procedure works directly with the wheel and rail profiles. Computation of contact forces is divided into the following tasks:

- computation of contact line on wheel;
- computation of contact patch;
- computation of normal force in contact patch;
- computation of creepages;
- computation of creep forces;
- computation of transformation of contact forces.

These tasks are described below.

The left and right coordinate systems used in ADAMS/Rail for the wheels and rails are shown in Figure 3.2.

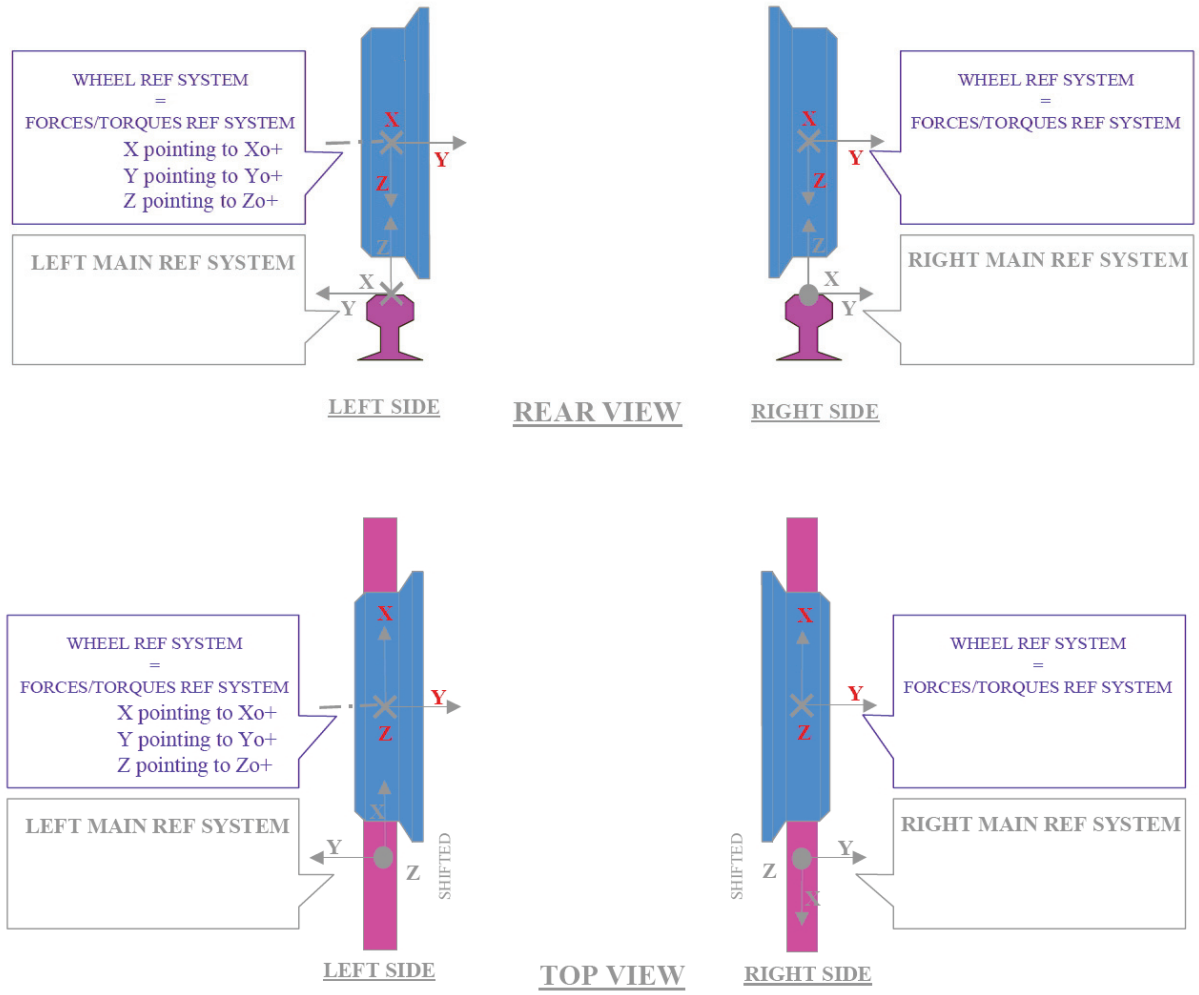

Figure 3.2: Orientation of wheel-rail element when used on left and right side. (Taken from ADAMS/Rail Help [2005].)

Contact between wheel and rail can be solved as a two-dimensional problem, as shown by Heumann [1950]. The projection of the wheel contour on a plane normal to the rail (plane of

the rail profile) is defined as the possible contact line. The computation of the contour or contact line is solved using the ellipses formed by the wheel tapes, as shown in Figure 3.3.

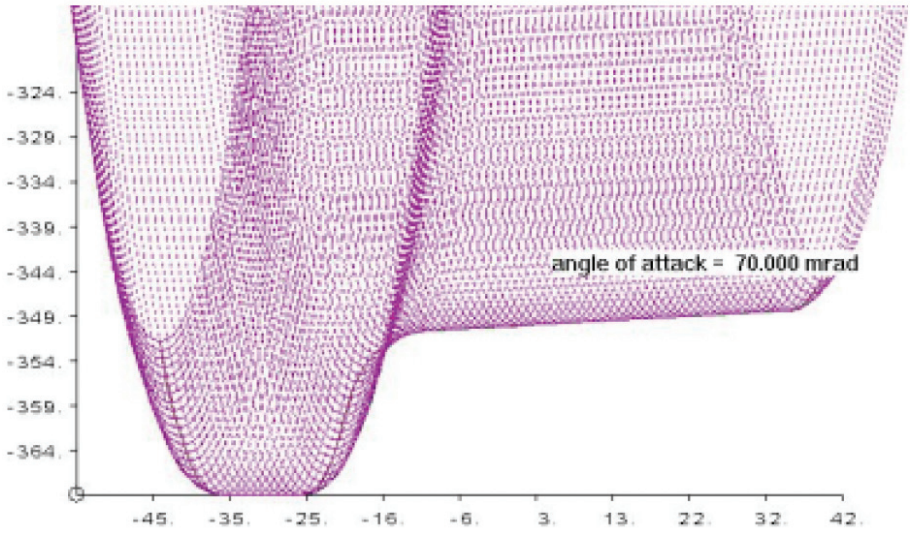

Figure 3.3: Wheel profile (contact line) for a wheel. (Taken from ADAMS/Rail Help [2005].)

The contact line is transformed into the rail coordinate system, and the undeformed penetration between rail profile and contact line is searched for. If no penetration occurs, there is no contact.

According to the approximation described by Kik and Piotrowski [1996], it is assumed that penetration of undeformed profiles, δ_u, describes elastic deformation, w_{el}. The ratio is:

$$\delta_u = \frac{w_{el}}{0.55}. \tag{3.27}$$

The intersection points of rail profile and contact line on the wheel describe the lateral width of the contact patch. It is assumed that the rail is straight in the longitudinal direction. The shape is computed by segmenting the area into stripes. Elongation for each of the stripes in the longitudinal direction computes the segment of the rolling circle:

$$a_i = \sqrt{-2w_i R_i - w_i^2}, i = 1,...,n \ , \tag{3.28}$$

where n is number of stripes, see Figure 3.4.

If an ellipse is computed, half diameter b in the lateral direction is equal to the lateral width. Half diameter a is computed assuming ellipse has the same area.

$$a = \frac{S_{contact}}{\pi b}. \tag{3.29}$$

The position of the contact point is defined as the centre of the area.

The normal force in the contact area is computed using the Hertz theory for a given ellipse with undeformed penetration.

The creep force computation is based on Johnson and Kalker theory (see Kalker [1990]); it is also possible to use the modified FASTSIM or the Polach method. Kalker's Table Book is based on Hertzian contact (contact ellipses), computed with the CONTACT program. Kalker's FASTSIM uses stripe theory with isotropic elastic layer and parabolic normal

pressure distribution. Functional approximation of Polach [1999] uses analytic functions to attain best fit for creep force relations.

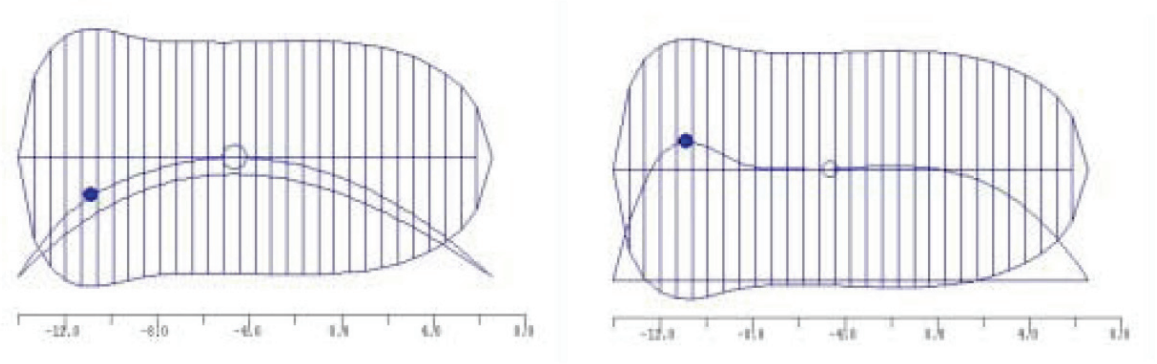

Figure 3.4: Penetration of undeformed profiles (left) and undeformed distance (right) and contact patch. (Taken from ADAMS/Rail Help [2005].)

As mentioned in the introduction to this chapter, analytic functions require less computing time than the FASTSIM algorithm. Table Book falls in the same range of computation time as analytic functions. It is possible to use the FASTSIM algorithm not only for elliptical, but also for non-elliptic contact patches.

The method proposed by Polach has been employed in various programmes. The algorithm is implemented in ADAMS/Rail as an alternative parallel to FASTSIM and the pre-calculated non-linear kinematic tables. The calculation time is faster than that of FASTSIM, and is usually faster than the tables. The proposed algorithm provides a smoothing of the contact forces in comparison with the tables, and there are no convergence problems during the integration.

3.4 Shakedown

In this section, the principles of shakedown in wheel/rail contact are briefly discussed. Additional information on this topic can be found in Tunna et al. [2006], and in Johnson [1985, 1989].

If the stresses produced in the wheel under contact conditions with the rail are below the elastic limit of the wheel material, no permanent deformation will take place. However, in practice, the stresses usually exceed the elastic limit, causing plastic flow and residual stress changes near the surface. Plastic flow raises the elastic limit for steel materials. Residual stress makes plastic flow less likely during subsequent loading cycles. The combined effect is known as “shakedown” or “work hardening”.

There is a limit – known as the “shakedown limit” – to the increase in hardening that the wheel material can achieve. If the stresses are above this limit, permanent plastic deformation will occur for each subsequent wheel revolution. If this continues, the plastic strain limit for the material will be exceeded and surface cracking will occur. This process is known as “ratchetting”.

Figure 3.5 presents an example of a shakedown diagram that is commonly used to compare contact conditions with the shakedown limit (see Johnson [1989], and Bower and Johnson [1991]). In Figure 3.5, p_0 is the maximum contact pressure [MPa], K_e is the shear yield strength of the material [MPa], Q is the tangential force in the contact patch [N], and P is the normal force [N]. The traction coefficient should not be confused with the coefficient of

friction; it is limited by the coefficient of friction and is sometimes called the utilised coefficient of friction.

Maximum contact pressure, p_0, is often estimated as $3P/2A$, where A is the contact area (mm^2). Shear yield strength can be calculated from a material's yield strength in direct tension, K_y, using the Von Mises criterion, as equation (3.30) shows. K_y can be estimated from the material's tensile strength, K_t, as equation (3.31) shows.

$$K_e \approx \frac{K_y}{\sqrt{3}}. \tag{3.30}$$

$$K_y \approx \frac{K_t}{\sqrt{3}}. \tag{3.31}$$

The limits shown in Figure 3.5 are based on laboratory tests under ideal conditions of line contact. Empirical limits, based on comparisons with observations in the field, are often used.

The shakedown diagram shows that surface flow can happen when the traction coefficient is high. This type of surface damage can occur in the flange root of wheels when the coefficient of friction is high; it is not discussed further in this thesis. The next two sections describe two other important types of surface damage, wear and rolling contact fatigue.

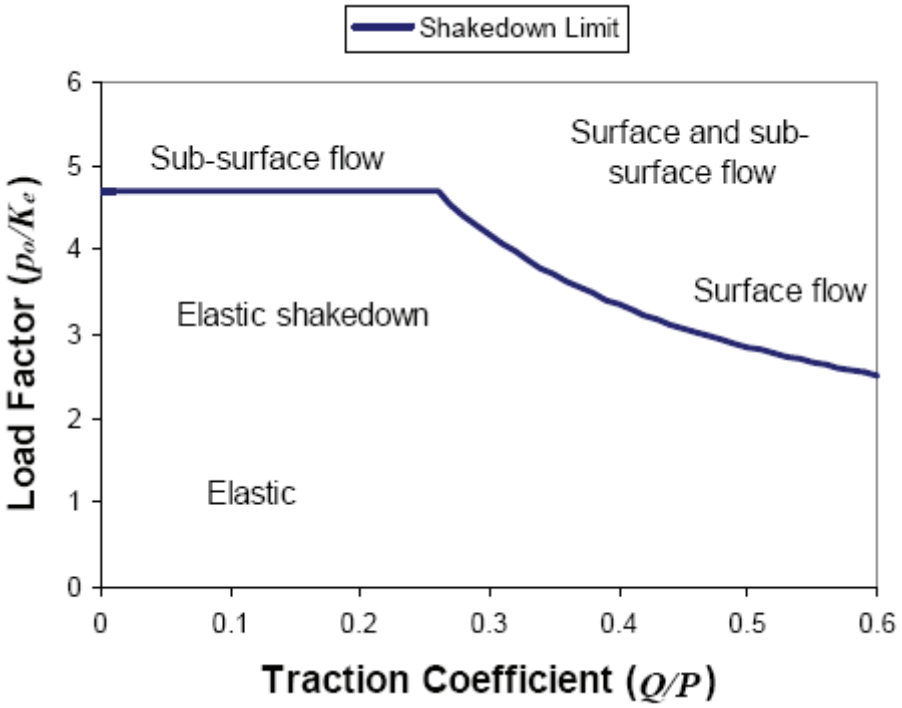

Figure 3.5: Example shakedown diagram.

3.5 Wear law in rolling contact

Wear is the principal cause of rail replacement on almost all railways. Wear tends to be concentrated on the gauge face of the high rail (i.e., the inner edge of the outer rail in curved track), where contact is made with the wheel flange root and on the rail top of the low rail. In straight track and large radius curves, vertical wear of the rail head is seen. If the rail wears severely, stress in the rail rises, particularly in the head and, eventually, the rail needs to be

replaced. All railways have different criteria for removing worn rail, but often these criteria call for replacement when about 30 to 50% of the head area has been lost.

The analogous situation with wheels is different, in that they can be reprofiled by machining (turning) when worn. This is undertaken either when the flange becomes too thin, or when tread wear has left the flange too high. Further, wheels are often machined when the profile has worn to a shape that causes the wheelset to have reduced steering ability. Wheels can be reprofiled if the contact surface is damaged due to flats, squaring, pitting, etc. As with rails, wheels are removed from service when metal has been lost to such an extent that stresses in the wheel are unacceptably high and can cause wheel fracture.

In railway engineering practice, three main wear regimes for wheel/rail materials have been defined as a result of laboratory twin disc experiments (Bolton and Clayton [1984], Lewis et al. [2003]): mild, severe and catastrophic. The regimes are described in terms of wear mechanism, as well as wear rate.

In the mild regime at low load and slip conditions, corrosive wear is most common. Corrosive wear is the result of the repeated removal by sliding action of the film of the product of chemical corrosion on the surface, formed during absence of contact. Corrosive wear rate is very low under normal environmental conditions. However, some metallic wear can also be present. Mild wear is typical for the wheel tread and for the rail head contact.

As slip and load in the contact are increased (to the levels experienced in a flange contact), severe wear occurs. Wear rate can increase tenfold comparing to mild regime. The wheel material wears out through a delamination process. During twin disk experiments it can be seen that a larger amount of plastic deformation occurs below the wheel disc wear surface, and crack formation just below the surface is visible, which leads to thin slivers of material breaking away from the surface. As the contact conditions become more severe, in the catastrophic regime, these cracks alter direction from running parallel to the wear surface and turning up, to turning down into the material, causing larger chunks of material to break away. These mechanisms are described in more detail in Lewis et al. [2004 b].

Wheel wear is closely related to conditions of force and slip in the wheel/rail contact. Two basic types of wear models are described in the literature on wheel/rail interaction (see Enblom and Berg [2005]):

1. Energy transfer models, which assume material loss to be a function of the energy dissipated in the contact patch.

2. Sliding models where material loss depends on combinations of sliding distance, normal force, and material hardness.

BR Research carried out pioneering work to understand and model wheel/rail wear behaviour. Empirical studies, both on a full-scale laboratory test rig and in the field (McEwen and Harvey [1986], Pearce and Sherratt [1990]), have shown that the wear of wheels and rails depends on the rate of dissipation of energy within the contact patch. It had been concluded that wheel wear rate could be related to the frictional energy expended through creepage in each wheel/rail contact. This can be shown to be the sum of the products of the individual creep forces, and creepages in the longitudinal and lateral directions. In most cases, the contribution from the spin term is assumed to be small and is ignored. Wheel wear is estimated using the wear index W that reads:

$$W = F_x \cdot \xi + F_y \cdot \eta \,, \tag{3.32}$$

where F_x is longitudinal creep force; ξ is longitudinal creepage (3.5); F_y is lateral creep force; and η is lateral creepage (3.6).

In unlubricated tests, McEwen and Harvey [1986] observe a mild wear regime (probably adhesive wear) if the wear number was less than 200N. A severe wear regime (probably delamination wear) was found for wear numbers greater than 400N. For wear numbers between 200N and 400N, either type of wear could occur.

3.6 Fatigue problem in rolling contact

Rolling contact fatigue (RCF) describes the phenomenon of crack growth in rails as a result of repeated contact loading. Normal loads, and longitudinal and lateral shear tractions, all contribute to RCF damage. Typical RCF cracks, called shells and spalls, occur on the gauge face of the outer rail, and the top surface of the inner rail in curved track carrying heavy-haul traffic. For rails, the traditional terminology is that spall refers to loss of metal from cracks initiated at the surface, while shell refers to loss of metal from cracks initiated below the surface. RCF cracks are known to propagate in and below the wheel surface but, in many cases, the cracks initiate by thermal mechanisms – either by thermal fatigue caused by the heat input from tread braking, or from sudden cracks formed in martensite produced when the wheel slides on the rail during braking.

For wheels, the terminology is different, and spall refers to loss of metal from defects initiated by a thermal mechanism. Shell refers to metal lost by a pure RCF process. RCF shells have been observed on coal trains in western Canada, but these are not typical of most cracks in wheels. Although wear attacks both the wheel and the rail, the evidence is that RCF is much more likely to initiate cracks in rails than wheels.

The fatigue failures of railway wheels can be divided into (at least) three different forms: surface initiated fatigue; subsurface initiated fatigue, and deep defects, each corresponding to different underlying mechanisms (see Ekberg and Marais [1999], Ekberg and Sotkovszki [2001]).

In surface initiated fatigue of railway wheels, fatigue cracks result from excessive plastic flow of the surface material. This will cause crack initiation due to ratchetting, and/or low cycle fatigue of the surface material. Once initiated, the cracks typically grow into the wheel material to a maximum depth of some 5 mm. Final fracture occurs as the cracks branch towards the wheel tread.

Surface initiated cracks are normally not a safety issue. However, they are the most common type of fatigue damage in wheels. They are costly in that they require reprofiling of the wheel, and that they cause unplanned maintenance. Further, if not attended to, non-round wheels may cause secondary damage to rail, bearings, etc.

In the case of subsurface fatigue, cracks will initiate several millimetres below the surface. They continue to grow under the surface, and final fracture will normally occur due to branching toward the surface. Such failure will break off a large piece of the wheel surface.

Material defects have a strong effect on resistance to subsurface initiated RCF. Below some 10 mm, nominal stresses due to rolling contact are very low, and fatigue can occur only if promoted by a material defect of sufficient size. Subsequent propagation occurs at approximately the same depth as the initiation. Due to the deep initiation point, such cracks are very dangerous. Final fracture may well occur as a branch towards the wheel hub and may cause a derailment (Ekberg and Marais [1999]).

Surface initiation of RCF stems from the same mechanism that causes delamination wear. Repeated plastic deformation of the surface layer eventually leads to the material reaching its plastic strain limit and a crack being initiated. If contact conditions are severe, wear by delamination will take place. If contact conditions are less severe, but are still above a certain threshold, cracks may propagate to form RCF, and the effect of fluid on crack propagation becomes important.

In this work, we use the methodology for estimation of RCF crack initiation developed by Ekberg et al. [1999, 2001].

In this work, material properties are considered to be prescribed. Therefore, fatigue models use as few material parameters as possible. In order to achieve this, the models predict the fatigue impact of a certain combination of load and contact geometry. The question of a material's resistance to this impact then becomes a separate issue. This strategy has the benefit of allowing fatigue assessments at the design stage, where the wheel material is not specified. Further, statistical uncertainties in the predictions, normally introduced by material fatigue parameters, are limited. Scatter due to random variations in load and contact conditions will, of course, still exist.

The fatigue index for surface initiated fatigue is based on the theory of elastic and plastic shakedown in general, and shakedown map theory in particular, as described in Section 3.4 (also see Johnson [1989]). The fatigue index is expressed as:

$$FI_{surf} = \mu - \frac{2\pi abk}{3F_z}, \tag{3.33}$$

where μ is the traction coefficient, a, b are the semiaxes of the Hertzian contact patch, F_z is the normal force magnitude, and k is the yield stress in pure shear. In this study, the traction coefficient μ is defined as the quotient between the tangential and normal forces in the contact patch:

$$\mu = \frac{\sqrt{F_x^2 + F_y^2}}{F_z}, \tag{3.34}$$

where F_x and F_y are the longitudinal and lateral creep forces, respectively. Fatigue is predicted to occur if the inequality $FI_{surf} > 0$ is fulfilled.

The index for subsurface initiated fatigue is based on the Dang Van equivalent stress (see Dang Van et al. [1989]); this is an approximation of the largest occurring equivalent stress during a wheel revolution. The index is expressed as:

$$FI_{sub} = \frac{F_z}{4\pi ab}(1+\mu^2) + a_{DV}\sigma_{h,res}. \tag{3.35}$$

Here, $\sigma_{h,res}$ is the hydrostatic part of the residual stress (positive in tension). The parameters F_z, a, b, and μ are the same as above, and a_{DV} is a material parameter that may be evaluated as:

$$a_{DV} = \frac{3\tau_e}{\sigma_e} - \frac{3}{2}, \tag{3.36}$$

where τ_e is the fatigue limit in alternating shear, and σ_e is the fatigue limit in rotating bending.

Fatigue is predicted to occur whenever the inequality $FI_{sub} > \sigma_{EQ,e}$ is fulfilled. Here, $\sigma_{EQ,e}$ is the fatigue limit in shear. To account for material defects, a reduced fatigue limit, σ_w, can be estimated as:

$$\sigma_w = \sigma_{EQ,e}\left(\frac{d}{d_0}\right)^{-1/6}, \tag{3.37}$$

where d is the diameter of the occurring defect, and d_0 is the defect size corresponding to the unreduced fatigue limit, according to Ekberg and Sotkovszki [2001].

For fatigue initiation at deep defects, this index is used:

$$FI_{def} = F_z, \tag{3.38}$$

where F_z is the magnitude of the vertical load. Fatigue is predicted to occur when this magnitude exceeds a threshold. To quantify this threshold is a complicated task and a topic of current research (see Kabo [2002 a,b]). Further details of the fatigue model can be found in Ekberg et al. [2002].

In this research, we focus mainly on surface fatigue problems, as they are the most frequently occurring problems on the Dutch railway network. Analysis of the formula (3.33) leads to the conclusion that decreasing the normal load F_z and traction coefficient μ as well as increasing the elliptic contact area of the Hertzian contact reduces surface fatigue occurrence. This conclusion will be used during design of a wheel profile.

3.7 Discussion

In this chapter, the basis of wheel/rail contact mechanics is described. Methods for calculation of creepages and creep forces are briefly explained. Significant consideration is given to wear and rolling contact fatigue problems.

The level of wear at the wheel and rail surface is indicated by the energy dissipated in the contact patch, and this is calculated by taking the product of creepage and creep force as shown in Section 3.5. A high value of energy is seen as indicating a high rate of wear of the wheel profile and is to be avoided. Some wear is however, seen as beneficial, as it removes small cracks that develop through rolling contact. Such cracks cannot then grow to a length where they cause spalls in rails or surface shells in wheels (Kapoor et al. in Bushan (ed.) [2001], Evans and Iwnicki [2002]). A very low level of wear is also undesirable, as it probably indicates that wear is taking place over a very limited section of the profile (hollow wear as an example), and that the shape of the profile will not then be stable.

One way to reduce the RCF problem is to increase wheel or rail wear rate by reducing hardness, which can be beneficial in certain situations. The corresponding increase in ductility decreases the incidences of RCF, and small RCF cracks are worn away before they can grow to compromise the integrity of the rail. However, rail life is inevitably reduced by the high wear rate.

The idea of removing small cracks to protect against RCF has led to the widespread use of rail grinding to control cracks, flakes, and spalls on the rail surface. This has been adopted on many railways, using in-track machines to grind the rail in situ; this is especially prevalent on heavy-haul railways, where it is a commonly used rail maintenance technique. Available machines are capable of grinding both rails simultaneously, and of applying desired profiles (to reduce contact stress or improve vehicle steering) at speeds in excess of 10 km/h.

Attempts have been made to define metal removal rates and grinding intervals to give the best rail surface condition at minimum cost, with some success (Kalousek et al. [1989]). Recent work on North American railways, however, indicates that the balance between wear and RCF is highly site-specific and rail-type–specific. That is, the propensity for RCF cracks depends critically on parameters such as track radius and structure, the type of rail installed, the speed of traffic, and operating practices (such as the presence of signalling systems that may require trains to brake and accelerate always on the same sections of track). There seems no doubt that, properly applied, rail grinding can reduce RCF and prolong rail life.

Until recently, the academic study of wear/RCF interaction has been limited. Observations from small-scale tests (Kalousek et al. [1989]; Beynon et al. [1996]) have indicated that a period of dry rolling prior to the application of water lubrication accelerates RCF cracking. This is thought to occur because surface tractions rise with friction, giving an increased rate of ratchetting strain accumulation at the surface of the steel, which leads to the initiation of cracks. Recent work has examined the effect of preventive grinding on rail surface damage using rail/wheel test discs (Ishida and Abe [1997]), with the conclusion that a metal removal rate 0.1 mm per 50 MGT (mega gross tons) has a significant effect on the reduction of RCF cracks. Based on field observations of grinding works, Schoech et al. [2006] propose 0.3 – 0.4 mm metal removal per 30 -40 MGT to control RCF.

The complex interactions between wear and RCF are of great commercial and safety significance to railways and merit further study.

4 Analysis of railway vehicle dynamics

This chapter examines principles of dynamic simulation of a railway vehicle along an arbitrary track. Section 4.1 explains why and how dynamic simulations are used to assess the behaviour of railway vehicles. Section 4.2 describes the application of ADAMS/Rail multi-body dynamic simulation software to real-world cases of railway vehicle dynamics. Models of railway vehicle and track are described as well. The wheel/rail contact models described in Chapter 3 are used here to model interaction between vehicle and track. The principles of the dynamics of railway vehicles on a straight track are discussed in Section 4.3, followed by Section 4.4, in which the dynamics of railway vehicles on curved track are explained. Special attention is given to derailment phenomena, described in Section 4.5. Section 4.6 concludes this chapter with a discussion.

4.1 Introduction

The large number of nonlinear components in a railway vehicle moving along a track creates a very complex mechanical system. In particular, interaction between wheel and rail is a very complex nonlinear element in the railway system. Wheel and rail geometries, involving both cross sectional profiles and geometry along the direction of movement, with varying shapes due to wear, have a significant effect on vehicle dynamic performance and operating safety.

With the advent of personal computers and faster processors, the use of analytical modelling programs has become less complicated, and far more practical. This is true in the area of rail vehicle modelling as well. The low cost of computer modelling compared with real-world testing is a significant benefit of the use of numerical modelling of railway vehicles. Such modelling allows a designer to test a new vehicle design without having to build a prototype and tie up a track for testing, thereby increasing productivity through saving valuable time and manpower. This cost savings advantage of railway vehicle modelling further magnifies the importance of its various uses and applications.

One such use is “what if” analysis. Computer modelling allows the user to test out various situations without spending the time, money, and use of equipment to test them on a track. Further, modelling can provide the means for derailment testing to enable prediction of when a given car might derail or overturn. Modelling can predict at what speeds derailment will occur, or under what conditions it may be prevented. Directly related to derailment studies is stability analysis; one can model multiple suspensions and loading options and examine dynamic responses.

Another important aspect of railway dynamics is ride comfort analysis, or predicting what travellers and cargo may experience under various conditions. Modelling software can predict forces and accelerations at various positions throughout the vehicle to model ride characteristics, or to evaluate ideas for improving ride quality.

The modelling programs that have received wide acceptance in recent years include:

- NUCARS,
- MEDYNA,
- VAMPIRE,
- SIMPACK,

- ADAMS/Rail,
- Universal Mechanism.

Although the above programs have differing attributes, they were all developed specifically for rail dynamic modelling. Each program includes different solution methodology, wheel/rail models, analysis methods, and user interface. Over the last several decades, ADAMS multibody simulation software, developed by MSC Software, has been widely used and has become the industry standard. The ADAMS/Rail module was developed within ADAMS to be used primarily for rail vehicle dynamic analysis. ADAMS/Rail provides a variety of output options that can be used for derailment and dynamic stability analysis, as well as for investigation of wheel/rail interaction.

The complete vehicle–track system can be split up into three subsystems: vehicle, wheel–rail contact, and track. In view of the vehicle and the track subsystems, the forces generated by wheel–rail contact can be regarded as external forces. The excitation of vehicle and track leads to motions. The corresponding kinematic quantities are fed back to the wheel–rail contact. The interchange of kinematics and the forces between the wheel–rail contact subsystem and the vehicle, and, respectively, the wheel–rail contact subsystem and the track occurs at nodes, where the subsystems are coupled.

The first step in every vehicle computer simulation is to set up a mechanical model appropriate to fulfil the desired simulation task. This model constitutes the basis for mathematical description using the equations of motion, obtained with the aid of physical principles and laws (Newton's laws, etc.). The multibody system (MBS) approach is a powerful and widely used method for this procedure, especially if the vehicle's running behaviour is to be analyzed. To avoid the time-consuming and error-prone task of compiling the mathematical model as a system of equations by hand, suitable professional software packages built upon this approach are commercially available. These provide the engineer not only with software tools for model setup, but also usually allow the application of a wide range of different numerical algorithms on the automatically generated system equations in a way optimised for the specific modelling and simulation task. A comprehensive survey of such simulation software in the field of wheel–rail systems is given in Iwnicki [1999]. The following descriptions are based on the simulation package ADAMS/Rail, a general multibody simulation tool with extended wheel–rail functionality. For detailed information about the modelling and simulation of railway vehicles, see for example Dukkipati [2000], Wickens [2003], and Iwnicki [2006].

To analyse the dynamic behaviour of railway vehicles running on arbitrary tracks under arbitrary manoeuvres, usually the vehicle (and if necessary the environment) is represented as a multibody system (see Figure 4.1). A multibody system consists of rigid bodies, interconnected via massless force elements and joints. Due to the relative motion of the system's bodies, force elements generate applied forces and torques. Typical examples of such force elements are springs, dampers, and actuators combined in primary and secondary suspensions of railway vehicles. Contrarily, joints give rise to constraint forces by constraining the relative motion of the system's bodies. The scope of application begins with simple single-axis rotational joints, and ends with highly complex and specific ones, like the so-called 'wheel–rail joints' guiding bodies along arbitrary tracks. Usually, the user can rely on extensive libraries of connecting elements in setting up the simulation model.

To take the flexibility of lightweight structures into account, an interface between MBS software and Finite Element (FE) software has been implemented in many simulation programs. In the first step, a number of mode shapes of the body to be modelled elastically are

calculated by FE analysis. Then the results are transferred to the multibody simulation, resulting in a "hybrid" model consisting of rigid and elastic bodies. Finally, on behalf of a dynamic stress analysis of the flexible body's most vulnerable locations, the dynamic forces and accelerations following from time-integration of the system equations can be shifted back to the FE software (Schupp et al. [2004]).

In the present research, MBS software package ADAMS/Rail is used to perform assessment of the dynamic properties of the railway vehicle running on a track with the newly designed wheel (and/or rail) profile. In this chapter, a general approach to vehicle and track modelling is described, with details on the particular vehicles used in the application cases of wheel profile design described in Chapter 7. Also, specific behaviour of the railway vehicle on straight and curved track is described. First, the modelling of a railway vehicle in ADAMS/Rail multibody software is described.

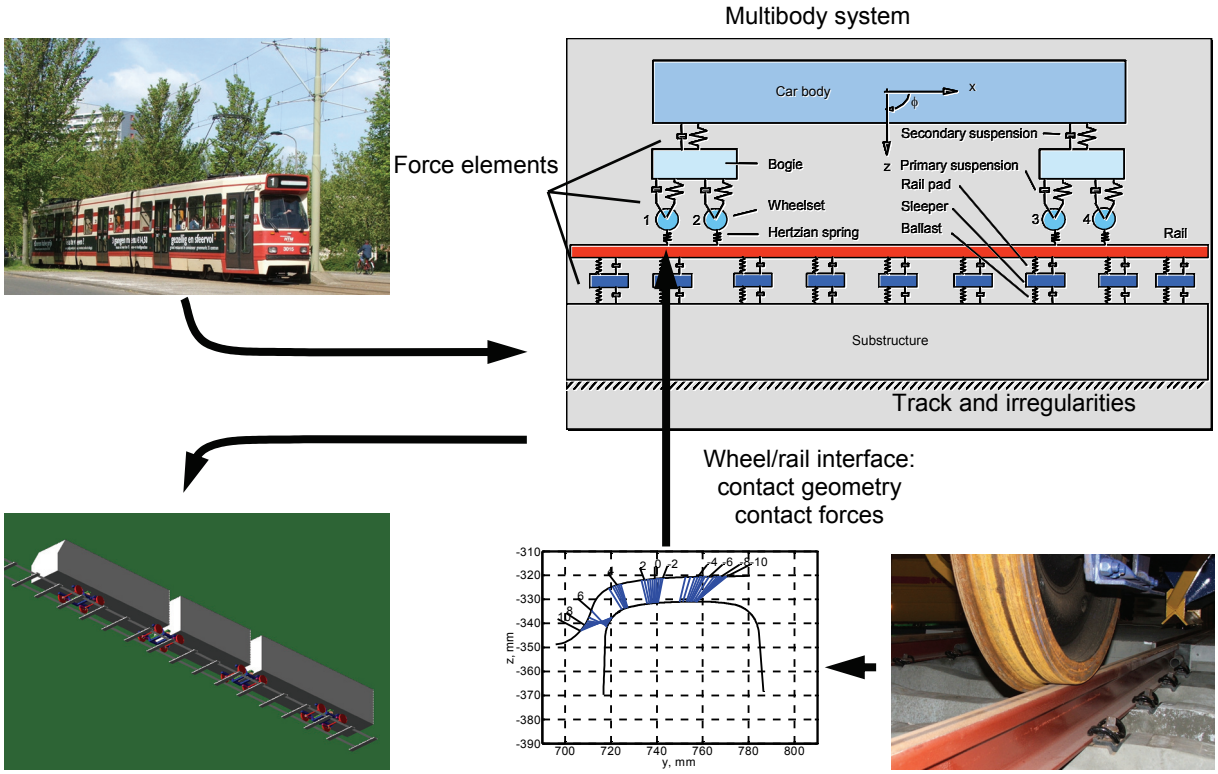

Figure 4.1: Generic simulation model for design and analysis of a railway vehicle's running behaviour.

4.2 Analysis of railway vehicle dynamics in ADAMS/Rail

In this section, the modelling of a railway vehicle in ADAMS/Rail is described. The multibody system rail vehicle analysis tool ADAMS/Rail is used in all time-domain simulations presented in this thesis.

4.2.1 ADAMS/Rail multibody computer package

The first step in wheel/rail profile evaluation procedure is the realisation of a multibody model of the complete railway vehicle and track combination. This is performed to evaluate contact-specific parameters, such as wheel/rail forces, relative positions, and creepages.

The complete railway system (see Figure 4.2) in ADAMS/Rail consists of a vehicle model, a track model, and contact elements. In the first stage, these models are built separately and, afterwards, they are assembled in order to obtain the complete railway system.

The vehicle model contains all necessary information (for the chosen level of discretisation) about the vehicle design: rigid bodies, suspensions, dampers, bumpstops, etc. The track model includes an analytical description of the track layout (horizontal and vertical curvature, cant, gauge variations, etc.), together with measured or analytically generated irregularities and a description of the rail profiles (constant or variable along the track). Contact elements are used to model wheel/rail interactions. As mentioned in Section 3.3, three different contact models are available in ADAMS/Rail:

- WRQLT – Quasi-linear contact, using wheel and rail profiles defined by equivalent conicity parameters, used for stability analysis;
- WRTAB – Tabular contact element. This uses a precalculated contact table to evaluate the contact geometry during the simulation;
- WRGEN – General contact element. This is the more detailed contact element; it uses the actual wheel/rail profiles at each simulation step, and it allows multipoint contact.

In the present work, the general contact element is used in all simulation cases, unless another contact model is explicitly mentioned. ADAMS/Rail provides information about the load and tractions applied to the entire wheel/rail contact patch and its location. In the current models, it is assumed that contact between wheel and rail can be approximated by an elliptical contact patch. This allows the use of a faster solution method to determine the traction and slip distribution within the contact. ADAMS/Rail provides the total normal force, the traction applied, and the semi-axes a and b for each elliptical contact patch. Using these values, local contact analysis is performed. For detailed information about the wheel/rail contact element in ADAMS/Rail see Section 3.3 and ADAMS/Rail [2005].

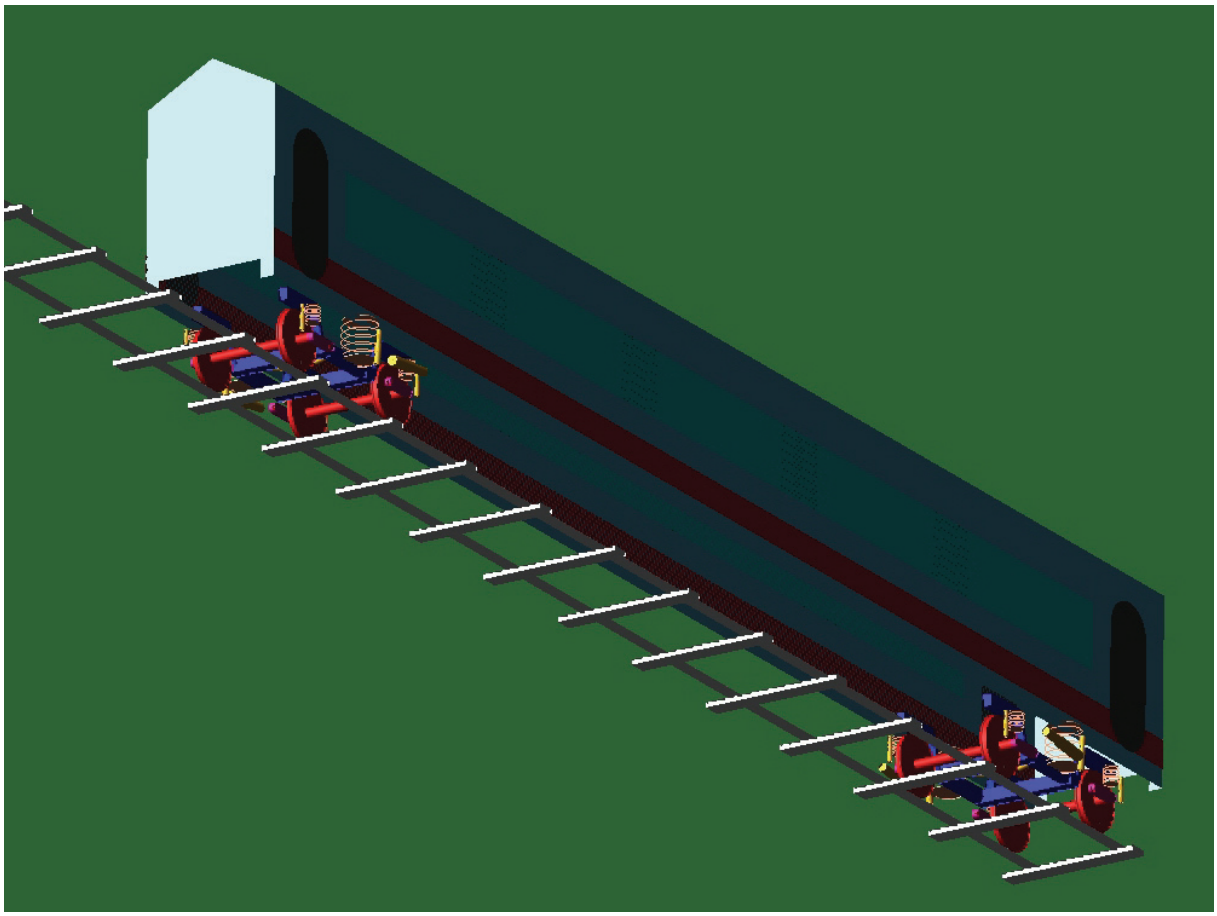

Figure 4.2: Complete railway system modelled in ADAMS/Rail.

In ADAMS/Rail, the dynamic behaviour of a railway vehicle can be analysed using three types of analysis:

- linear analysis, for the evaluation of the vehicle model eigenvalues;
- stability analysis, used for the evaluation of the critical speed of the vehicle;
- dynamic analysis, to simulate the actual behaviour of the railway system in operating conditions.

The linear analysis (also called modal analysis) performs an eigenvalue calculation on the matrices that represent the equations of motion. This will indicate the natural frequencies of the various modes of oscillation. The motion can be self-exciting and become unstable, and the eigenvalue analysis can indicate the critical speed at which this instability, or hunting, may occur. In practice, vehicle speed gradually increases until the real part of the complex eigenvalues is not negative, but equal to zero. This speed corresponds to the critical speed of the vehicle.

The stability analysis performs a series of vehicle dynamic simulations with multiple equivalent conicity values (using linearised wheel/rail contact), providing the value of the critical vehicle speed for each conicity value. Vehicle stability is discussed further in Section 4.3.

The dynamic analysis method is used to calculate, as a function of time, all meaningful quantities related to the dynamic behaviour of the vehicle and the wheel/rail contact. In order to integrate calculation of wheel wear and RCF and the results of dynamic analysis, the output must be enhanced to include such quantities as contact patch dimensions and contact forces, necessary for wear, RCF, and dynamics evaluation. Additionally, a specific toolkit has been created to export calculation data in ASCII format. The quantities discussed in Chapter 3 and included in the output file are shown in Table 4.1.

Table 4.1: Quantities calculated from dynamic analysis.

Quantity	Symbol	Units
Simulation time	t	S
Contact ellipse longitudinal semi-axis	a	M
Contact ellipse lateral semi-axis	b	M
Contact point position on wheel and rail profiles	CPw, CPr	M
Normal and tangential contact forces	F_z, F_x, F_y	N
Longitudinal creepage	ξ	
Lateral creepage	η	
Spin creepage	ϕ	
Rolling radius at contact point	r	m
Longitudinal velocity	V	m/s
Actual friction coefficient at contact point	μ	

4.2.2 Equations of motion of multibody systems

The first stage in setting up a computer model is to prepare a set of mathematical equations that represent the vehicle – track system. These are called the equations of motion and are usually second order differential equations that can be combined into a set of matrices. The equations of motion can be prepared automatically by the computer package; a user interface collects vehicle parameters, described in graphical form or by entering sets of coordinates,

along with other data describing all the important aspects of body, and suspension components.

The vehicle is represented by a network of bodies connected to each other by flexible, massless elements. This is called a multibody system, and the complexity of the system can be varied to suit the simulation and the type of results required. Each of the rigid bodies can be considered to have a maximum of six degrees of freedom, three translational and three rotational. Physical constraints may mean that not all of these movements are possible, and the system can be simplified accordingly. Application of the constraint equations results in a set of equations of motion which are ordinary differential equations (ODE) or linear algebraic equations (LAE) and ODEs, depending on how the constraint equations are used.

There are various coordinates and formalisms that lead to suitable descriptions of multibody systems, each possessing relative advantages and drawbacks for derivation of the equations of motion of the system. It is outside the scope of this dissertation to discuss what is the most efficient multibody methodology that could be applied to vehicle dynamics analysis. In this work, the methods presented are based on the use of Cartesian coordinates, which lead to a set of differential-algebraic equations that need to be solved. It is assumed that appropriate numerical procedures are used to integrate the type of equations of motion obtained with the use of Cartesian coordinates. It is also assumed that the various numerical issues that arise from the use of this type of coordinates, such as the existence of redundant constraints and the possibility of achieving singular positions, are also solved. For a more detailed discussion of the numeric aspects of this type of coordinates, the interested reader is referred to Nikravesh [1988], Petzold [1994], and Augusta Neto and Ambrósio [2003].

A typical multibody model is defined as a collection of rigid or flexible bodies that have their relative motion constrained by kinematic joints that are acted upon by external forces. An example of multibody representation of a railway vehicle is presented in Figure 4.3. Let the multibody system be made of *nb* bodies. The equations of motion for the system of unconstrained bodies are

$$\mathbf{M}\ddot{\mathbf{q}} = \mathbf{g}, \tag{4.1}$$

where $\mathbf{M}$ is the mass matrix, which includes the masses and inertia tensors of the individual bodies, $\mathbf{q}$ is the vector of generalized coordinates, and correspondingly $\ddot{\mathbf{q}}$ is the acceleration vector, and $\mathbf{g}$ is the vector with applied forces and gyroscopic terms.

The relative motions between the bodies of the system are constrained by kinematic joints, which are mathematically described by a set of *nc* algebraic equations, written as

$$\mathbf{\Phi}(\mathbf{q}, t) = 0. \tag{4.2}$$

The first and second time derivatives of equation (4.2) constitute velocity and acceleration constraint equations, respectively, written as

$$\begin{aligned} \dot{\mathbf{\Phi}}(\mathbf{q}, t) &\equiv \mathbf{D}\dot{\mathbf{q}} = \upsilon, \\ \ddot{\mathbf{\Phi}}(\mathbf{q}, \dot{\mathbf{q}}, t) &\equiv \mathbf{D}\ddot{\mathbf{q}} = \gamma, \end{aligned} \tag{4.3}$$

where $\mathbf{D}$ is the Jacobian matrix. For a system of constrained bodies, the effect of the kinematic joints can be included in equation (4.1) by adding to its right-hand side the equivalent joint reaction forces $\mathbf{g}^{(c)} = -\mathbf{D}^T\boldsymbol{\lambda}$, leading to

$$\mathbf{M}\ddot{\mathbf{q}} = \mathbf{g} - \mathbf{D}^T\boldsymbol{\lambda}, \tag{4.4}$$

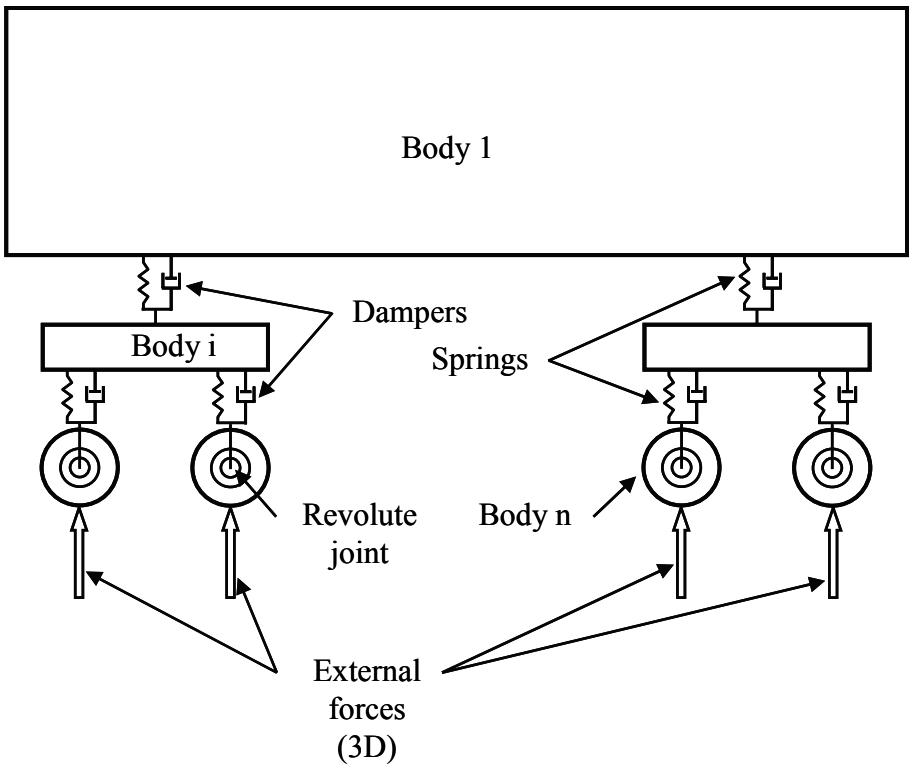

Figure 4.3: Generic multibody system of railway vehicle.

where $\boldsymbol{\lambda}$ is a vector with *nc* unknown Lagrange multipliers. Equation (4.4) has $nb+nc$ unknowns that must be solved together with the second time derivative of the constraint equations. The resulting system of differential-algebraic equations is

$$\begin{bmatrix} \mathbf{M} & \mathbf{D}^T \\ \mathbf{D} & \mathbf{0} \end{bmatrix} \begin{bmatrix} \ddot{\mathbf{q}} \\ \lambda \end{bmatrix} = \begin{bmatrix} \mathbf{g} \\ \gamma \end{bmatrix}. \tag{4.5}$$

Note that the solution of equation (4.5) presents numerical difficulties resulting from the need to ensure that the kinematic constraints are not violated during the integration process.

After grouping the force matrixes according to coordinate vectors, the equations of motion for the vehicle will have the following form:

$$\mathbf{M}\ddot{\mathbf{q}}(t) + (\mathbf{H} + \Omega_0 \mathbf{G})\dot{\mathbf{q}}(t) + (\mathbf{K} + \Omega_0^2 \mathbf{Z})\mathbf{q}(t) = \mathbf{h}(t), \tag{4.6}$$

where the vector $\mathbf{q}(t)$ contains the generalized coordinates, matrix $\mathbf{M}$ is the mass matrix, matrix $\mathbf{H}$ is the damping matrix resulting from viscous coupling elements between the wheelset, the bogie frame, and the car body, and matrix $\mathbf{K}$ is the stiffness matrix resulting from the elastic coupling elements and the modal stiffnesses of the wheelsets. The matrices $\Omega_0 \mathbf{G}$ and $\Omega_0^2 \mathbf{Z}$ describe gyroscopic and centrifugal forces, respectively. The vector $\mathbf{h}(t)$ represents generalized external forces resulting from wheel–rail contact, from gravitation, and from nonlinear yaw damping. Because of the symmetric structure of the vehicle, the equations of motion can be split up into two separate systems for symmetric and asymmetric motions.

Dynamic analysis of a multibody system requires that the initial conditions of the system, i.e., the position vector $\mathbf{q}^0$ and the velocity vector $\dot{\mathbf{q}}^0$, are given. With this information, equation (4.6) is assembled and solved for the unknown accelerations, which are in turn integrated in time together with the velocities. The process, schematically shown in Figure 4.4, proceeds until a system response is obtained for the required period.

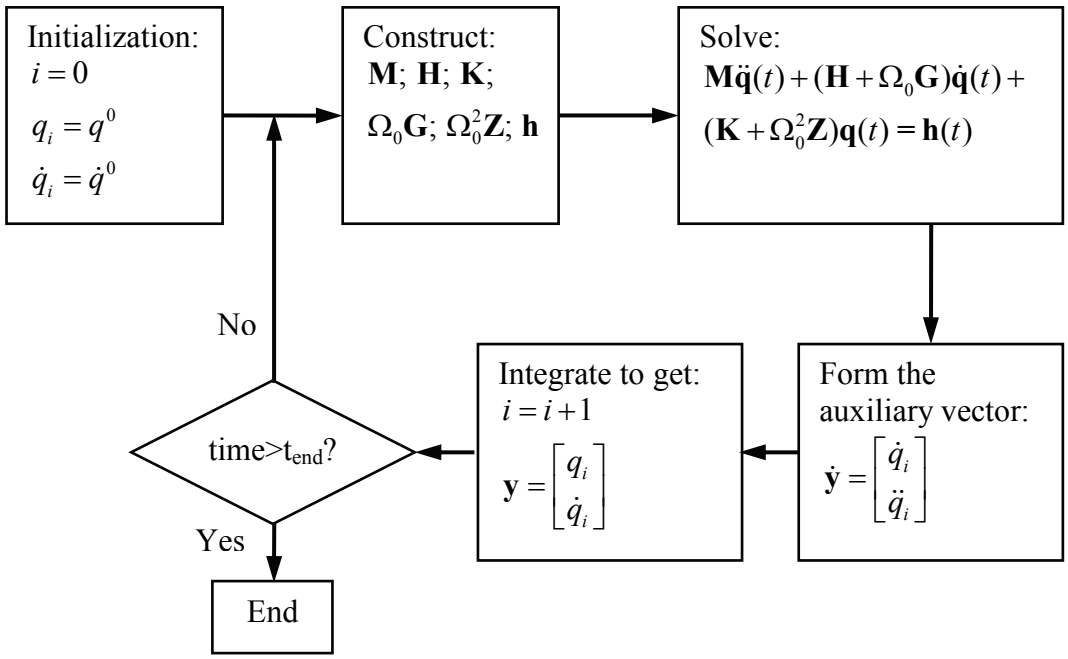

Figure 4.4: Flowchart representing the dynamic analysis of a multibody system.

Thus, the problem is reduced to solving a set of differential-algebraic equations (DAE). Furthermore, all time-domain analyses are performed with the second order Runge-Kutta integration method.

Once equations of motion can be compiled and integrated, they can provide us with the information about variation in response for different vehicle designs. Three vehicle designs are discussed in the next subsection.

4.2.3 Model of a railway vehicle

The typical model of a railway vehicle is presented in Figure 4.2, and is composed of the three sub-assemblies: the car body, the front bogie, and the rear bogie. Each bogie consists of the bogie frame, the bolster, and two wheelsets. In this research, the car body and bogie frames, as well as the wheelsets are treated as rigid bodies and are defined by their mass–inetria characteristics (mass, moments of inertia, and the position of the centre of gravity), and by the relative position of the bogies with respect to the car body itself. Each rigid body has six degrees of freedom, viz. three translations and three rotations. All bodies are connected by linear and non-linear springs and dampers, representing the primary and secondary suspensions, as shown in Figure 4.5. Primary and secondary suspensions are often used to support the car components and to provide vibration isolation. The primary suspension is connected between the wheelset and the side frame, while the secondary suspension is connected between the bolster and the side frame. The primary and secondary suspensions consist of spring, damper, and friction elements.

Passenger railway vehicle suspensions are designed to ensure that the natural frequencies associated with the rigid body modes of the bogie and the car body are below 10 Hz, in order to provide adequate vibration isolation. Knothe and Grassie [1993] emphasize this fact and pointed out that at this low frequency range, the track behaves as a relatively stiff spring. As the frequency increases, track inertia becomes increasingly important.

Depending on their mode of utilization, railway vehicles can have differing designs and composition. Below, three railway vehicle designs are considered, in particular, tram, metro

and passenger coach. Later, models of these vehicles will be used to assess currently existing and designed (hypothetical) wheel and rail profiles. First, we consider the passenger coach as the most classical example of railway vehicle design.

4.2.3.1 Model of a passenger coach

Figure 4.2 presents a typical view of the passenger coach in the ADAMS/Rail environment. One vehicle is considered only, i.e., there are no coupled vehicles to form a train. In Figure 4.5, a view zoomed to the bogie model is shown. A short overview of the main vehicle properties is presented in Table 4.2. The data are used for ERRI (European Railway Research Institute) model of passenger coach (see ADAMS/Rail [2005]). The front and rear bogies are equal, except for the position of the yaw dampers, which is symmetrical with respect to the middle of the car body. The single bogie basically comprises the bogie frame, two wheelsets, suspensions, and dampers connecting the bogie frame to the wheelsets and to the car body. The masses of other components in the bogie, like auxiliary elements, springs, and dampers, are reduced to the bogie frame.

Primary and secondary suspensions are represented with linear and non-linear elastic elements, while the corresponding dampers are treated as viscous elements.

The connections between the bogie frame and the wheelsets are represented by the primary suspension vertical springs, and by concentrated elastic bushing elements representing the axlebox-wheelset connection. The yaw damper is represented by a viscous damper in series to a spring.

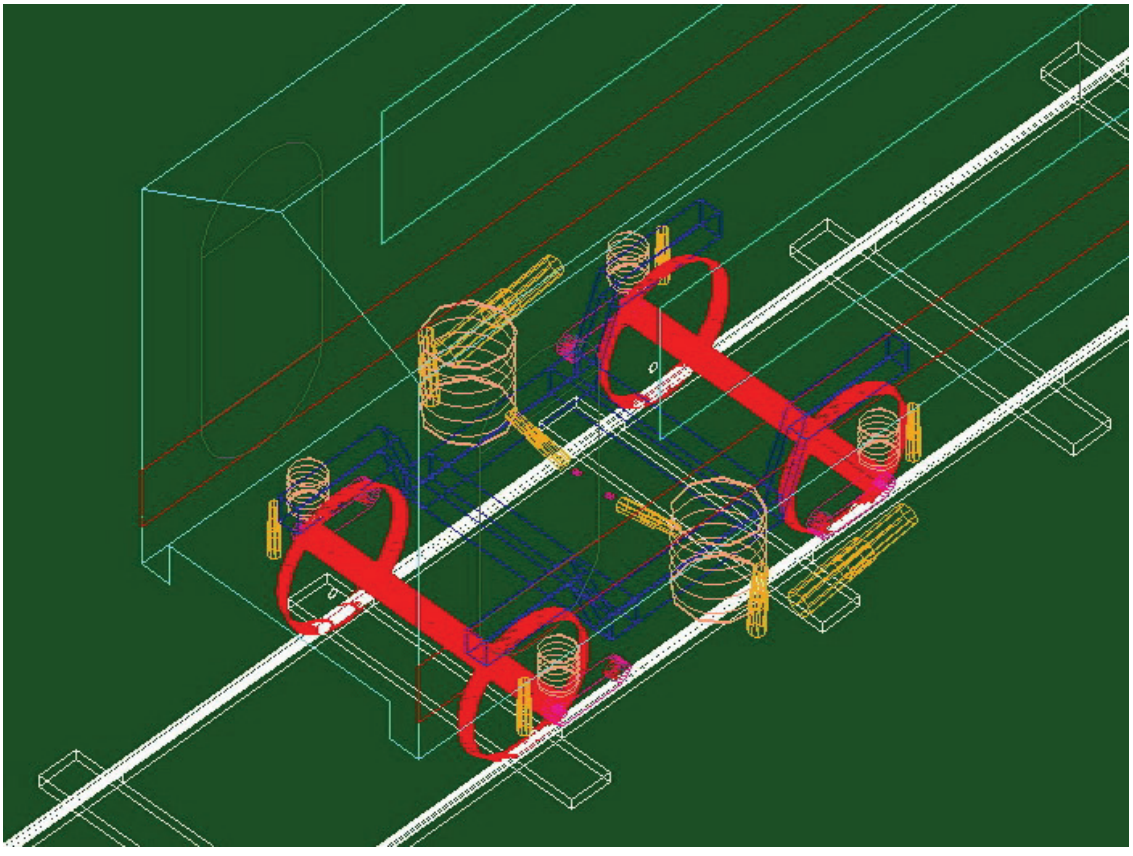

Figure 4.5: Multi-body model of the vehicle (zoomed on one bogie).

Table 4.2: Overall data for a passenger coach.

Parameter	Value	Units
Total mass	32000	kg
Total length	24	m
Bogie distance	19	m
Wheelset distance	2.56	m
Nr. of wheelsets	4, in 2 bogies	
Wheel radius	0.460	m
Track gauge	1.435	m
Minimum curve radius	25	m

4.2.3.2 Model of a metro coach

The metro vehicle, shown in Figure 4.6, is used by Rotterdamse Electrische Tram N.V. company (RET, Rotterdam, The Netherlands) in their operations. It is an electric two-car unit composed of two powered vehicles with an articulated bogie in the middle.

Due to absence of realistic mass–inertia properties, and the stiffness and damping values of the RET metro vehicle, the vehicle model used here was made geometrically similar with regard to wheel/rail contact, while body and suspension properties were taken from an ERRI vehicle. Therefore, calculated values cannot be used in an absolute sense, but only for comparison between different wheel and/or rail profiles. A characteristic feature of this vehicle is its smaller wheel radius (390 mm) in comparison with the conventional passenger coach.

Figure 4.6: Metro train, RET. Courtesy of www.retmetro.nl.

4.2.3.3 Model of a tram

The trainset, shown in Figure 4.7, is used by Haagsche Tramweg Maatschappij N.V. company (HTM, The Hague, The Netherlands) in their operations. It is an electric three-car unit composed of two powered end-coaches and one intermediate coach that rests on articulated bogies. A short overview of the main properties of this tram is presented in Table 4.3.

Railway bogies can be classified as non-articulated or articulated, according to the suspension. Two non-articulated bogies usually support one railcar body (see Figure 4.2), but one articulated bogie supports the back end of the forward car and the front end of the rear car (see middle bogies in Figure 4.7). Although the articulated bogie has some disadvantages, such as complex structure, increased axle load due to support of one body by one bogie, and difficult maintenance, it offers various advantages, including a lower centre of gravity, better ride comfort because car ends do not overhang bogies, and reduced length of trainset, as couplers are absent.

Only the front vehicle is modelled in the present study; this is done to reduce simulation time in ADAMS/Rail. Simulation time increases proportionately to the number of wheel/rail contact problems. Therefore, for a vehicle with eight wheelsets, the calculation time is twice as long as that for a vehicle with four wheelsets. The front bogie of the tram experiences the greatest flange wear; therefore, our primary investigation is focused on the dynamic behaviour of the front bogie. Consequently, simplification of the tram model to a model of the front vehicle is feasible, as far as the front bogie is concerned.

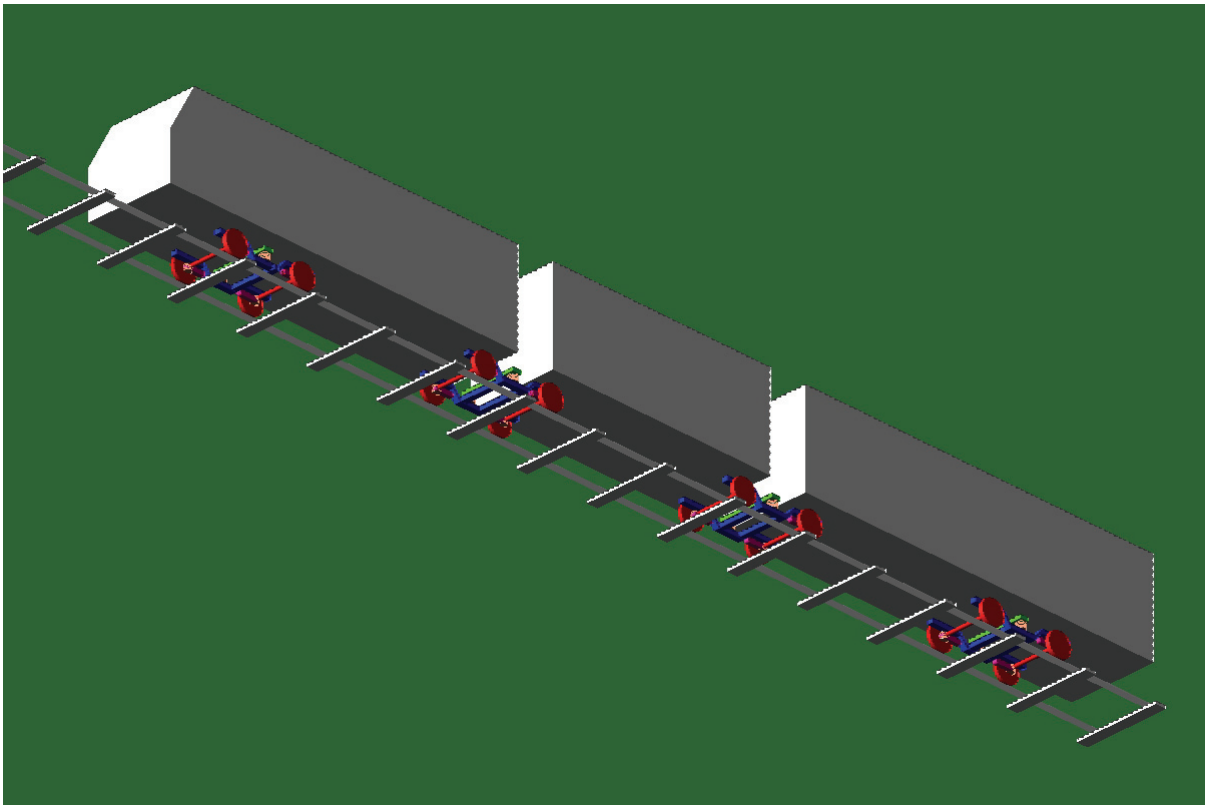

Figure 4.7: Tram modelled in ADAMS/Rail.

Table 4.3: Overall tram data (from Wiersma [2000]).

Parameter	Value	Units
Total mass	38800 (empty)	kg
Mass of the front car body	8700	kg
Mass of the middle car body	5600	kg
Mass of the rear car body	8200	kg
Total length	27.000	m
Length of the front car body	9.960	m
Length of the middle car body	5.820	m
Length of the rear car body	9.960	m
Bogie distance	6.9 front and rear cars 5.4 middle car	m
Wheelset distance	1.905	m
Nr. of wheelsets	8, in 4 bogies	
Wheel radius	0.331	m
Track gauge	1.435	m
Minimum curve radius	17	m

4.2.4 Model of railway track

A characteristic feature of railway vehicles is the support and guidance of the vehicle by a railway track. Standard track geometry is composed of sections such as straight track (tangents), curve entries (transition curves), constant radius curves, superelevations, grades and vertical curves, crossovers, switches, etc. To simulate manoeuvres on arbitrary tracks, standard track designs or measured tracks can be incorporated into the track layout description. In reality, the layout of a track deviates from the desired geometry. The causes for these deviations (or irregularities) can be traced to temperature variations, design tolerances, excessive dynamic and static loads, deterioration, and wear. In ADAMS/Rail simulations, analytical or measured track irregularities can be used. Analytic irregularities are defined as lateral, vertical, cant, or gauge deviations from the ideal track centre line. The measured irregularities are defined as vertical, lateral, or both vertical and lateral, deviations from the nominal geometry for right and left rail, separately. Stochastic irregularities can be defined either directly as measured data, or by the power spectral density, that is, as a stochastic, stationary process.

In ADAMS/Rail, the nominal track geometry (layout) is defined by the length and curvature of a curve, the length and curvature of transition curves, track cant, track gauge, rail profile, and rail inclination.

For simplicity, the rack used in this research is modelled as rigid. However, in ADAMS/Rail, the flexibility of the track can be taken into account. The track flexibility model is based on the concept of so called “moving track piece”, which follows under each wheelset and incorporates four distinct rigid bodies: two rails, a track piece and a ground. The ground is fixed. Each rail is connected laterally and vertically with the track by linear springs in series with linear dampers. In the same manner, the track piece is connected laterally and vertically with the ground.

As mentioned, the vehicle model and the track model are connected through the wheel/rail contact model, described in Section 3.3. Once a model of a railway system is completed, the dynamic behaviour of railway vehicles on straight and curved track can be investigated.

4.3 Dynamics of vehicles on straight track

In the absence of large track irregularities, the dynamics of a railway vehicle on a straight track mainly depend on the stability of vehicle motion. Stability of running vehicles is one of the important design criteria for railway and road vehicles. Railway vehicle stability is based on kinematics, as well as on contact mechanics. This area of research stretches back to the 19th century, and had its first breakthrough in the works of Carter [1926] and Rocard [1935] on the stability of locomotives. During the 1960s, a theoretical comprehension of railway vehicle stability emerged as a result of studies based on linearised models. Representative of this development are the works of Matsudaira, Wickens, De Pater and Joly. More detail about historical development of stability research can be found in Wikens [1998, 2003], Gilchrist [1998], and Knothe and Bohm [1999]. Research in this field still continues, with the works of True [1999], Polach [2006], and other researchers.

4.3.1 Definition of stability

The meaning of stability can be easily explained with respect to wheelset motion. Stability means that for a slight lateral displacement or yaw angle, the wheelset moves back into its central position with a damped oscillatory parasitic motion. The wheelset motion is considered to be unstable if, for some small irregularity, an excited vibration takes place, such that the maximum amplitude increase and the oscillating parasitic motion is finally restricted only by wheel flange contact.

This unstable behaviour is called hunting and can result in damage or derailment. The speed at which hunting initiates is called the critical speed for the vehicle. If only the wheelsets and bogies are subject to unstable movement, this is called bogie instability or bogie hunting. If the wheel/rail contact conditions lead to low frequency oscillations, the car body sometimes moves together with the bogies. This is called car–body instability, or car–body hunting.

The frequency of sinusoidal wheelset and bogie motion is related to wheel/rail contact geometry. The linear, purely kinematic motion of a single wheelset was solved by Klingel, see equation (2.1) in Section 2.2.1.1. For a two-axled vehicle or a bogie with rigid primary suspension and a rigid frame, purely kinematic motion is no longer possible.

The wheel/rail profile combination is one of the most important factors influencing railway vehicle stability. Wickens [1965a, 1965b] was the first to solve the problem of railway vehicle instability theoretically. He refined the equations of motion, and took into account additional effects such as gravitational stiffness (which is of importance for worn profiles) and damping. Basic mechanical aspects, as well as mechanical techniques for solving the stability problem, were presented very clearly. Finally, the influence from various parameters was investigated carefully, such that a basis for better bogie design would become available. Through his parametric studies, Wickens was able to show that it is possible to choose parameters such that car body instability could be avoided. Since that time, many papers have been published on various aspects of railway vehicle stability problems.

4.3.2 Stability analysis

An eigenvalue analysis of a vehicle can be used to obtain information about the stability of vibrations at each mode; this is useful in establishing the critical speed of a vehicle, above which hunting instability will occur. This approach is briefly discussed in Section 4.2.1. However, this method for establishing the critical speed of a vehicle should be used with caution, as it relies on the linearised equations of motion. The wheel/rail interface is highly nonlinear even for small displacements, and the linearised conicity parameter, which must be

used for a linear analysis, cannot fully represent this situation. This problem is investigated by Polach [2006].

At present, linear stability analyses are performed for newly designed vehicles. Linear stability analysis is integrated in most computer programs for multibody systems, for example, ADAMS, SIMPACK, MEDYNA, NUCARS or VAMPIRE. An alternative method is to perform time-step integration to find limit cycles for railway vehicles. A time-domain simulation using the full nonlinear equations of motion allow the determination of the speed at which the oscillations of vehicle motion (especially wheelset lateral displacement) damp out after a disturbance. However, application of computer codes does not always provide an ideal solution. Regarding railway vehicle dynamics, none of the computer codes is able to calculate automatically nonlinear critical speed.

An example of vehicle hunting with an increase of the vehicle speed is presented in Figure 4.8. In this figure, lateral displacement versus travel distance is shown for the first wheelset. The vehicle is moving on a straight track with a single horizontal lateral ramp at 50 m from the beginning of the track. This ramp initiates vehicle oscillation, which is damped out if the vehicle is stable. From Figure 4.8, it can be seen that with an increase in speed from 90 to 100 m/s, the amplitude of wheelset lateral displacement significantly increases. This amplitude reaches its limit value, defined by the flange clearance, and the wheelset is then moving from one side of the track to the other making flange contact with the rails. As is evident, at 100 m/s this vehicle is unstable.

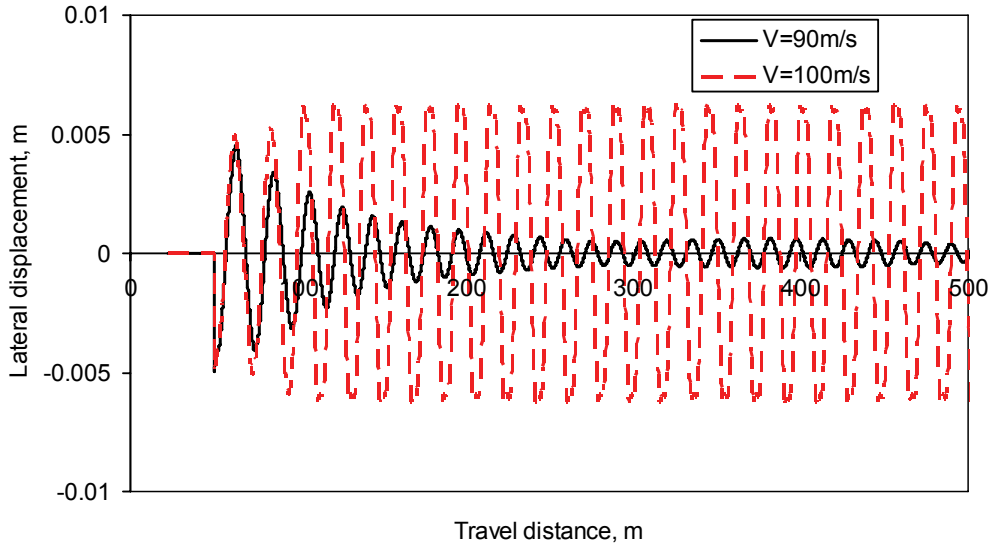

Figure 4.8: Lateral displacement of the first wheelset with S1002 wheel profile at 90 m/s and 100 m/s.

The influence of wheel profile on wheelset behaviour is evident in Figure 4.9. Two wheelsets move at 90 m/s. One wheelset is equipped with S1002 wheel profile, while another is equipped with the Conical profile (see Figure 2.18 from Section 2.4). Both wheelsets are stable, because wheelset oscillations are damping out. However, oscillations of the wheelset with curvilinear S1002 profile are damping out faster than oscillations of the wheelset with a linear conical profile. Figure 4.9 confirms the importance of wheel profile for vehicle stability on straight track.

The effect of equivalent conicity (see section 2.2.1.3) on the critical speed for a passenger vehicle equipped with purely conical wheels is presented in Figure 4.10. As is evident from

this figure, with an increase of the equivalent conicity, the critical speed of the vehicle is reduced.

It should be noted that in the cases presented (Figure 4.8 - Figure 4.10), the simulations have been performed with the ERRI model of the passenger vehicle. This vehicle is designed for high speed; therefore, it is stable at such speed (90 m/s). Other vehicles with the same wheels as considered here may have different critical speeds.

After the problems of railway vehicle motion on a straight track have been considered, our attention shifts to the vehicle moving on a curved track.

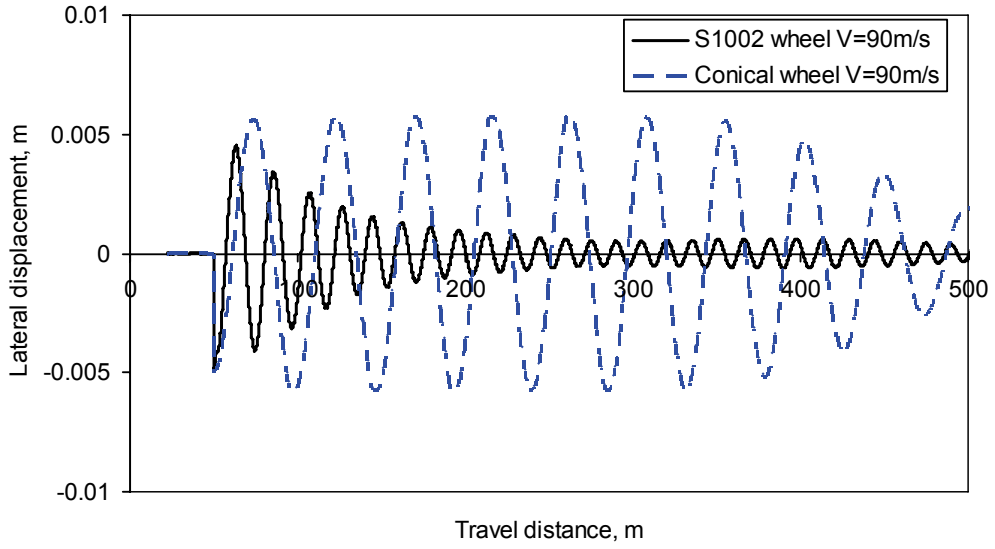

Figure 4.9: Lateral displacement of the first wheelset with S1002 and Conical wheel profiles at 90 m/s.

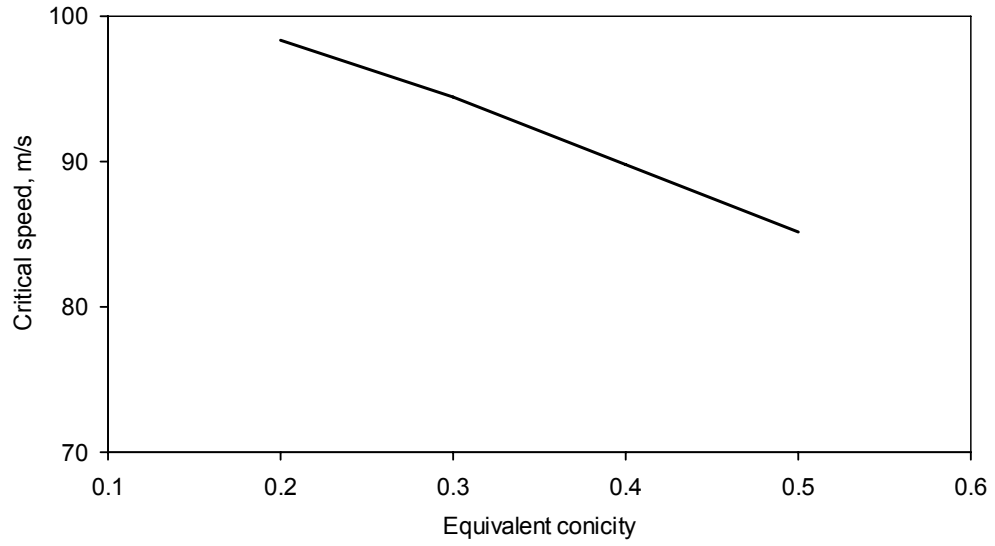

Figure 4.10: Effect of effective conicity on critical speed of a passenger vehicle.

4.4 Dynamics of vehicles on curved track

The dynamic behaviour of a railway vehicle on a curved section of track is significantly different from one on a straight track. Newland [1968] and Boocock [1969] independently derive equations of motion of the curving vehicle. Newland's model makes useful

simplifications, but Boocock analyses several configurations, including a complete bogie vehicle, a two-axle vehicle, and vehicles with cross-braced bogies. He also includes in equations of motion the effects of gravitational stiffness and spin creep. Most important of all, Boocock was able to obtain experimental full-scale confirmation of his theory using the two-axle research vehicle HSFV-1. These linear theories are valid only for large radius curves. On most curves, the curving of conventional vehicles involves the same nonlinearities due to creep saturation and wheel – rail geometry that are noted in hunting. At the present time, general vehicle dynamic simulation programs are used for the analysis of curving behaviour of the railway vehicle (see Section 4.1).

Railway vehicles use one of two methods to negotiate curved sections of track. Shallow curves are negotiated with lateral wheelset displacement, which produces a difference in the rolling radii of the right and left wheels, and generates a turning motion. For sharper curves, the bogies use wheel flange contact to generate large wheel/rail contact forces, and to increase the turning moments about their centres of gravity. As the wheelsets are constrained by longitudinal and lateral springs connecting them to the bogie, the wheelsets are not able to take up the radial attitude of perfect steering described by Redtenbacher (see Section 2.2.2).

Since the wheels have a conical shape and taper toward the outside of the track, wheelset lateral displacement causes a difference in the rolling radii of the left and right wheels. This, in turn, causes a difference in wheel velocities, and leads to yawing of that wheelset. The wheelset balance a yaw couple applied to it by the suspension by moving further in a radial direction. This generates equal and opposite longitudinal creep forces in left and right wheel/rail contact and wheelset balance a lateral force by yawing further. For the complete vehicle, the position of the vehicle in the curve and the set of forces acting upon it, are obtained by solving the equations of equilibrium. If all the wheelsets of the bogie displace to one side, a common turning motion translates to yawing of the bogie and allows it to roll smoothly through the curve. Figure 4.11 shows the two-axle bogie displaced to the left to negotiate a shallow, right hand curve.

Lateral movement of the wheelsets creates the rolling radii difference that allows the wheelsets to roll through the curve. As the curvature increases, the wheelset displaces more and generates a larger difference of the wheel radii, increasing the rate of yaw rotation. The yaw rotation rate, and hence the curvature that the wheelset can smoothly roll through, is limited by the maximum wheel radii difference. This, in turn, is limited by the clearance between the wheel flanges and the rail (the gauge clearance). For the sharper curves, the bogie curves with flange contact, as shown in Figure 4.12 and discussed below.

Beyond a certain curvature, flange contact occurs at the outside wheel of the first axle. This generates a large wheel/rail contact force and increases the magnitude of the bogie turning moment. This additional moment increases the bogie yaw rate, allowing it to negotiate the tighter curve. As curvature increases, the bogie yaws more into the outside rail to increase the contact force on the wheel flange. Eventually, the bogie yaws enough for the inside wheel on the trailing axle to contact the rail. Now, flange forces at both the outside lead wheel and the inside trailing wheel generate turning moments about the bogie centre of gravity, producing a higher rate of yaw. For still sharper curves, the bogie becomes pinched between the rails. The magnitudes of the flange contact forces increase with increasing curvature, first causing rail damage and eventually leading to the wheels climbing the rail.

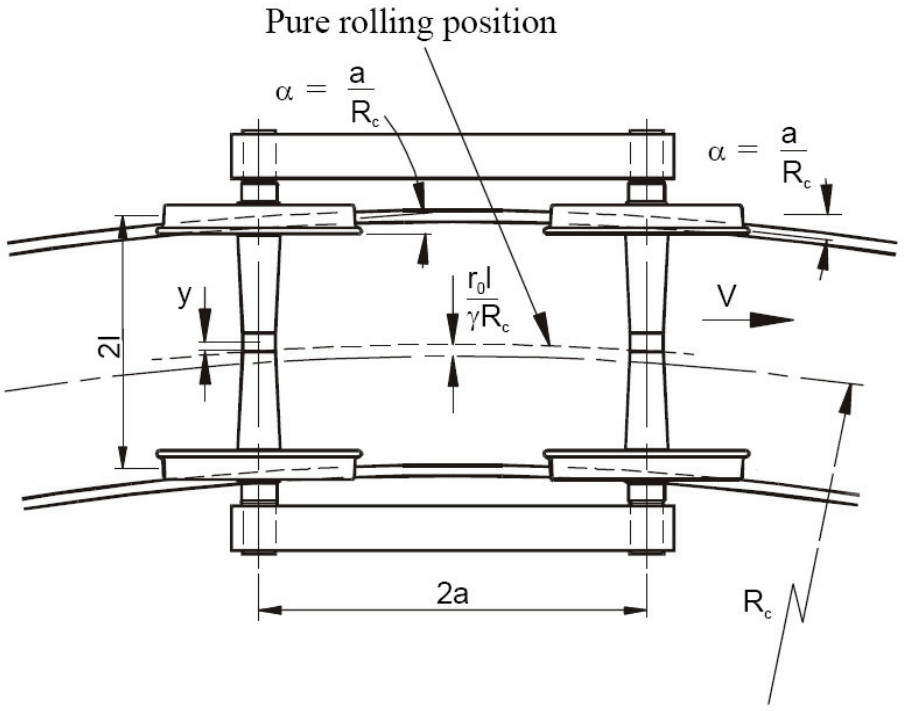

Figure 4.11: Lateral displacement of the bogie in a curve at equilibrium position.

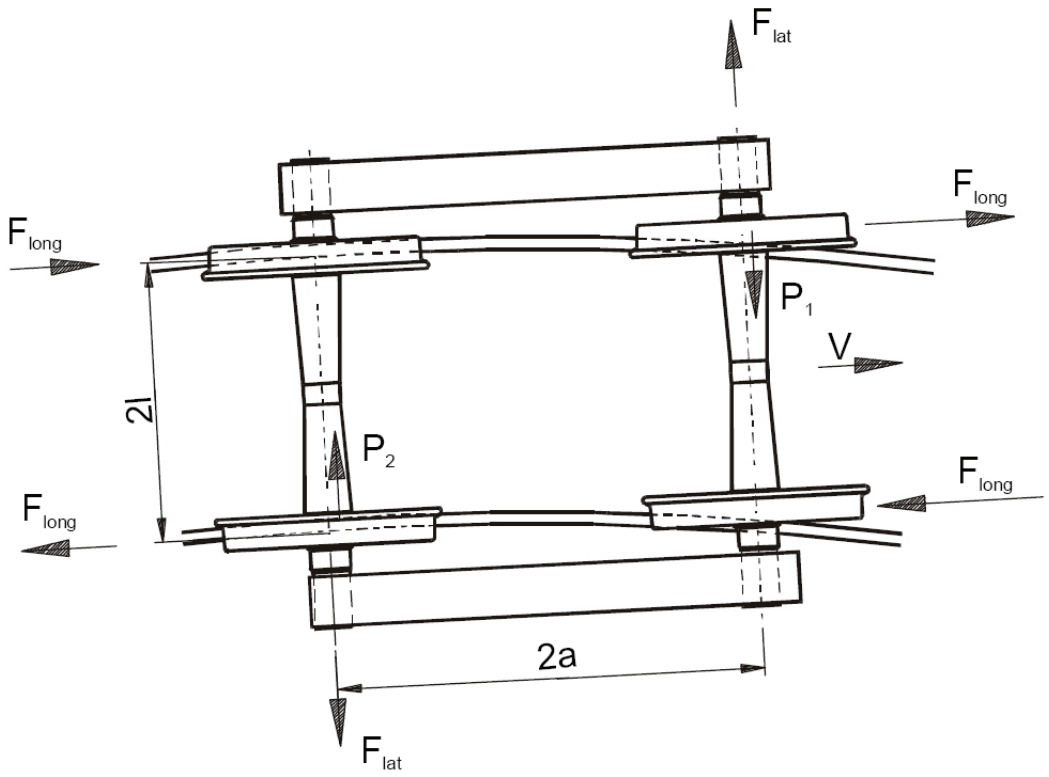

Figure 4.12: Lateral displacement of the bogie in a curve at flange contact.

A railway vehicle should run stable on a straight track and safely negotiate curves. This can be achieved with the correct choice of vehicle suspension parameters. A high stiffness of primary suspension implies that both wheelsets remain essentially parallel to one another, and hence may not attain a radial position in a curve. There is thus a limit on the ability of the bogie to negotiate sharp curves without flange contact. This limit is a function of:

- track gauge,
- bogie wheelbase,
- equivalent conicity of wheels,
- gauge clearance and
- bogie rotational resistance.

Theoretical investigations and experiments show that wheelset stability increases with increasing stiffness of the connection to the bogie frame. However, the nature of this dependence is highly nonlinear, and the relationship between suspension stiffness and the mass and conicity of the wheels influences the critical speed. Increasing the longitudinal stiffness of the primary suspension impairs the guidance properties of the wheelset in curves, while increasing the lateral stiffness reduces the ability of the wheelset to safely negotiate large lateral irregularities.

Therefore the requirements for stability on straight track, and good curving with safe negotiation of track irregularities are antagonistic. The in-plane (lateral and longitudinal) stiffnesses must therefore be selected to give the best compromise for the conditions under which the vehicle will operate.

The choice of appropriate equivalent conicity that insures vehicle stability and good curving is as important and complicated as the choice of the parameters of the primary suspension. The equivalent conicity of the wheel/rail pair should be minimised to increase the critical speed of the vehicle. For passing curves, the required rolling radii difference should be available and the wheel must be able to provide this RRD, for which an increase in the equivalent conicity is required. As a result, requirements for high speed stability on straight track and good curving with safe negotiation of track irregularities are contradictory. The wheel/rail profile combination must be selected to give the best compromise for the conditions under which the vehicle will operate.

4.5 Limits applied on running behaviour of railway vehicle

4.5.1 General limits

In general, to be allowed to exploit a railway network, a railway vehicle must fulfil national and international norms. UIC fiches and EN norms are examples of international norms. Some local or national requirements may take priority over international norms. In all cases, the most recent norms must be fulfilled for the newly designed rolling stock.

The UIC 518 fiche describes methods, conditions and limit values used for the assessment of railway vehicles. The limit values can be defined in terms of values concerning the safety of the vehicle, and values concerning fatigue and running behaviour of the vehicle. The safety values are described in the next subsection. In this subsection, the fatigue and running behaviour values are briefly discussed.

4.5.1.1 Track loading forces

The UIC 518 fiche sets a maximum static load of 112.5 kN per wheel, and a maximum dynamic vertical force equal to

$$Q_{\text{lim}} = Q_0 + 90, \tag{4.7}$$

where Q_0 is the static load on each wheel, with forces expressed in kN.

The maximum dynamic vertical force from one wheel is limited to between 160 kN (for vehicle speed less then 160 km/h), and 200 kN (for vehicle speed less then 300 km/h), depending on the maximum vehicle speed (see UIC518 leaflet).

In small radius curves, the quasi-static vertical force exerted from one wheel on a track must not exceed 145 kN, and the quasi-static lateral force must not exceed 60 kN.

4.5.1.2 Ride characteristics

The ride characteristics of the vehicle provide assessment of the dynamic behaviour of the vehicle through analysis of accelerations at the vehicle body, whereas ride comfort assesses the influence of vehicle dynamic behaviour on the human body. Although both criteria use acceleration signals, the analysis and limit (or target) values differ.

To simulate the dynamic behaviour of a vehicle on a track, measured track irregularities or synthesised irregularities with specified spectral density are usually applied. Track irregularity data often used in European countries are the “low level” and “high level” spectral density according to ORE B176.

The most widely used comfort analysis methods are the comfort index analysis according to UIC 513, Root Mean Square (RMS) method specified in ISO 2631, and Sperling’s method (comfort value Wz).

For assessment of ride comfort, filtered RMS accelerations are used, measured at the floor of the vehicle over the bogies and weighted according to ERRI Question B153. The lateral and vertical values of the accelerations are considered.

The limit values can be found in UIC 518 and UIC 513 leaflets. In general, maximum amplitude of lateral and vertical accelerations should not exceed 2.5 m/s^2 for passenger rolling stock and locomotives.

4.5.2 Running safety and derailment prevention

The limits to prevent vehicle derailment due to rail breakage were considered in the Section 4.5.1.1. There are four main modes for derailment of a railway vehicle not associated with fatigue:

- wheel drop derailment, when one of the wheels drops from the rail inside of the track;
- vehicle overturning, when a vehicle turns around a rail on one side of the track and falling down from the track;
- track shift derailment, when a vehicle distorts the track superstructure by large wheel/rail contact forces;
- wheel flange climb derailment, when one of the wheels rolls over the rail to the outside part of the track.

Each derailment mode and corresponding safety limit are described below.

4.5.2.1 Wheel drop

Track gauge widening can cause wheel drop derailment. This usually involves a combination of wide track gauge and large lateral rail deflection (rail roll). Large lateral forces from the wheels act to spread the rails in curves. Both rails may experience significant lateral translation and/or railhead roll, which often causes the non-flanging wheel to drop between rails.

The safety margin $S_{\lim}$ represents the minimum overlap of wheel and rail required on the non-flanging wheel, when the flanging wheel contacts the gauge face of the rail. To prevent wheel drop between the rails, the geometry of wheelset and rail track must satisfy the following expression (see Wu et al. [2005]):

$$S_{\lim} \le WG + W_w + f_w - TG, \tag{4.8}$$

where TG, WG, W_w and f_w represent track gauge, wheels back-to-back space (wheelset inside (or inner) gauge), wheel width, and flange thickness respectively (see Figure 2.1).

4.5.2.2 Vehicle overturning

Very low vertical forces in wheel/rail contact can indicate that a vehicle is susceptible to derailment by rolling over, or by failing to follow the twists in the track. The UIC518-1 leaflet supplement introduces the overturning criterion:

$$\eta_{\lim} = \frac{\sum_{bogie} Q_{iA} - \sum_{bogie} Q_{iB}}{\sum_{bogie} Q_{iA} + \sum_{bogie} Q_{iB}}, \tag{4.9}$$

where Q_{iA} and Q_{iB} are the vertical wheel forces at wheelset i on the A and B (left and right) sides of the vehicle respectively. To take into account any possible asymmetry of the vehicle, the effect of quasi-static acceleration toward the two vehicle sides must be treated separately for each side. The risk of overturning exists when the overturning coefficient is equal to 1 ($|\eta_{\lim}| < 1$).

4.5.2.3 Track shift

The high wheel/rail forces in the lateral direction can cause distortion of the track superstructure (in the case of ballasted track). To prevent this, the PrudHomme limit is used, which prescribes that maximum track shifting force at one wheelset should be less than:

$$Y_{\lim} <= 10 + \frac{2Q_0}{3}, \tag{4.10}$$

where $Y_{\lim}$ is the lateral force and all values are in kN.

Lateral forces of very short duration are not likely to shift the track, therefore forces are filtered with sliding mean over 2m of track; i.e., only forces that act for more than 2 m of track length are taken into account.

4.5.2.4 Wheel flange climb

When one of the wheels rolls over the rail to the outside part of the track, this is called wheel flange climb derailment. Various formulae exist for analysis of this derailment process, which

give the ratio between the lateral and vertical forces for a particular wheel/rail combination. This ratio is usually called the "derailment ratio", denoted here as Y/Q (also known as L/V ratio), where Y (L) and Q (V) are, respectively, the lateral and vertical forces in the flange contact. The derailment ratio Y/Q is used as a measure of the running safety of a railway vehicle. Several theories have been developed to establish the Y/Q ratio. One of the most widely used is the Nadal [1908] derailment criterion which describes the conditions necessary to sustain equilibrium of the forces in flange contact. Description of the Nadal theory can be found in Dukkipati [2000].

Nadal's formula takes into account the influence of the wheel flange angle, the wheel/rail friction coefficient, and wheel/rail forces on the possibility of wheel climb derailment. This principle is expressed in Nadal's formula:

$$\frac{Y}{Q} = \frac{\tan\alpha - \mu}{1 + \mu\tan\alpha}, \tag{4.11}$$

where α is the angle between the wheel flange and horizontal line; μ is the friction coefficient.

The wheel flange angle is defined as the maximum angle of the wheel flange relative to the horizontal axis, as illustrated in Figure 4.13.

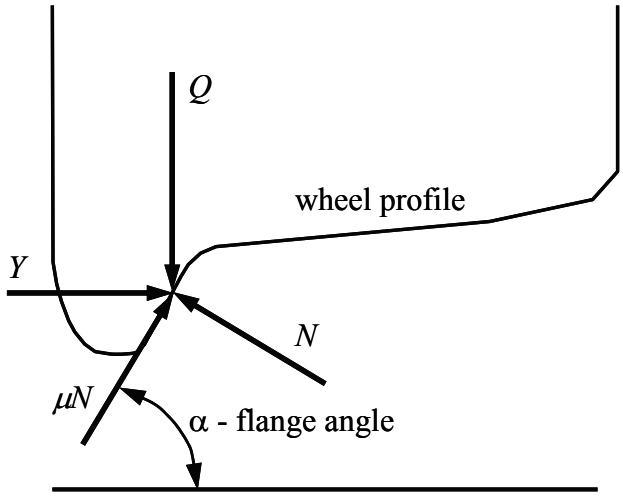

Figure 4.13: Flange angle and flange forces.

The limiting Y/Q ratios for various combinations of the friction coefficient and contact angles are shown in Figure 4.14. For a particular combination of the friction coefficient and contact angle, the derailment can occur if the Y/Q ratio exceeds the corresponding limiting value. The theory of Nadal is used to establish the limit for the Y/Q derailment ratio. In the UIC 518 regulations, the limiting value of Y/Q is set to 0.8 (see Figure 4.14).

Since Nadal's pioneering work a century ago, many studies have shown that Nadal's limit is extremely conservative for most practical cases (see Gilchrist and Brickle [1976], Cheli et al. [2003]). Gilchrist and Brickle [1976] applied Kalker's theory of creep in a re-examination of Nadal's analysis, and they show that Nadal's formula is correct only for the most pessimistic case, when the angle of attack is large and the longitudinal creep on the flange is small. In the Nadal model, it is assumed that the friction force at the contact point between the wheel flange and rail is oriented in the lateral direction (perpendicular to the track). In reality, however, there are components in both the longitudinal (along track) and lateral directions

that cause the lateral friction force to be somewhat less than μN. For high angles of attack, the longitudinal friction force is small, and Nadal's limit is a reasonably conservative estimate of the critical Y/Q ratio. For low angles of attack, however, increased longitudinal creep reduces the lateral component of friction force, and it makes Nadal's limit excessively conservative. Most recent research on wheel derailment phenomena can be found in Barbosa [2004], Wu et al. [2005] and Braghin et al. [2006].

Another problem with Nadal's limit is the choice of values for the flange angle and coefficient of friction. With flange angle of 65° and coefficient of friction of 0.5 from formula (4.1), we obtain a critical Y/Q ratio of 0.8, which complies with the UIC 518 requirement. In practice, however, the flange angle varies from 70° for new wheels to anything in the range of 60° to 75° for worn wheels. Additionally, the coefficient of friction between the wheel and rail in the field is usually lower than 0.5; in most cases, it ranges from 0.15 to 0.40.

Therefore, while being conservative in nature, Nadal's limit of 0.8 takes into account the reduction of the wheel flange angle due to wear, and assumes high friction coefficients, which are, most probably, the most realistic conditions for real-life derailments.

The conservativeness of the Nadal limit is valid for the wheelset with the rigidly connected wheelsets. In the case of independently rotating wheels, the critical Y/Q ratio precisely fits the Nadal limit, as the influence of the contact force from the wheel on the other side of the wheelset vanishes.

In the present paper, the main focus is on wheel flange climb derailment, as it is directly connected to wheel/rail contact geometry. Wheel drop derailment, vehicle overturning, and track shift are mostly dependent on track layout, track and vehicle conditions, and vehicle/track dynamics, while less dependent on wheel/rail profiles. Wheel flange derailment also depends on track layout, and track and vehicle conditions, but is very influenced by vehicle dynamics and wheel/rail profile interaction.

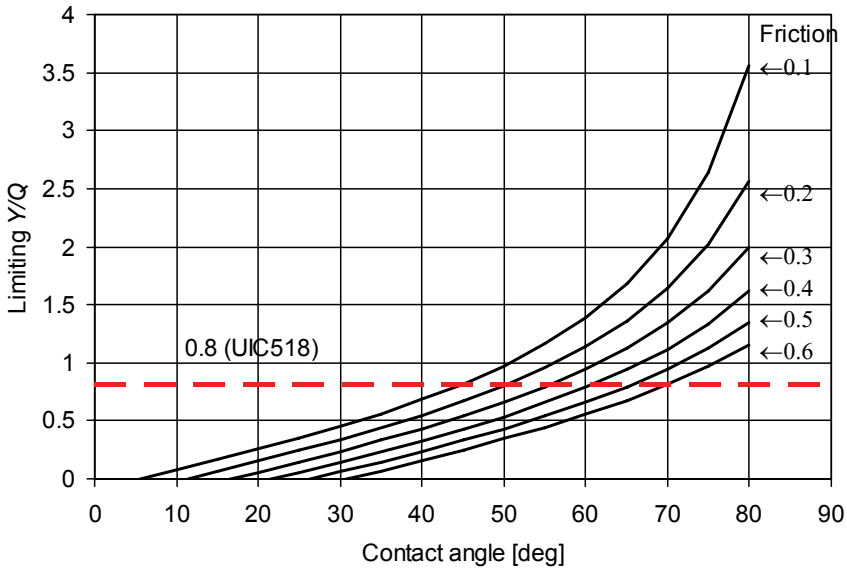

Figure 4.14: Nadal's derailment criteria.

4.6 Discussion and conclusions

The multibody simulation methods used to simulate dynamic behaviour of railway vehicles are described in this chapter. Models of the railway vehicles and track are introduced. The specific features of railway vehicle dynamics on straight and curved tracks are illustrated. Limits applied on running behaviour of the vehicle are described. In this section, research issues related to wheel/rail interface and vehicle dynamics are discussed.

One important issue that requires further investigation is the interaction between the railway vehicle and flexible railway track. In this research, railway track is assumed to be rigid; however, rail vibrations play an important role in the dynamics of railway vehicle systems. Given the speed, acceleration, and wheel profile, vehicle system dynamics are significantly influenced by the layout and flexibility of the rails. The layout factor is taken into account and includes the rail profile, the track turns, track twists, track elevations, track grades, and the track irregularities. The track flexibility factor, which is ignored in simulations in the present research, is important because the track dynamics and inertia can be significant sources of disturbance to the multibody rail vehicles. The inclusion of track dynamics is important because it contributes to the creepages at the wheel/rail contact point, which in turn contributes to the calculation of the contact forces and spin moment.

Another research issue omitted in multibody models is flexible body modelling. In addition to the state of the art wheel/rail contact models, other important considerations in developing a simulation model for vehicle–track systems include kinematic and dynamic nonlinearities, and deformable body flexibility. Ignoring kinematic nonlinearity results in errors that lead to misunderstanding of the dynamic behaviour and vibration characteristics of the railway vehicle system. Ignoring flexibility would eliminate the option of properly modelling the deformable components, such as car bodies and rails. The inclusion of flexibility using nonlinear dynamic formulations becomes more urgent as the demand for higher speed and the selection of lighter materials for vehicle-track systems increases. The high dynamic loads, which result from high operating speeds, impacts, or track irregularities, can excite flexible motion of the car body, which is coupled with the rigid body dynamics of other components of the vehicle system. If these couplings are not properly accounted for, the calculations of the joint displacements and velocities where two bodies come in contact will be incorrect.

Certainly development of the vehicle model, even with the MBS software, is not a simple task. It requires understanding of the mechanical principles of the railway vehicle, along with knowledge of the construction design and availability of the data describing geometric and physical (dynamic) properties of the modelled vehicle. However, significant reduction of costs and time required for the dynamic simulations, especially in comparison with the field tests, brings them on the leading positions in the task of design and verification of the new vehicle's components.

In the last few years, multibody simulation has become a standard tool for the design process in the railway industry. Modern simulation packages such as ADAMS/Rail offer a wide range of modelling possibilities, not only for standard calculations but also for unusual simulation tasks such as running through a switch. Calculation times are sufficiently short so as to allow complex examinations when, for example, wheel and rail profiles must be optimised.

In the present research, vehicle dynamic simulations are used to examine the dynamic properties of the existing and designed (new) wheel and rail profiles. In some cases, the obtained dynamic values cannot be used in an absolute sense, but only for comparison between two different profiles. However, dynamic simulations are an essential tool in the present research. Otherwise, lengthy and expensive field tests would be required, with an

inevitably limited quantity of variants of the test profile. With the dynamic simulations researcher is only limited by the available computational time, which is much cheaper nowadays.

Every railway vehicle must satisfy the corresponding railway norms. However, innovative designs can come into conflict with the existing norms. For example, the lower flange angle increases the possibility of derailment. On the other hand, the lower flange angle can improve wheel/rail contact through better distribution of contact points, and consequently reduce wear. Therefore, optimisation of wheel flange angle is the tradeoff between improvement of safety and improvement of performance. Nevertheless, safety norms must be satisfied unconditionally. It should be noted that for the case of wheelsets with rigidly mounted wheels, the Nadal formula is known as the very conservative. The real risk of derailment is lower than the one calculated from the Nadal formula. For wheelsets with independently rotating wheels, Nadal's formula is exact. Therefore, constraint on a flange angle for such wheel must be stricter than for the wheelsets with rigidly mounted wheels.

The wheel/rail profile combination is a significant factor influencing vehicle stability and negotiation of curves. Reduction of the (equivalent) conicity of the combination of wheel and rail profiles increases wheelset stability and, consequently, the critical speed of the vehicle. However, to negotiate a curve without high slip and without flange contact, conicity of the wheel profile must be sufficiently high to produce the required rolling radii difference. A fundamental conflict therefore exists between the requirements of wheel and rail profile combinations for high speed stability on straight track, and good curving.

One of the possible solutions for this problem is the use of different rail profiles on straight tracks and in curves. Rail profiles of curved segments of track can be modified in such a way that they increase rolling radii differences for the wheelsets rolling in the curves, just improving curving behaviour of the vehicles. Also, preferred ranges of effective conicity can be defined for specific vehicle/bogie combinations. The goal is to set limits on effective conicity, and thus on wheel and rail profiles, such that the speed of hunting can be reasonably guaranteed to be above the required operating vehicle speed, and good curving is achieved for the selected range of curves.

Obviously, wheel profile design must satisfy conflicting requirements to provide stability on a straight track and good curving. Optimisation methods are helpful in the search for the best wheel (or rail) profile that gives the best compromise for the conditions under which the vehicle will operate. The numerical optimisation method used in this research is described in the next chapter.

5 Numerical optimisation method

To find the optimum shape of the wheel (or rail) profile, the optimisation problem must be formulated and solved. Therefore, knowledge of the principles of shape optimisation is essential. In this chapter, formulation of the optimisation problem and the solution method are described. An introduction to shape optimisation is given in Section 5.1. Section 5.2 describes, in general terms, the optimisation problem. Section 5.3 gives a description of the multipoint approximation method, which is used to solve the optimisation problem in the present research. Section 5.4 finalises this chapter with a discussion of implementation and conclusions.

5.1 Introduction

Any design must be driven by a combination of objectives and constraints, for example function, weight, cost, aesthetics, and manufacturing and other technical requirements. The objective of any optimisation procedure is to determine that layout and shape of an object that provides the optimum combination of objectives within the applied constraints. Shape optimisation, in particular, pursues optimal determination of the dimensional variables that maximise the ability of the part to perform the intended function under the prescribed operating conditions. Recent practical demands from the automotive and aerospace industries concerning reduction of construction weight and material volume place great emphasis on optimal shape with respect to any particular application. It is, therefore, no surprise that shape optimisation problems attract the attention of many investigators; the results of their efforts are widely available in the literature.

Computer-aided geometric design (CAGD or CAD) becomes more popular and accepted in engineering applications, therefore it become natural to couple the CAD system with structural optimisation. This trend is being followed by many commercial software companies. Esping [1985] applied a CAD approach to the minimum weight design problem. A structure can be defined by a set of governing entities. For example, a truss structure can be described as a set of lines, a membrane or shell structure as a set of surfaces, and solid structures can be described by solid entities. In all cases, points are the basic information. The values of the design variables are determined by manipulating the points. It is then natural to connect design variables to point coordinates. Braibant and Fleury [1984, 1985] used the CAD philosophy of geometric description to formulate a shape-optimal design of an elastic structure. The structure to be optimised is decomposed into a set of simple subregions, called design elements, and the shape of these elements is described through properly chosen master nodes. Parametric curves and surfaces of CAD actuate the interpolation process in the design elements. The advantage of this approach is that it makes unnecessary both the piecing together of design elements such that they agree with shape complexity, and the restriction of shape variation. Wang, Sun and Gallagher [1985] use a similar geometric description in their sensitivity analysis for shape optimisation of continuum structures. For an interested reader, Seireg and Rodriguez [1997] describe a number of shape optimisation examples using mechanical elements and structures.

Shape optimisation problems can be efficiently formulated with the incorporation of an appropriate optimisation procedure. Knowledge of optimisation techniques enables the designer to select the most suitable one for a particular problem, and to incorporate it as an integral part of the synthesis procedure. The primary tool utilised in the past for most optimisation problems was differential calculus. However, with the advent of high speed

computing, numerical methods for the solution of differential equations are now a realistic option, thus providing very powerful tools for more complex analyses of optimisation problems. In reference to numerical methods, two main groups of algorithms are notable:

- algorithms used for the solution of the actual differential equation(s) resulting from the physical laws governing the problem;
- algorithms based on approximation methods for the formulation of the problem at hand.

In the first group, numerical analysis theories have resulted in the development of helpful solution algorithms for partial differential equations. Many textbooks and technical reports have addressed the most efficient ways of solving linear and non-linear equations. On the other hand, approximation techniques were used as early as the late 1950s, combined with newly available high speed computing. Techniques ideal for computer implementation, such as the Finite Element Method (FEM), became a dominant force in the engineering optimisation field. These approximation techniques basically discretise the continuum field, and define a new set of discrete variables that represents the entire domain of the problem; therefore, the differential equations that represent the original problem are replaced by a system of algebraic equations for the new discrete vector.

5.2 General optimisation problem

When the optimisation process is started for a given engineering problem, important assumptions are made: that a solution of the given problem exists, and that the formulation of the problem can provide sufficient flexibility for the type and range of the needed modifications to the initial design. Once that is assumed, the next step in the optimisation process is the mathematical formulation of the problem. To make use of numerical optimisation techniques, an optimisation problem should be stated in a general form as follows:

Minimize

$$F_0(\boldsymbol{x}) \rightarrow \min, \quad \boldsymbol{x} \in R^N \tag{5.1}$$

subject to

$$F_j(\boldsymbol{x}) \leq 1, \quad j = 1,...,M \tag{5.2}$$

and

$$A_i \leq x_i \leq B_i, \quad i = 1,...,N, \tag{5.3}$$

where

F_0 is the objective function;

F_j, $j = 1,...,M$ are the constraints;

$\boldsymbol{x} = [x_1,...,x_N]^T$ is the vector of design variables;

A_i and B_i are the side limits, which define lower and upper bounds for the i-th design variable.

The components of the vector $\boldsymbol{x}$ can represent various parameters of a mechanical structure, such as geometry, material, stiffness, and damping properties. These properties can be varied

to improve design performance. Additionally, design variables can be continuous or discrete. Continuous design variables can take any magnitude in a given range; discrete design variables can take values only from a specific set of permissible magnitudes (e.g., integers). Material properties are often discrete variables, while geometry parameters are usually continuous ones.

Another important definition in the optimisation formulation is the objective function. This constitutes the actual system function that can be improved. In some cases, the objective function is a combination of several independent variables, and is called the multiobjective function. Dealing with multiobjective functions is complex and is usually avoided. Possible ways of getting around this problem are: a) definition of a composite objective function, and b) selection of a main objective function through, for instance, a Pareto optimality.

The third important component of the formulation is the specified constraints. If limits are introduced for the design vector, they are called side constraints, which are usually treated in a special way by the solution procedures, because of their simplicity. Constraints that impose upper and/or lower limits on parameter magnitudes are called inequality constraints. Equality constraints impose stronger limitations by specifying a single value (usually zero), but it is common practice to implicitly include them in the objective function.

Depending on the problem under consideration, the objective and constraint functions (see equations (5.1) and (5.2)), can describe various structural and dynamic response quantities such as weight, reaction forces, stresses, natural frequencies, displacements, velocities, accelerations, etc. Also, cost, maintenance, and safety requirements can be used in the formulation of the optimisation problem. The objective function provides a basis for design improvements, whereas the constraints impose necessary limitations on the properties or behaviour of the structure.

In general, numerical searching techniques start from an initial design and proceed in an iterative fashion, with small steps intended to improve the value of the objective function, as well as the degree of compliance with the specified constraints. The searching process ends when no further significant improvement can be made on the objective without violating some of the constraints. The exact quantification of the word "significant" is usually problem-dependent, and it basically means: no, or very little, progress. This numerical search for the optimum takes place in N-dimensional space, where N is the number of elements in the design vector, and every point in this space constitutes a possible solution.

In optimisation problems of mechanical components, the constraints that are imposed on the design, such as stresses, displacements, or frequency constraints, are very important; this is because the optimum design will be affected by some of these constraints. Thus, the optimum value of the objective function is not as good as it could have been without constraints. Constraints divide N-dimensional space into two regions: feasible domain and infeasible domain. The feasible domain contains all the possible design points where all the constraints are satisfied, and the infeasible domain is where at least one constraint is violated. This concept is sketched in Figure 5.1.

It is not unreasonable to expect the optimum design to be located at the boundary between the feasible and infeasible domains. The constraints defining this particular boundary are called active constraints, while all other constraints are called inactive or passive. One should be careful with the concept of active constraints, since it simply indicates presence at the location of optimum design, and not any special effect on the optimum.

A common characteristic of all design problems is the existence of many feasible solutions. The selection of the best possible design depends on the ability to clearly define the

interaction between the system variables, and to explicitly state the design objective. An appropriate method should then be devised to seek the optimum solution according to the stated criterion. Formulated in the form (5.1)–(5.3), the optimisation problem can be solved using the conventional method of Nonlinear Mathematical Programming (NMP). Here, the Multipoint Approximations based on the Response Surface fitting (MARS) method is used to solve the optimisation problem (5.1)–(5.3) (see Markine [1999], Toropov [1989], Toropov et al. [1993], Toropov et al. [1999]). This method is described in the next section.

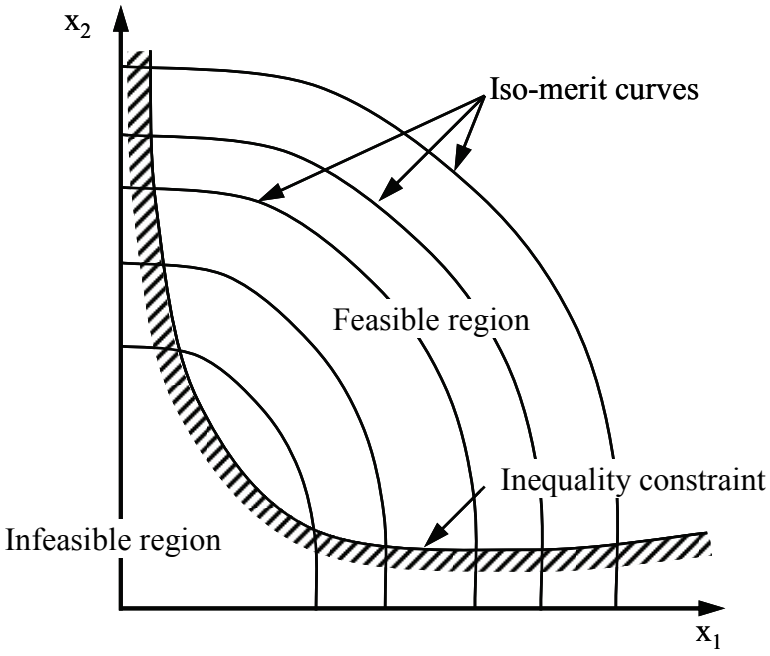

Figure 5.1: Graph of feasible and infeasible regions.

5.3 MARS method

To solve the optimisation problem formulated in the previous section, the MARS method is used. The main features of this method are briefly described below.

5.3.1 Approximation concept

The optimisation problem (5.1)–(5.3) can be solved using a conventional method of mathematical programming. However, when a complex system is to be analysed, evaluation of the objective and constraint functions can be time consuming. As a result, the total computational effort of the optimisation might become prohibitive. This difficulty began to be mitigated starting in the mid-1970s with the introduction of approximation concepts (see Barthelemy and Haftka [1993]).

The typical structure of the multipoint approximation method is shown in Figure 5.2. According to the approximation concepts, the original functions (5.1)–(5.2) are replaced with approximate ones, which are computationally less time consuming. Instead of the original optimisation problem (5.1)–(5.3), a succession of simpler approximated subproblems, similar to the original one and formulated using the approximation functions, is to be solved. Each simplified problem then has the following form:

Minimize

$$\tilde{F}_0^k(\boldsymbol{x}) \to \min, \quad \boldsymbol{x} \in \boldsymbol{R}^N \tag{5.4}$$

subject to

$$\tilde{F}_j^k(\boldsymbol{x}) \le 1, \quad j = 1,...,M \tag{5.5}$$

and

$$A_i^k \le x_i \le B_i^k,\ A_i^k \ge A_i,\ B_i^k \le B_i,\ i = 1,...,N, \tag{5.6}$$

where the superscript k is the number of the iteration step, $\tilde{F}$ is the approximation of the original function F, and A_i^k and B_i^k are move limits defining the range of applicability of the approximations.

Since the functions (5.4)–(5.5) are chosen to be simple and computationally inexpensive, any conventional method of optimisation can be used to solve the problem (5.4)–(5.6). The solution of the problem $\boldsymbol{x}_*^k$ at the k-th iteration step is then chosen as a starting point for the next $(k+1)$-th step, and the optimisation problem (5.4)–(5.6), reformulated with the new approximation functions $\tilde{F}_j^{k+1}(\boldsymbol{x}) \le 1, \quad (j = 0,...,M)$ and move limits A_i^{k+1} and B_i^{k+1}, is to be solved. The process is repeated iteratively until the convergence criteria are satisfied.

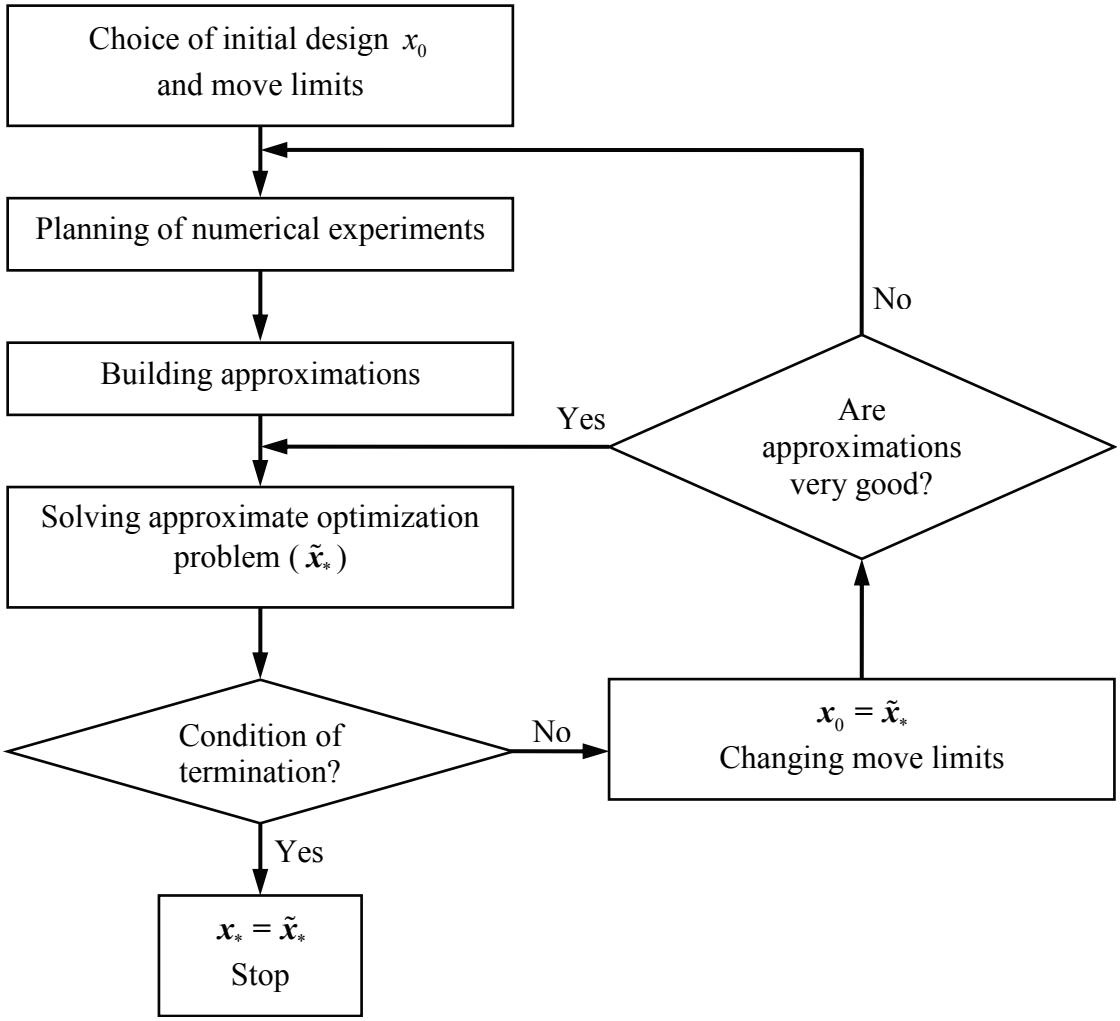

Figure 5.2: Flowchart of multipoint approximation method (from Markine [1999]).

5.3.2 MARS optimisation technique

Each approximation in (5.4)–(5.5) is defined as a function of the design variables $\boldsymbol{x}$ and tuning parameters $\boldsymbol{a}$ (for brevity, the indices k and j will be omitted). To determine the components of vector $\boldsymbol{a}$ the following weighted least-squares minimization problem is to be solved (Toropov [1989], Toropov et al. [1993], Toropov and Markine [1996], Markine [1999]):

Find vector $\boldsymbol{a}$ that minimizes

$$G(\boldsymbol{a}) = \sum_{p=1}^{P} \{ w_p [F(\boldsymbol{x_p}) - \tilde{F}(\boldsymbol{x}_p, \boldsymbol{a})]^2 \} . \tag{5.7}$$

Here $F(\boldsymbol{x_p})$ is the value of the original function from (5.1)–(5.2), evaluated at the point of the design parameters space $\boldsymbol{x}_P$, and P is the total number of such plan points; w_p is a weight factor that characterises the relative contribution of the information about the original function at point $\boldsymbol{x}_P$. It should be noted that if the design sensitivities of the original functions are available, they can easily be used in the building of approximations. Function G in (5.7) then reads

$$G(\boldsymbol{a}) = \sum_{p=1}^{P} \{ w_p [F(\boldsymbol{x_p}) - \tilde{F}(\boldsymbol{x}_p, \boldsymbol{a})]^2 + \gamma \delta_p \sum_{i=1}^{N} [F_{,i}(\boldsymbol{x_p}) - \tilde{F}_{,i}(\boldsymbol{x}_p, \boldsymbol{a})]^2 \} , \tag{5.8}$$

where $\delta = 1 / \sum_{1=1}^{N} [F_{,i}(\boldsymbol{x}_p)]^2$ is the normalizing coefficient, and $0 < \gamma < 1$ reflects the weight of the sensitivity information as compared to the information on the function values.

The choice of approximation function $\tilde{F}(\boldsymbol{x})$ is important for the success of optimisation. The basic requirements for such function are:

- it must depend on the same design variables as the original function;
- it must contain tuning parameters defined using the general (non-linear) least-squares method;
- it must be simple enough to be used in numerous repeated calculations;
- it should not contain any considerable level of numerical noise in order not to cause convergence problems in the optimisation process.

Simple but quite efficient approximations are intrinsically linear (with respect to the tuning parameters) models, that is linear and multiplicative models:

$$\tilde{F}(\boldsymbol{x}) = a_0 + \sum_{i=1}^{P} x_i a_i \text{ and } \tilde{F}(\boldsymbol{x}) = a_0 \prod_{i=1}^{P} (x_i)^{a_i} . \tag{5.9}$$

These models have been successfully applied to various design optimisation problems (Markine [1999], Toropov et al. [1999]).

Recently, a new type of approximation that uses simplified numerical models was introduced:

$$\tilde{F}(\boldsymbol{x}, \boldsymbol{a}) \equiv \tilde{F}(f(\boldsymbol{x}), \boldsymbol{a}) , \tag{5.10}$$

where $f(\boldsymbol{x})$ is the function representing the structural response using the simplified model (Toropov and Markine [1996]). The simplified model can be obtained by simplifying the

numerical analysis (e.g., using a coarser FE mesh) or numerical model (e.g., using simpler geometry). Depending on the manner of introduction, and the number of tuning parameters in the simplified expressions (5.10), the following approximations are introduced by Toropov and Markine [1996]:

linear and multiplicative:

$$\tilde{F}(\boldsymbol{x},\boldsymbol{a}) = a_0 + a_1 f(\boldsymbol{x}) \text{ and } \tilde{F}(\boldsymbol{x},\boldsymbol{a}) = a_0 f(\boldsymbol{x})^{a_1}, \tag{5.11}$$

models with the correction function $C(\boldsymbol{x},\boldsymbol{a})$:

$$\tilde{F}(\boldsymbol{x},\boldsymbol{a}) = f(\boldsymbol{x}) + C(\boldsymbol{x},\boldsymbol{a}), \quad C(\boldsymbol{x},\boldsymbol{a}) = a_0 + \sum_{l=1}^{N} a_l x_l \tag{5.12}$$

and

$$\tilde{F}(\boldsymbol{x},\boldsymbol{a}) = f(\boldsymbol{x})\, C(\boldsymbol{x},\boldsymbol{a}), \quad C(\boldsymbol{x},\boldsymbol{a}) = a_0 \prod_{l=1}^{N} a_l x_l \tag{5.13}$$

parameters of a model as tuning parameters:

$$\tilde{F}(\boldsymbol{x},\boldsymbol{a}) \equiv f(\boldsymbol{x},\boldsymbol{a}). \tag{5.14}$$

Other approximations include those constructed using genetic programming methodology. For details of the approximations of the MARS method, the interested reader is referred to Toropov [1989], Toropov et al. [1999].

The optimisation process is controlled by changing the move limits in each iteration step. The main rules governing the strategy for changing the move limits employed in the method are:

- if the approximating functions do not adequately represent the original ones in the current optimum point, which means that the search subregion is larger than the range of applicability of the current approximations, the move limits (5.6) are changed to reduce the size of the search subregion;
- if the approximations are good and the solution of the optimisation problem (5.4)–(5.6) is an internal point of the search subregion, then it could be considered as an approximation of the solution of the original optimisation problem (5.1)–(5.3); the search subregion is to be reduced in this case;
- if the current optimum point belongs to the boundary of the search subregion (at least one of the move limits is active), and the approximations are good, the size of the subregion is not changed on the next iteration.

The iteration process is terminated if the approximations are good, none of the move limits is active, and the search subregion is small enough. More information about the weight coefficient assignment, the move limits strategy, and the most recent developments in the MARS method can be found in Toropov [1989], Toropov et al. [1993], Markine [1999], Toropov et al. [1999], and Markine and Toropov [2002].

5.4 Discussion and conclusions

In this chapter, a general numerical optimisation problem is described with an aim to applying it to design of the shape of wheel and rail profiles. The MARS method is chosen as a method of solution of the optimisation problem. The main features of the method are briefly described.

It is worth pointing out that practical design goals for finding design variants and special proposals almost always fall outside of the scope of mechanics. The main goals of practical optimisation are:

- reduced manufacturing costs;
- reduced manufacturing and construction time;
- reduced maintenance costs;
- improved quality and durability.

Optimisation of wheel/rail interface addresses the last two goals. Good wheel/rail profile combination improves quality of vehicle motion and durability of wheels and rails, at the same time reducing maintenance costs. The challenge for the designer is to translate these requirements into mathematical form. Chapter 6 deals with this intricate problem.

At the present time, many problems of optimum design of mechanical systems are solved using a synthesis of individual disciplines:

- design modelling, e.g., by methods of computer-aided geometric design;
- structural analysis, e.g., FE methods and/or MBS simulations;
- behaviour sensitivity analysis;
- mathematical optimisation;
- interactive graphical user interface (GUI).

The methods have achieved remarkable sophistication and have been used as design tools to improve structural quality in many industrial applications, especially in the aircraft and automotive industries. The key to structural optimisation is to join together interdisciplinary dependencies in a clear, integrated overall model, and to convert this model into an efficient and practical computer code.

This study provides insight into the formulation and interactions among the models. The models are ordered hierarchically: the analysis model is generated with respect to the design model, which itself is affected by the overall optimisation model. Several characteristic or so-called "natural" variables can be selected as optimisation variables; these may be either typical design variables such as certain geometric parameters defining the overall shape of the structure, or structural parameters. These variables, in turn, are subsets of the entire group of either design or structural parameters; some of them may already be automatically generated from previous variables.

The geometric part of the problem description defines the design model and is primarily based on CAGD concepts. The mechanical part is integrated in the analysis model with the help of, for example, multibody simulation or the finite element method, and provides the structural response. It is important to realize that this procedure can be supplemented by an efficient sensitivity analysis; this supplies important gradient information for the optimiser. Structural data are transformed satisfying the requirements for optimisation, i.e., objective, constraints, and the related derivatives are calculated. This is the starting point for the mathematical optimiser, which finally delivers a new proposal for the structure.

The same approach is used in the design of wheel and rail profiles. The optimum profile design problem is solved using a synthesis of several disciplines:

- profile design modelling, using methods of computer-aided geometric design;

- behaviour analysis, using geometric wheel/rail contact ;
- structural analysis, using multibody system simulations and rolling contact mechanics;
- mathematical optimisation, using MARS method.

In a practical design situation, it is seldom an easy task to choose a mathematical programming technique to formulate and solve the shape optimisation problem. Difficulties of all kinds may arise during the formulation and the solution of the problems, and such solutions are not always clear. Experience emerges as the best tool for selecting a method. Relationships, specifications, environment, and available analysis tools are some of the important aspects to take into account. All details of wheel and rail profile design procedure are described in the Chapter 6, and examples of real-life applications are presented in Chapter 7.

6 Design procedure of wheel and rail profiles

In this chapter, the general procedure for wheel and rail profile design is described. An introduction is given in Section 6.1. Methods of profile variation are described in Section 6.2. Criteria for wheel and rail profile optimisation, and the complete design procedure are described in Sections 6.3 and 6.4, respectively. Section 6.5 ends the chapter with a discussion of the profile design procedure, along with final remarks.

6.1 Introduction

Wheels and rails are important elements of the railway vehicle–track system; they not only bear the load from the rolling stock to the ground, but they also guide the rolling stock along a track. During operation of the rolling stock on the railways the contact surfaces of wheels and rails wear out. Wear of wheels and rails can lead to undesirable changes in their cross-sections (profiles), and consequently to changes in contact properties, which are followed by increased wear rates, vehicle instability at operational speeds, and RCF problems. Furthermore, initial (unworn) profiles of wheels and rail could mismatch, leading to the problems described above. However, the appropriate match of wheel and rail profiles can reduce wear rate, provide vehicle stability at operational speeds, and reduce (or prevent) RCF problems. Below, the theoretical basis of wheel/rail interface optimisation is described.

6.1.1 Factors influencing wheel/rail interface

Five main factors determine the requirements for shaping the contact surfaces of wheels and rails:

- wheel/rail wear;
- RCF;
- wheelset (vehicle) dynamics on a straight track (maximisation of stability);
- wheelset (vehicle) dynamics in a curve (minimisation of L/V and track forces);
- safety requirements.

Safety requirements consist of prevention of derailment due to wheels climbing over the rail, and to fracture of the wheel and/or rail. A limit on minimum flange angle is applied to address wheel climb phenomena (Nadal's formula). A limit on contact forces is dealt with the fracture of the wheels and rails.

The relation of wear intensity from the various factors can be presented as a function (Ushkalov [1998])

$$\mathrm{I} = \mathrm{I}(\mathrm{Y}, \varphi, \mu, \rho), \tag{6.1}$$

where Y is the guiding force or force of wheel/rail interface, φ is the angle of attack of a wheel on a rail, μ is the friction coefficient, and ρ is the relation of wheel and rail material hardness.

Values of Y and φ are determined through a process of dynamic vehicle-track interaction, and curving behaviour. These are dependent on the cross-sectional profiles of wheels and rails, conditions of track and vehicle, design and parameters of the rolling stock, travelling speed, and axle load, etc.

Vehicle dynamics can be divided roughly according to curving behaviour of the vehicle, and stability of the vehicle on a straight track. Both are dependent on wheel and rail profiles, as well as on the design and parameters of rolling stock and railway track. Wear has a deteriorative effect on vehicle dynamics. Hollow wear of the tread part of the wheel induces wheelset instability on straight track, however, hollow wear can increase effective conicity, thereby influencing curving behaviour. Flange and flange root wear reduce rolling radii, which increases creepage of the wheels in curves. In contrast, hunting on straight track, and flange contact in curves increase the wear rate of wheels and rails, causing changes to wheel and rail profiles, which in turn influences vehicle dynamics.

The influence of the friction coefficient μ on the intensity of wheel/rail wear can be decreased by lubrication of wheel flanges and gauge sides of the rail, especially in curves of small radius (R<=650 m). However, lubrication of wheels and rails can lead to negative consequences; therefore, this technique should be used with caution.

The wear rate of wheels and rails can be significantly reduced by appropriate selection of hardness of wheel and rail steels, i.e., relation ρ should provide the lowest wear rate.

The development of rolling contact fatigue in rails depends on the relationship between crack growth, which is governed by contact stress and the tangential force at the contact patch, and wear, which depends on tangential force (again) and creepage at the contact patch. These parameters are dependent on a large number of interdependent factors, in particular (Evans and Iwnicki [2002]):

- curve radius;
- vehicle configuration – wheelbase, axle load, wheel diameter;
- suspension design – in particular primary yaw stiffness;
- wheel profiles – nominal profile and state of wear;
- rail profiles – nominal profile and state of wear;
- wheel/rail friction;
- cant deficiency (depends on speed, radius and cant);
- traction and braking forces;
- track geometry quality;
- wheel and rail material properties.

Wheel/rail interface is influenced by all these parameters, and most of them are prescribed such that track design and layout are given, and cannot be changed. Vehicle design is given as well, and in most cases cannot be modified. Curving behaviour and stability of a vehicle on a straight track are dependent on wheel/rail coupling, which can be altered, and on vehicle configuration and suspension design, which are given. Changes to wheel and rail materials are rather expensive and time consuming. Wheel/rail friction management (lubrication) is a powerful tool, but cannot optimise wheel/rail geometric interaction. Finally, only the geometry of wheel and rail profiles remains as a possible solution to the wheel/rail interface optimisation problem. Due to the fact that rail replacement is much more expensive than wheel replacement, and that wheels are more frequently reprofiled, it would appear more attractive to design a new wheel profile to fit an existing rail profile.

6.1.2 Wheel and rail functional regions

Wheel and rail profiles can be divided according to three functional contact regions, as shown in Figure 6.1 (see Harris et al. [2001]):

- region A: Contact between the central region of the rail head and wheel tread;
- region B: Contact between the gauge corner of the rail and the wheel flange root (including flange);
- region C: Contact between the field sides of both rail and wheel.

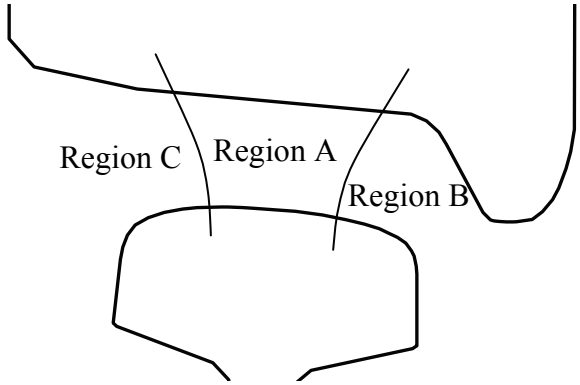

Figure 6.1: Functional regions of wheel/rail contact.

6.1.2.1 Contact region A: central region of the rail crown and the wheel tread

Contact is made most often in this region and occurs as the vehicle negotiates tangent track, mild curves (non-steering bogies), or tight curves (steering bogies). As a result of these conditions and wheel/rail profile geometry:

- contact stresses are the lowest stresses encountered between rail and wheel;
- lateral creepages and forces are low; particularly if the vehicles are not subject to tracking inaccuracies or instabilities;
- longitudinal creepages and forces are significant in relation to lateral creepages and are a dominant consideration for vehicle stability;
- vehicle speeds are higher than in sharper curves.

This region is thus primarily designed to optimise vehicle stability while providing a radius differential to curve according to the Newland model [1968], with non-steering bogies in mild curves and with adequate radius differential for self-steering in tighter curves. To reduce the rate of wear across this region, the conicity should be as low as possible within the curving requirements to “spread” the occurrence of contact as wide as possible across the wheel tread. The rail crown has two radiuses over this region, and a profiled wheel is preferred.

Conicity and radius differential may be calculated according to geometric methods or according to the more sophisticated numerical methods used in vehicle multi-body dynamic routines. When assessing conicity, a balance should be drawn between lower contact stresses resulting from more conformal contact (equal wheel and rail profile curvature), and the resulting high conicity causing vehicle instability. Two-point contact is to be avoided at all costs because of the high resultant conicities, and because of the wear associated with two-point contact.

Adequate gauge clearance on tangent track must be associated with decreased conicity and the spread of contact over the wheel, promoting pummelling. This clearance may be obtained by increasing the nominal gauge, decreasing flange thickness (if flange wear is under control), or decreasing the "back-to-back" dimension across flanges on a wheelset, or a combination of all three measures.

If excessively soft rail is used, a large difference in the rail and wheel profile radii may have to be used to counter the "flattening" effect caused by material flow. This design action may have to be accompanied by grinding.

The conicity of new and worn profiles must be considered. Good tracking may result in a hollowing of the wheel tread, and in altering the initial design conicity. This should be limited, to retain conicities within vehicle stability limits. Contact toward the field side of the rail and wheel should be encouraged by continuing the wheel profile radius beyond the taping line to the field side of the rail.

Care should be taken with the straight track parts to avoid concentrated contact in just one portion of the wheel tread. Concentrated contact can lead to excessive wheel hollowing.

Flange clearance has an influence on the RRD in curves. Too narrow a gauge can limit the RRD (and therefore the yaw displacement of the wheelset in curves), inducing wear, especially to high rails in curves. However, too wide a gauge can increase the risk of gauge widening derailment.

6.1.2.2 Contact region B: contact between the gauge corner and flange root

As the contact patch in this region is small, contact is often made under the most arduous stress conditions. If two-point contact occurs, high wear rates and material flows are present.

If single point contact occurs, high contact stresses prevail together with spin creep and high longitudinal creep. Contact in the gauge corner is invariably associated with high angles of attack and lateral creepage.

Flange contact will inevitably occur at some points on the track, in tighter curves, and at locations on the track where alignment is not good. This also occurs at locations on the track where there are discontinuities in the running profile, such as at points and crossings, rail joints, and skid marks. If flange contact is not designed properly, rail and wheel damage may occur, or vehicle guidance or stability may be impaired.

There are three generic options that the profile designer must consider when examining flange contact; these are two-point contact, single-point contact, and conformal contact, as Figure 2.21 illustrates.

Two-point contact is associated with gross slippage and wear if a flange force and lateral creep are present, as is the case in curves. Under these conditions, wheel flange wear is accelerated until the flange shape conforms to that of the rail.

Contact is often so severe that material flows occur on the flange of the wheel. Experience shows that under this condition, the flange often cuts under any lubricating film applied to the contact zone.

It is often argued that two-point contact is less damaging to the rail because the vertical load is carried away from the gauge corner. In addition, two-point contact is often applied to rails exhibiting gauge corner fatigue defects as a result of improper past maintenance. It does limit, however, the amount of radius differential and steering ability available in a curve. If taken to the conclusion, two-point contact could result in even worse contact conditions.

First, the gauge corner of the rail is removed, then the wheels eventually wear, because of two-point contact, to the new gauge corner. Then, the gauge corner is further removed, and so on. This procedure should be undertaken under tight control, as it could possibly end in dangerous, extremely high conicity, one-point contact between the wheel and the rail on straight track. Notwithstanding the disadvantages described above, gauge corner relief does give a short-term extension to rail life.

Single-point contact between wheel flange root and rail gauge corner is probably most damaging to vehicle and track. The high contact stresses occurring under high creep conditions result in fatigue of the gauge corner.

A case may be made, however, for single-point contact on tangent track, as it is difficult to imagine that the low angles of attack encountered would result in excessive wear and an alteration to a designed wheel profile. This would also help reduce conicities, and hence improve vehicle stability on straight track.

This should not be taken to an extreme, as it will impair the ability of the vehicle to centralize itself on straight track, resulting in wheel and flange wear, which may become non-symmetric and damage the vehicle's tracking ability. This, in its mildest form, produces head checks, and in its worst form, a breaking-out of the gauge corner of the rail. It is associated with high longitudinal creepages, causing rail material flow but, more dangerously, vehicle instability in the form of hunting, and associated alternating side wear on the track.

Single-point contact occurs as a result of:

- incorrect wheel and rail design;
- a flattening of the railhead in service;
- excessive hollowing of the wheel tread.

Conformal flange contact is observed as the gauge-corner and flange wear to a common profile under hard flange contact in curves. This is a remarkably common form under different flange contact conditions, and on different railways. An example of a conformal profile design is given in Figure 2.21. Care should be taken not to confuse this profile with those developed on the gauge corner as a result of single-point contact.

Rail and wheel profiles produced to conformal shape maintain their shape and perform successfully in terms of fatigue life. The advantages of using this profile type are:

- it retains its shape;
- gauge corner fatigue is controlled under prevailing axle loads;
- lubricating films are supported due to low specific pressures;
- conicity is "neutral" as it would seem that the wheelset does not experience the high conicities associated with single-point contact.

It is recommended that wheel and rail profiles be designed to a conformal profile. Wheels and rails may be profiled during maintenance; rails may be rolled or profiled (grinded) immediately on installation. What is important in designing these profiles include the following:

- radius and lengths of the profile arcs;
- tangential contact in blending flange root with the tread part to ensure the minimum of two-point contact on the tread and flange root of profiles;

- a certain liberty is available in choosing the flange angle to suit existing maintenance standards;
- gauge corner radii should follow the flange profile to blend in with the rail crown profile without producing two-point wheel/rail contact.

6.1.2.3 Contact region C: contact between the field sides of both wheel and rail

Region C is probably the most difficult to optimise because contact between rail and wheel ends in this region, and eventually, notwithstanding the efforts of the designer, either high contact stresses are generated as the outer edge of the wheel profile bears on the rail (Figure 6.2), or contact ends before the edge of the wheel, giving rise to the development of a false flange on the field side of the tread.

Often, both effects develop simultaneously as both contact conditions prevail at different locations, giving rise to the contact condition shown in Figure 6.2, where both high contact stresses occur together with high longitudinal creepage, steering the wheel in the incorrect sense. This is associated with accelerated flange wear.

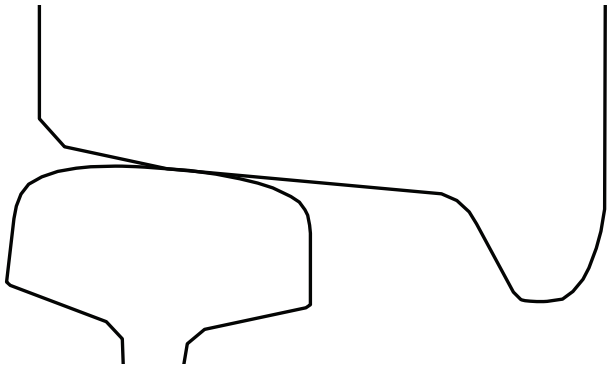

Figure 6.2: High contact stresses regions on field side of wheel/rail contact.

The wheel profile can be continued from the tread radius design suggested, until the profile is conical. This spreads contact on the field side as much as possible.

Adverse field contact may be minimized or controlled by controlling for the level of maximum wheel hollowing, applying suitable field side relief to the rails.

6.1.3 Requirements for optimised wheel and rail profiles

Obviously, an optimum profile is a compromise between stability, curving, wear, and RCF. Of course, safety requirements must be fulfilled without any compromises. Optimised wheel and rail profiles should satisfy the following requirements (Magel and Kalousek [2002]):

- avoid high contact stresses greater than three times the strength of material in shear;
- avoid closely conformal and severe two-point contact with rail to improve curving and reduce wear;
- design appropriate steering capability;
- ensure effective conicity that is within the conicity window of the truck to insure optimum compromise between curving and stability requirements;
- arrange for as many contact points across the wheel tread as possible;
- provide sufficient flange angle to reduce the risk of flange climb derailment;

- ensure that all dimensional requirements for a specific wheel profile are met.

In the past, such a compromise would have been achieved by manually modifying the wheel shape to find satisfactory contact characteristics in combination with a given rail. However, this design approach is quite time consuming and expensive. Therefore, it seems attractive to develop and use numerical methods to design the wheel and rail profiles.

As shown in Chapter 2, the rolling radii difference function is an important characteristic of the contact between wheelset and railway track. The rolling radii of the left and right wheels are present in the equations of wheelset motion (see Dukkipati [2000]). Therefore, RRD function is important for the dynamic behaviour of a wheelset. From another perspective, the RRD function is defined by the wheel and rail cross-sectional profiles. Track and wheelset geometric parameters of course influence RRD function as well, but they are considered to be constant.

But if the shape of the RRD function is defined by wheel and rail profiles, then the opposite is also valid; that is, the RRD function can define the shape of the wheel or rail profile. In computational modelling, variation of the RRD function can change dynamic behaviour of the wheelset to achieve the required performance. This modified RRD function virtually corresponds to a new combination of wheel/rail profiles. For a given rail profile, one can try to solve an inverse problem in order to find a wheel profile to match the modified RRD function. The inverse problem can be solved using an optimisation method. This idea is used as a foundation for the creation of the procedure for wheel profile design.

In the wheel profile design procedure, the optimisation searches for an optimum wheel profile by minimizing the difference between target (desired) and actual RRD functions. To solve the minimization problem, an optimisation procedure based on Multipoint Approximations based on Response Surface fitting (MARS method) is used. Different constraints can be applied in the optimisation procedure to reflect safety, construction, and other requirements to the designed profile.

Static analysis of geometric wheel/rail contact is used as a first step in the design of appropriate profiles. Dynamic analysis is needed to verify that the designed profiles will perform well under given vehicle and track conditions. Limited track tests should also be conducted, if possible, to confirm the analysis results.

Below, in Section 6.4, the complete procedure for the design of wheel and rail profiles is described. Methods of profile variation, criteria of optimisation of the wheel/rail contact, and the design procedure itself are described in detail in their corresponding sections.

6.2 Methods of profile variation

In this section, requirements for wheel profile description, and methods of profile variation that achieve a new shape of profile are discussed.

6.2.1 Wheel profile drawing

The designed shape of a wheel is represented by wheel profile drawing. For wheel manufacturing, wheel profile drawings generally have all dimension descriptions required for the machine production of such a profile. However, for designers and rolling stock maintenance staff, several additional parameters are required to assess features of the wheel profiles. The requirements for wheel profile drawings are described below.

Wheel flange angle is defined as the maximum angle of the wheel flange relative to the horizontal axis, as illustrated in Figure 4.13. As discussed in Section 4.5, maximum flange

angle is directly related to the wheel L/V ratio required for wheel flange climb. A higher flange angle has a lower risk off flange climb derailment. Therefore, it is very important to clearly denote the flange angle in the wheel drawing. Within a given manufacturing tolerance range, the flange angle should not be smaller than a specified minimum required value.

In the drawings, wheel profiles are generally described by a series of circular arcs and straight lines. For the convenience of both wheel/rail contact analysis and vehicle modelling, it is suggested that the coordinates of intersection points and arc centres be listed on the drawings.

MiniProf software calculates standard values to analyse wheel wear (Sd, Sh, qR). It calculates flange thickness (Sd), flange height (Sh) and the flange gradient (qR), for the selected profile. See Figure 6.3 below for definitions of parameters and results. For most railway wheels, the default values of the parameters are L1 = 2 mm, L2 = 70 mm, and L3 = 10 mm. For tram or light rail systems, these parameters can have different values.

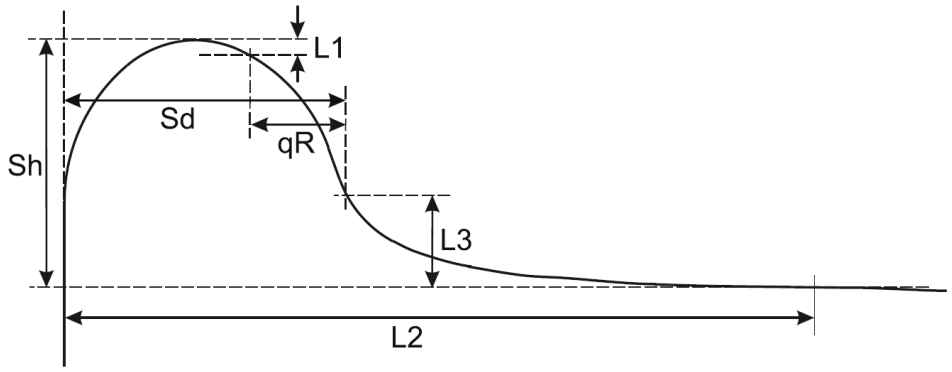

Figure 6.3: Wheel profile standard values.

In contrast to manufacturing processes, where wheel and rail profiles are represented by arcs and straight lines, in wheel/rail contact analysis, profiles are usually represented in analytical form (as a function), or in a discrete form, as a sequence of profile coordinates. To describe the geometry of a wheel (or a rail) profile, a number of points on the wheel's flange, flange root, and tread parts are chosen. Usually, these basis points are stored with a step of 0.1 mm, but larger spacing between points is also possible. Note that here the node points of the profile are mentioned. To solve the geometric contact problem, a smaller step between profile discrete points is required. To achieve this, interpolation methods are used. Connected by a spline or a piecewise cubic Hermite interpolating polynomial, the node points define the shape of the wheel profile, as shown in Figure 6.4. The positions of these node points can be varied in order to modify the profile.

In geometric contact programs, wheel and rail profiles are represented as a sequence of profile coordinates in the Cartesian coordinate system. However, there exist a number of possibilities to change (vary) the wheel (or rail) profile; these methods are described below. For simplicity, we will address wheel profile description. Rail profile can be represented and varied in a similar way.

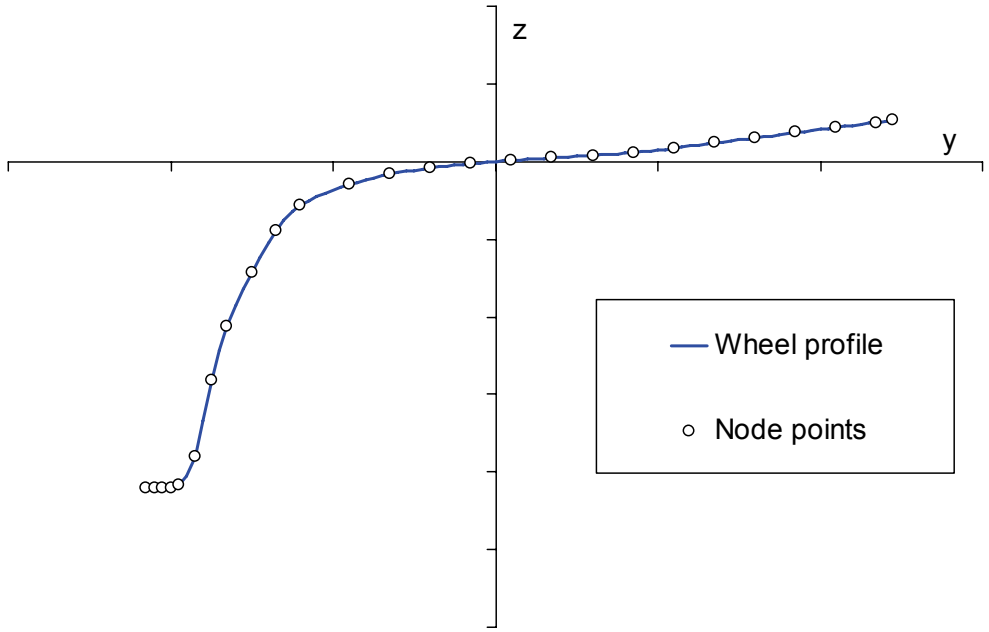

Figure 6.4: Wheel profile and node points.

6.2.2 Circular arcs

For many years, researchers have been using arcs and straight lines to draw wheel and rail profiles. Smith and Kalousek [1990] developed a procedure for design of a wheel profile described by a series of arcs. These authors developed a wheel profile specifically for steered axle vehicles. However, the most important aspects of this procedure can be applied to the design of a wheel profile for conventional systems. For example, the drawing of the S49 rail is shown in Figure 6.5. As shown in Figure 6.5, the head of the rail S49 consists of three radii, namely R=300 mm, R=80 mm and R=13 mm. Therefore, the corresponding wheel profile, which provides evenly distributed contact points, can also be built from a series of circular arcs.

Multiple contact points between wheel and rail are highly undesirable. As discussed in Section 2.4.1.2, to avoid this, the radius of a wheel profile at the contact point must always be greater than the radius of a rail profile at the same contact point.

The following procedure for design of a wheel profile made up of a series of circular arcs was originally proposed by Smith and Kalousek [1990] and later adapted by the author:

1. The position of the initial contact point (contact point at zero lateral displacement of a wheelset) on the rail must be chosen. From known values of track gauge, rail width, and inner wheelset gauge, the position of the mean wheel circle can be calculated.
2. For tangent parts and large radius curves, the radius of the tread part should provide the required RRD within the required lateral displacement of the wheelset. This is the first arc.
3. The second arc, of smaller radius than the first, is connected to the first arc, the tangents at the point of connection being coincident. The end of the first wheel arc is located at the last contact point with the first rail arc. Correspondingly, the end of second wheel arc is located at the last contact point with the second rail arc.

4. The third arc is connected in the same way as the second arc. The radius of the third arc should meet two requirements: first – provide required RRD within the remaining lateral excursion, and second – provide required wheel flange width.
5. The top of the flange is connected with third arc by the fourth circular arc, with opposite curvature.
6. The field side of the wheel profile can be made from a circular arc or a straight line with certain conicity. The field side part is to be connected to the first arc at its highest point, or at the point where the tangents of the two parts coincide.

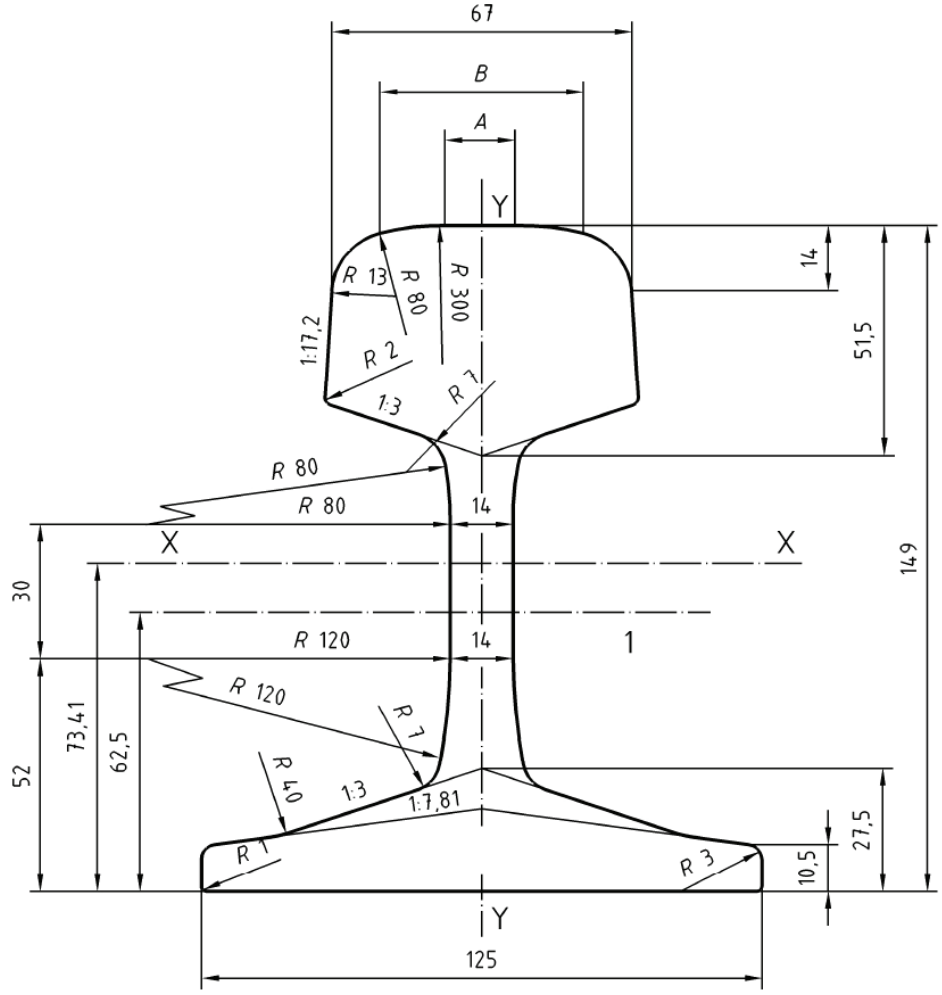

Figure 6.5: Drawing of S49 rail.

A schematic representation of the wheel profile consisting of the three circular arcs corresponding to the circular arcs of the S49 rail profile is shown in Figure 6.6.

Advantages of circular arcs:

1. shape of profile is smooth, first derivative is continuous;
2. zigzag on profile is avoided;
3. global shape control;
4. even distribution of contact points along unworn wheel and rail profiles is achieved due to arched shapes of the profiles;
5. uses basic principles of wheel and rail design;
6. profiles are immediately represented as a drawing.

Disadvantages of circular arcs:

1. all parts of profile are rigidly linked to each other. For example, modification of the first part of the profile will lead to a shift in all other parts of the profile, or will require recalculation of the entire shape of the profile;
2. inflexible method, difficult to use for worn rail profiles;
3. for geometric contact programs, conversion from arc and straight line representation into discrete points is required;
4. calculation of a worn shape is complex.

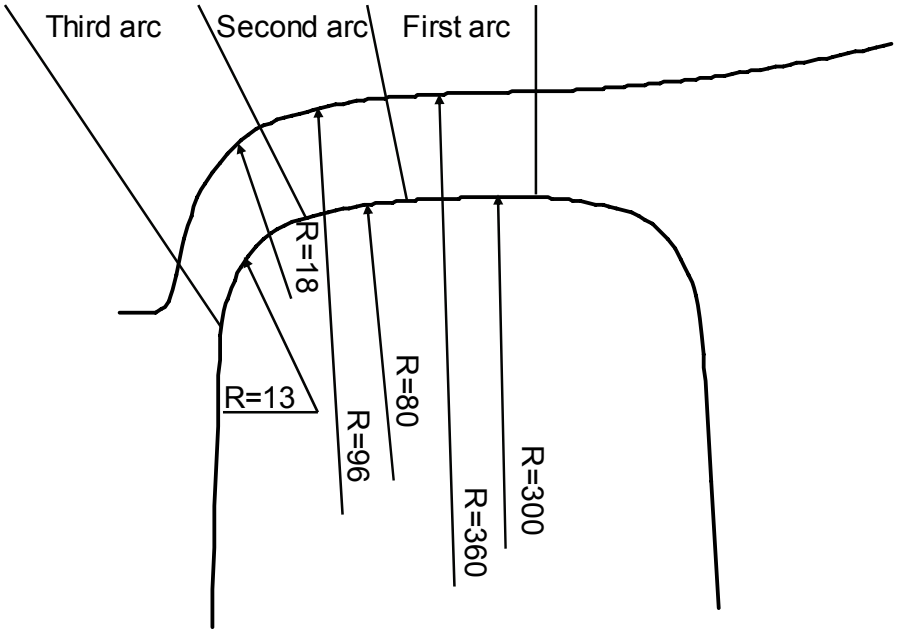

Figure 6.6: Schematic representation of designed wheel and S49 rail.

6.2.3 Cartesian coordinates

After arcs and straight line representation, one of the simplest methods of wheel profile variation is representation of wheel profile by node points evenly spread along the profile in the Cartesian coordinate system, as shown in Figure 6.7. The node points are connected by a piece-wise cubic Hermite polynomial function. During optimisation (or wear simulation), the vertical positions of the node points can be varied, whereas the lateral positions of the node points are prescribed (fixed). This alone reduces the number of design variables in the optimisation problem by a factor of two.

The number of the moving points on a wheel profile, and their location, must be determined through analysis of wheel/rail contact characteristics beforehand. To reduce the computational costs of the optimisation, the positions of the points on the flange top and on the field side of the conical part of the profile are not varied during the optimisation, since these parts of the wheel profile do not participate in wheel/rail contact. For tangent track, only the points ambient to the wheel tread are considered. In this case, stability is the dominant factor. In curves, points ambient to the flange root and the field side are selected. Here, wear and contact stresses are dominant.

Advantages of the use of Cartesian coordinates:

1. simple to visualize and analyse;
2. ready to use, does not require any significant modification of computer program;
3. easy for calculations, straightforward method;
4. easy to change and restore profile (back–forward transformation);
5. horizontal coordinates of profile node points are fixed, thus reducing number of design variables in the optimisation procedure;
6. can be used with virtually any rail shape.

Disadvantages of the use of Cartesian coordinates:

1. possible appearance of zigzag on profile, in optimisation problem additional requirements will be needed to avoid unrealistic shapes of the profile;
2. wear of profile is simulated in vertical direction instead of normal, unless special procedure is applied;
3. variations of node points are different on tread part than on flange;
4. second derivative of profile is discontinuous.

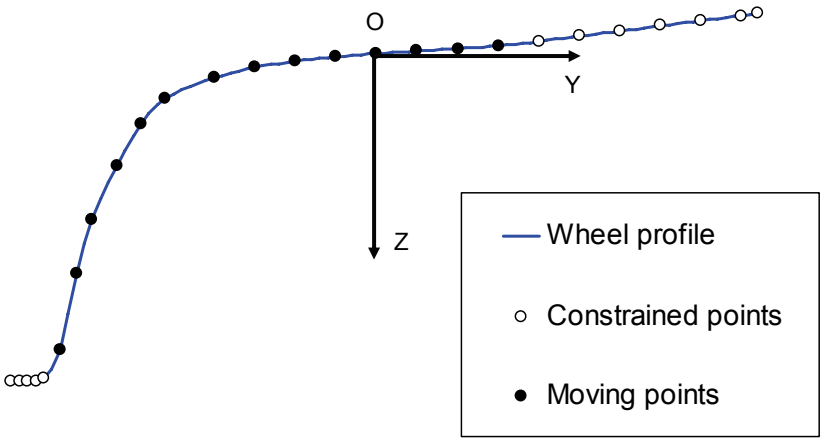

Figure 6.7: Example of Cartesian coordinate system.

6.2.4 Curvilinear coordinates

Polar coordinates are presented by angle between horizon and radius and length of the radius, as shown in Figure 6.8. Node points can be evenly distributed along a wheel profile, or evenly distributed using constant angle step. In the first case, angles differ between adjacent node points. In the second case, node points are not evenly distributed along the wheel profile.

Advantage of polar coordinates:

1. possible to deal with vertical parts of profile (points are better distributed along vertical part, whereas for spline in Cartesian coordinates this is not possible).

Disadvantages of polar coordinates:

1. possible appearance of zigzag on profile;
2. transformation from original Cartesian coordinates to the polar coordinates must be implemented via software modification;

3. radius coordinates can be not normal to the wheel profile, introducing distortion in the shape of the wheel during variation of the profile;
4. wear of profile cannot be simulated in normal direction, unless special procedure is applied;
5. distance between node points (measured along profile) is changes with variation of profile.

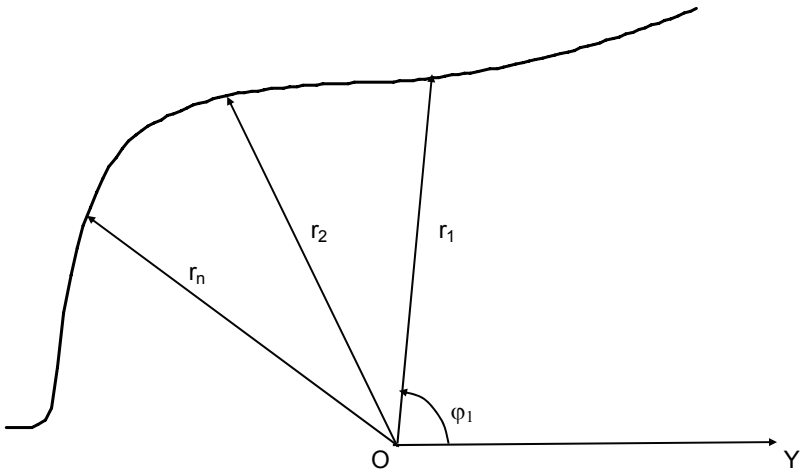

Figure 6.8: Example of polar coordinate system.

Normal coordinates represent a modification of the polar coordinate system. Wheel profile is taken as the basis of the coordinate system. Node points are (evenly) distributed along the wheel profile. Changes in the wheel profile (i.e., modification of the wheel profile) are performed in the normal direction to the original (reference) profile (see Figure 6.9). Profile variation is measured using the scaled normal sections placed in the node points.

Advantages of normal coordinates:

1. wear of profile is correctly calculated, as it is advance in direction normal to profile;
2. easy to see changes in profile;
3. highly suitable for profile modification or wear calculations.

Disadvantages of normal coordinates:

1. possible appearance of zigzag on profile;
2. transformation from original Cartesian coordinates to the normal coordinates must be implemented via software modification;
3. dependent on the reference wheel profile;
4. the coordinate system normal to the reference profile can be non-perpendicular to the modified profile.

The last problem can be dealt with through variation of the profile in the normal direction to the wheel profile. However, this will lead to a shift of the node points, and consequently to a shift of the coordinate system. Special procedures are required to address this, and intermediate results must be stored. This is difficult to realise in an optimisation procedure.

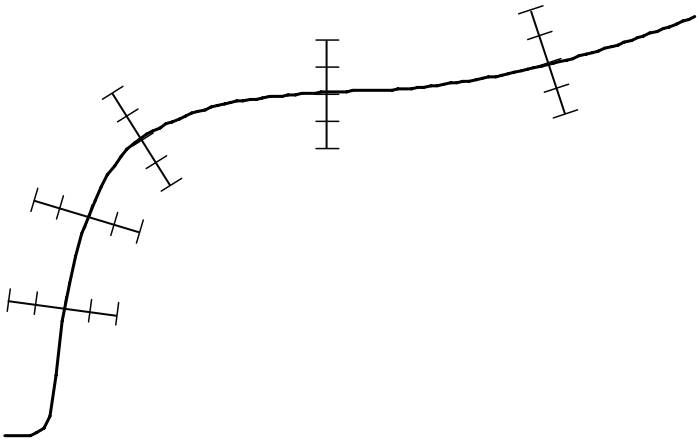

Figure 6.9: Example of normal coordinate system.

6.2.5 B-splines

The geometry of a wheel profile is described by B-spline. Braibant and Fleury [1984] proposed the use of B-spline for shape optimisation problems due to B-spline's flexibility. With B-splines, it is no longer necessary to piece together design elements such that they agree with shape complexity, nor to restrict shape variations. Furthermore, the additional optimisation constraints that are needed to avoid unrealistic wheel profile designs are automatically taken into account in the new formulation. A mathematical formulation of B-spline functions, as well as information about Computer Aided Geometrical Design (CAGD), can be found in the work of Böhm, Farin and Kahmann [1984].

A number of nodes along the wheel flange, flange root, and tread are chosen to compose B-spline. These nodes define the shape of a wheel profile as shown in Figure 6.10. The positions of these nodes can be varied in order to modify the profile. To reduce the computational costs of the optimisation, the positions of the nodes on the flange top and on the field side of the profile are not varied.

One of the features of the B-splines is that some nodes do not coincide with the wheel profile (see Figure 6.10), while node points of the ordinary splines coincide with the function they are describing.

The nodes are moving in the direction normal to the initial wheel profile. This is done to take advantage of the normal coordinate system. The number of moving nodes and their location along the wheel profile is determined from the analysis of wheel/rail contact properties beforehand.

Advantages of the B-splines with normal coordinates:

1. shape of profile is smooth, second derivative is continuous, zigzag on profile is avoided;
2. modification of profile is made in a normal direction to profile;
3. global–local shape control;
4. represent local and global changes of the wheel profile.

Disadvantages of the B-splines with normal coordinates:

1. transformation from original Cartesian coordinates to the normal coordinates must be implemented via software;
2. dependent on the reference wheel profile;
3. the coordinate system normal to the reference profile can be non-perpendicular to the modified profile;
4. linear displacement of the nodes leads to non-linear modification of the profile shape.

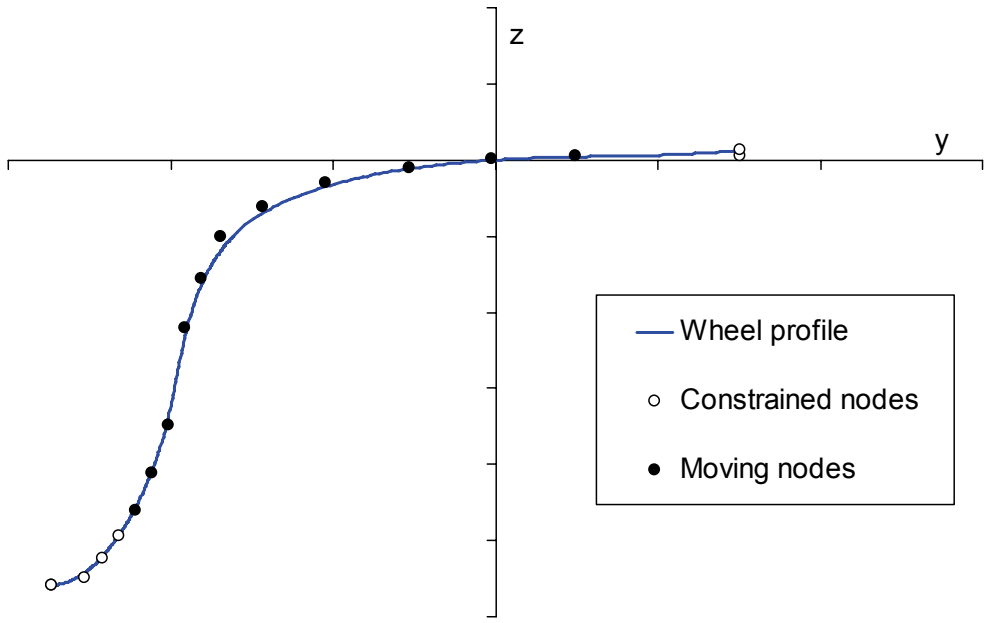

Figure 6.10: Wheel profile, constrained and moving nodes. Note that nodes do not coincide with the wheel profile.

6.3 Criteria of optimisation

In this section, the requirements for and constraints on the designed profile are discussed.

6.3.1 Wheelset dynamics

As discussed in Chapters 2 and 4, a railway wheelset must satisfy two contradictory requirements: it must provide the required critical speed, and it must pass curves without excessive slippage. It has been shown by Wickens [1965], Newland [1968] and Boocock [1969], that wheel profile has a tremendous effect on bogie dynamics both on straight track and in curves. Behaviour of the railway bogie is defined not only by wheel/rail profiles, but also by bogie geometry and suspension characteristics. During wheel profile design, we assume that all bogie parameters are given, therefore, the wheel profile should match given thresholds.

For increased critical speed of the vehicle, the (equivalent) conicity of the wheel/rail pair should be minimised. For passing curves, the required RRD should be available and the wheel must be able to provide this RRD, for which increase of (equivalent) conicity is required. A fundamental conflict therefore exists between the requirements for high speed stability on straight track, and good curving with safe negotiation of track irregularities. The wheel profile must therefore be selected to give the best compromise for the conditions under which the vehicle will operate.

6.3.2 Wheel/rail wear

The level of wear at the wheel and rail surface is indicated by the energy dissipated in the contact patch; this is calculated by taking the product of creepage and creep force, as shown in Section 3.5. A high value of energy here is seen as indicating a high rate of wear of the wheel profile and is to be avoided. Some wear is however, seen as beneficial, as it removes small cracks that develop through rolling contact. A very low level of wear is also undesirable, as it probably indicates that wear is taking place over a very limited section of the profile (hollow wear as an example), and that the shape of the profile will not then be stable.

Wheel wear is estimated using the wear index W taken from the English Normatives (British Rail) that reads:

$$W = F_x \cdot \xi + F_y \cdot \eta \,, \tag{6.2}$$

where F_x is the longitudinal creep force; ξ is the longitudinal creepage; F_y is the lateral creep force; η is the lateral creepage.

As can be seen from formula (6.2), to reduce wheel wear, one should reduce tangential creep forces and (or) creepages in wheel/rail contact. Of course, for wheel/rail profile optimisation, we do not consider traction and braking regimes where creep forces and creepages are significant. As is shown later in the examples, the wheel tread – rail top contact produces the lowest wear index, due to low creep forces and creepages. This type of wear is called “mild wear”. This is valid for the case of a single point contact. Double point contact increases the wear index due to larger creepages in the contact. In this case, wear can vary from mild to severe.

Wheel flange root – rail gauge corner contact produces a larger wear index due to increased creepages and creep forces. Usually in this area, severe wear is observed. When a double point contact situation occurs between flange root and gauge corner, the wear index increases significantly due to increased creepage and creep forces. Wear then becomes catastrophic.

Contact between wheel flange and rail gauge corner leads to high wear index, especially in the case of double point contact, where the wheel also has contact on a tread part. In this case, wheel flanges experience a catastrophic wear regime, while wheel tread remains in a mild regime (also due to lower tangential forces in the contact patch).

6.3.3 RCF problem

High levels of contact stress are likely to result in rolling contact fatigue or other rail or wheel damage. To estimate the possibility of rolling contact fatigue in a railway wheel, an engineering model developed by Ekberg et al. [2002] is used in the present study. The prediction of surface fatigue defects (head checks) is defined by the surface fatigue index FI_{surf}:

$$FI_{surf} = \mu - \frac{2\pi abk}{3F_z} > 0 \,, \tag{6.3}$$

where μ is the traction coefficient, a, b are the semiaxes of the Hertzian contact patch, F_z is the normal force magnitude, and k is the yield stress in pure shear. In the present study, the traction coefficient μ is defined as the quotient between the tangential and normal forces in the contact patch:

$$\mu = \frac{\sqrt{F_x^2 + F_y^2}}{F_z}, \tag{6.4}$$

where F_x and F_y are the longitudinal and lateral creep forces.

If the inequality (6.3) is satisfied, then fatigue damage is predicted to occur.

Analysis of formula (6.3) leads to the conclusion that decreasing the normal load F_z, and traction coefficient μ, as well as increasing the elliptic contact area of the Hertzian contact, reduces surface fatigue occurrence. This conclusion will be employed during wheel profile design.

6.3.4 Other requirements

Besides main criteria, such as wheelset dynamics, wear, and RCF, many other requirements can be applied to wheel profile design. These requirements can represent geometric limits, requirements for wheel/rail contact properties, or to wheel profile maintenance process. Several major requirements are described below.

6.3.4.1 Geometric constraints

The designed wheel profile should meet all dimensional requirements. Flange width, flange height, and wheel band width, must conform to the dimensions used in the system for which a new wheel profile will be made. Designers should pay close attention to existing practice at the particular network. For example, inappropriate modifications in the field side of the wheel profile can lead to problems in passing switches or during wheel reprofiling.

Higher flange angle is necessary to reduce the risk of flange climb derailment in curves. Using Nadal's criteria, the safe minimal flange angle $\alpha^{\min}$ can be found for each specific railway system. Further, constraint on flange angle α of the designed wheel can be introduced:

$$F_i \equiv \left(\alpha^{\min} - \alpha\right) \Big/ \alpha^{\min} \geq 0. \tag{6.5}$$

Effective conicity must be selected to give the optimum compromise between curving and stability requirements for the particular vehicle design and track system. Equivalent (or effective) conicity γ_e (2.4) is considered as the parameter defining stability of the bogie (see Wikens [1965 a,b]). For various types of railway vehicles, wheels with differing equivalent conicity should be used to achieve required critical speeds. High conicity can result in dynamic instability or "hunting" of the vehicle, which severely impairs its ride characteristics and can seriously damage the track. The equivalent conicity limit value $\gamma_e^{\max}$ for a wheel can be set to avoid excessively high conicity of a new wheel; it reads:

$$F_i \equiv \left(\gamma_e^{\max} - \gamma_e\right) \Big/ \gamma_e^{\max} \geq 0. \tag{6.6}$$

With the use of numerical modelling methods, designers must take care that designed profiles have realistic shape, as in numerical methods it is easy to obtain unrealistic topology. Spline functions can easily bend the profile line, or the choice of the position of the node points can produce zigzags in the profile.

To avoid this, additional constraints can be introduced in the numerical optimisation. For example, such constraints were implemented in Shevtsov et al. [2003], where constraints on

angles between the adjacent parts of the profile were introduced to avoid zigzags of the wheel profile, and thus to exclude unrealistic wheel designs during optimisation. Node points are numbered from 1 to n, starting from the low-left side to the upper-right of the profile, see Figure 6.7. Constraints for point number j are written as

$$F_i \equiv 1 - \frac{\gamma_{j+1}}{\gamma_j} \geq 0\,,\ j = 1,...,m, \tag{6.7}$$

for the concave part of the profile. Accordingly, for the convex part of the profile, these requirements read:

$$F_i \equiv 1 - \frac{\gamma_j}{\gamma_{j+1}} \geq 0\,,\ j = 1,...,n. \tag{6.8}$$

The γ_j is the angle between the y-axis of the wheelset (see Figure 6.7), and the straight line connecting points j and $j+1$ of the wheel profile. In a similar way, constraint on the wheel flange angle is introduced to satisfy the safety limits according to Nadal criteria, see equation (6.5).

To avoid additional constraints, advanced methods of CAGD can be used, as described in Section 6.2.5. Use of B-splines can prevent the appearance of zigzags on profiles.

6.3.4.2 Contact point distribution

While designing rail and wheel profiles, designers must keep in mind the following basic considerations:

1. Contact points are not spread over the whole rail and wheel surface. The contact point is limited to the regions highlighted in Figure 6.11. The safe operation of wheel and rail profiles precludes contact on the edges. This means that, during exploitation, the shape of both wheel and rail will change, however, some parts of the profile will remain unworn. This means that both the wheel and rail profiles will change shapes, and consequently wheel/rail contact properties will be altered. One question concerns the limits to allowable profile change. Usually the answer to such a question can be obtained only from practise, by studying the worn shapes of wheels and rails. One example of such research can be found in Sawley and Wu [2005], where the influence of hollow worn wheels on the stability of vehicles is investigated.

2. Contact points are not evenly distributed over the regions shown in Figure 6.11. The incidence of contact over the rail and wheel profile on straight track is highest on the centre of the tread. It is more sharply defined if pure conical wheel profiles are used on rails with high profile curvatures, and less so with profiled wheel treads on flatter rails. The contact band is also more sharply defined when the track gauge is more consistent. Two-point contact between wheel tread and rail crown on straight track is to be avoided, as it produces high-conicity contact (i.e., the danger of vehicle instability), and high wear due to the increase of slip in contact points. To address the problem of concentration of the contact points on a wheel tread, it is possible to use two different rail profiles on different parts of the straight track, as proposed by Magel et al. [2003]. These rail profiles should provide two concentrations of the contact points on the wheel tread.

Contact on the wheel profile in curves is invariably symmetric, if there is a balance between left- and right-hand curves. Contact on the rail is unsymmetrical and depends on the sense of the curve. In the case of profiled wheels, the outer wheel of the leading wheelset makes

contact closer to the gauge corner and flange root than the outer wheel of the trailing wheelset. Similar differences in contact occur on the low leg. These contact differences can be beneficial, as they reduce the number of fatigue cycles "seen" by both wheel and rail. Contact stresses and creepages are invariably higher in curves. For conical wheels, contact remains centrally placed on the top of the rail. On the wheel tread, it moves off-centre to the taping line by the amount of the lateral deflection of the wheelset. This effect of concentrating the contact on wheel and rail is considered detrimental to the fatigue life of the rail. The conical shape of wheel treads is transient, as they quickly wear to a more conformal profile, thus the use of this wheel profile type is not pursued further.

These two considerations lead us to the conclusion that the design of wheel and rail profile should provide good distribution of contact points along the whole working area of the profile. This will prevent profiles from local wear leading to alteration of profile contact properties, and from the concentration of RCF damage at one location leading to crack initiations. To achieve this, additional constraints can be introduced in the formulation of the optimisation problem. These constraints can be applied to the position of contact points, just distributing them along profile.

Another approach to reducing RCF damage is to avoid contact between wheel and rail in the area where contact stresses exceed the shakedown limit. For example, if RCF arises in the flange root – gauge corner contact, than wheel (or rail) profile can be modified in such a way that contact will not occur in this region. To achieve this, positions of contact points can be constrained, preventing appearance of contact in the problem region.

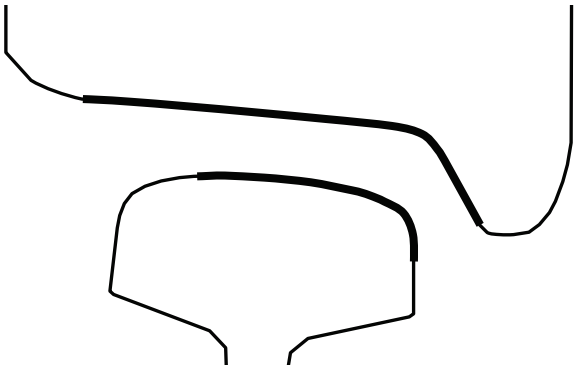

Figure 6.11: Potential contact on wheel and rail.

6.3.4.3 Cost reduction

Prolongation of the life cycle of a wheelset can be achieved not only by reducing wear of the wheel, but also by increasing the number of possible reprofilings for the wheelset.

During calculations, we find the area of cross section of the worn wheel S_{worn} and the area of cross section of a wheel after reprofiling into new profile S_{new}. To increase the number of such reprofilings, the difference between these two areas, i.e., the shaded area in Figure 6.12, should be minimal. Therefore, this constraint can be written as:

$$F_i \equiv \left(S_{worn} - S_{new}\right)/S_{worn} \rightarrow \min . \qquad (6.8)$$

Using this method, one can also try to optimise maintenance intervals of the wheelset. By using worn profile measurements through the entire wheel life, it is possible to find an optimum point, where the amount of natural wear, the amount of cut material, and the frequency of reprofilings will be minimal.

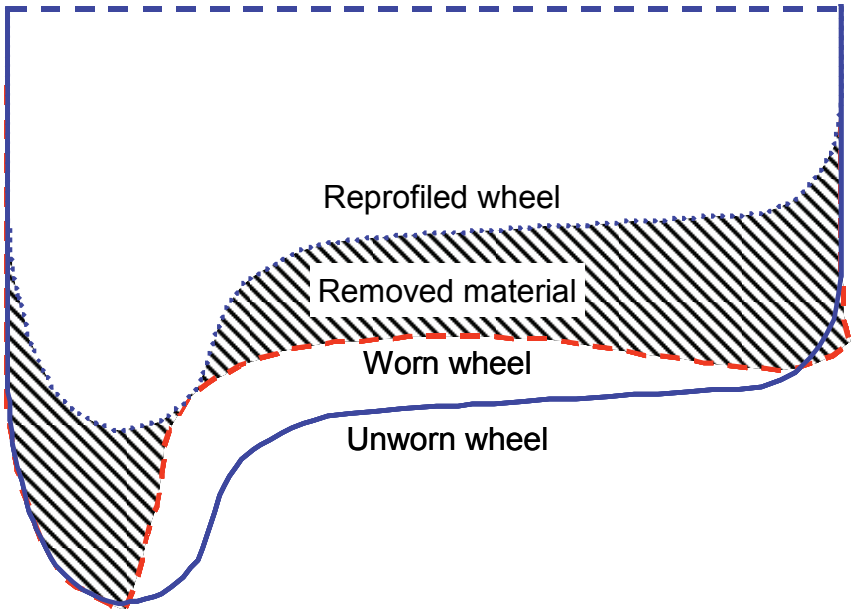

Figure 6.12: Reprofiling of worn wheel.

6.4 Design procedure for wheel and rail profiles

A wheel profile design procedure is developed using the idea that RRD function describes wheel/rail contact properties. Therefore, for the known "optimal" RRD function, a wheel profile can be found which provides the requested contact properties. Below, the design procedure is described in detail.

6.4.1 General scheme of design procedure for wheel profile

The procedure of wheel profile design used here is schematically shown in Figure 6.13. It consists of a number of steps. The first step consists of collection of data about wheelset and track geometric parameters. Also, the type of railway system (tram, metro, train) is very important. The dynamic parameters of the railway vehicle for which the new wheel profile is to be designed must be known. Of course, an analysis of the current wheel/rail profiles and their contact properties is of vital importance. Wheel and rail profile measurements are used to collect data on new and worn profiles. In the next step, the contact properties (RRD curve) for various wheel and rail combinations are analysed. After the analysis of the initial data, the designer must determine the constraints to be applied to the wheel profile (described in the previous section). Subsequently, the limiting (target) RRD function has to be obtained. In the case of improvement of an existing wheel/rail interface, wheel and rail profile measurements may be used to analyse wheelset contact properties in order to design a target RRD function. Three ways of defining a target rolling radii difference function are presented and discussed in Shevtsov et al. [2002 a, b, 2003]. The strategy for designing a limiting RRD function is presented in the following section.

In the next step of the procedure, the problem of finding a wheel profile corresponding to the target RRD function is formulated as an optimisation problem. The problem can be solved using the MARS optimisation method, which is successfully employed in various real-life applications (see Markine [1999], Markine and Toropov [2002]). Since the dynamic properties of a vehicle are not directly controlled during the optimisation process, which in fact reduces the computational efforts of the optimisation, they must be verified afterwards. The optimised profile is tested for stability, wear, and dynamic contact stresses using the ADAMS/Rail computer package (see ADAMS/Rail [2005]). If the dynamic performance of a

vehicle with the resultant wheel profile does not satisfy the imposed requirements, the RRD function and/or constraints should be adjusted, and the optimisation should be performed again in an iterative process. Otherwise, the resultant wheel profile is considered optimal.

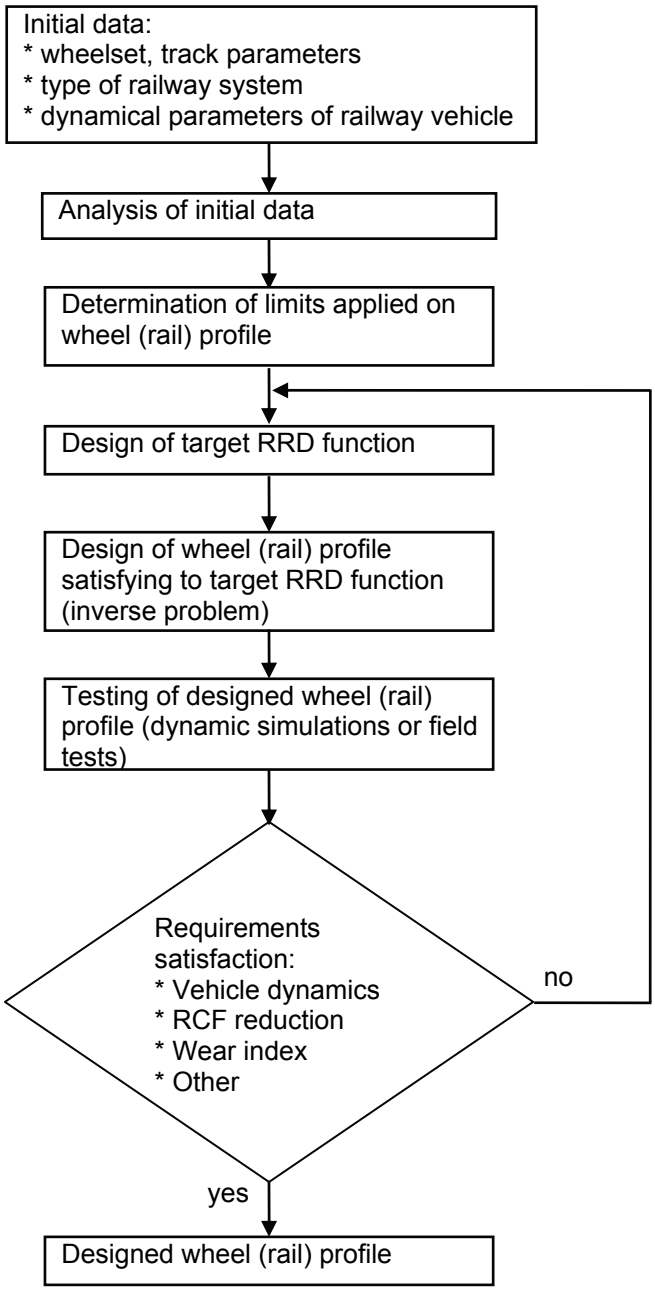

Figure 6.13: Flowchart of wheel (rail) profile design procedure.

Since the optimum wheel profile is defined by the target RRD, the difference between its RRD and the target RRD should be as small as possible. The requirement for the minimum discrepancy between the target rolling radii difference function Δr^{tar} and the RRD function of the designed wheel profile Δr^{calc} can be written as

$$F_0(\boldsymbol{x}) \equiv \frac{\sum_{i=1}^{K}\left(\Delta r^{tar}(y_i) - \Delta r^{calc}(\boldsymbol{x}, y_i)\right)^2}{\sum_{i=1}^{K}\left(\Delta r^{tar}(y_i)\right)^2} \to \min, \tag{6.9}$$

where y_i is the i-th discretisation point of the lateral displacements of a wheelset; K is the number of such points. The function (6.9) is taken as the objective function of the optimisation problem (5.4)-(5.6).

6.4.2 Design of limiting RRD function

In this section, the strategy of design and the constraints on RRD function are discussed.

6.4.2.1 Strategy of design of limiting RRD function

A target rolling radii difference function can be obtained in several ways:

- It can be a modification of a RRD function for an existing wheel/rail profile combination, when a problem in wheel/rail contact can be clearly identified. An example of such a case is presented in Section 7.3 (also see Markine, Shevtsov et al. [2003, 2004 a, b]).
- The designer can use the average RRD curve for worn wheels and rails; however, care must be taken on equivalent conicity to avoid the instability problem with the designed wheels. An example of such application is found in Shevtsov et al. [2003, 2005].
- The limiting RRD function can be built based on designer experience, or the RRD function of the successful wheel/rail profile combinations from a similar railway system can be used.

The target RRD function is divided into three parts that are responsible for tangent track, curved track and sharp curves, as discussed in Chapter 2. For tangent track, conicity at $y = 0$ should be maintained in the range 0.025–0.2 for, respectively, high-speed trains, and passenger trains to provide a sufficiently high vehicle critical speed. On a curved track with a large radius, the corresponding rolling radius difference must allow the wheelset to find the radial position in a curve to prevent wheel creepage (see Section 2.2.2). In sharp curves, wheels are expected to encounter heavy flange contact. In such a case, the RRD must be as high as possible. The complete procedure for selection of the target RRD function is described below.

6.4.2.2 Constraints applied on limiting RRD function

Let us consider design methodology for limiting RRD function using as an example a tram wheel/rail contact. This example is chosen because tram wheels have much more pronounced contact regions due to relatively small wheel width and a large variety of curve radiuses, ranging from very large to very small, which requires very efficient use of the whole contact surface of the wheel profile. Also, relatively small lateral displacement of the wheelset is required to achieve top flange contact. An example of a tram wheel contacting a rail is presented in Figure 6.14. The corresponding RRD function is presented in Figure 6.15.

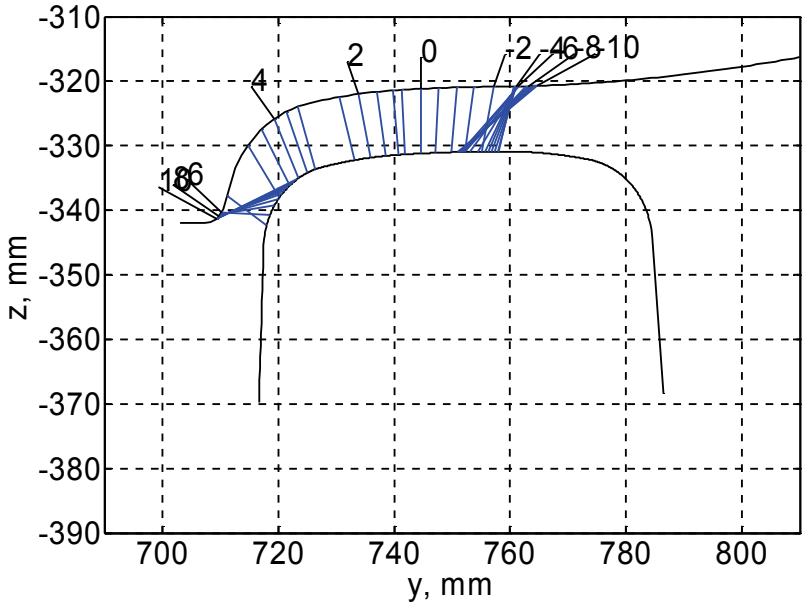

Figure 6.14: Positions of contact points for tram wheel profile with S49 rail profile.

In Figure 6.15, one can see the base points applied on RRD function. The first point is Y_s, corresponding to wheelset lateral displacement on a straight track. Within this lateral displacement, the RRD function should provide that Δr such that equivalent conicity γ_e will be below the maximum permissible equivalent conicity γ_e^{max}. Maximum permissible equivalent conicity ensures that vehicle motion is stable in the required speed range. The next point is Y_c, corresponding to the wheelset lateral displacement in curve. Between points Y_s and Y_c, RRD function must increase up to the maximum required (or available, if required RRD is too high) value, following formula (2.7) and Table 2.1. Required RRD value is dependent on the minimum curve radius existing on an examined railway network. Available RRD is dependent on wheel radius, track width, and wheel profile dimensions. For point Y_{fw}, the value of wheelset lateral displacement corresponds to the wheel contact point where wheel flange width is measured. Generally, the width of the wheel flange is prescribed by norms; therefore, RRD function must pass through this point. Maximum feasible wheelset lateral displacement is achieved at point Y_{max}, above which the contact point moves to the top of the flange, and the wheelset can derail. Point Y_{fh} corresponds to the area of top flange contact, which is easy to visualise for tram wheels due to the short wheel flange.

In Figure 6.16, the RRD function of a tram system is compared with the RRD functions for a metro and a train railway system. Here, one can see the influence of various railway parameters on the behaviour of RRD function. Due to larger flange clearance at metro and train systems, the RRD functions have wider area for contact on straight track and in curves. Points $Y_{s(train)}$ and $Y_{c(train)}$ are shifted relative to the corresponding points Y_s and Y_c of a tram system. Point $Y_{fw(train)}$ is also shifted relative to point Y_{fw}.

Using these five constraint points, Y_s, Y_c, Y_{fw}, Y_{max} and Y_{fh}, with the corresponding Δr's, a designer can describe the shape of the desired RRD function. This is shown in the following example. Let us consider the RRD function for a train system, shown in Figure 6.17 by dashed line. Assuming that only five points will be used in the description of RRD function,

namely Y_s, Y_{fw} and Y_{max}, as well as (0,0), and the endpoint of RRD function, just skipping the Y_c point. In this particular case, Y_{fh} is not used, as top flange contact is reached at a wheelset lateral displacement far beyond our point of interest. Using cubic spline interpolation, one can obtain a new design of RRD function, shown by a solid line. As is evident, the correlation between original and designed RRD functions is not satisfactory, due to the absence of the Y_c point. However, if the Y_c point is added to the description of the designed RRD function, the result is much better, as shown in Figure 6.18. Here, one sees very good correlation between original and designed RRD functions.

Using node points of the designed RRD, and referring to the rolling radii difference values required for the particular railway system, one can design a limiting RRD function that can be used in the wheel profile design procedure. Of course, the designer should keep in mind the available space at the wheel and rail profiles to fit the contacts within the existing area. If necessary, some additional constraints can be introduced on the limiting RRD function, describing supplementary properties of wheel/rail contact.

6.4.3 Test of dynamic properties of the profile

Static analysis of wheel/rail contact can be used as a first step in the design of appropriate profiles. Dynamic analysis is needed to verify that the designed profiles will perform well under given vehicle and track conditions. Limited track tests should also be conducted, if possible, to confirm the analysis results.

At the present time, three methods exist to test the dynamic properties of the designed wheel (or rail) profile:

- dynamic simulation;
- test on a (scaled) roller rig;
- field tests on a test ring or on a real track.

With the development of reliable multi-body dynamic software packages able to simulate railway vehicle dynamics, dynamic simulations have become the cheapest way to test designed wheel/rail profiles (and the whole vehicle as well). Of course, reliable vehicle models and representative track layouts must be available to perform such simulations. The problems of projecting the dynamic simulations on a real railway system still exist, as variation in real track conditions is much wider than can be simulated with a computer program. Nevertheless, dynamic simulations are a very reliable tool. Tests of wheel/rail profile dynamics on a roller rig are not very practical, as this is comparably time and cost intensive. The problem of scaling results from roller rig tests to a real life system is complex, as it includes not only dynamics of the railway vehicle, but also dynamics of the roller rig itself. Nowadays, roller rig tests are mostly used to perform controlled experiments to study tribological properties of wheel/rail contact. Field tests on a test ring or on a real track are most reliable, especially the latter. These tests are comparatively expensive, since they involve real rolling stock, but results obtained reflect a real-world operating environment.

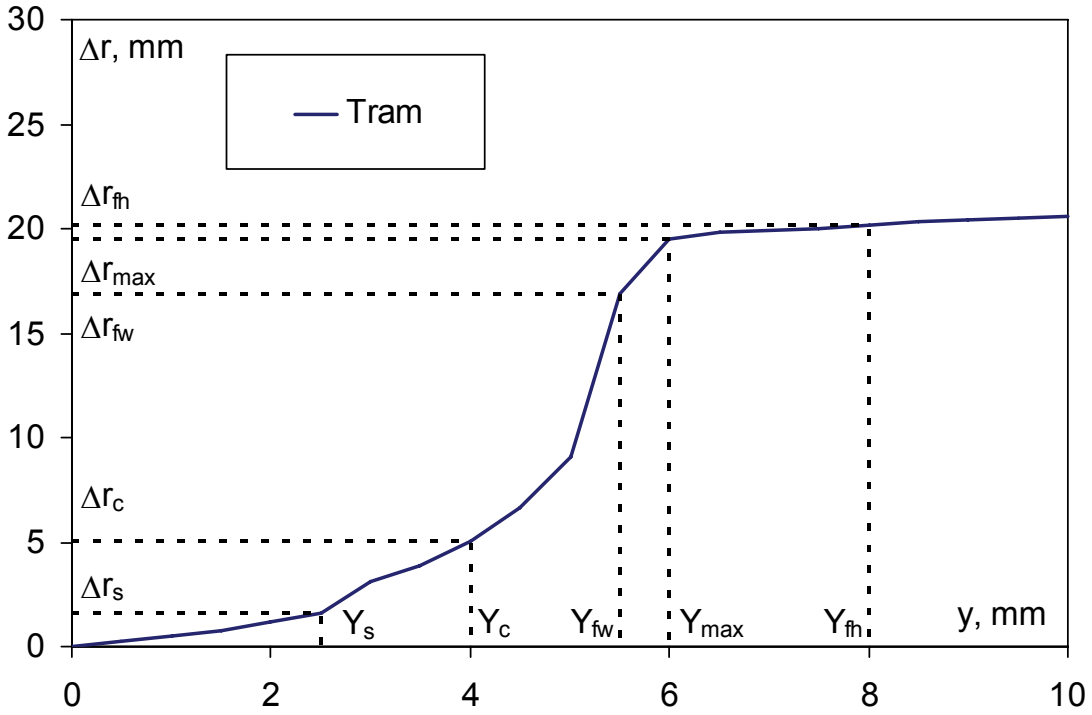

Figure 6.15: RRD function for tram system.

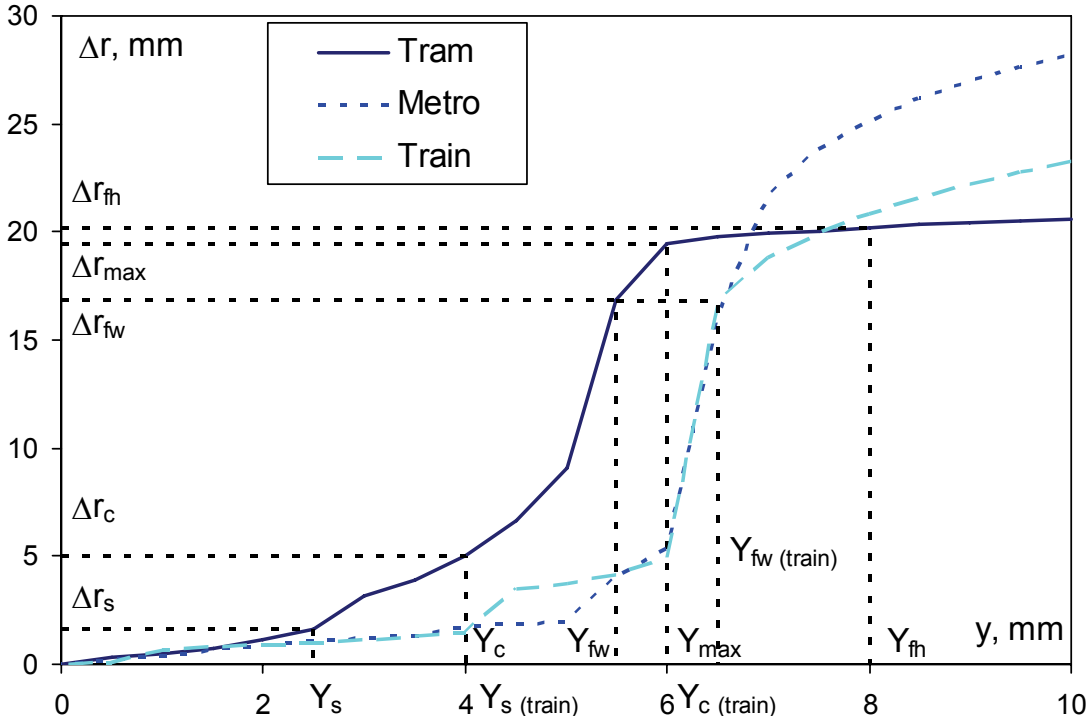

Figure 6.16: RRD functions for the tram, metro and train systems.

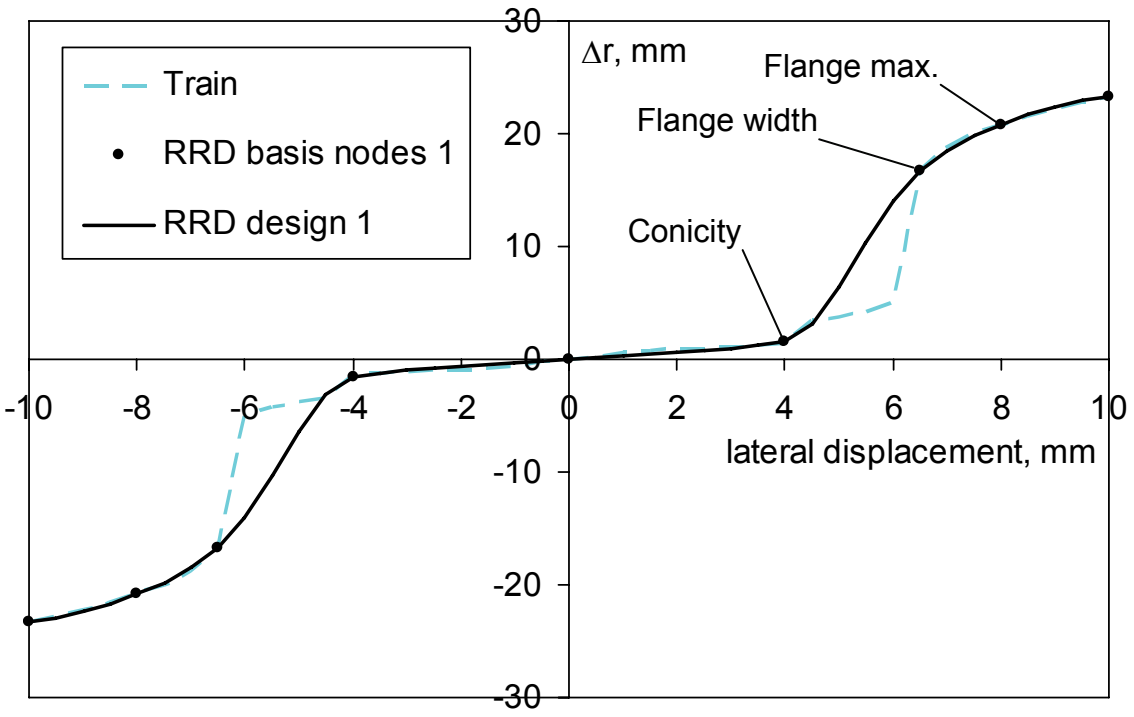

Figure 6.17: RRD function for train system, basis nodes, and designed RRD function (without point Y_c).

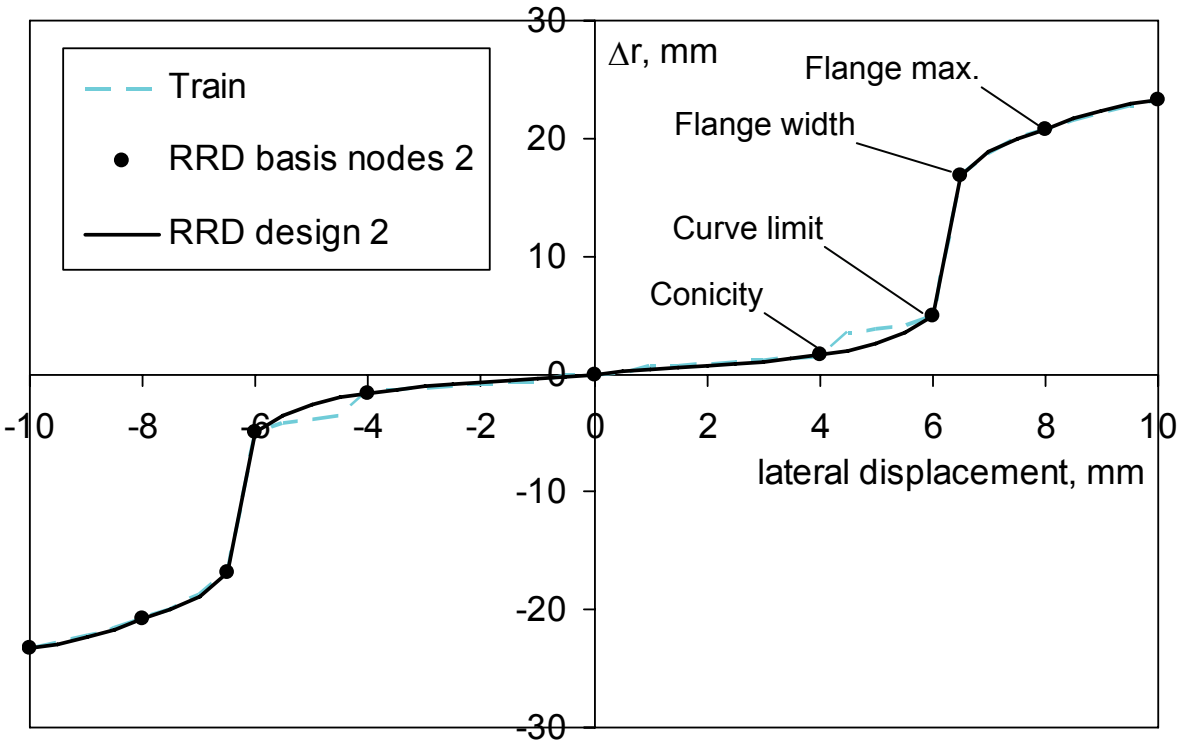

Figure 6.18: RRD function for train system, basis nodes, and designed RRD function (with point Y_c).

At present, dynamic simulation can be divided into three main categories according to the complexity of the dynamic simulations and wheel/rail interface models:

1. quasi-static approach:
   1.1. "Pummelling" model (Magel and Kalousek [2002]);
   1.2. "Quasi-static" model (Zakharov and Zharov [1998, 2002]);
2. dynamic simulation (a number of home-made and commercial software packages);
3. modelling of wheel (rail) profile evolution with mileage (Pearce and Sherratt [1990], Li [1998, 2001], Jendel [2000, 2002], Lewis et al. [2004 a]).

These simulation methods are used depending on various factors – available data, permitted simulation time, purpose of the research. Usually, a quasi-static approach requires a number of measured worn rail (wheel) profiles, with which tests of the designed wheel (rail) can be performed. Modelling of the evolution of the designed wheel (rail) profile requires fine tuning of the wear model using data from a real railway structure. Because such experimental data was not available during the work on this manuscript, dynamic simulation of the railway vehicles will be used. Dynamic simulation allows us to assess properties of the designed wheel (rail) using the criteria of optimisation described in Section 6.3, while not requiring large amounts of experimental data.

6.4.4 Design of wheel profile using contact stresses

High contact stresses (higher than the yield limit of the material) in repeated rolling contact between wheel and rail can lead to development of cracks in the material. With the importance of the RCF problem, one can decide to optimise wheel/rail contact to reduce the contact stresses that are responsible for the initiation of the cracks. An example of use of optimisation techniques to minimize rail contact stresses can be found in Smallwood et al. [1990].

The wheel profile optimisation procedure must be adapted to take into account contact stresses. Contact stress calculation programs (such as Kalker's "Contact" program) can be incorporated directly into optimisation procedures, and constraints can be introduced to minimize contact stresses. However, this will increase the computation time of the optimisation procedure. To avoid this, we invoke the basic principles of contact mechanics. Equation (6.3) clearly shows that a reduction of contact stresses can be achieved through increasing the contact area between wheel and rail. This can be achieved by increasing the transversal radiuses of the profiles, or by increasing the conformity of the profiles. Corresponding constraints can be incorporated in the optimisation procedure without leading to increased computation time.

One possible engineering solution for the reduction of RCF damage at the flange root and the rail gauge corner is the removal of the contact between the wheel flange root and the rail gauge corner. With this purpose in mind, a rail profile with a removed gauge corner can be designed and implemented in the curves. Also, wheel profiles can be modified in order to avoid flange root contact with the rail. An example of such a modification of the wheel profile can be found in Shevtsov et al. [2006, 2008], and will be described in Section 7.4.

6.4.5 Design of wheel profile using dynamic simulation

Development of fast computing, as well as reliable computer software packages now allows the simulation of the dynamic behaviour of the railway vehicle, brought to further development in the wheel/rail profile design problem. Here, we follow the works of Persson

and Iwnicki [2004], and Novales et al. [2006]. The flowchart of wheel (rail) profile design procedure using dynamic simulation is presented in Figure 6.19.

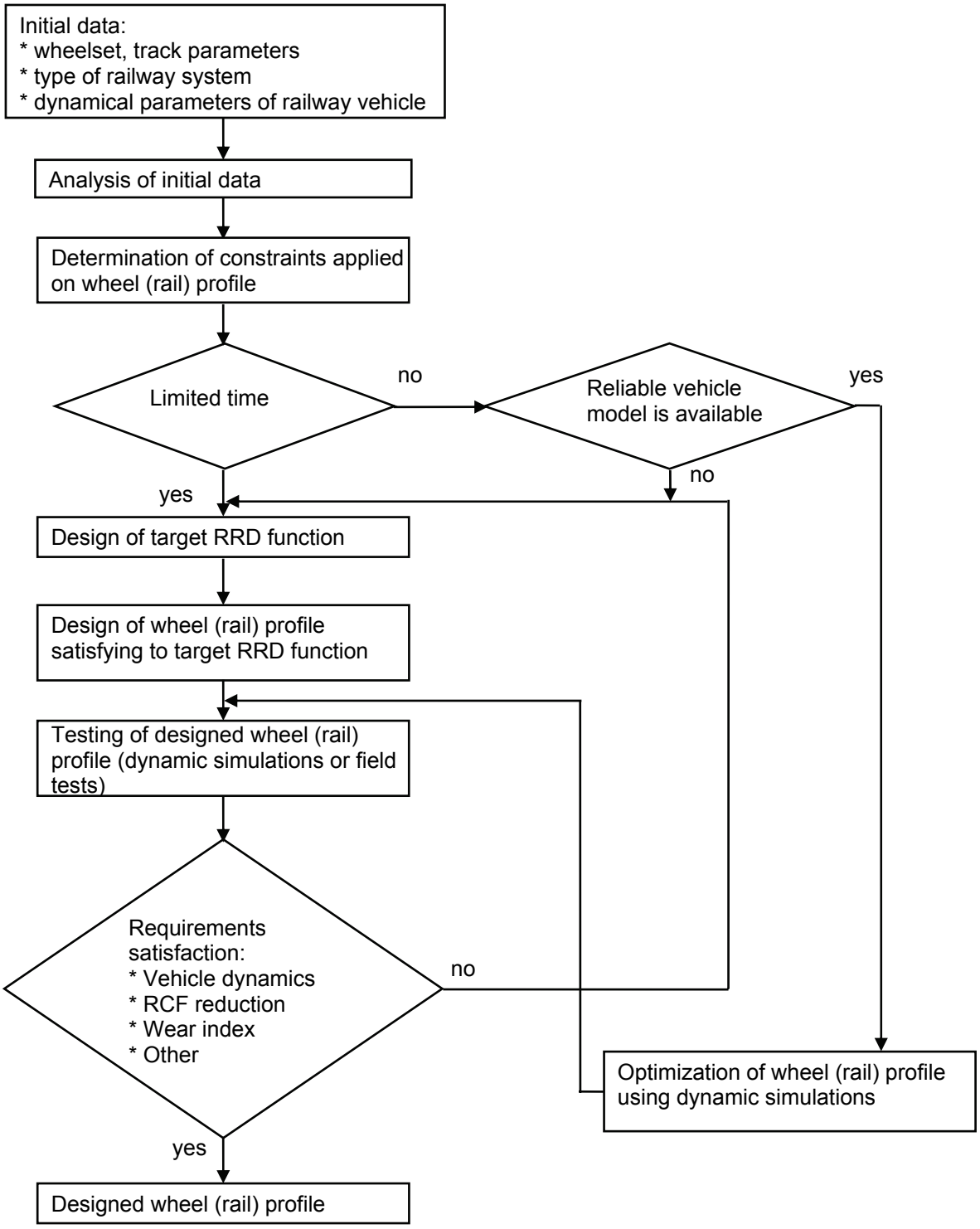

Figure 6.19: Flowchart of wheel (rail) profile design procedure using dynamic simulations.

Wheel profile can be optimised on the basis of responses obtained from dynamic simulations of the railway vehicle. The wheel profile is varied during the optimisation process. The varied wheel profile is incorporated into an ADAMS/Rail (or any other simulation software) simulation model of railway vehicles. Railway vehicles are simulated on a specially designed track, and various vehicle parameters are obtained in order to evaluate vehicle behaviour and

wheel/rail interaction. Wheel profile is varied until no further improvement of objective function is seen.

The track selected for the simulation tests must be a representative section of a railway line. After running through the selected track part the simulation is stopped and the results are used to calculate the objective function.

In order to evaluate the effectiveness of each profile, an objective function can be introduced which is calculated after each simulation run. The aim of the objective function is to provide an assessment of vehicle behaviour in a single value.

For wheel profile optimisation, several factors can be included in the objective function to reflect the maximum contact stress (or maximum surface fatigue index): the maximum lateral force on the track; the maximum derailment quotient (lateral force divided by vertical force at the contact point); total wear; and the total ride index. The objective function is the sum of individual penalty factors.

Each of the factors that make up the objective function can be weighted to reflect their importance to the designer or the particular service type. Other factors could also be included in the objective function if they were felt to be important.

6.4.6 Design of rail profile

On curved track, the outer rail is laid higher than the inner rail. This outer or “high” rail has been found to be susceptible to rolling contact fatigue, resulting in the initiation of cracks from the running surface of the rail. These shallow cracks can develop into squats or head checks, which can either link together, resulting in the loss of surface material, or turn and propagate transversely through the rail. It is known (see Chapter 3) that both contact stress and creepage have a significant effect on RCF life. One of the approaches to reduce RCF damage can be a modification of rail head geometry to create a low contact stress profile. An example of such optimisation can be found in Smallwood et al. [1990]. Another idea consists of providing “relief” to the rail contact surface by removing material from the gauge corner of the high rail, just avoiding contact between wheel flange root and rail gauge corner. Such a profile is known as the Anti Head Check (AHC) rail profile. The latest generation of aggressive grinding trains are able not only to remove the required amount of metal from the rail in just one train passage, but also to grind the rail to the required profile, making practical the application of the designed rail profiles (see Magel and Kalousek [2002], Schoech and Heyder [2003]).

Of course, the effects of the suggested new rail profiles on vehicle behaviour must be investigated using computer simulation and field tests.

Comparably small modifications are required to adapt wheel profile design procedure to the problem of rail profile design. Two things are required. First, modification of the rail profile must be implemented, and second, in a curved track, the condition of track symmetry is not fulfilled, therefore left and right (low and high) rail profiles must be considered separately in the contact program.

6.5 Discussion

A procedure for the design of a wheel profile using numerical optimisation is described in this chapter. This procedure uses optimality criteria based on the Rolling Radius Difference function that to a large extent defines the contact properties of the wheel and rail. The design procedure allows creation of wheel profiles with *a priori* defined contact properties.

Different representations of the shape of profile have been investigated. The most advantaged approach is to use B–splines for the description of the wheel and rail profiles. Description of wheel (or rail) profiles with B-splines in a shape-optimal design problem is a powerful and rather general approach.

There are several possibilities for effectively using the described design procedure:

- Obtaining wheel profiles for the new rail profile (e.g., upgrade of rail type due to track renewal), when previous wheel/rail profile combination was satisfactory. The RRD function of the previous wheel/rail couple must be used as the target RRD function. In this way, the new combination of wheel/rail profiles will have the same contact conditions as the previous one.
- When existing wheel and rail profiles mismatch each other, as clearly seen from their geometric wheel/rail contact. In this case, RRD function must be modified to remove unwanted contact behaviour thus improving wheel/rail contact.
- When current wheel/rail behaviour must be changed for new conditions, for example, vehicle must be used on a track with another rail inclination, operational speed must be increased, or sharper curves are introduced. In this case, current RRD function can be modified to satisfy new conditions, and consequently new wheel profiles can be designed.

The disadvantage of this method is that vehicle dynamic responses (wear index, wheelset dynamics) cannot be obtained before the wheel profile is designed by optimisation software. Possibly several modifications of limiting RRD function must be tested before good result will be obtained. Features of the rolling stock cannot be directly incorporated in the optimisation procedure. The problem of RCF reduction must be solved by applying additional constraints, or in a separate block.

The advantage of this method is that it is much less computationally expensive than the optimisation of wheel profile using vehicle dynamic simulations. Another advantage of this method is that obtained profiles have the required contact properties.

This method can be modified by including a contact program in the design procedure to address the RCF reduction problem.

This method can be used together with the optimisation of wheel profile using vehicle dynamic simulation. Geometric wheel/rail contact is used as the first approach to wheel design. Then the optimisation of wheel profile using vehicle dynamic simulation is performed for the fine tuning of wheel profile. The disadvantages of this method are that precise vehicle and track models are required, as well as the fact that it is a very computationally expensive method. The advantages are that the wheel profile is optimised for exact railway vehicle and track conditions.

Optimisation of the wheel/rail interface is highly effective when a “closed” railway system is present. A railway system is called “closed” when only one type of rolling stock is running on one track. In the case of “open” systems, optimisation of the wheel/rail interface is difficult, because different types of rolling stock have varying influences on the development of rail profile, and it is very difficult to distinguish this influence.

A new wheel profile may be requested for a completely new rail system, starting with new wheels and new rails. The design emphasis under this condition is to establish desirable starting wheel/rail contact features to help new vehicles meet their performance requirements. Simulations and trial tests should be conducted on vehicles with the new wheel profiles under the specified operating conditions, to ensure that the specified requirements have been meet.

The likely wear patterns may be predicted to further determine vehicle performance under worn wheel/rail shapes.

A new wheel profile may also be requested for an existing rail system with worn wheels and rails. Under this condition, the existing worn wheel/rail shapes should be taken into consideration when designing the new wheel profile, for example when adopting a new wheel profile with a higher flange angle to replace an existing low flange angle wheel. If the profile change is significant compared to the existing design, it is likely that a temporary profile (more than one, when necessary) will be needed to gradually approach the desired profile. Further, a transition program should be carefully planned by considering the capacity of both wheel truing and rail grinding on the system.

Optimisation of the wheel/rail interface is made under certain restrictions, which come from existing designs of railway vehicles and track structures, safety regulations, exploitation parameters, etc.

A brief summary of the wheel/rail profile design problem:

Methods of profile description:

1. Geometric. Wheel profile is composed of straight lines and circles. Tread is made by straight line with different conicity (e.g., 1:10, 1:20, 1:40, etc.) or by large radius circle (R=300 mm). Flange is made by straight line inclined on angle of 70 degrees. Flange and tread parts are connected by circle or set of circles. Rail profile comprises 3 circles with different radii (e.g., 300 mm, 80 mm, 13 mm). Advantages of this method: conventional method, direct use by reprofiling machines. Disadvantages of this method: non flexible, requires hand work, discontinuities in contact.
2. Numerical. Wheel profile is presented by array of x-y coordinates. Node points are connected by polynomial functions or by spline. Advantages of this method – flexible, possible to avoid discontinuities in first and second derivatives, possible to work with measured (worn) profiles. Disadvantages of this method – polynomial functions can give oscillations of line, possible deviations from node points. The closest results can be achieved by Hermite piece-wise polynomial spline or by B-spline.

Methods of profile design:

1. Geometric. Wheel profile described by straight lines and circles. Tread conicity and circle radii adjusted to the existing rail profile to achieve required properties (increase critical speed, contact on wheel flange root, increase flange angle).
   1.1. Tread conicity is varied to increase critical speed.
   1.2. Wheel profile obtained by expansion of rail profile to achieve single point contact.
2. Optimisation of wheel profile using different methods (contact stress minimization, minimization of wear, dynamic parameters).
   2.1. Target function is pre-described (RRD function, contact angle function).
   2.2. Objective function is calculated in dynamic simulation model or in contact program.
3. Design of wheel profile using measured worn wheels. Shape of worn wheels usually a better match to rail profiles.

Methods of wheel/rail interface evaluation:

1. Dynamic simulations.
   1.1. Quasi-static approach.
      1.1.1. “Pummelling” model (Kalousek, Magel).
      1.1.2. “Quasi-static” model (Zakharov, Zharov).
   1.2. Dynamic simulations(ADAMS/Rail, Medina, Vampire, Sympack).

2. Estimation of worn wheel (rail) profile (Li, Jendel, Dwyer-Joyce).
3. Laboratory test on roller rig.
4. Field tests on test ring or real track.

Profile is optimised by means of improvement of its performance, together with satisfaction of different conditions and restrictions.

Criteria of optimisation:

1. Reduction of big (more than 10 mm) jumps of contact point on wheel and rail profiles. Contact points are evenly spread along profiles.
2. Reduction of contact stresses.
3. Calculated RRD function close to the target RRD function.
4. Increase of critical speed.
5. Reduction of wear index.
6. Improvement of ride comfort.
7. Lateral track-shifting force.
8. Maximum derailment quotient.
9. Increased number of reprofilings.

Limits applied on profile:

1. Geometric constraints.
1.1. Absence of zigzags on profile.
1.2. Fitted in to given size limits (flange height, wheel width, flange thickness).
2. Maximum contact stresses.
3. Required critical speed (maximum conicity).
4. Maximum derailment quotient.
5. Maximum wear index.
6. Number of reprofilings.
7. Limiting ride comfort values.

Criteria of profiles evaluation:

1. Geometric contact.
2. Wear index.
3. Dynamic parameters.
4. Safety parameters.
5. Contact stresses.

Limiting values of criteria to be determined by norms.

Ways of profile evaluation:

1. Dynamic simulations (ADAMS/Rail, Medina, Vampire, Sympack).
2. Field test on test ring.
3. Field test on real track.
4. Combination of dynamic simulations and field tests.

Technique of keeping profile properties in exploitation:

1. Grinding for rail, reprofiling for wheel (preventive).
2. Design of wheel profile which is stable in exploitation.
3. Transformation of open systems with many profiles into closed systems with one set of profiles.

The optimisation of wheel/rail interface via modification of wheel and rail profiles is an essential and powerful method. However, the influence of track and vehicle designs, track irregularities, and rolling stock deviations, can have a tremendous effect on wheel/rail wear, vehicle dynamics, the RCF problem, and safety. These factors should not be overlooked in the process of wheel/rail interface optimisation. In general, if analysis of geometric wheel/rail contact does not reveal problems, this means that other than wheel/rail profiles, sources of problems (e.g., excessive wear, instability, RCF) should be checked (e.g., track and rolling stock design, conditions, and maintenance). In the following Chapter 7 three real cases of wheel profile optimisation will be described.

7 Application cases of wheel profile design procedure

In this chapter, design cases of new wheel profiles for three types of railway vehicle are described. An introduction is given in Section 7.1. Section 7.2 presents the design of a wheel profile for a tram. Section 7.3 deals with the design of a wheel profile for a metro vehicle. The design of wheel profiles for passenger coaches of the conventional railway is described in Section 7.4. Section 7.5 finalises the chapter with conclusions and a discussion.

7.1 Introduction

Modern railways are developing systems. Numerous changes have been introduced over time to increase productivity, serviceability and profitability. However, in the field of wheel/rail interface, any modification should be carefully investigated before being applied in the field. Moreover, as will be shown in this chapter, even when no difference is expected in system behaviour as a result of the track renewal, unexpected side effects can negatively impact this behaviour. The development of appropriate combinations of wheel/rail profiles improves vehicle–track dynamic interaction and reduces wear and RCF.

In this chapter, we use all previously described theories, which are combined into the wheel profile design procedures described in Chapter 6, and apply them to practical cases.

7.2 Case 1: Design of wheel profile for tram (HTM case)

7.2.1 Description of problem

During the last decade, the increasing wear of wheels and rails has became a serious problem for HTM (Haagsche Tramweg Maatschappij N.V.), The Hague tram company. An example of an HTM tram is presented in Figure 7.1. Since the beginning of the 1990s, newly laid tracks on the HTM network have had different rail profiles, namely S49 and Ri60n, instead of S41 and Ri60. The wheel profile was not adapted for the new rail profiles at that time. After increased wear problems, the wheel profile was changed to one (HTM2) similar to the S1002 wheel profile, with an inner wheel gauge of 1389+0/-2 mm, a deliberate introduction of high conicity to increase the self-steering effect. HTM considers this profile to be non-optimal, since the problems of wear and hunting are not solved.

TU Delft (Section of Railway Engineering) was asked to perform a study of the contact situation between wheels and rails used by HTM, and to find the sources of high wear and hunting. Advice on a new profile was also requested.

Results from the investigation of contact situation, wheel profile design procedure based on optimisation technique and designed profile Opt26f, along with dynamic simulations of the tram vehicle in the ADAMS/Rail computational package are presented in the report 7-03-220-3 (Esveld, Markine and Shevtsov [2003]). The main findings of this report are detailed below. After completion of report 7-03-220-3, research on the wheel/rail contact situation at HTM continued, as several additional questions arose from HTM. The influence of the various unworn and worn wheel profiles and track gauge variations are studied as well. Design procedure is modified to use circular arcs in the design of wheel profile, which allows even spreading of the contact points along the wheel and rail profiles. Designed wheel profile CWdesign3 is extensively tested using ADAMS/Rail simulation. A complete description of

this testing can be found in the report 7-05-220-9 (Esveld, Markine and Shevtsov [2005]). Results from this study are described in the following sections.

It must be mentioned that the Opt26f wheel profile was not implemented in practise, while the CWDesign3 profile was successfully tested. The design processes of both profiles are presented together, according to the steps of the design procedure.

Figure 7.1: HTM tram. Delft - The Hague, The Netherlands. (Photo by the author).

7.2.2 Solution

In this section, the application of the wheel profile design method is shown step by step.

7.2.2.1 Analysis of problem

First, the geometry of the wheel and rail profiles must be analysed. In addition to the presently used HTM2 curvilinear wheel profile, a conical wheel profile HTM1 is considered. This profile was in use before the HTM2 profile was implemented. In Figure 7.2, the unworn HTM1, HTM2, and S1002 wheel profiles are shown. All profiles are aligned to cross the horizontal axis at the coordinate 53 mm (wheel tape line). It is clearly seen that the shapes of two curvilinear profiles are close to each other at the tread and flange root part. The flange of the S1002 profile is longer than the flanges of the tram wheels. The shape of the field side of the wheel tread of the S1002 profile differs as well, which is rather important for wheel/rail contact, as will be shown later. The HTM2 wheel profile has a 0.8 mm wider flange, as compared to the S1002 wheel profile, which increases wheelset outer gauge. In contrast to the HTM2 and S1002 wheel profiles, the HTM1 wheel profile is purely conical. This is an old-fashioned wheel profile. In this section, the HTM1 wheel profile is used for comparison purposes only.

The HTM company uses Ri60n and S49 rail profiles. The shapes of S49 and Ri60n rails are presented in Figure 7.3. Ri60n grooved rail is used without inclination, while S49 rail is used

with inclination 1:40. Ri60n rail profile is designed to match inclined 1:40 S49 rail. Therefore during analysis, only S49 rail profile inclined 1:40 is used in this section. In all figures, the rail S49 is shown with inclination 1:40.

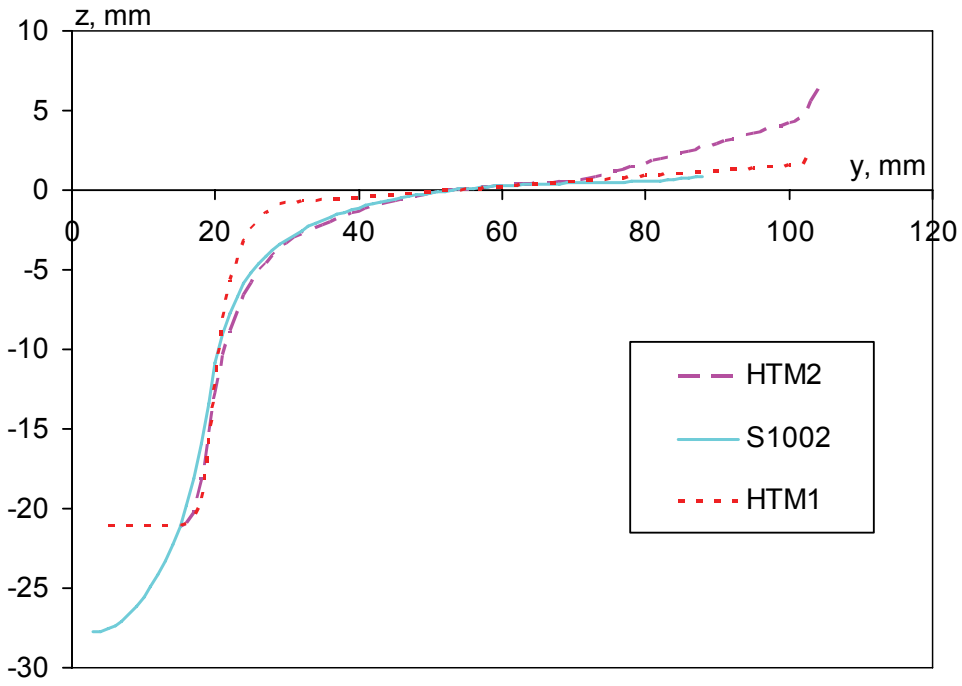

Figure 7.2: Wheel profiles HTM1, HTM2 and S1002.

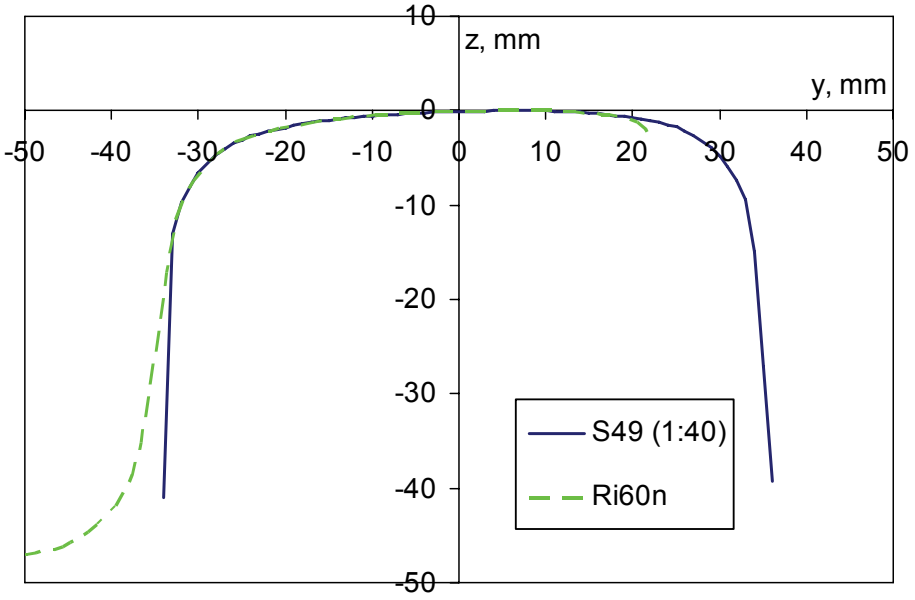

Figure 7.3: Rail profiles S49 and Ri60n (grooved part of the rail is not shown).

After the geometry of wheel and rail profiles is known, the properties of geometric wheel/rail contact are studied. The rail gauge is 1435 mm, measured at 14 mm below the track top, the wheel radius is 331 mm, and the wheelset inner gauge is 1385 mm. Wheelset inner gauge and track gauge are taken as constants unless mentioned otherwise.

The properties of geometric contact of the HTM1, HTM2, and S1002 wheel profiles with the

S49 rail profile are studied. The HTM2 profile is derived from the S1002 profile; therefore, the S1002 profile is present in this study. For the analyses of geometric contact properties, the contact situation between the wheels and rails for various lateral displacements of the wheelset are considered. The results of the calculations are shown in Figure 7.4, Figure 7.5 and Figure 7.6, where the contact situations for the right wheel and rail are presented. The contact situation for the left side wheel and rail is symmetrical, due to the symmetry of the track and the wheelset. In the wheel/rail contact figure, the lines between the wheel and rail profiles connect the corresponding contact points, which are calculated per 0.5 mm of the lateral wheelset displacement. The lateral wheelset displacements are shown above the wheel profile. The coordinate system in this figure is the wheelset coordinate system $y_w Oz_w$ (Figure 2.4), with the origin in the centre of the wheelset in neutral position. It should be noted that in this figure the wheel is shifted vertically 10 mm upwards from its actual position. Please, pay attention, that z -values are plotted with negative value to show graphs in convenient perception.

The HTM1 wheel profile is a classic example of a conical, double point contact wheel profile. In Figure 7.4, it can be clearly seen that the HTM1 wheel has contact on top of the rail at one point (for +/– 5 mm of the lateral displacement). For the larger displacements, the contact point jumps to the top of the wheel flange. Although not shown in Figure 7.4, in the region of +/– 5 mm of lateral displacement, the HTM1 wheel profile has simultaneous contact on the tread and flange part, creating a double point contact situation. This is a perfect example of a contact situation that leads to high wear.

For the HTM2 and S1002 wheel profiles, the contact situation is completely different from the HTM1 profile, as one can see from Figure 7.4, Figure 7.5 and Figure 7.6. For the curvilinear profiles, the contact points are more evenly distributed along the wheel and rail profiles. The contact with the rail top is not located at just one point, but creates a contact band. The flange root part also participates in the contact, in contrast to the HTM1 wheel.

For the HTM2 wheel profile, the contact points are spread on the top of rail and wheel tread up to 3 mm of the wheelset lateral displacement. Between 3.5 and 5 mm, the HTM2 wheel has contact on the flange root. The flange contact appears for 5.5 mm of the lateral displacement and is located on the top of the flange. For the S1002 wheel, the contact on the tread part is similar to the contact of the HTM2 wheel, but on the flange the contact is different. On the S1002 wheel profile, a jump from the flange root to the flange exists. By comparing Figure 7.5 and Figure 7.6, one can see that the contact points of the HTM2 wheel are located almost on the top of the flange, whereas on the contact points of the S1002 wheel they are spread along the flange. The non-participation of flange (except flange top) in the contact is a very undesirable situation. As a result, high wear will occur at one point instead of being spread along the profile. This means that the HTM2 profile can be improved.

In Figure 7.7, the rolling radius difference (RRD) functions for the HTM1, HTM2, and S1002 wheel profiles, and the S49 rail profile, are presented. The RRD function for the HTM1 wheel is piecewise-linear. A very large jump in the RRD function can be observed at +/– 5 mm of the lateral displacement when the contact point jumps from the tread to the flange. The RRD functions for the HTM2 and S1002 wheels are non-linear, and wider range of RRDs can be achieved during the lateral displacement of the wheelset before the flange contact. Curvilinear profiles provide better curving performance as compared to the purely conical HTM1 wheel.

It should be noted that the HTM2 wheel profile has 0.8 mm wider flange as compared to the S1002 wheel profile; this is why the flange contact appears earlier for the HTM2 wheel. In other words, the wheelset outer gauge with the HTM2 wheels is 1.6 mm wider as compared to the one with the S1002 wheels.

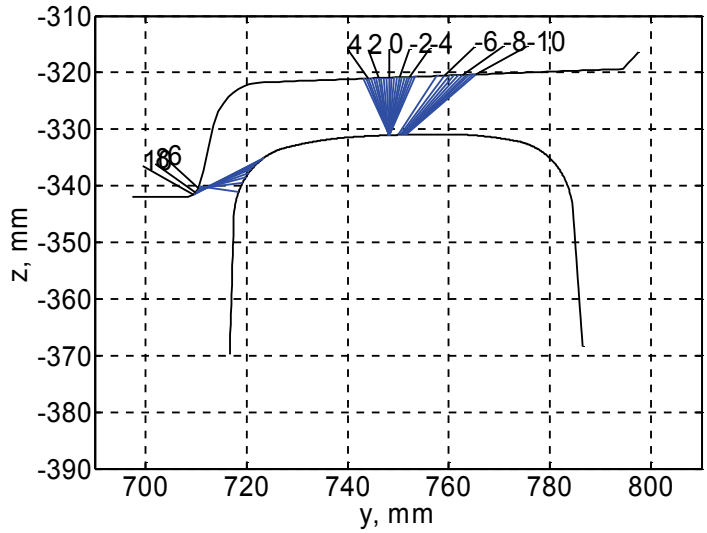

Figure 7.4: Positions of contact points for HTM1 wheel profile with S49 rail profile.

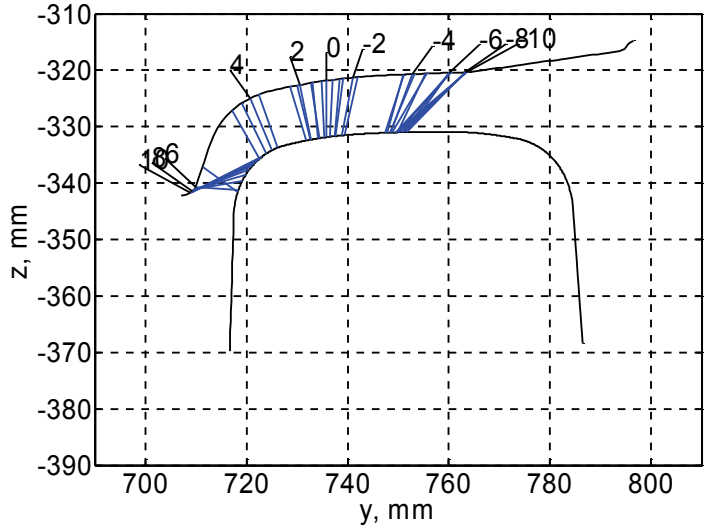

Figure 7.5: Positions of contact points for HTM2 wheel profile with S49 rail profile.

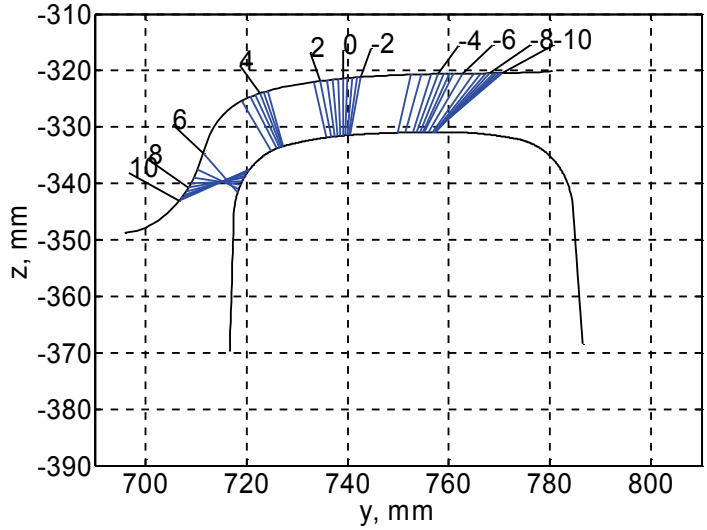

Figure 7.6: Positions of contact points for S1002 wheel profile with S49 rail profile.

For the S1002 wheel, the RRD function is divided into three regions, as can be seen in Figure 7.7. The first corresponds to the tread contact (+/– 2.5 mm), the second corresponds to the flange root contact (+/– 3–5.5 mm), and the third is related to the flange contact (after +/– 6 mm). The first region is responsible for motion on straight track, the second is responsible for the curves with large radius, and the third is responsible for sharp curves. Such a division provides necessary RRD for stability on the straight track and passing curves. On a straight track, the RRD should not exceed certain values in order to have the required critical speed, depending on the type of the vehicle. On a large radius curve, the wheelset will have steady motion because RRD provides a stable region for a certain range of lateral displacement (+/– 3–5.5 mm).

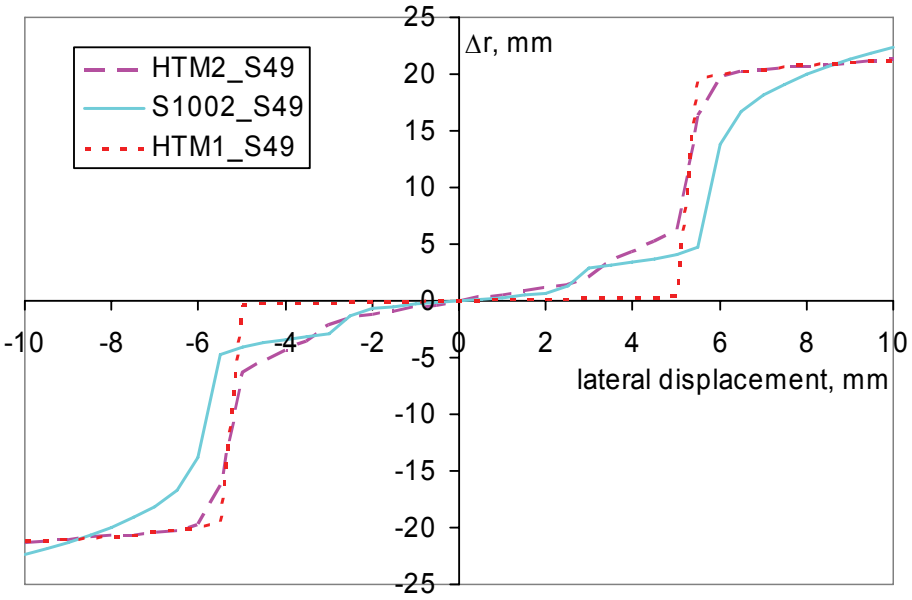

Figure 7.7: RRD functions for combination of HTM1, HTM2, and S1002 wheels on S49 rail.

7.2.2.2 Applied limits

As discussed in Chapter 6, during profile design, a number of limits (or constraints) can be applied on a designed wheel profile. Two safety requirements are considered in this case. The first is the requirement for wheel flange thickness, which is checked after optimisation. The second is the requirement to avoid derailment of the vehicle, which is achieved through restriction of the minimum flange angle. This requirement is checked for the optimised profile as well.

For the Opt26f profile, it the decision is taken to check fulfilment of the requirements for the obtained profile, not to apply the limits during optimisation. For CWDesign3, profile flange angle and flange thickness constraints are used during the optimisation process, not afterwards. The values from HTM standards for tram wheels are used for CWDesign3 profile. The unworn wheel flange width should be at least 19.2 mm for HTM tram wheels. The wheel flange angle should be between 65 and 70 degrees for the considered trams.

Constraints on angles between the adjacent parts of a profile are introduced to avoid zigzags of wheel profile, and thus to exclude unrealistic wheel designs during optimisation. Moving points are numbered from 1 to N, starting from the low left side to the upper right side of the profile (see Figure 7.10). Constraints for point number i are written as

$$F_j \equiv 1 - \gamma_{i+1}/\gamma_i \geq 0, \quad j = 1,...,k, \tag{7.1}$$

for the concave part of the profile. Accordingly for the convex part of the profile, these requirements read:

$$F_j \equiv 1-\gamma_i/\gamma_{i+1} \geq 0\,,\ j=k+1,...,N+1. \tag{7.2}$$

The γ_i is the angle between the y-axis of the wheelset and the straight line connecting points i and $i+1$ of the wheel profile. Some moving points located on the flange can be absent in (7.1)-(7.2), since their positions are already constrained by the side limits (5.3).

7.2.2.3 Design of limiting RRD function

In this section, the design of limiting (or target) RRD function for the case of an HTM tram is described. The general theory of design of target RRD function is described in Section 6.4.2. The target RRD function is used in the optimisation procedure for the design of a new tram wheel profile. The optimisation of the wheel profile is performed for S49 rail.

Two design cases are considered. In the first design of target RRD function, it is decided to not apply many constraints on the shape of the function. The idea is to improve contact situation, not completely redesign wheel profile. The S1002 wheel and S49 rail have good contact properties on the tread part of the wheel. However, the contact properties of the flange contact are not as good for this wheel/rail combination. A big jump of contact point from the tread to the flange can be observed. A decision was made to use the S1002 profile as the starting profile in optimisation, and to improve the flange contact of this profile. The modified RRD function of the S1002 wheel and S49 rail is used as a target function. As can be seen from Figure 7.8, from 0 to 5.5 mm of lateral displacement RRD function of the S1002/S49 combination is left without changes. After 5.5 mm to 10 mm of lateral displacement of the wheelset, target RRD function is smoothed to achieve smooth flange contact. The end point of the target RRD function is placed lower than the end point of S1002/S49 RRD function and almost coincides with the end of the RRD function for the HTM2/S49 combination. This is because the flange of the S1002 profile is longer than the flange of the tram wheel (see Figure 7.2). As a result, the RRD value for the top flange contact is higher for the S1002 profile. In this optimisation problem, 21 mm flange height of tram wheels is used. Therefore, the RRD values should coincide for top flange contact of the wheels with the same flange height, see "Target" and "HTM2_S49" lines at 10 mm of lateral displacement. In the first case, the general procedure of target RRD design was simplified and not all possible constraints were included.

Now the second design of the target RRD function is described. Originally, the second design of RRD was made based on experience with the design case of the Opt26f wheel profile for rail S49. However, for consistency, the second design of target RRD function is now described. The target RRD function is designed based on the procedure described in Section 6.4.2. Several additional requirements to the designed wheel profile are imposed based on experience with the design of the Opt26f wheel profile. These requirements were added after consultation with HTM to explicitly meet their standards. According to the standards, wheel flange width should be at least 19.2 mm, as in the HTM2 wheel. The wheel flange angle should be between 65 and 70 degrees. The newly turned wheels have 70-degree flange angle, while the average angle of the worn HTM wheel profiles is 65 degrees. Keeping the wheel flange angle within these limits guarantees safety against derailment.

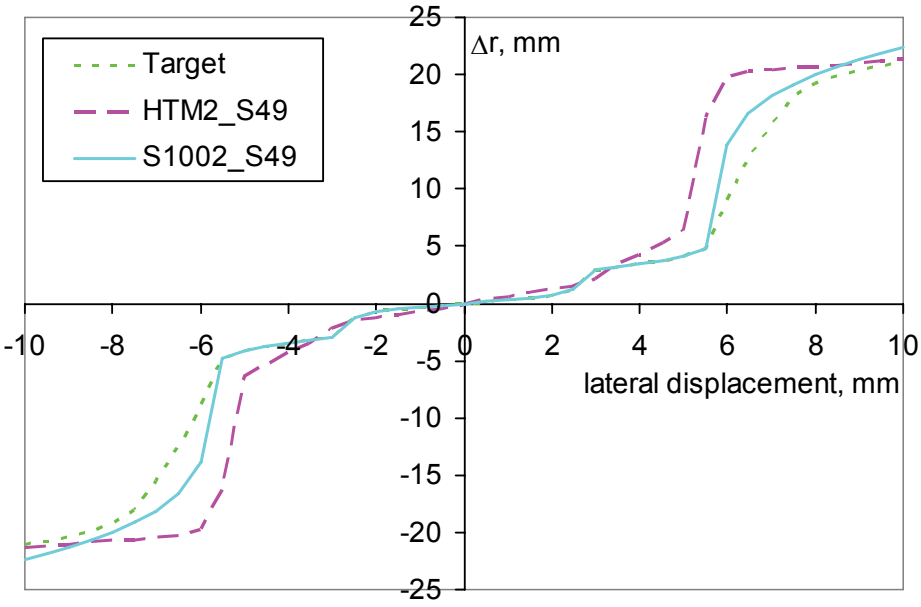

Figure 7.8: RRD functions for the HTM2 and S1002 wheel profiles on S49 rail and target RRD function.

Several constraints were applied on a target RRD function in the second design case. This procedure is thoroughly described in Section 6.4.2.2. In the optimisation problem, the usual 21 mm flange height of the tram wheels is used and, as a result, the RRD values of designed wheels for top flange contact will be the same as, for example, "Target" and "HTM2_S49" lines at 10 mm of lateral displacement (see Figure 7.9). Consequently, this is the first constraint on the target RRD function, point [Y_{fh} , Δr_{fh}], (see Section 6.4.2.2).

At the HTM company, a wheel flange width is measured at a level 15 mm below mean wheel circle. Let us name this point FW (Flange Width). The HTM2 profile has the flange width of 19.2 mm. To obtain a profile with flange width equal to 19.2 mm, the corresponding point on the target RRD function must be at a certain point. The HTM2 profile has contact at point FW at a wheelset lateral displacement equal to 5.5 mm, and the corresponding RRD is equal to 16.5 mm. Therefore, during the design of the target RRD function (line "Target_8"), the point [Y_{fw} , Δr_{fw}] is placed at Y_{fw} =5.5 mm and Δr_{fw} =16.5 mm. The "Target_8" and "HTM2_S49" functions have a common point at 5.5 mm of lateral displacement (see Figure 7.9). This point serves to obtain the required wheel flange width, and is used as the second constraint of the target RRD function.

The "Target_8" RRD function has four working areas corresponding to: tread contact, flange root contact, flange contact, and top of flange contact. The tread contact area is defined for 0–2.5 mm of lateral displacement and corresponds to motion on a straight track. The target function is made in such a way that wheel conicity smoothly rises from 0.24 to 0.38, providing the required critical speed. The flange root contact area starts from 2.5 mm of lateral displacement and continues to 4.5 mm. The RRD for that area rises from 1.9 mm to 7.3 mm, which satisfies the condition of passing curves with radius from 300 m up to 100 m, as shown in Table 2.1. The flange contact area starts after 4.5 mm, and continues until 7.5 mm of lateral displacement. The corresponding RRD rises from 7.3 mm up to 21 mm (top flange contact). The top of the flange contact area cannot be optimised; it is left without changes. The target RRD function is designed smooth with the help of cubic spline approximation.

Equivalent conicity of the HTM2_S49 RRD function is 0.30, and of the "Target_8" RRD function it is 0.325. The equivalent conicity is calculated for 2 mm of lateral displacement,

which corresponds to wheel tread contact. According to the ADAMS/Rail calculations, the equivalent conicity, 0.325, should provide the critical speed for a tram vehicle of 29 m/s, as will be shown later in this thesis.

After the design of target RRD function is defined, next the method of profile variation must be chosen.

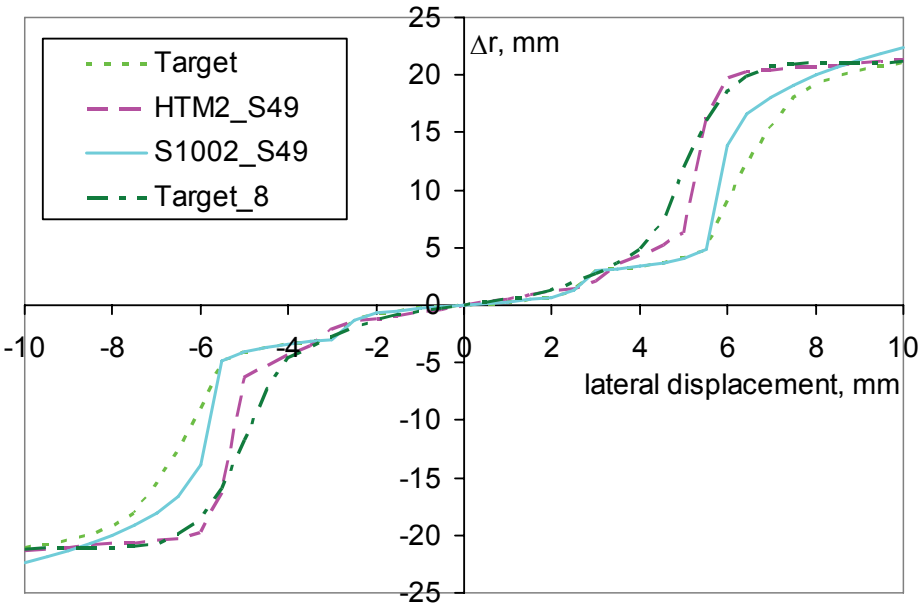

Figure 7.9: RRD functions for the HTM2 and S1002 wheel profiles on S49 rail and target RRD function.

7.2.2.4 Choice of profile variation

In this case, two profile variations are used. For "Target" RRD function, variation of the design points in Cartesian coordinates is chosen as the method for profile modification (see Section 6.2.3). This is done because only part of the profile will be varied during optimisation. For "Target_8" RRD function, the wheel profile is designed using circular arcs, as described in Section 6.2.2.

For "Target" RRD function, only part of the function is modified; therefore, only corresponding parts of the wheel profile can be modified, to reduce the number of design variables and, consequently, computation time. Starting profile, together with the shown positions of chosen constrained and moving points, is presented in Figure 7.10. S1002 wheel profile was used as the source of coordinates for the starting profile. Top of flange points are taken from HTM2 profile. Vertical position of the moving points changes during the optimisation procedure to find the optimum profile. Contact at the modified area corresponds to 5.5–8 mm of wheelset lateral displacement. Therefore, the contact problem can be calculated only for the range 5.5–8 mm of lateral wheelset displacement, to reduce the computation time of the optimisation procedure.

For "Target_8" RRD function, the whole wheel profile is modified. For this RRD function, contact problems are calculated for +/– 8 mm of wheelset lateral displacement.

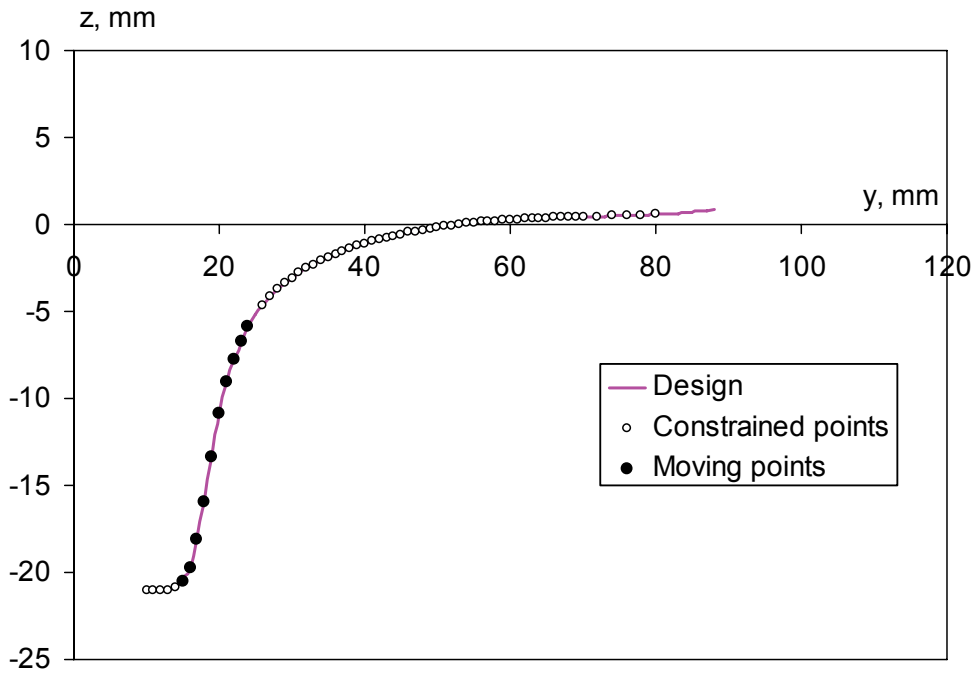

Figure 7.10: Starting (design) wheel profile, constrained, and moving points.

7.2.3 Results

After the problem is analysed, constraints on wheel profile defined, target RRD function designed, and variation of wheel profile chosen, the optimisation problem can be solved. In this section, the results of wheel profile design for an HTM tram using the optimisation procedure are described.

7.2.3.1 Results of wheel design

First, results of the optimisation for "Target" RRD function are described. The results of the optimisation are presented in Figure 7.11 and Figure 7.12. Comparing the wheel profiles in Figure 7.11, one can see that flange angle of the optimised profile Opt26f is reduced, and flange root radius is increased. Furthermore, on the field side of the tread, lower conicity is introduced as compared to HTM2 profile. The optimisation was performed for the range 5.5–8 mm of lateral displacement of the wheelset as described earlier. In Figure 7.12, lines "Target" and "Opt26f_S49" are very close to each other within the range 5.5–8 mm. The discrepancy between these two lines after 8 mm of lateral displacement is not significant because the corresponding top flange contact has not been taken into account in the optimisation.

Let us compare the contact situation for Opt26f wheel profile shown in Figure 7.13 with the contact situation for HTM2 wheel profile shown in Figure 7.5. For Opt26f profile, contact points are evenly spread along the flange, in contrast to the contact situation on the flange of HTM2 profile, where contact is moved to the flange top part. Such evenly spread contact allows a greater variety of RRD. This provides the possibility of better adjustment of the wheelset in a curve and accordingly, wheel flange wear will decrease.

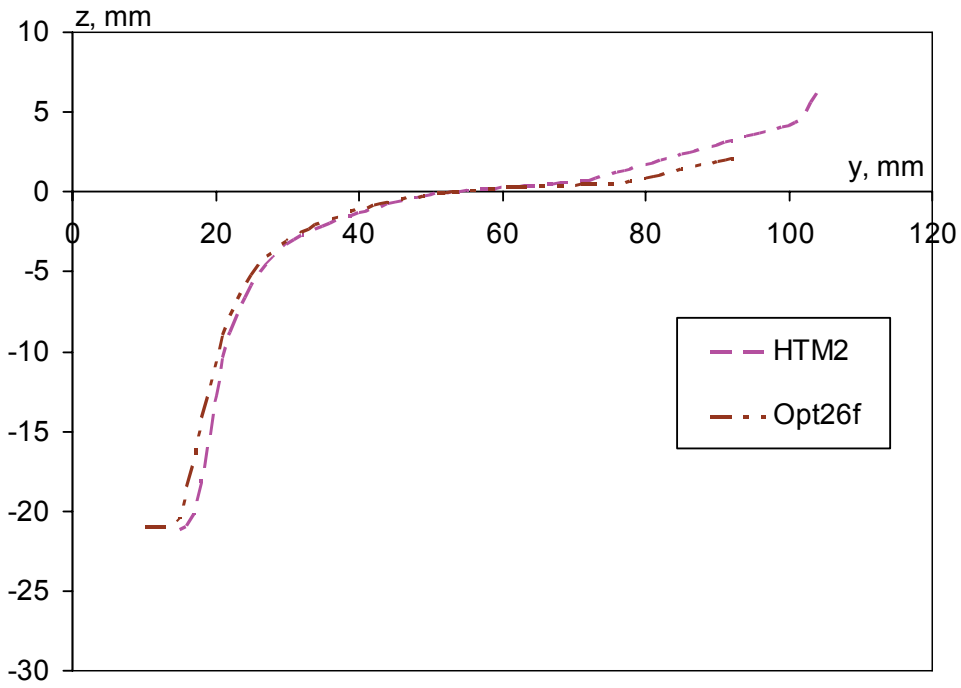

Figure 7.11: HTM2 and designed Opt26f wheel profiles.

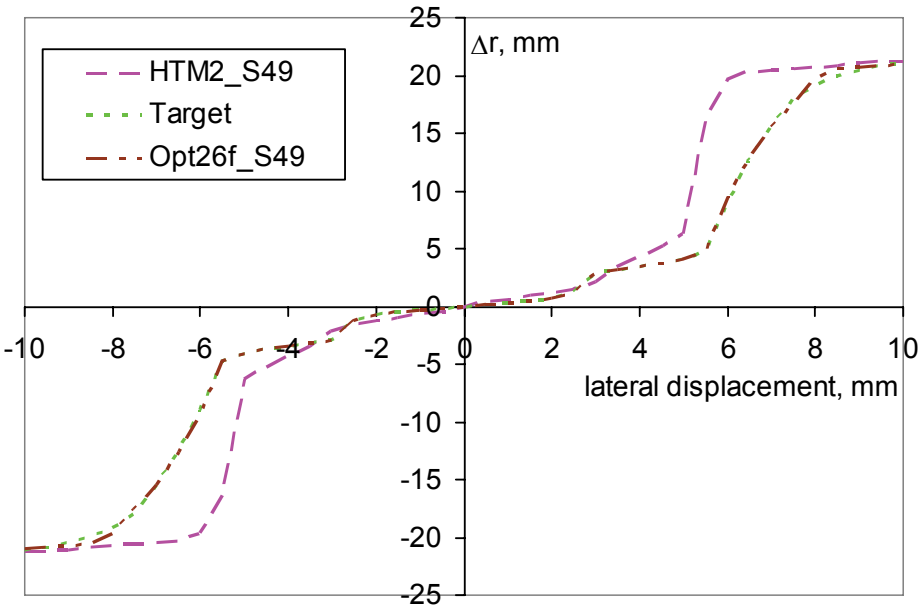

Figure 7.12: RRD functions for HTM2 and Opt26f wheel profiles on S49 rail and target RRD function.

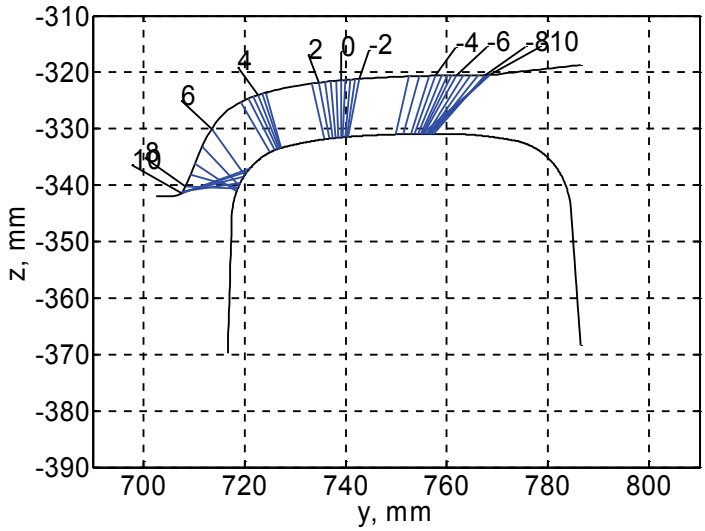

Figure 7.13: Positions of contact points for Opt26f wheel profiles with S49 rail profile.

Now, results of the optimisation for "Target_8" RRD function are described. As mentioned in the previous section, constrains on wheel flange width and wheel flange angle are introduced in the second design case. Wheel flange width should be at least 19.2 mm. Wheel flange angle should be between 65 and 70 degrees.

Preliminary calculations had shown that the flange angle of 70 degrees could not be achieved without jump of the contact point on the wheel flange and consequently, on the RRD function. Furthermore, the HTM2 wheel profile has a 68.08-degree flange angle, and the S1002 profile has a 67.8-degree flange angle. However, these two wheel profiles have a large jump of the contact point along the flange (see Figure 7.5 and Figure 7.6). From preliminary calculations, a small jump of the contact point was obtained for 67-degree flange angle. Therefore, it was decided to design a wheel profile with 67-degree flange angle.

A new wheel profile for the S49 rail is obtained using the design procedure described in Section 6.2.2. The contact surface of the new profile consists of the three circular arcs with R=360 mm, R=96 mm, and R=18 mm, as shown in Figure 6.6. The resulting wheel profile CWdesign3 and the HTM2 profile are shown in Figure 7.14. The zero point of the designed wheel was changed from 53 mm (HTM2) to 57 mm in order to shift the initial contact point to the top of the rail. The wheelset inner gauge for the CWdesign3 wheel profile is 1386 mm, which is 1 mm wider than for the HTM2 wheel profiles. This inner gauge was chosen to match the track width, 1500 mm (1386 mm + 2*57 mm = 1500 mm).

The rolling radii difference functions for the HTM2 and CWdesign3 wheel profiles, together with the "Target_8" function are shown in Figure 7.15. From this figure, it can be seen that for lateral displacements of +/– 2.5 mm, the RRD functions of the CWdesign3 and HTM2 profiles are almost identical. For larger lateral displacements, the CWdesign3 wheel profile provides the larger rolling radii difference compared to the HTM2 wheel profile, which is preferable for passing sharp curves without slippage.

Positions of the contact points for the CWdesign3 profile with the S49 rail for various lateral displacements of a wheelset are shown in Figure 7.16. Let us compare the contact situation for the CWdesign3 wheel profile shown in Figure 7.16 with the contact situation for the HTM2 wheel profile shown in Figure 7.5. For the CWdesign3 profile, the contact points are evenly spread along the profile in contrast to the contact situation for the HTM2 profile, where the contact points have large jumps and contact along the flange is absent. Such evenly spread

contact will allow greater variety of RRDs, which will allow a wheelset to find the radial position (without slippage) and as a result, wheel wear (especially flange wear) will decrease.

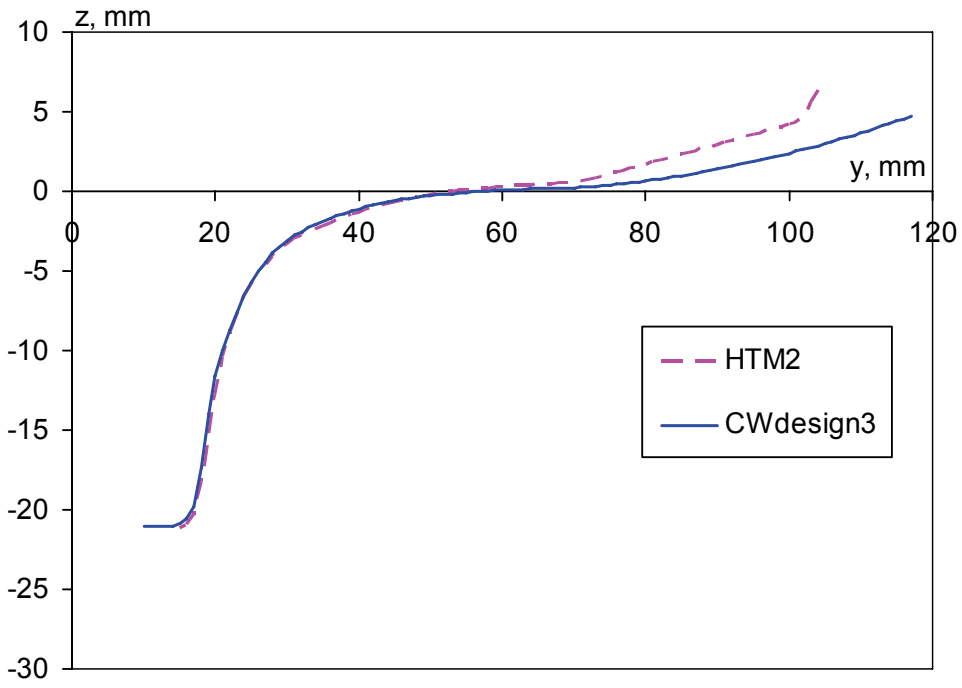

Figure 7.14: Designed CWdesign3 and HTM2 wheel profiles.

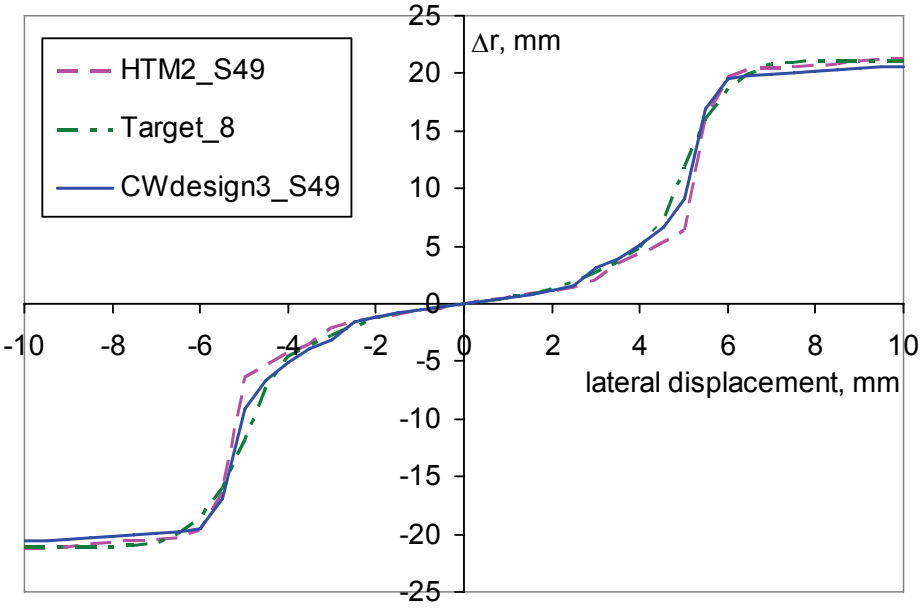

Figure 7.15: RRD function for HTM2 and CWdesign3 wheel profiles on S49 rail and “Target_8” RRD function.

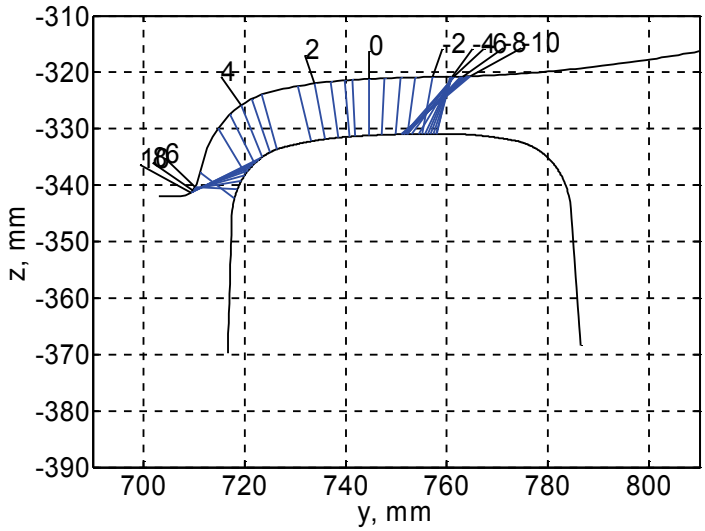

Figure 7.16: Positions of contact points for CWdesign3 wheel profile with S49 rail profile.

In contrast to the contact situation of a purely conical wheel, when the contact points are evenly spread along the tread of the wheel profile but concentrated in one point on a rail (see Figure 7.4), the wheel profile designed from a set of circular arcs provides even distribution of the contact points on both wheel and rail (see Figure 7.16).

The previously designed wheel profile Opt26f is shown in Figure 7.17, together with the HTM2 and CWdesign3 wheel profiles. The rolling radii difference functions for the HTM2, Opt26f and CWdesign3 wheel profiles on the S49 rail, and also “Target” and “Target_8” functions, are shown in Figure 7.18. The geometric contact points of the Opt26f profile on the S49 rail for various lateral displacements of a wheelset are shown in Figure 7.13.

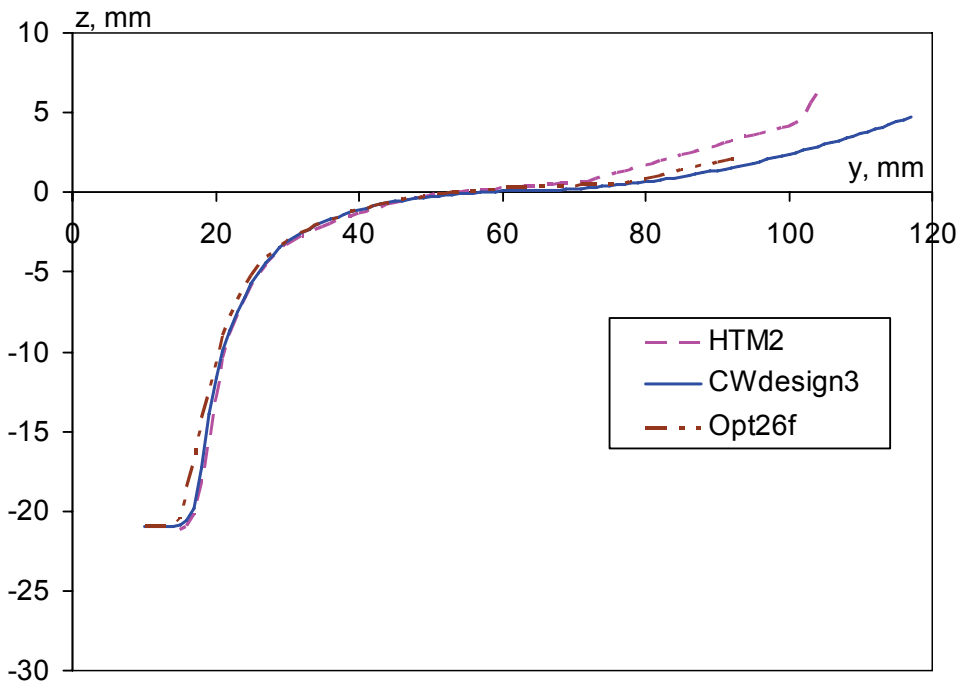

Figure 7.17: HTM2, CWdesign3 and Opt26f wheel profiles.

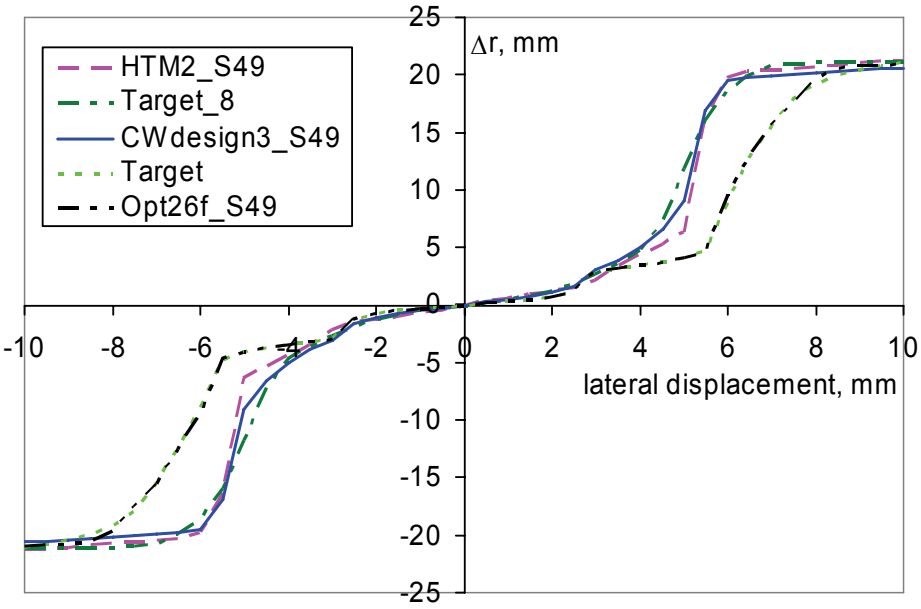

Figure 7.18: RRD functions for the HTM2, CWdesign3 and Opt26f wheel profiles on S49 rail; "Target" and "Target_8" RRD functions.

As can be seen from comparison of Figure 7.13 and Figure 7.16, the Opt26f wheel profile has better distribution of contact points on the flange as a result of the smaller flange angle and flange width of this profile in comparison to the CWdesign3 wheel profile. From Figure 7.17, it can be seen that the CWdesign3 wheel profile has wider flange and larger flange angle, compared to the Opt26f wheel profile. On the other hand, the CWdesign3 profile has evenly distributed points on the tread and flange root parts. Moreover, CWdesign3 profile can provide larger RRD for the smaller lateral displacement, which should result in better curving performance as compared to the Opt26f profile. The conclusion can be reached that the CWdesign3 profile has better contact characteristics than the Opt26f wheel profile (except on the flange). This conclusion is tested in the following section using ADAMS/Rail dynamic simulations.

The geometric parameters of several wheel profiles are presented in Table 7.1. The initial conicity of the wheel profiles is calculated at the initial contact point (zero lateral displacement of wheelset). Equivalent conicity of wheel profile is calculated for 2 mm of the lateral displacement. This is different from train application, where 3 mm of the lateral displacement is used. Obviously, the initial conicity of conical profile HTM1 is equal to its equivalent conicity. However, the initial conicity of the non-conical profiles (all other profiles in Table 7.1) is not the same as the equivalent conicity. The flange angle is measured as the angle between the horizontal line and the line that connects the points on the flange at 10 mm and 16 mm above the mean wheel circle. The flange width is measured at 15 mm below the mean wheel circle (see Section 6.2.1 and Figure 6.3).

The wheelset outer gauge for the CWdesign3 and HTM2 wheel profiles is the same. However, the flange width of the CWdesign3 and HTM2 wheel profiles is different (18.7 mm and 19.2 mm correspondingly). Equal wheelset outer gauge is obtained by the 1 mm difference between the wheelset inner gauge for the CWdesign3 (1386 mm) profile and the wheelset inner gauge for the HTM2 (1385 mm) wheel profiles. If necessary to increase the flange width of the CWdesign3 wheel profile, this 1 mm difference can be added to the inner side of the CWdesign3 wheel flanges, and flange width will then be 19.2 mm (i.e., for each wheel,

0.5 mm should be added to the inner gauge side of the wheel). Correspondingly in this case, 1385 mm wheelset inner gauge must be used.

According to the HTM regulations, the flange angle of the wheels should be between 60 and 80 degrees, while the new wheels should have an angle of 70 degrees. Values for the flange angles for several wheel profiles are presented in Table 7.1. Using Nadal's derailment criteria (equation 4.11 from Section 4.5.2.4) it is possible to calculate that for the limiting L/V = 0.8 and friction coefficient 0.4, the wheel flange angle should not be lower than 60.46 degrees (65.22 degrees for the friction coefficient 0.5). In these cases, UIC regulation will be not violated. The conclusion can be drawn that Opt26f wheel profile is safe up to 0.4 friction coefficient, and CWdesign3 profile is safe up to 0.5 friction coefficient. In typical contact conditions, friction coefficient remains below 0.4. Therefore, both designed profiles satisfy safety criteria against derailment.

Table 7.1: Wheel profile properties.

Profile	Initial conicity	Equivalent conicity (measured for 2 mm of lateral displacement of wheelset on S49 rail)	Flange angle, degree	Flange width, mm (measured 15 mm below mean wheel circle)
HTM1	0.03	0.03	75.97	19.3
HTM2	0.12	0.30	68.09	19.2
S1002	0.08	0.17	67.92	18.4
Opt26f	0.08	0.17	63.49	17.7
CWdesign3	0.05	0.28	66.59	18.7

Lower flange angle increases the possibility of derailment. On the other hand, lower flange angle can also improve wheel/rail contact. Therefore, optimisation of wheel flange angle is a tradeoff between improvement of safety and improvement of performance. It should be noted that the Nadal formula is regarded as very conservative, and the real risk of derailment is lower than that calculated using the Nadal formula. Such results are obtained by Cheli et al. [2003].

The flange angle of 63.5 degrees (Opt26f wheel profile) is rather close to the limiting value (60 degrees). Analysis of the flange angles of typical HTM worn profiles reveals that most of the worn profiles have a flange angle between 64 and 67 degrees. From this observation, it can be concluded that during operation, the initial 68 degree flange angle will be reduced. As is known from practise, wheels are subject to greatest flange wear during the first weeks of their exploitation. This means that during this period, the wheel flange is adapting to the contact conditions, and later becomes stable. Therefore, with the introduction of the optimised wheel profile with an initial flange angle of 63.5 degrees, wheel wear will decrease due to omission of the initial "grinding" of the wheel flanges.

The CWdesign3 wheel profile has a flange angle of 66.58 degrees, which is close to the upper bound of the flange angle of the measured worn wheels. This flange angle provides higher safety against derailment as compared to the Opt26f profile while it still has a good distribution of contact points along the flange. It seems advantageous to use the CWdesign3 wheel profile for trams. This conclusion will be further tested through dynamic simulation.

7.2.3.2 Results of dynamic simulations

Analysis of tram dynamics is performed using the ADAMS/Rail model described in Section 4.2.3.3. Prior to analysis of dynamic behaviour, the critical speed of the tram vehicle with

each wheel profile is investigated. The critical speed is obtained using closed-loop stability analysis. Closed-loop stability analysis is based on an initial value of velocity and a velocity step. ADAMS/Rail automatically increments the velocity until the railway system reaches the critical velocity. Analysis is performed for a set of differing conicity values, representing the various wheel/rail profile combinations. The results of closed-loop analysis for a tram are presented in Table 7.2. Apparently, higher equivalent conicity leads to lower critical speed of the vehicle.

As is evident from Table 7.2, all curvilinear wheels on rail S49 have critical speeds around 30 m/s. HTM1 wheel has critical speed lower than 20 m/s, which is due to very low conicity and consequently, very low centring effect.

Table 7.2: Critical speed of vehicle with various wheel/rail profiles.

Wheel profile	Critical speed from closed-loop stability analysis	Equivalent conicity (measured for 2 mm of lateral displacement of wheelset on S49 rail)
HTM1	<20.0 m/s	0.03
HTM2	29.0 m/s	0.30
S1002	31.2 m/s	0.17
Opt26f	31.2 m/s	0.17
CWdesign3	30.5 m/s	0.28

To check the results of the closed-loop stability analysis, simulations with a tram vehicle on a straight track with horizontal ramp at various speeds is performed. For these simulations, a 700 m straight track is modelled in ADAMS/Rail. At a distance of 50 m from the beginning of the track a horizontal ramp (height 5 mm, width 0.1 m) is introduced. The ramp produces initial disturbance for the wheelset, leading to oscillation motion in the bogie. The motion associated with a particular wheel profile is considered stable if, after passing through the lateral ramp, the oscillations of the bogie are damped out quickly. In such case, the tram is stable with a given wheel profile at a given speed.

The lateral displacement of the first wheelset vs. time for five wheel profiles on S49 rail at speeds of 20, 30 and 40 m/s are presented in Figure 7.19-Figure 7.23. The simulations on the straight track with horizontal ramp show that the vehicle with HTM1 wheel profile is unstable at 20 m/s (at 10 m/s, the oscillations of the wheelset are slowly damped out as shown in Figure 7.19). For the vehicle with HTM2 and CWdesign3 wheel profiles, the wheelset starts hunting at running speeds higher than the calculated critical speed (40 m/s vs. 30 m/s), as shown in Figure 7.20 and Figure 7.23. The vehicle with the S1002 and Opt26f wheel profiles is stable at the speed 40 m/s, as can be seen from Figure 7.21 and Figure 7.22.

Dynamic simulations of a tram running on straight track at the speed of 20 m/s are analysed to check the dynamic behaviour of the designed wheel profiles. This speed is the maximum operational speed of a tram, and it is below the critical speed. After passing the lateral ramp, the oscillations of the wheelset with the designed wheel profiles are damped out quickly. Hence, at operational speeds, the tram is stable with the designed wheel profiles.

From analysis of the simulation results, it is concluded that the wear index for a wheelset with different wheel profiles running at the same speed is practically the same, so long as such wheelset with the particular wheel profile is stable. During stable motion, the tram produces much less wear on straight track than the hunting vehicle. The wear index of a hunting wheelset is higher as compared to non-hunting wheelsets. In other words, wear is not the

critical factor on a straight track. For motion on a straight track, the critical speed is the most important parameter determining the quality of the wheel profile.

The maximum operating speed of the tram is 20 m/s (72 km/h). Consequently, the existing HTM2 and newly designed wheels Opt26f and CWdesign3 satisfy the operational conditions regarding critical speed.

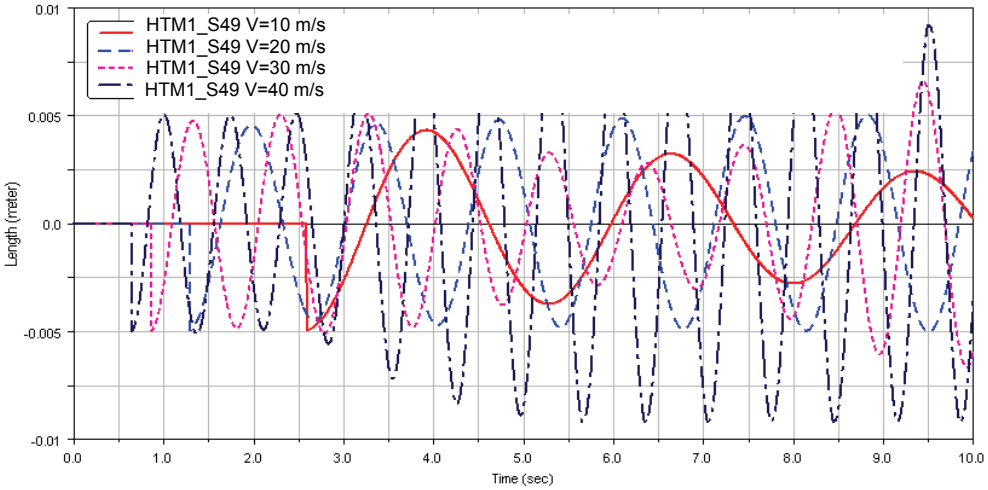

Figure 7.19: Lateral displacement of the first wheelset vs. time. Wheel HTM1 and rail S49. Running speed is 10, 20, 30, and 40 m/s.

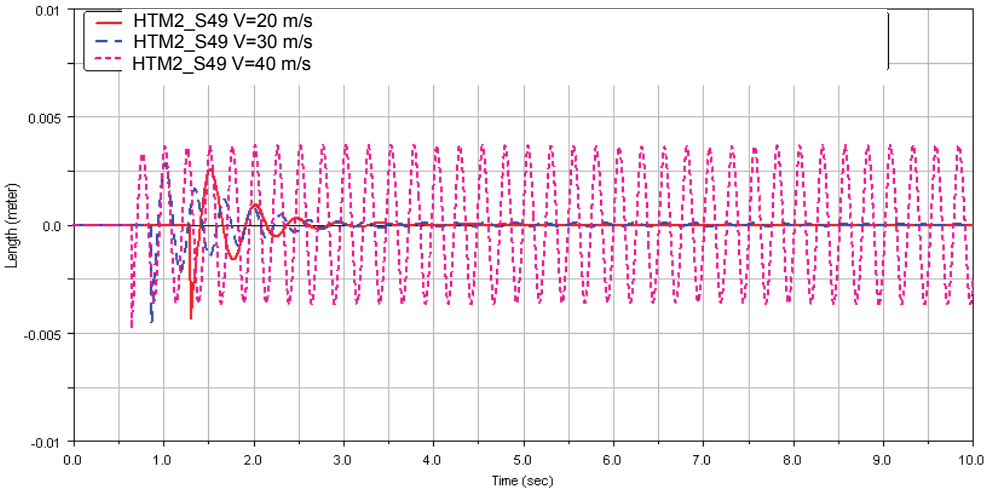

Figure 7.20: Lateral displacement of the first wheelset vs. time. Wheel HTM2 and rail S49. Running speed is 20, 30, and 40 m/s.

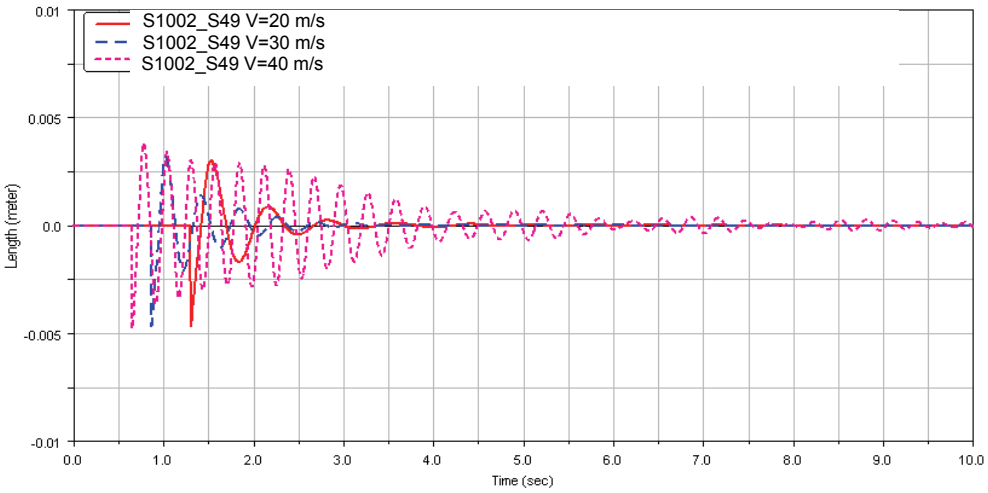

Figure 7.21: Lateral displacement of the first wheelset vs. time. Wheel S1002 and rail S49. Running speed is 20, 30, and 40 m/s.

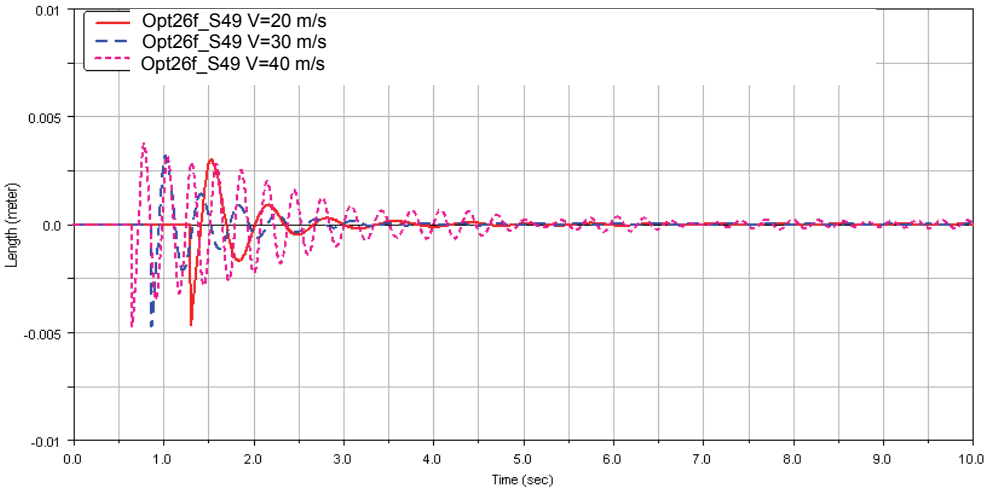

Figure 7.22: Lateral displacement of the first wheelset vs. time. Wheel Opt26f and rail S49. Running speed is 20, 30, and 40 m/s.

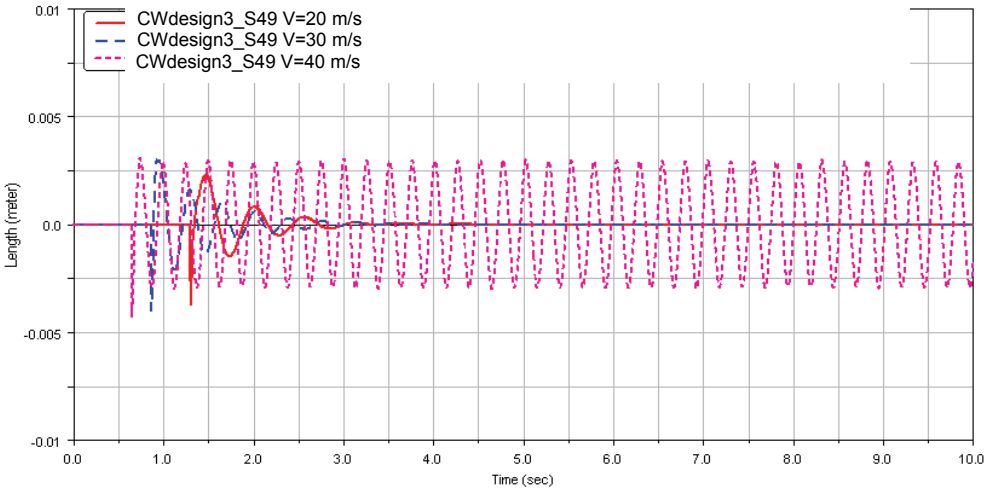

Figure 7.23: Lateral displacement of the first wheelset vs. time. Wheel CWdesign3 and rail S49. Running speed is 20, 30, and 40 m/s.

Dynamic simulations of a tram vehicle passing the curve, and related wheel/rail wear rate calculations are performed in ADAMS/Rail on specially designed tracks. Two curved tracks are used, one with radius R=150 m (shallow curve), and the other one with radius R=30 m (sharp curve). The shallow curve track consists of the following consecutively connected sections: 50 m straight track, 40 m transition curve, 50 m right turn curve (R=150 m) without cant, 30 m second transition curve, and 230 m straight track. The sharp curve track consists of the following consecutively connected sections: 50 m straight track, 10 m transition curve, 40 m right turn curve (R=30 m) without cant, 10 m second transition curve, and 290 m straight track. The total length of the track is 400 m.

The wear index W (6.2) for the left wheel of the first wheelset and the lateral displacement y of the first wheelset are chosen as the most representative quantities in the dynamic check. The results of the dynamic simulations of the tram running with the speed of 5 m/s on the curved track with 30 m radius are presented in Figure 7.24 and Figure 7.25. On the curved track with 150 m radius, a tram was run with the speed of 10 m/s. The results of this simulation case are presented in Figure 7.26 and Figure 7.27.

The HTM2, S1002, Opt26f and CWdesign3 curvilinear wheel profiles have lower wear index on the curved track as compared to the conical HTM1 wheel profile. In the curve R=30 m, the CWdesign3 wheel has the smallest wear index, as shown in Figure 7.25. The wear index of the Opt26f profile is smaller compared to the HTM2 wheel. The S1002 wheel has the highest wear of all the curvilinear profiles. The wear index of the CWdesign3 wheel profile is 1.3 times less than the wear index of the HTM2 wheel profile.

In the curve R=150 m, the wear indexes of the CWdesign3 and HTM2 wheel profiles are practically the same, as shown in Figure 7.27. The wear indexes of the S1002 and Opt26f wheel profiles are also close to each other, but they both are higher than the wear indexes of the CWdesign3 and the HTM2 wheel profiles.

In the performed simulations, the top flange contact is not achieved for the curvilinear profiles; on the curved tracks, the contact points are situated on the flange root part of the profiles. In the 30 m radius curve, the CWdesign3 wheel profile has only single-point contact, whereas all other profiles have double-point contact. This single point contact provides such low wear index for the CWdesign3 wheel profile. In 150 m radius curve, all curvilinear profiles have mainly single point contact – this is why wear index is almost the same.

In curves, the HTM1 wheel profile always has two contact points: one on the tread part, and one on the flange. In the curve R=30 m, the HTM1 wheel profile has about 2.53 times higher wear index as compared to the CWdesign3 wheel profile (1.86 times higher than for the HTM2 profile), as can be seen in Figure 7.25. In the curve R=150 m, the HTM1 wheel profile has about 3.7 times higher wear index as compared to the CWdesign3 and HTM2 wheel profiles, as shown in Figure 7.27. Based on this, it can be concluded that replacement of the HTM1 wheel profile with the HTM2 wheel profile should lead to significant (2–3 times) decrease of wheel flange wear. From HTM's experience, introduction of HTM2 wheel profile led to about a 3-times reduction in flange wear.

The wear indexes for each of the four wheels of the first bogie running on 30 m and 150 m radius curves are shown in Figure 7.28 and Figure 7.29, respectively. It is clearly seen that in the sharper curve, the wear index is larger than in the curve with the larger radius. In the sharp curve (R=30 m), the first left and the second right wheels have the highest wear indexes, which is typical for sharp curves. In the curve with radius 150 m, the first and the second left wheels have the highest wear indexes.

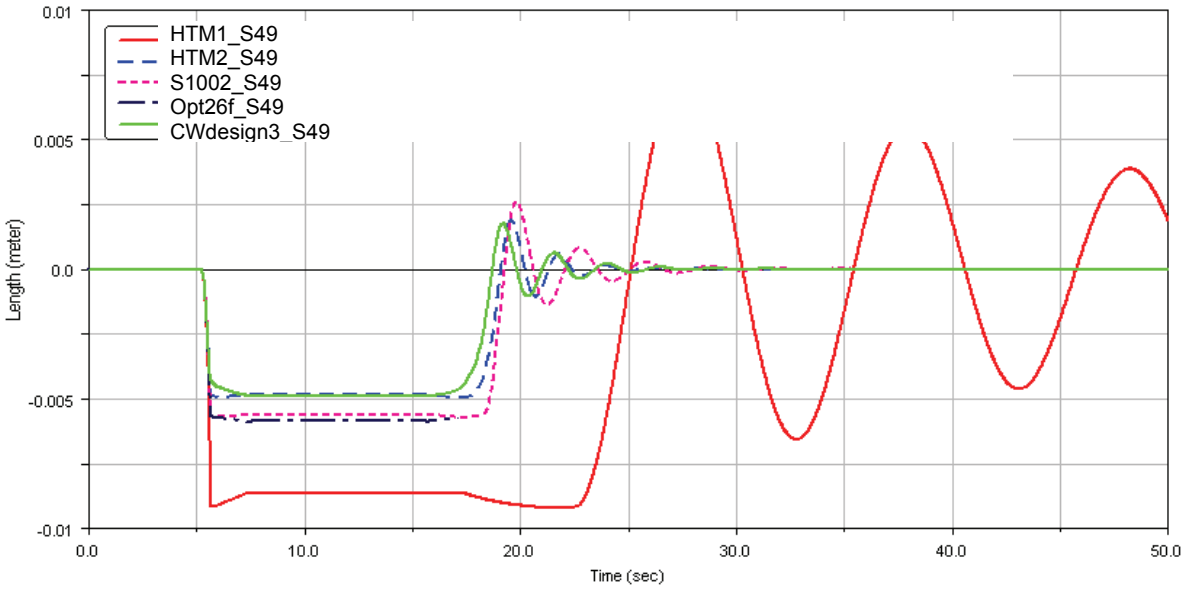

Figure 7.24: Lateral displacement of the first wheelset vs. time. HTM1, HTM2, S1002, Opt26f and CWdesign3 wheels running on rail S49. Curve radius is 30 m. Running speed is 5 m/s.

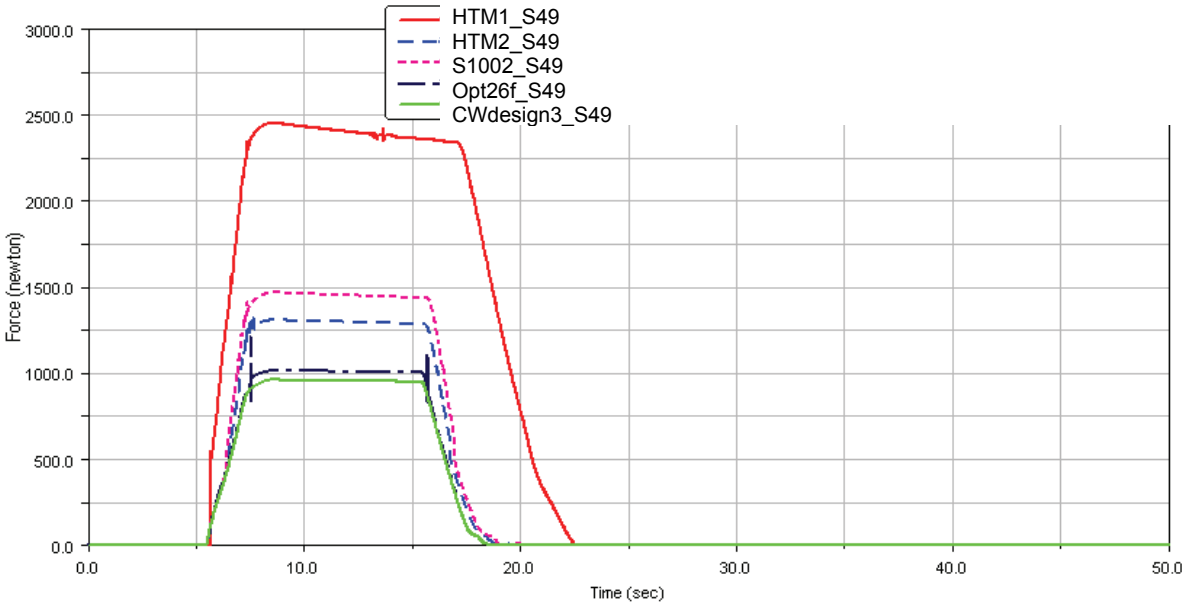

Figure 7.25: Wear index of the left wheel on the first wheelset vs. time. HTM1, HTM2, S1002, Opt26f and CWdesign3 wheels running on rail S49. Curve radius is 30 m. Running speed is 5 m/s.

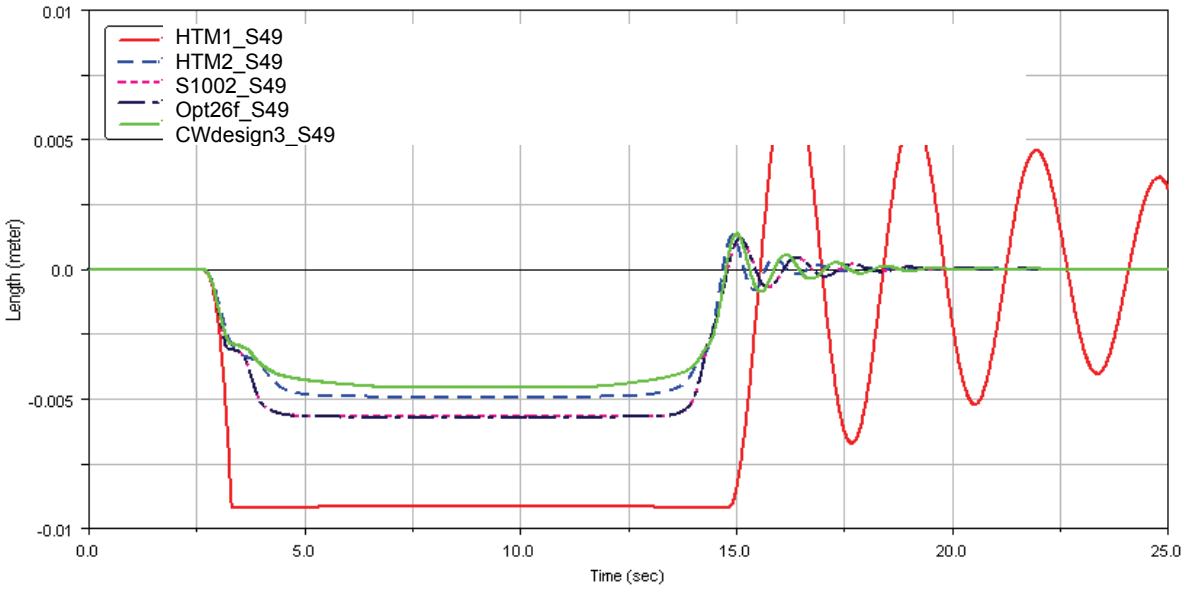

Figure 7.26: Lateral displacement of the first wheelset vs. time. HTM1, HTM2, S1002, Opt26f and CWdesign3 wheels running on rail S49. Curve radius is 150 m. Running speed is 10 m/s.

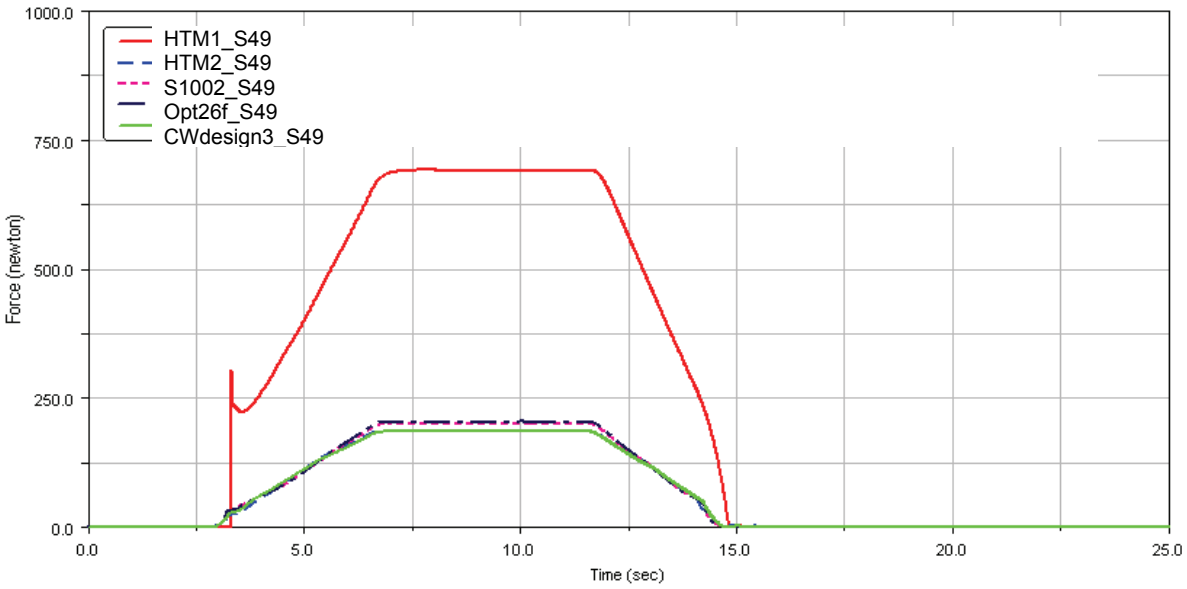

Figure 7.27: Wear index of the left wheel on the first wheelset vs. time. HTM1, HTM2, S1002, Opt26f and CWdesign3 wheels running on rail S49. Curve radius is 150 m. Running speed is 10 m/s.

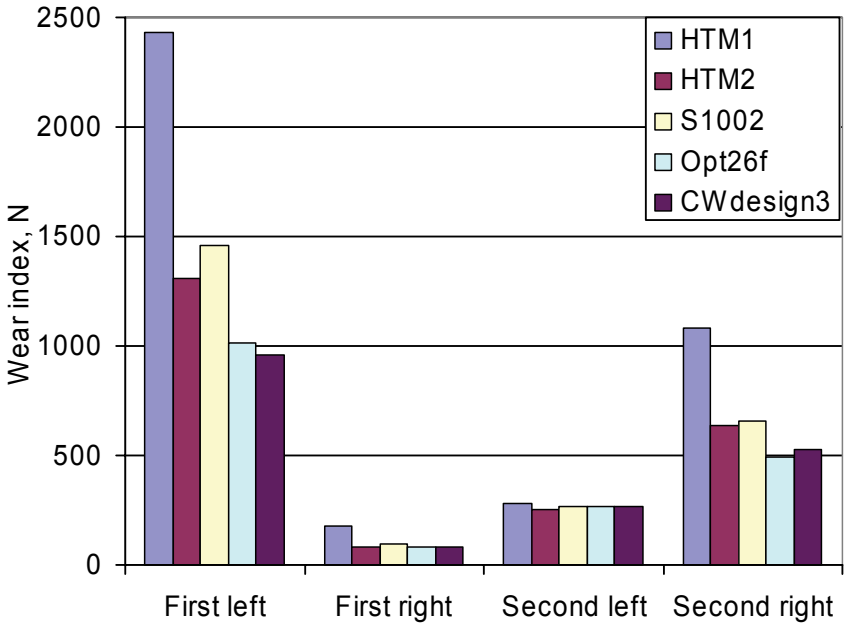

Figure 7.28: Wear index of the wheels of the first bogie. HTM1, HTM2, S1002, Opt26f and CWdesign3 wheels running on rail S49. Curve radius is 30 m. Running speed is 5 m/s.

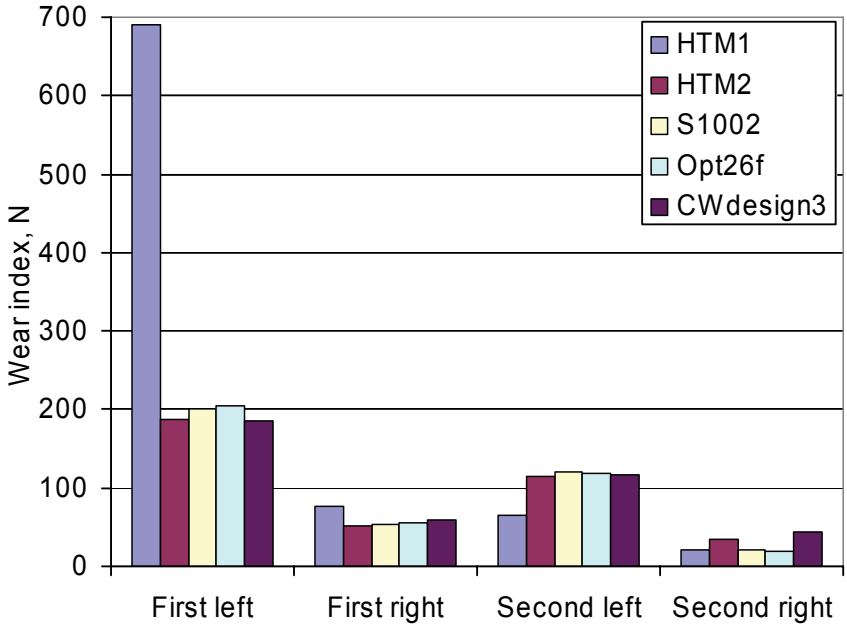

Figure 7.29: Wear index of the wheels of the first bogie. HTM1, HTM2, S1002, Opt26f and CWdesign3 wheels running on rail S49. Curve radius is 150 m. Running speed is 10 m/s.

Based on simulation results, a conclusion can be drawn that with the replacement of the conical profile HTM1 by the curvilinear profile HTM2, a quite significant (2–3 times) decrease in wheel flange wear should be observed. Nevertheless, the better distribution of the contact points on the flange of the CWdesign3 profile (resulting from lower flange angle), rather than the concentrated contact on the top of the flange of the HTM2 profile, should reduce wear of the wheel flange. Implementation of the CWdesign3 wheel profile should lead to a 30% reduction in wear in sharp curves, as compared to the HTM2 profile.

7.2.3.3 Results of field tests

The proposed CWDesign3 wheel profile was tested on HTM's network. Wheels with CWdesign3 profile showed a good distribution of contact along the rolling surface of the wheel. Due to organisational reasons, it was not possible to compare the tested profile with the current one. However, the general tendency of the wear was promising. Based on the results of these tests, CWDesign3 wheel profile was accepted by the HTM company for exploitation.

7.2.4 Conclusions

During the design of the wheel profile for an HTM tram, analysis was performed of the geometric contact of the new and worn wheel profiles with different rail profiles.

Replacement of the HTM1 wheel profile with the HTM2 wheel profile was concluded to be a significant improvement from the perspective of wheel flange wear. This replacement was able to reduce wear by a factor of 2 to 3.

Two wheel profile design variation methods were used, one using points along the profile, and another using circular arcs for the profile design. Two wheel profiles were obtained using this design procedure. CWdesign3 wheel profile showed better contact characteristics. With the CWdesign3 wheel profile, the initial contact point is situated on top of the rail. The contact points are evenly spread along the wheel and rail profiles, providing superior geometric contact between wheel and rail, and resulting in better wear performance. The new, designed wheel has the same dynamic performance as the current HTM2 profile on straight track. In 150 m radius curve, the new profile has practically the same wear index as does HTM2 profile. In 30 m radius curve, the CWdesign3 wheel profile provides 30% reduction of wear compared with HTM2 profile.

The new profile design satisfies the derailment safety criteria.

For trams, wear is a dominant factor in wheel/rail contact; therefore RCF occurrence was not included as an optimisation factor.

From dynamic simulations on curved tracks, an obvious conclusion can be made: smaller curve radius leads to higher wear of wheels and rails.

The new wheel profile has been implemented on the HTM trams. Field tests of CWDesign3 wheel profile show good performance for the new design.

7.3 Case 2: Design of wheel profile for metro (RET case)

7.3.1 Description of problem

The wheel profile design procedure described in Chapter 6 is applied to improving performance of the metro trains of RET (Rotterdamse Electrische Tram N.V.), the Rotterdam metro network. An example of a metro train from RET is presented in Figure 7.30. In 1999, the existing NP46 rail was replaced by S49 rail. The profiles looked similar, and therefore no difference in train performance was expected. However, after the introduction of the new rail profile, the metro trains began to experience severe lateral vibration. At the same time, a high level of wheel wear was observed after relatively small mileage. In fact, these vibrations were caused by worn wheels. Immediately after these vibrations were observed, the wheels were re-profiled to prevent derailment. Thus, due to rail replacement, the lifetime of the wheels was reduced from 120,000 km (with rail NP46) to 25,000 km (with rail S49). The average monthly mileage of a metro train is 10,000 km. The Railway Engineering Group of TU Delft was commissioned to research ways to improve vehicle stability and wheel life.

Results from the investigation of contact situation, wheel profile design procedure and designed profile, along with dynamic simulations of the metro vehicle in the ADAMS/Rail computational package are presented in the report 7-03-220-2 (in Dutch) (Markine, Shevtsov and Esveld [2003]). A comprehensive description of this research can be found in Markine, Shevtsov and Esveld [2004 a,b, 2006] and in Esveld, Markine and Shevtsov [2006]. Results from this study are described in the following sections.

Figure 7.30: RET metro, Rotterdam, The Netherlands. Courtesy of www.retmetro.nl.

7.3.2 Solution

In this section, application of the wheel profile design method in the case of a metro is shown step by step.

7.3.2.1 Analysis of problem

The problem is analysed in several steps. First, a comparison of the old and new rails is performed. It should be noted that S49 rail is installed with an inclination of 1:40, whereas NP46 rail is used without inclination. S49 rail has a cant of 1:40 in the track in order to achieve the shape of the NP46 rail used without cant. Even though rail profiles NP46 and S49 look similar (Figure 7.31), there is a small difference between these two profiles, which becomes visible only through zooming into the top of the rails, as shown in Figure 7.32. It is interesting that such a small difference (tenths of millimetre) in the shape of rail profile results in substantial changes in the dynamic behaviour of a vehicle, since the problems in the RET network were caused by rail replacement.

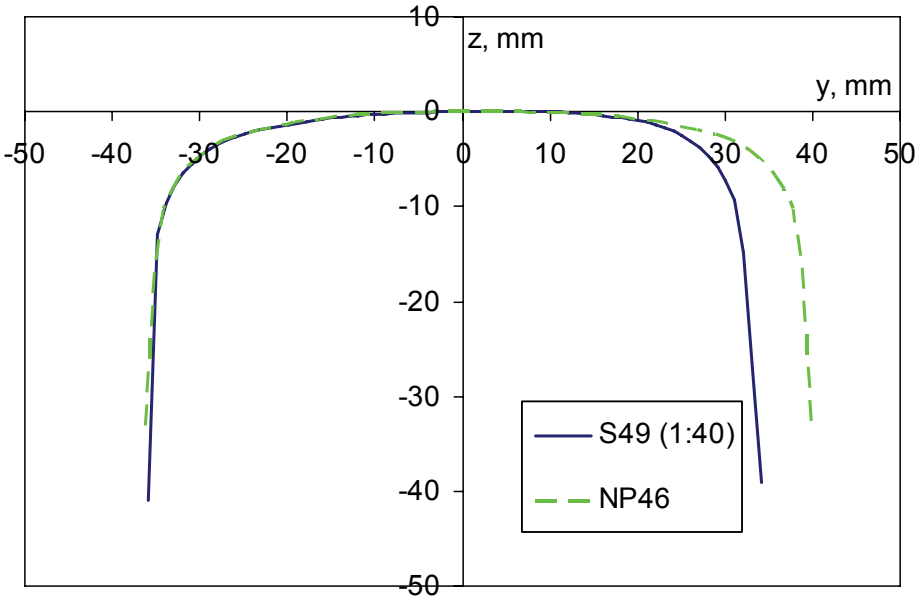

Figure 7.31: Comparison of rails NP46 and S49 (not zoomed).

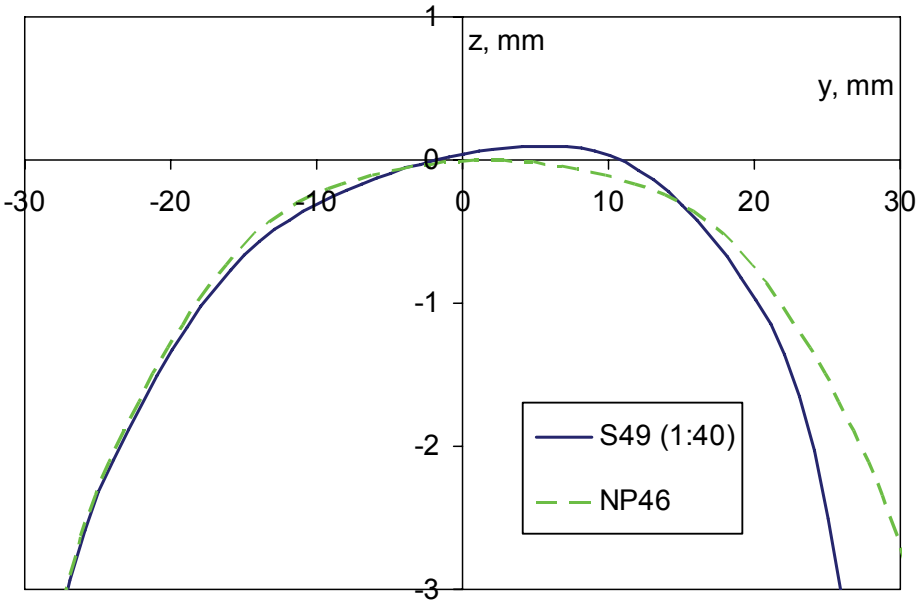

Figure 7.32: Comparison of rails NP46 and S49 (zoomed).

In the next step, the wheel/rail contact characteristics of the old and new situations are investigated. The wheel/rail contact points for new (unworn) wheel profile UIC510 with the unworn NP46 and S49 rails are shown in Figure 7.33 and Figure 7.34, respectively. In the wheel/rail contact figure, the lines between the wheel and rail profiles connect to the corresponding contact points, which are calculated per 0.5 mm of lateral wheelset displacement. The lateral wheelset displacements are shown above the wheel profile. The coordinate system in this figure is the wheelset coordinate system $y_w Oz_w$ (Figure 2.4), with the origin in the centre of the wheelset in neutral position. It should be noted that in this figure the wheel is shifted vertically 10 mm upwards from its actual position.

By comparing Figure 7.33 and Figure 7.34, one observes that there is a discontinuity (a large jump) in the position of the contact point on the S49 rail for the +/– 2 mm lateral displacement of the wheelset. Since the displacements in this range (+/– 2 mm) typically correspond to straight track motion of a wheelset, many such jumps will occur during vehicle motion. Due to these contact point jumps, the wheel profile wears very rapidly, which ultimately results in very large jumps in the contact point, as is shown in Figure 7.35. This figure shows the contact points of a worn (measured) UIC510 wheel profile on S49 rail. These large jumps in the contact point are also the source of the vibrations observed in the metro trains. On the other hand, the wheel/rail combination UIC510/NP46 has more uniformly distributed contact points on a straight track (corresponding to wheelset displacements of +/–2 mm), as shown in Figure 7.33. As a result, the wear rate of the UIC510 wheels on NP46 rail is much lower, and therefore wheel life is relatively long (120,000 km).

As mentioned earlier, rolling radius difference plays an important role in vehicle dynamics. Therefore the RRD functions are next investigated. The RRD functions for the UIC510 wheel profile on, respectively, NP46 and S49 rail are shown in Figure 7.36. From this figure, one observes that for small displacements of a wheelset, the RRD function of the UIC510/S49 wheel/rail combination has much higher inclination compared to the UIC510/NP46 wheel/rail combination. This means that the corresponding equivalent conicity (2.5) for S49 rail is higher than that for NP46 rail. High equivalent conicity for small lateral displacements of the wheelset is the reason of high tread wear, vehicle vibration, and ultimately the relatively short wheel life.

After the source of vehicle instability is found, the next step is to optimise the wheel profile. To reduce computation time, only problem parts of the profile are modified if such parts do not interfere with wheel/rail contact on the other parts of the profile. Vehicle instability corresponds to the motion on a straight track when wheels are running on the tread part of the profile. Consequently the tread contact part of the wheel profile must be modified. Therefore, only the tread is modified, while the flange and the field side of the profile are left untouched. Such approach influences the applied limits (constraints), design of limiting RRD function, and choice of profile variation, as described in the following sections.

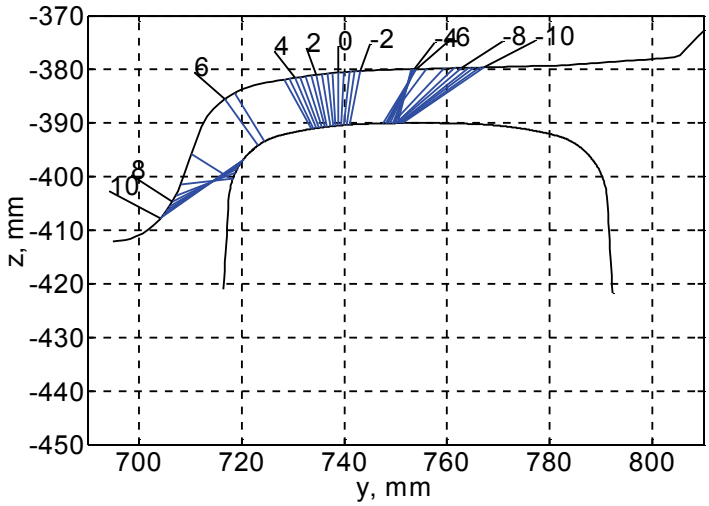

Figure 7.33: Positions of contact points for unworn UIC510 wheel profile with NP46 rail profile.

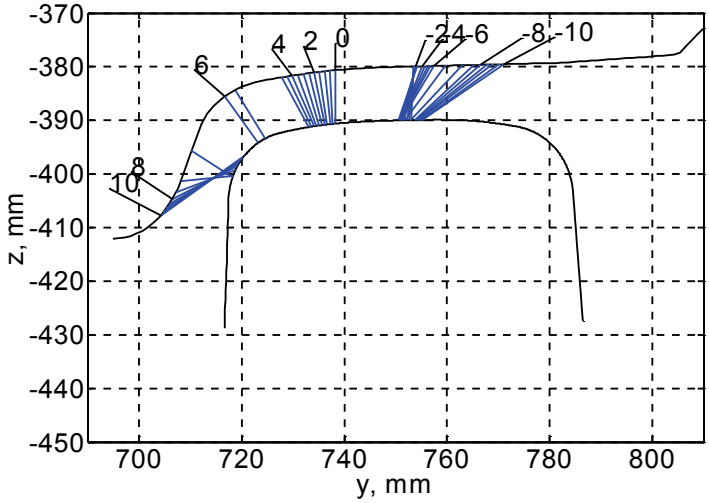

Figure 7.34: Positions of contact points for unworn UIC510 wheel profile with S49 rail profile.

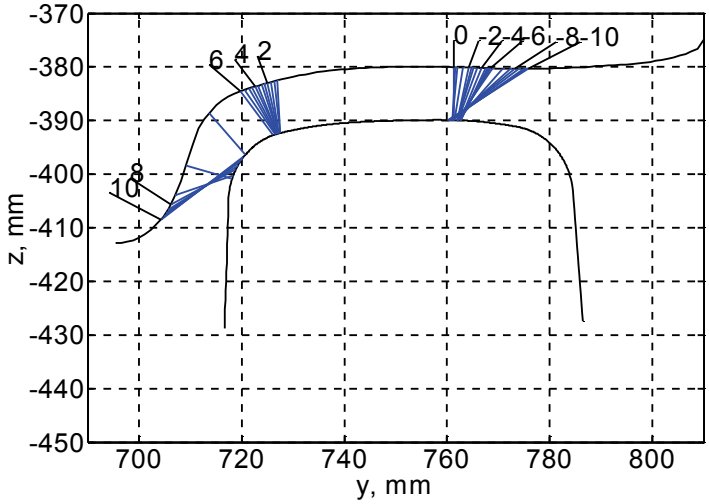

Figure 7.35: Positions of contact points for worn (measured) UIC510 wheel profile with S49 rail profile.

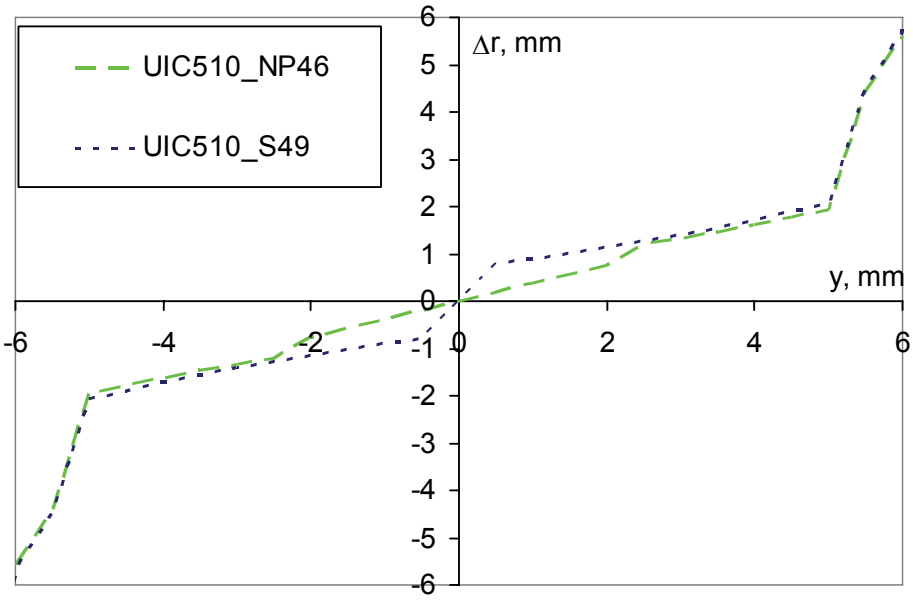

Figure 7.36: RRD functions for combination of UIC510 wheel on NP46 and S49 rails.

7.3.2.2 Applied limits

Due to modification of only the tread part of the profile, a number of limits (or constraints) on the designed wheel profile can be omitted, as they are superfluous. The requirements for wheel flange thickness and minimal flange angle are not used, because wheel flange is not modified.

Constraints on angles between the adjacent parts of a profile are introduced to avoid zigzags of wheel profile, and thus to exclude unrealistic wheel designs during optimisation, as described in Section 7.2.2.2. Moving points are numbered from 1 to N, starting from the low left side, to the upper right side of the profile (see Figure 7.37). For the concave part of the profile, constraints are used in the form of equation (7.1). Accordingly, for the convex part of the profile, constraints are written in the form of equation (7.2).

7.3.2.3 Design of limiting RRD function

In this section, the design of limiting (or target) RRD function for the case of a metro is described. General theory of design of target RRD function can be found in Section 6.4.2. The target RRD function is used in an optimisation procedure for the design of a new metro wheel profile. Optimisation of wheel profile is performed for S49 rail.

As mentioned above, the metro requires improvement in the contact situation on the tread part of the profile, but not a complete redesign of the wheel profile. The UIC510 wheel on NP46 rail has good contact properties on the tread part of the wheel, as can be seen from Figure 7.33. The UIC510/NP46 wheel/rail combination (see Figure 7.36) has a conicity of 0.2 for 3 mm of wheelset lateral displacement. The metro vehicle is stable on wheels with such conicity. RRD functions for UIC510 wheel on NP46 and S49 rail after +/– 6 mm of wheelset lateral displacement are not of interest for this problem, as this corresponds to flange contact of the wheel, which we do not intend to modify. Therefore, RRD above +/– 6 mm is not included in the design problem.

The RRD function of UIC510/NP46 wheel/rail combination in the range of +/– 6 mm lateral displacement is chosen as the target RRD function for the optimum wheel profile design

procedure, as described in the previous chapter. Additional constraints on RRD function are automatically included through the use of RRD function for which good wheel/rail contact and proper dynamic behaviour are known in advance.

7.3.2.4 Choice of profile variation

Variation of the design points in Cartesian coordinates is chosen for the metro profile design (see Section 6.2.3). This is done because only part of the profile will be varied during optimisation. The starting profile, together with the shown positions of chosen constrained and moving points, is presented in Figure 7.37. To reduce the number of design variables in the optimisation problem, only the tread part of the wheel profile is modified. Furthermore, only the gauge part of the tread is modified (between 30 and 70 mm, see Figure 7.37), while the field part remains fixed. This is feasible due to the symmetry of wheel profiles on one wheelset. UIC510 wheel profile is used as the source of coordinates for the starting profile. The field part of the tread (after 70 mm) is modified. This part of the profile is made straight, with inclination 1:40 to match inclination of the rail. The flange points are taken from UIC510 profile as well and are fixed, as is evident from Figure 7.37. The vertical position of the moving points changes during optimisation to find the optimum profile. Contact on modified area corresponds to the 0 - +6 mm of wheelset lateral displacement. Therefore, the contact problems can be calculated only for the range 0 - +6 mm of lateral displacement of wheelset to reduce computation time of the optimisation procedure.

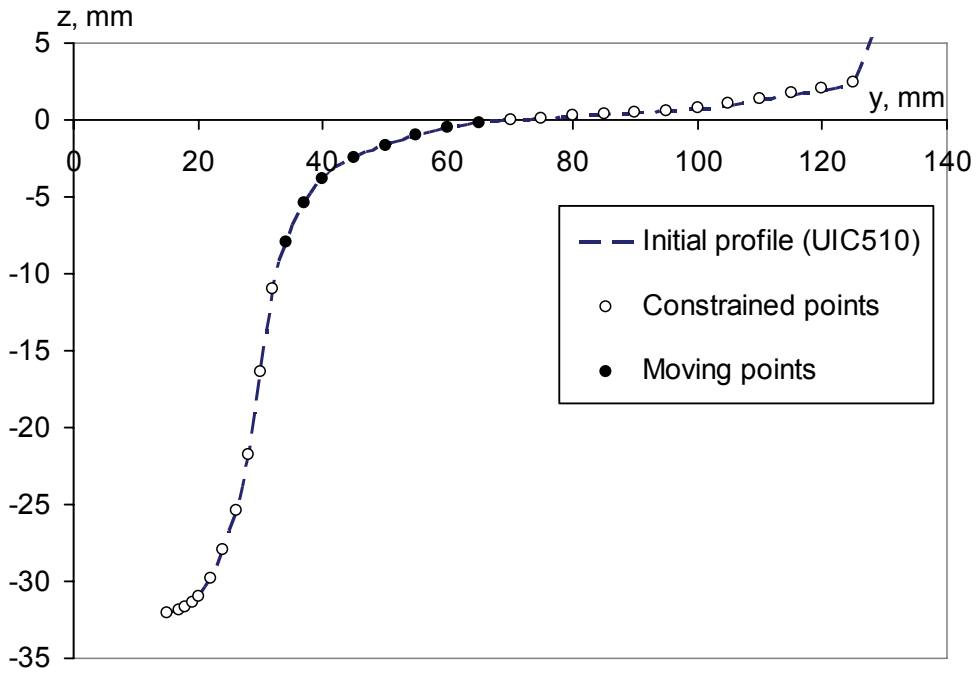

Figure 7.37: Initial wheel profile, constrained and moving points.

7.3.3 Results

In this section, results of wheel profile design for RET metro using the optimisation procedure are described.

7.3.3.1 Results of wheel design

The shape of the optimum designed wheel profile is shown in Figure 7.38. The tread part of the wheel profile is modified, while flange root and flange are left unchanged. Even though

the changes in the shape are not significant, they result in quite substantial changes in the RRD function, as shown in Figure 7.39. The RRD function of the optimised profile on S49 rail is very close to the target RRD, which means good results from optimisation. Wheel/rail contact points are shown in Figure 7.40. It can be observed that the contact points are very well distributed in the range from −4 mm to 4 mm of wheelset lateral displacement. The large jump of the contact point around the neutral position of the wheelset typical for UIC510 wheel on S49 rail (see Figure 7.34) is removed. The new contact conditions will result in significantly lower wheel wear. This conclusion is tested in the following section, using ADAMS/Rail dynamic simulations.

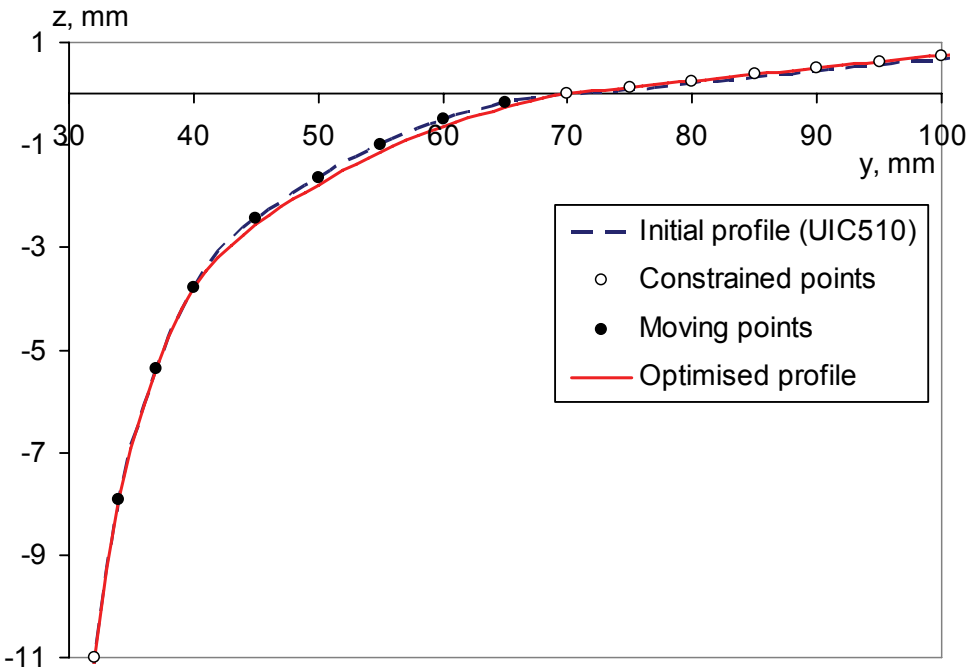

Figure 7.38: Initial and optimised wheel profiles with constrained and moving points, zoomed to modified part.

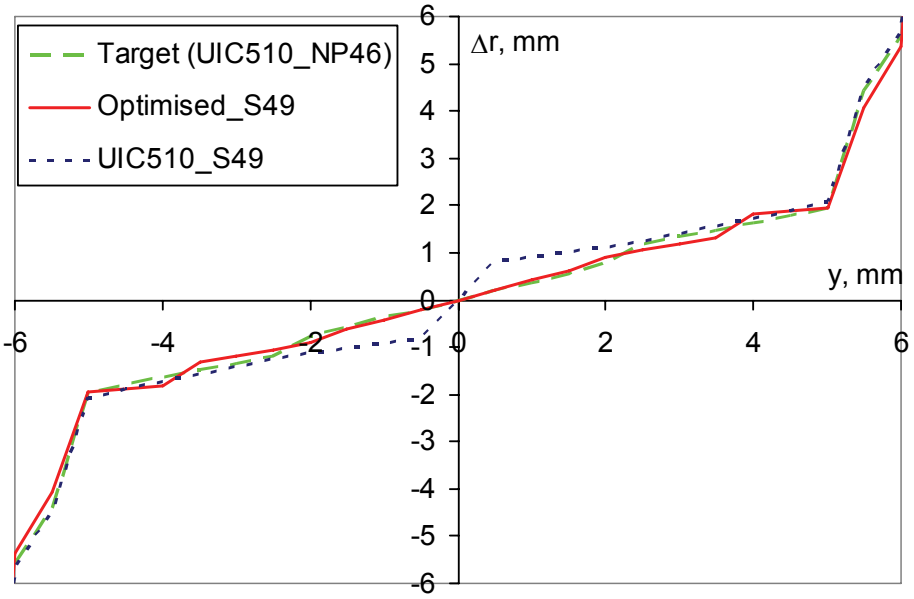

Figure 7.39: RRD functions for combination of UIC510 wheel on NP46 and S49 rails and optimised wheel profile on S49 rail.

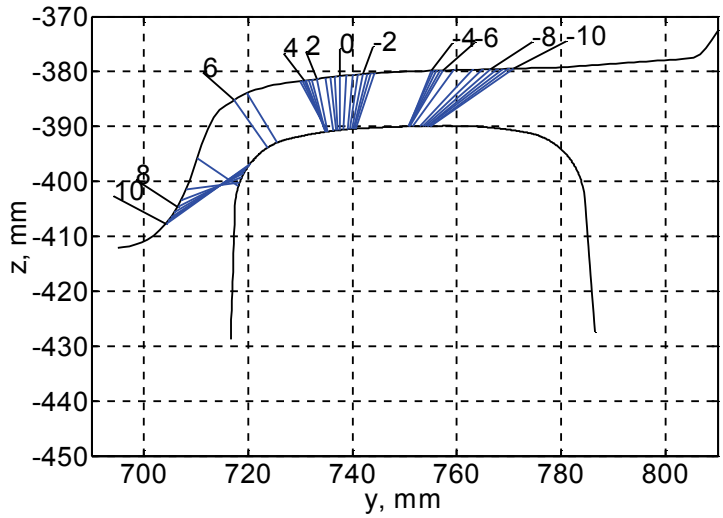

Figure 7.40: Positions of contact points for optimised wheel profile with S49 rail profile.

7.3.3.2 Results of dynamic simulations

After the optimum profile is obtained, the dynamic behaviour of a metro vehicle is then analysed. Analysis of metro vehicle dynamics is performed using the ADAMS/Rail model described in Section 4.2.3.2. First, the critical velocities of the metro train with UIC510 and optimised wheel profiles on S49 rail are evaluated; these are collected in Table 7.3. These velocities are obtained by performing closed-loop stability analysis and are confirmed by the dynamic simulation of a metro train running at various velocities on a straight track with lateral ramp. From this table, it is evident that, as a result of optimisation, the critical velocity of a metro train is increased (compare $V_{crit} = 50\, m/s$ for unworn UIC510 and $V_{crit} > 60\, m/s$ for optimised wheel profile). Critical speed is an important characteristic of vehicle stability. Critical velocity for the worn UIC510 profile is much lower, which also explains the stability problem observed in the metro trains.

It must be noted that results of simulated critical speed overshoot real critical speed. This is due to the absence of reliable vehicle suspension data for the metro model in ADAMS/Rail. Therefore these results may be used only in a relative sense.

Table 7.3: Critical speed of a metro train for various wheel profiles on S49 rail.

Wheel profile	Critical speed from closed-loop stability analysis	Equivalent conicity (measured for 3 mm of lateral displacement of wheelset on S49 rail)
UIC510 unworn	50.0 m/s	0.23
UIC510 worn	30.0 m/s	0.53
Optimised	>60.0 m/s	0.20

After analysis of the critical velocities, dynamic simulations of a metro train on a straight track are performed in order to analyse vehicle stability and wheel wear. The track has a length of 700 m. At 50 m from the beginning of the track, a horizontal ramp (height: 5 mm, width: 0.1 m) is introduced. The ramp induces initial disturbance to a wheelset, leading to oscillation of the bogie.

The lateral displacements of the first wheelset with various wheel profiles are shown in Figure 7.41 and Figure 7.42. Figure 7.41 presents an example of the unstable behaviour of a wheelset

with worn UIC510 profile. In this figure, the lateral displacements of the metro train wheelset with the optimised and (worn and unworn) UIC510 wheel profile travelling on S49 rail with velocity 30 m/s are shown. UIC510 and optimised wheel profiles are stable at this speed. The worn UIC510 profile is unstable in this case. For comparison, stable behaviour is shown in Figure 7.42. The metro train travels on a straight track with a speed of 20 m/s. From this figure, it is evident that the oscillations of the wheelset due to the lateral ramp are damping out relatively quickly and that the amplitude of these oscillations is not large. Therefore, it can be concluded that the motion of a metro vehicle with optimised wheel profile is stable at the operational speed of 20 m/s. From Figure 7.42, one can also see that the unworn UIC510 wheel profile on S49 rail delivers stable wheelset behaviour at 20 m/s as well, as is observed in practice.

The wear indexes of a wheelset with optimised and UIC510 wheel profiles are shown in Figure 7.43. From this figure, it is evident that the wear index for the unworn UIC510/S49 wheel/rail combination is significantly higher than that calculated for the optimised wheel profile (which means that the optimised wheel will wear more slowly). The explanation for this can be found in Figure 7.44, where the positions of the wheel contact point(s) for these combinations are shown. As is shown, the optimised wheel on S49 rail always has single-point contact, while the unworn UIC510/S49 wheel/rail combination always has double-point contact on the tread part of the wheel. Double-point contact normally results in a high wear rate for wheels. This is the case for the UIC510/S49 wheel/rail combination in the RET metro network. Due to elimination of double-point contact, the metro train with the optimised profile should show less wheel wear on a straight track.

The high wear of the tread part of the wheel leads to a hollow worn wheel profile, which in turn results in instability (hunting) of the vehicle due to high or negative conicity. Such instabilities are observed in RET metro trains. Immediately following such observation, the wheels must be reprofiled or replaced with the new ones in order to prevent vehicle derailment. Therefore, the reduction of wheel wear will also lead to increased wheel life.

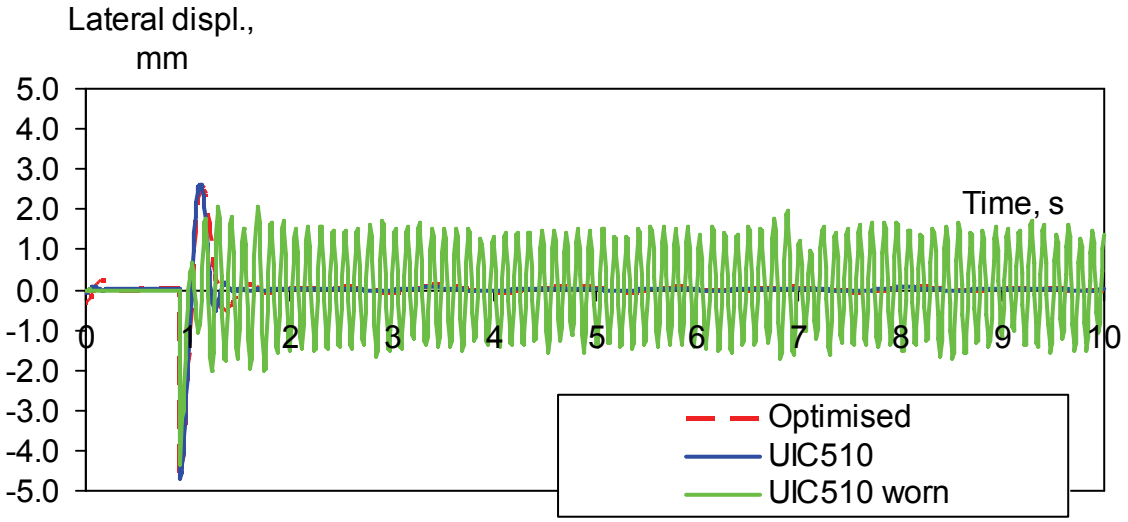

Figure 7.41: Lateral displacement of wheelset with optimised, UIC510 and worn UIC510 wheel profiles on S49 rail, velocity 30 m/s. Worn UIC510 wheel profile is unstable.

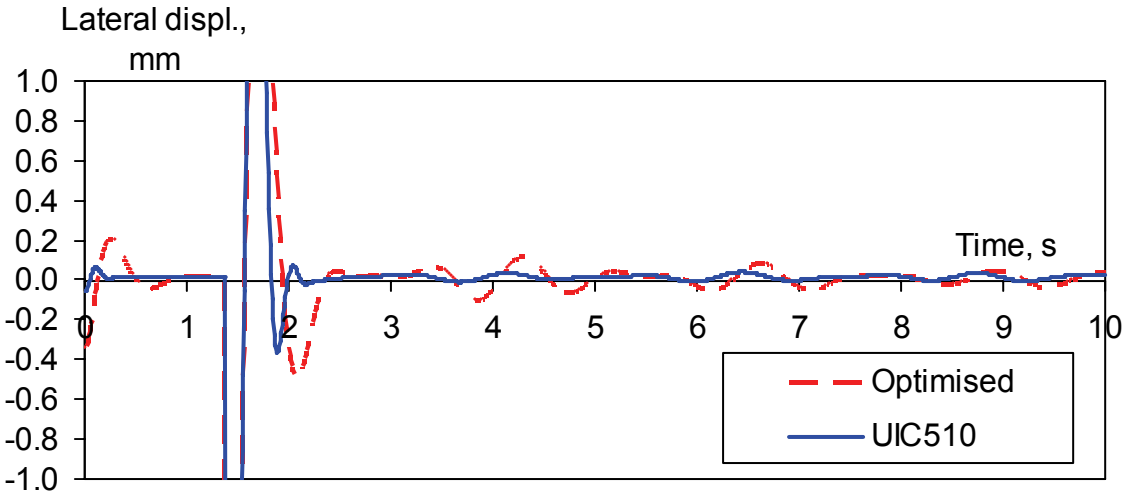

Figure 7.42: Lateral displacement of wheelset with optimised and UIC510 wheels on S49 rail, velocity 20 m/s.

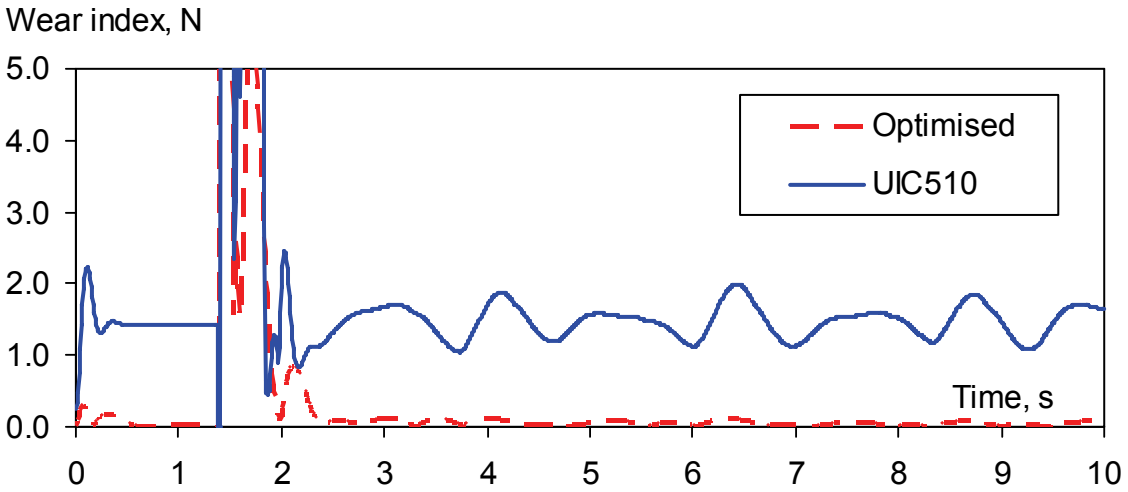

Figure 7.43: Wear index of the left front wheel. Optimised and UIC510 wheel profiles on S49 rail, velocity 20 m/s.

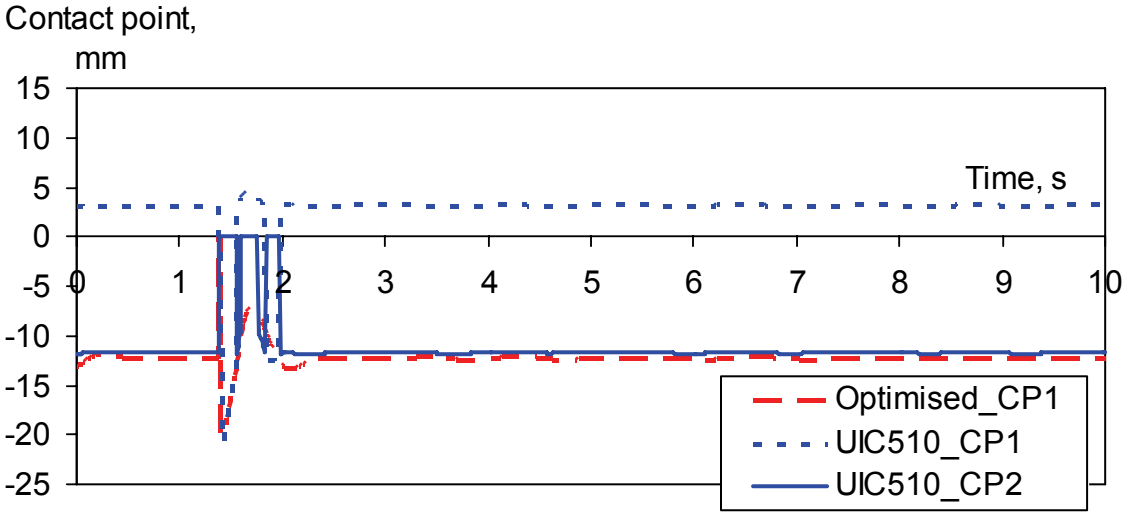

Figure 7.44: Position of contact point(s) (CP) on the left front wheel. Optimised (single-point contact) and UIC510 (double-point contact) wheel profiles on S49 rail, velocity 20 m/s.

7.3.3.3 Results of field tests

The optimised wheel profile was applied to metro trains in Rotterdam (The Netherlands). Unexpectedly low lifespan of the designed wheel profile was observed during the first tests. The wheels ran only 55,000 km before the occurrence of hunting. Nevertheless, this represented an improvement over the initial 25,000 km. However, the goal of 120,000 km was not achieved.

A follow-up investigation was undertaken. This investigation found that the track gauge, which was assumed as the standard 1435 mm during the optimisation of the wheel profile, was actually 2 mm narrower. Based on this finding, the optimised wheel profile was adapted to the narrower gauge by reducing flange width. After this adaptation, the mileage of the wheels did reach 120,000 km, and no lateral vibrations in metro trains using the optimised wheel profile have been observed. This application demonstrates that the performance of railway vehicles can be significantly improved by improving wheel/rail contact properties, and that the proposed optimum wheel design procedure can be successfully applied to such problems.

7.3.4 Conclusions

Using the design procedure described in Chapter 6, the wheel profile design for RET metro trains was determined and tested. The target RRD function was obtained through modification of the RRD function of the existing wheel and rail profiles used on the RET network. The results of the dynamic simulations show that the performance of a railway vehicle may be improved by addressing the contact properties of wheel and rail.

Double point contact between wheel tread and rail top produces high wear and leads to hollow wear of wheels.

Thinner wheel flange is used to increase flangeway clearance, and consequently to adapt wheelsets to narrower track gauge.

The new wheel profile has been implemented on the RET metro trains. Due to the application of the optimised wheel profile, instability on the metro trains has been eliminated, and the lifetime of the wheels has increased from 25,000 km to 120,000 km.

7.4 Case 3: Design of wheel profile for trains (NS case)

7.4.1 Description of problem

Recent developments in wheel and rail materials, as well as changes in railway policy towards increasing speed and vehicle load with regard to the essential increase in passenger traffic versus freight, has produced new problems in wheel/rail interface. Earlier, the wear of wheels and rails in curves was the essential problem for railway operators. Now, due to reduction of wheel/ rail wear, a head checks (HC) problem has appeared. Grinding of rail gauge sides to remove HC cracks, and thus reducing contact with wheel profile, seems to be a powerful but artificial measure, which does not eliminate the source of the problem. Grinding may be regarded as a solution for surfaces damaged by cracks, whereas design of wheel and rail profiles that remove RCF, and reduce wheel/rail wear, is the real challenge for researchers. In this section, a wheel profile design procedure to solve this problem is presented.

Investigation of new types of rail defects caused by RCF began in the Netherlands in the mid-1990s (see Smulders [2003]). Later, these defects were found to be HC and squats. HC occur primarily in curves and switches.

In the past, RCF problems were not present on the NS (Nederlandse Spoorwegen, Dutch Railway) network or were present only to a limited degree. The immediate cause of the problem is excessive tangential stresses overloading the rail surface. But it is clear that changes in the design of infrastructure and rolling stock, in network usage, and in maintenance practices over a long period, are the real causes.

There has been close cooperation between ProRail, Network Rail, AEA Technology (recently Delta Rail), NedTrain Consulting (now Lloyd's Register Rail Europe (LRRE)) and TU Delft in the investigation of the RCF problem. ProRail started its investigations into the RCF phenomenon as early as 1996. Initially, the investigations concerned RCF crack initiation, and the crack growth speed associated with it. At the beginning of 2000, investigations were initiated into modification of rail quality and rail head geometry.

The results of the investigations show that one reason (among other factors) for the increase in RCF problems was the replacement of NP46 rail (inclined 1:20) with UIC54 rail (inclined 1:40). The rails with UIC54 profile in a moderate and large radius curves are suffering from the frequent occurrence of the head checks. This rail change also resulted in a reduction of wheel mileage of 50% (from 300,000 km to 150,000 km between wheel reprofiling). The reason for this was that the wheels are now replaced due to RCF defects much more frequently and at an earlier stage (e.g., hair like cracks on a wheel contact surface, along with flats, squaring, pitting, etc.). Of course, wheel flats and squaring are due to higher accelerations and decelerations of the vehicles. Cracks on a wheel contact surface are appearing partly due to changes of rail profile and partly due to higher creepages in a wheel/rail contact patch. Smulders et al. [2003] provide an overview of the situation on the NS network.

ProRail also commissioned the Railway Engineering Group of TU Delft to perform research to examine the RCF phenomenon at the Dutch railway network (NS). As part of this project, the wheel/rail profile optimisation procedure was modified to take into account RCF. A complete description of this research can be found in Shevtsov et al. [2006] and Shevtsov, Markine and Esveld [2008]. The results of wheel profile optimisation to reduce RCF are presented below.

The NS fleet comprises several types of rolling stock. Some of the most common rolling stock is presented in Figure 7.45. For this research, the passenger coach was chosen (middle coach of ICM trainset, presented in Figure 7.46), as its dynamic properties are close to the ERRI passenger coach model, which is available in ADAMS/Rail.

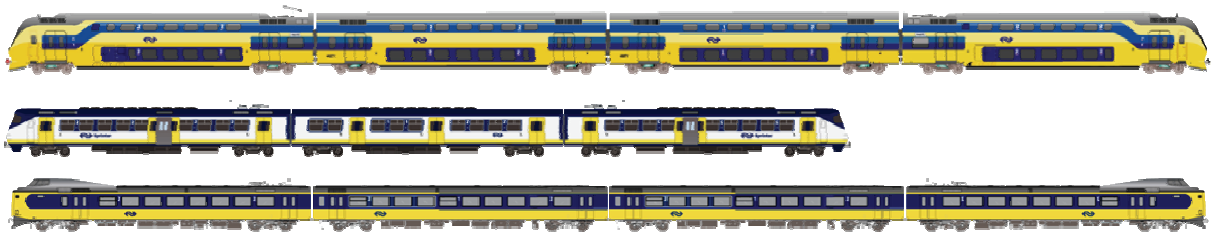

Figure 7.45: Trains of the NS fleet (from top to bottom: VIRM, SGM, ICM), NS, The Netherlands. Courtesy LRRE.

Figure 7.46: ICM trainset (NS) at Rotterdam Centraal station, The Netherlands. (Photo by the author).

7.4.2 Solution

In this section, application of a wheel profile design method for the RCF problem is shown step by step.

7.4.2.1 Analysis of problem

To find the sources of the head checks problem, the contact behaviour of the wheel and rail profiles currently used by the Dutch railways is studied. The standard S1002 wheel profile is used together with the UIC54 rail profile inclined 1:40. Previously, the NP46 rail with cant of 1:20 was used on the network.

Wheel/rail contact is analysed in several steps. First, a comparison of the old (NP46) and new (UIC54) rail profiles is performed (see Figure 7.47 and Figure 7.48). It should be noted that UIC54 rail is shown with an inclination of 1:40, whereas NP46 rail is shown inclined 1:20. There is a significant difference between these two profiles (Figure 7.47), which becomes visible when the top of the rails is zoomed in upon, as shown in Figure 7.48. This difference, mainly the result of the different rail inclinations, is responsible for the substantial changes in the wheel/rail contact, and consequently in wear and rolling contact fatigue behaviour.

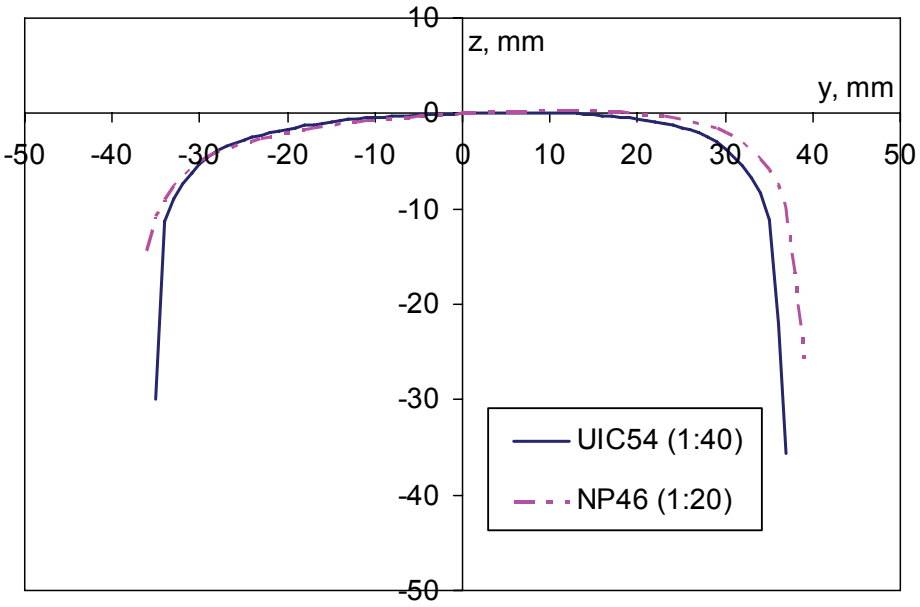

Figure 7.47: Comparison of rails UIC54 and NP46 (not zoomed).

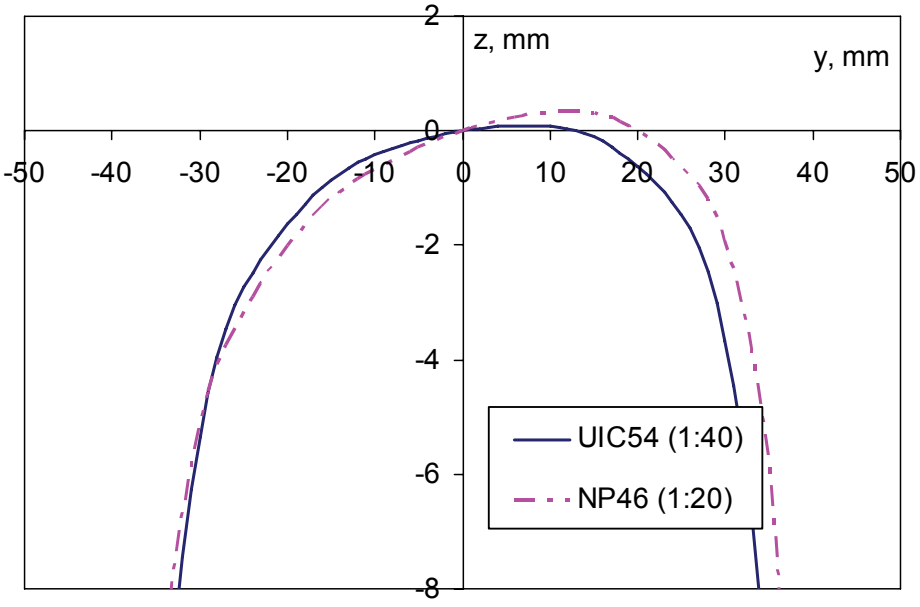

Figure 7.48: Comparison of rails UIC54 and NP46 (zoomed in).

In the next step of this analysis, wheel/rail contact characteristics of the old and new situations are investigated. The wheel/rail contact points for the new (unworn) wheel profile S1002 with the unworn UIC54 and NP46 rails, respectively, are shown in Figure 7.49 and Figure 7.50. In the wheel/rail contact figure, the lines between the wheel and rail profiles connect

corresponding contact points, which are calculated per 0.5 mm of lateral wheelset displacement. The lateral wheelset displacements are shown above the wheel profile. The coordinate system in this figure is the wheelset coordinate system $y_w Oz_w$ (Figure 2.4), with the origin in the centre of the wheelset in neutral position. It should be noted that in this figure, the wheel is shifted vertically 10 mm upwards from its actual position.

By comparing Figure 7.49 and Figure 7.50, one can observe a discontinuity (a large jump) in the position of the contact point on the NP46 rail around 6 mm of lateral displacement. This displacement typically corresponds to the motion of a wheelset on a curved track. Therefore, during the curve negotiation double point contact will occur, resulting in high wear rates. On the other hand, the wheel/rail combination S1002/UIC54 has more uniformly distributed contact points on a straight track and in curves, as shown in Figure 7.49. As a result, the wear rate of S1002 wheels on UIC54 rails is much lower. However, as will be shown later, such contact can lead to RCF problems.

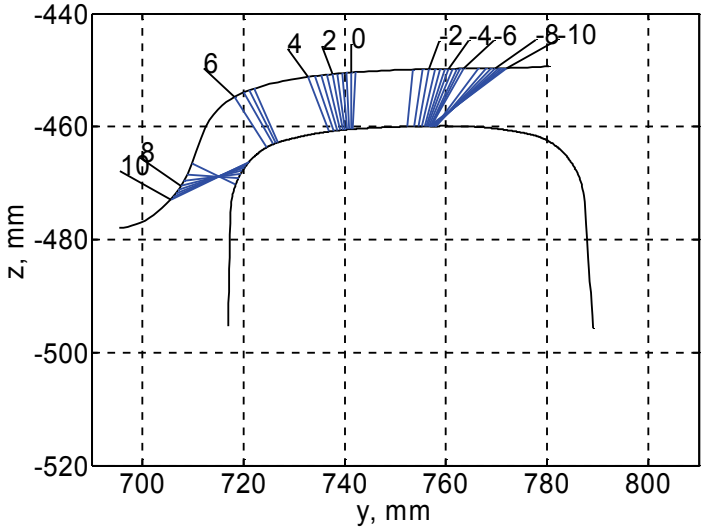

Figure 7.49: Positions of contact points for S1002 wheel profile with UIC54 (1:40) rail profile.

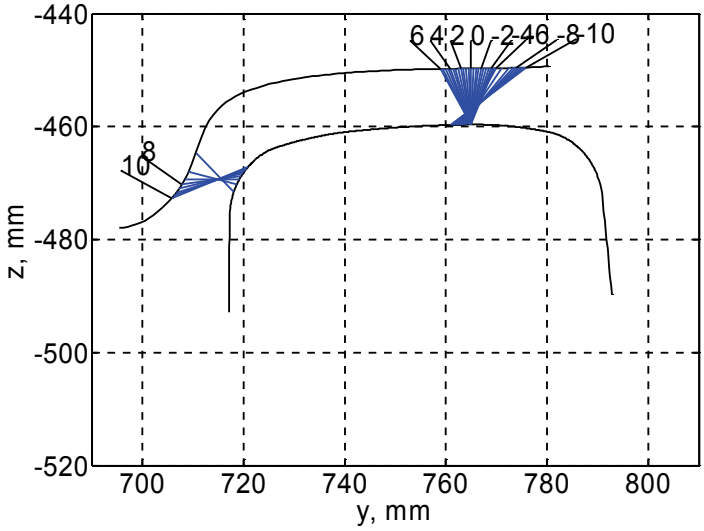

Figure 7.50: Positions of contact points for S1002 wheel profile with NP46 (1:20) rail profile.

As was mentioned earlier, rolling radius difference plays an important role in vehicle dynamics and is investigated next. The RRD functions of the S1002 wheel profile on,

respectively, UIC54 and NP46 rails are shown in Figure 7.51. This figure reveals that the S1002/UIC54 wheel/rail combination has much higher inclination of RRD function compared to the S1002/NP46 combination, which means that the corresponding equivalent conicity (2.5) is higher for the UIC54 rail than for the NP46 rail. The higher conicity allows a vehicle to pass curves at the required RRD. However, due to stiff primary suspension, a hunting problem does not occur with the S1002/UIC54 wheel/rail profile combination at the operational speed.

To take into account RCF, the design procedure of a wheel profile was modified using available knowledge on the RCF problem. ProRail, together with AEA Technology and NedTrain Consulting (see Smulders et al. [2003]), discovered that the so-called RCF region starts at the gauge side of the rail 15 mm from the rail zero point (see Figure 7.47). This was determined from simulations of the dynamic behaviour of NS rolling stock using measured wheel profiles. A set of worn S1002 wheel profiles was tested, and the worn S1002 wheel profile measured after 75,000 km shows the best compromise between distribution of contact point position and contact stresses. Field tests of the modified S1002 (worn) wheel profile were successfully performed, showing reduction of the RCF problem in comparison with the standard S1002 wheel profile.

In this section, a wheel profile is designed by following a practical approach. Let us consider surface fatigue index (3.33). In our case, the normal load F_z and the traction coefficient μ from formula (3.33) are defined by rolling stock and track conditions, which in our case are given (cannot be changed). From formula (3.33), a conclusion can be made that by increasing the wheel/rail contact area, fatigue occurrence can be reduced. The contact area can be increased by increasing the radiuses of the wheel and the rail profile. This is difficult to achieve at the flange root / gauge corner area due to the given design of the rail profiles. However, head checks can be eliminated by shifting the contact points from the RCF sensitive region to the top side of the rail profile and to the tread part of the wheel. Thus, constraints can be imposed on the positions of the contact points to omit gauge side area after the 15 mm from the rail zero point (see Figure 7.47). The RRD function of the S1002/UIC54 wheel/rail combination can be used as the target RRD function with the aim to keep unchanged the dynamic properties of the new wheel. Now, we describe constraints on designed wheel profile.

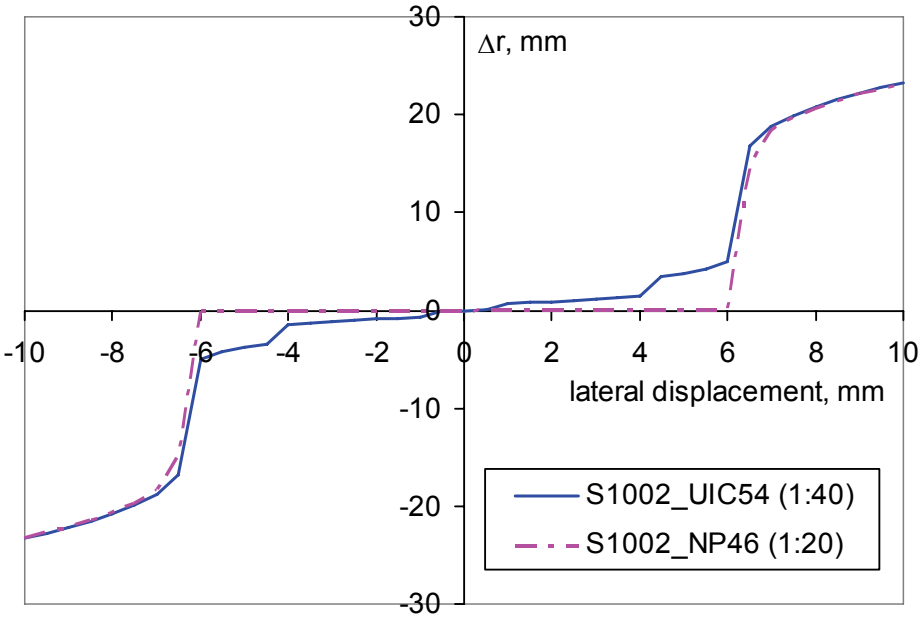

Figure 7.51: RRD functions for combination of S1002 wheel on UIC54 and NP46 rails.

7.4.2.2 Applied limits

As discussed in Chapter 6, during wheel profile design, a number of constraints can be applied on a designed wheel profile. Two safety requirements are considered in this case. Wheel flange thickness is the first requirement and is checked after optimisation. The second requirement is the constraint applied on the flange angle. The wheel flange angle is chosen to be 68º, the same as that of the S1002 wheel profile.

As described below in Section 7.4.2.4, wheel profile is described using B-splines. Use of B-splines does not require constraints on angles between the adjacent parts of the profile to avoid zigzags of the wheel profile. Therefore, these constraints are omitted in this case.

As described above, to avoid contact at the RCF-sensitive region of the rail, constraints on the position of contact points on the rail must be introduced. Contact points, corresponding to wheelset lateral displacement from 4.5 mm to 6 mm, are numbered 1 to 4, in the order of increase in wheelset lateral displacement (see Figure 7.49). The constraint for point number i is written as:

$$F_i \equiv 1 - y_{ci} / y_{ri} \geq 0\,,\ i = 1,...,4, \tag{7.3}$$

where y_{ri} is the horizontal coordinate of the contact point on the rail, and y_{ci} is the horizontal coordinate on the rail, which the contact point should not exceed. In the particular case of UIC54 rail, the value of y_{ci} is taken as:

$$y_{ci} = 735 - 0.1 \cdot (4 - i)\,,\ i = 1,...,4. \tag{7.4}$$

Each constrained contact point has a limit y_{ci} shifted along a rail profile at 0.1 mm from the limit y_{ci+1} for the next constrained contact point. This is done to promote spread contact along the rail profile and does not concentrate contact on a rail at one point.

Constraints on positions of the contact points in the form (7.3)–(7.4) assure that designed wheels will omit rail gauge side area after 15 mm from the rail zero point (see Figure 7.47). Consequently, contact points are moved from the RCF-sensitive region to the top side of the rail profile, and to the tread part of the wheel, reducing RCF damage to the rail.

However, the position of contact points on wheel and rail influence RRD function, which in turn defines the dynamic behaviour of the vehicle. To avoid the negative consequences of the introduced constraints, the proper limiting RRD function must be chosen.

7.4.2.3 Design of limiting RRD function

In this section, design of the limiting RRD function for the case of a passenger coach is described. The limiting RRD function is used in the optimisation procedure for the design of a new wheel profile. Optimisation of wheel profile is performed for UIC54 rail. The general theory of design for limiting RRD function can be found in Section 6.4.2.

As mentioned above, passenger coach is needed to modify contact situation on a rail, however, the dynamic properties of the coach should not be worsened. Therefore, the RRD function of the S1002/UIC54 wheel/rail combination (Figure 7.51) is used as the limiting RRD function, with the aim of keeping unchanged the dynamic properties of the designed wheel. Additional constraints on RRD function are automatically included through the use of existing RRD function for which proper dynamic behaviour and required wheel profile dimensions are known in advance.

The contact area on the wheel profile that is of interest for modification corresponds to the 0 - +8 mm of wheelset lateral displacement. Therefore, the contact problems can be calculated only for the range 0 - +8 mm of wheelset lateral displacement, to reduce computation time of the optimisation procedure.

7.4.2.4 Choice of profile variation

The geometry of the designed wheel profile is described via B-spline (see Section 6.2.5). Such description is used because the whole contact surface of the profile will be varied during optimisation. With B-splines, it is no longer necessary to piece together parts of the profile in order to agree with the shape complexity, nor to restrict the shape variations. Furthermore, the additional optimisation constraints that are needed to avoid unrealistic wheel profile designs are automatically taken into account in the new formulation (see Section 7.4.2.2).

A number of nodes along the wheel flange, flange root, and tread are chosen to compose B-spline. These nodes define the shape of a wheel profile as shown in Figure 7.52. The positions of these nodes can be varied in order to modify the profile. To reduce the computation costs of the optimisation, the positions of the nodes on the flange top and on the field side of the profile are not varied, as these do not participate in contact with a rail in the given range of wheelset lateral displacement. S1002 wheel profile is used as the source of coordinates for the starting profile.

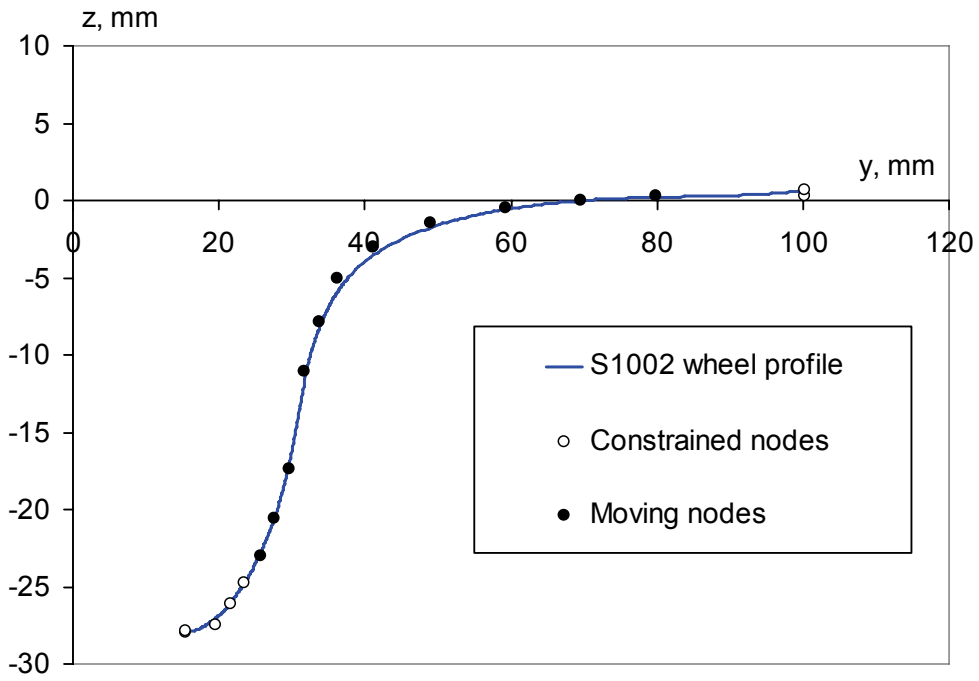

Figure 7.52: Wheel profile, constrained and moving nodes.

During optimisation, the nodes are moving in a direction normal to the initial wheel profile. This is done to take advantage of the normal coordinate system. The number of moving nodes and their location along the wheel profile must be determined from the analysis of wheel/rail contact properties beforehand. In the present case, 11 moving nodes are chosen for the profile variation.

The optimisation procedure consists of modifying the wheel profile that satisfies the target RRD function, while preventing high contact stresses. A solution to the optimisation problem is then taken as a new wheel profile. Wheels with such profile have the required contact

characteristics, which results in improved wheelset dynamics, reduction of wheel/rail wear, and prevention of HC occurrence. The results of the wheel design procedure are presented in the next section.

7.4.3 Results

In this section, the results of wheel profile design for a railway vehicle, using optimisation procedure, are described.

7.4.3.1 Results of wheel design

The approach described in the previous section was applied to the design of a new wheel profile that would reduce the RCF problem and would have the pre-described contact properties. RRD function of the S1002/UIC54 wheel/rail combination is used as the target RRD function. A wheel profile is designed for the UIC54 rail inclined 1:40. The S1002 wheel profile is modified into the pv11opt16start wheel profile (Figure 7.53), which is used as the initial wheel profile for the optimisation problem. The pv11opt16start wheel profile has no contact in the RCF region (between wheel flange root and rail gauge corner), making the starting design of the optimisation feasible.

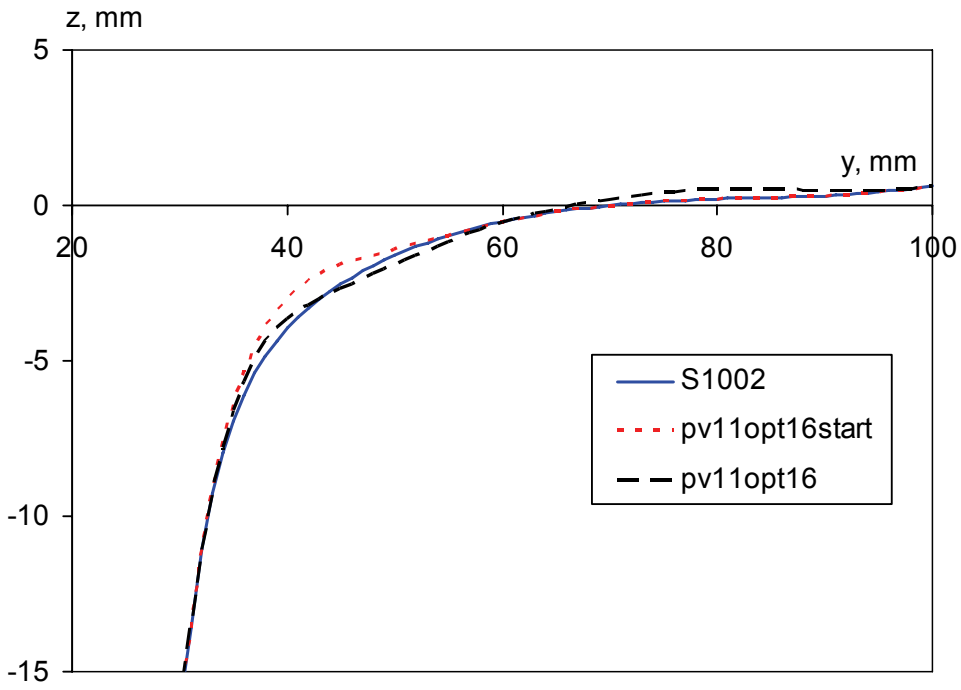

Figure 7.53: S1002, initial pv11opt16start and designed pv11opt16 wheel profiles. Only flange root and tread parts of profiles are shown.

The shape of the optimised wheel profile pv11opt16 is shown in Figure 7.53, together with the S1002 and pv11opt16start wheel profiles. The optimised wheel profile is significantly different from the S1002 and initial wheel profiles. From comparison of their RRD functions in Figure 7.54, it can easily be seen that for 4–6 mm of lateral displacement (corresponding to wheel/rail contact in a curve), the rolling radii difference of the pv11opt16 wheel profile is larger than the rolling radii difference of the initial profile, although it is smaller than the rolling radii difference of the S1002 wheel profile. This difference in RRD functions results from constraints on the position of the contact points on the rail profile. As can be seen from Figure 7.55, the pv11opt16 wheel profile has no contact at the rail gauge corner, i.e., beyond

15 mm from the top of the rail. From Figure 7.55 and Figure 7.49, one can see the changes in contact point distribution of the pv11opt16 wheel profile in comparison with the S1002 wheel profile. Absence of contact at the rail gauge corner should reduce contact stresses, and consequently prevent the RCF problem. However, the reduction of the jump of contact points from a wheel tread to a flange for the pv11opt16/UIC54 wheel/rail combination in comparison with the S1002/NP46 wheel/rail combination can also reduce wheel wear. This will be investigated in the next section using dynamic simulations of the passenger railway vehicle.

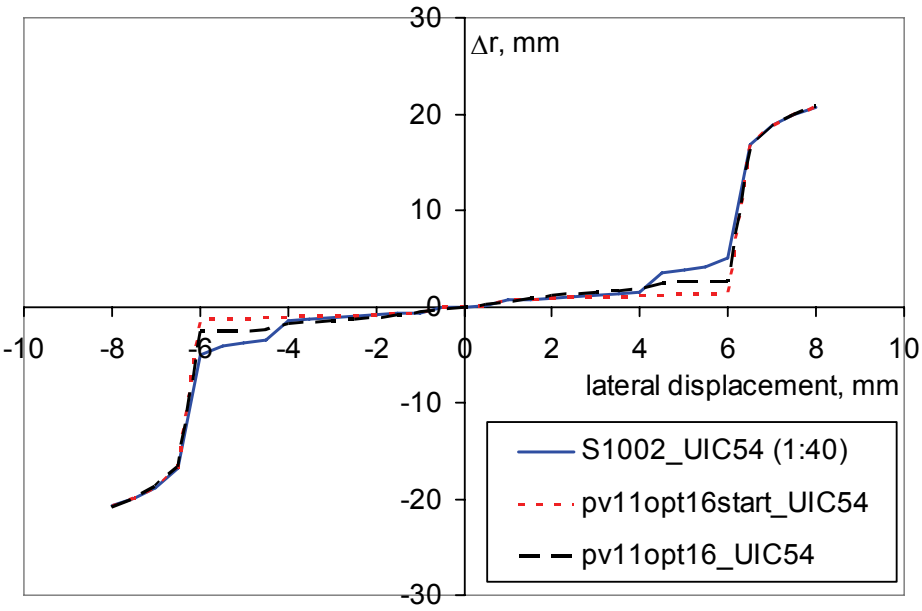

Figure 7.54: RRD functions for combination of S1002, pv11opt16start and pv11opt16 wheels on UIC54 rail.

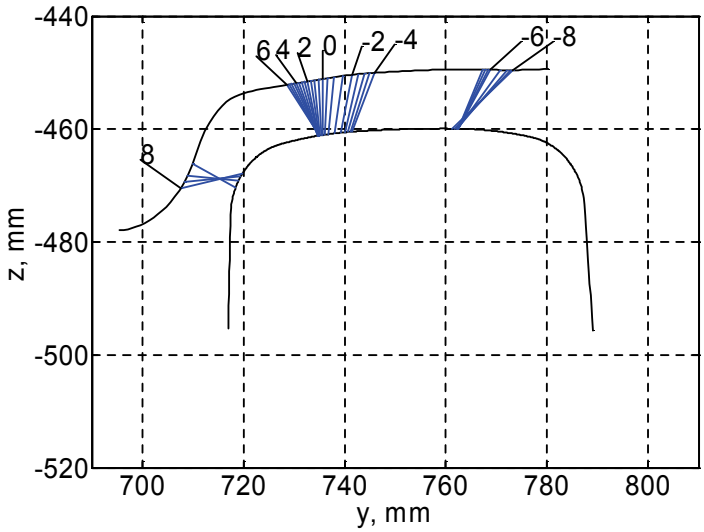

Figure 7.55: Positions of contact points for pv11opt16 wheel profile with UIC54 (1:40) rail profile.

7.4.3.2 Results of dynamic simulations

Analysis of passenger railway vehicle dynamics is performed using the ADAMS/Rail model described in Section 4.2.3.1. In this particular case, we concentrate on dynamic simulations in curved track, as we are mainly concerned with the RCF problem in large radius curves. A

passenger railway vehicle is simulated on a track consisting of 50 m straight track, continuing into a 100 m transition curve, then switching into a 400 m right turn curve with R=1000 m, then a 100 m transition curve, and ending with 850 m straight track. The vehicle travels at a speed of 20 m/s. In this research, other curve radiuses and vehicle speeds are also investigated; however, for the sake of brevity, these cases will not be presented here.

Wear index W and surface fatigue index FI_{surf} calculated for the left wheel of the first wheelset and lateral displacement y of the first wheelset are chosen as the most representative quantities in this dynamic analysis. Based on lateral displacements of the wheelset, one can judge its stability.

Dynamic simulation of the passenger vehicle is performed using the following three wheel/rail combinations – S1002/UIC54, S1002/NP46, and pv11opt16/UIC54. The lateral displacements of the first wheelset are shown in Figure 7.56. From this figure, it can be seen that the motion of the vehicle is stable at a speed of 20 m/s. The S1002/NP46 wheel/rail combination, due to low conicity, produces low steering forces. As a result, the oscillations, after the curved track, damp out slowly for the S1002/NP46 wheel/rail combination.

The wear (3.32) and surface fatigue (3.33) indexes of the left front wheel are shown in Figure 7.57 and Figure 7.58 correspondingly. The yield stress in shear is here taken as $k = 600\text{MPa}$, which corresponds to the premium sorts of the wheel and rail steel, that are more and more frequently used by the railways. It should be noted that in case of double point contact, the wear index is calculated as the sum of the wear indexes for each contact point, whereas the surface fatigue index is presented for each contact point separately. In Figure 7.58, the fatigue index for the second contact point is represented by dots. From Figure 7.57, it is evident that the wear index for the S1002/NP46 wheel/rail combination is significantly (1.5 times) higher than that calculated for the S1002/UIC54 combination. The wear index for the pv11opt16/UIC54 combination is 1.2 times higher than the wear index for the S1002/UIC54 combination. Analysis of Figure 7.58 shows that surface fatigue index on a curved track exceeds the fatigue limit (is positive) for all tested wheel/rail profile combinations. The S1002 wheel on UIC54 rail has the highest surface fatigue index, due to single point contact. On NP46 rail, it has a slightly lower surface fatigue index, due to double-point contact. It should be noted that at the first contact point, the fatigue index of the S1002 wheel on the NP46 rail does not exceed the fatigue limit. The surface fatigue index for the pv11opt16 wheel on the UIC54 rail is the lowest of these three wheel/rail combinations, which means that the chance of RCF occurrence is lower for this wheel/rail combination.

Dynamic simulation of a passenger vehicle in a curve with R=1000 m shows single and double contact situations for the wheel/rail combinations. The wheels with the S1002 profile on the UIC54 rail profile have a single point of contact, situated at the wheel flange root and the rail gauge corner. The wheels with the S1002 profile on the NP46 rail profile have double-point contact, situated, respectively, at the wheel tread and flange, and at the rail head and rail gauge corner. Due to single point contact, the wear index of the S1002 wheel on the UIC54 rails is significantly lower than on the NP46 rails. Using the formula (3.33), it is found that the contact stresses for the S1002 wheel profile on the UIC54 rail exceed the shakedown limit, and therefore RCF damage will occur (see Figure 7.58). The stresses for the S1002 wheel profile on the NP46 rails also exceed the shakedown limit (still, they are lower than those on the UIC54 rail). This means that RCF damage will occur for the S1002/NP46 combination as well. However, in practice (see Smulders et al. [2003]), RCF damage was observed only for the S1002/UIC54 wheel/rail combination, and high wear was observed for the S1002/NP46 wheel/rail combination. The absence of RCF damage for the S1002/NP46 wheel/rail

combination can be explained by the high wear, due to which the surface fatigue cracks were removed and therefore RCF damage was not observed.

Due to the absence of contact on a rail gauge corner, the pv11opt16 wheel profile has double point contact with the UIC54 rail during its motion in a curve. By analysing the results of the dynamic simulations, one can see that the surface fatigue index shown in Figure 7.58 is lower for the designed wheel profile pv11opt16, as compared to the S1002 wheel profile. Due to double point contact, the wear index for the pv11opt16 wheel is higher than for the S1002 wheel on UIC54 rail (see Figure 7.57); however, this is the price for the reduction of the contact stresses and for the corresponding reduction of the chances of RCF damage. It seems realistic that a small increase in wear for the designed wheel will preventively remove surface fatigue cracks. Due to reduction in RCF damage and relatively small increase of wear, the pv11opt16 wheel profile can be considered a good compromise with respect to wear and RCF.

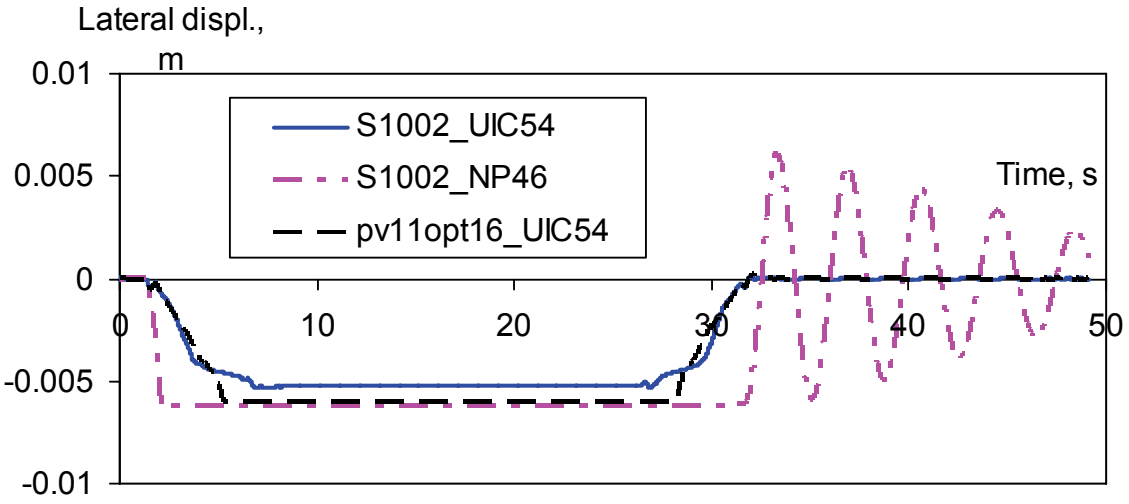

Figure 7.56: Lateral displacements of front wheelset vs. time for S1002/UIC54, S1002/NP46 (1:20) and pv11opt16/UIC54 wheel/rail profiles. Curve radius is 1000 m. Running speed is 20 m/s.

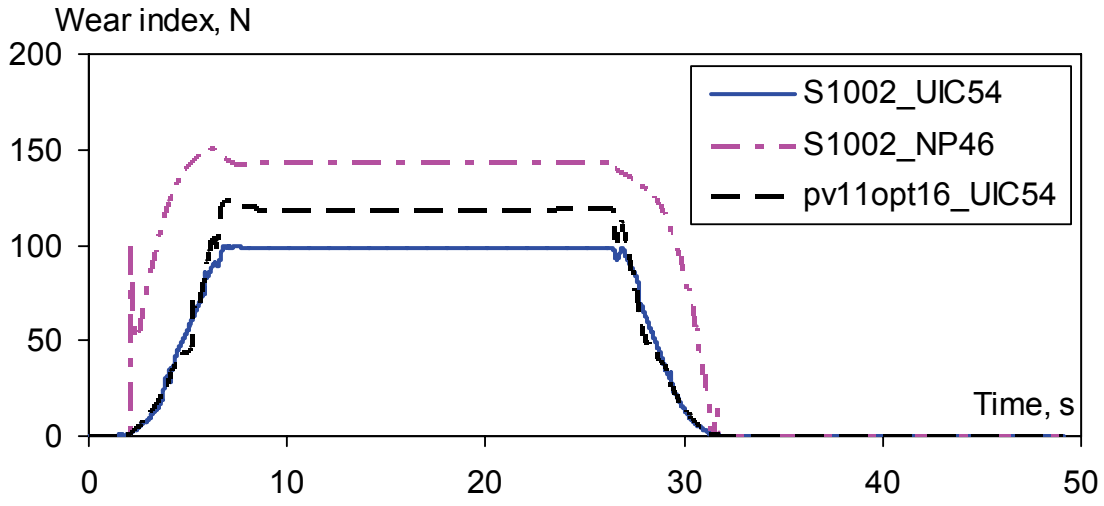

Figure 7.57: Wear index of the left front wheel vs. time for S1002/UIC54, S1002/NP46 (1:20) and pv11opt16/UIC54 wheel/rail profiles. Curve radius is 1000 m. Running speed is 20 m/s.

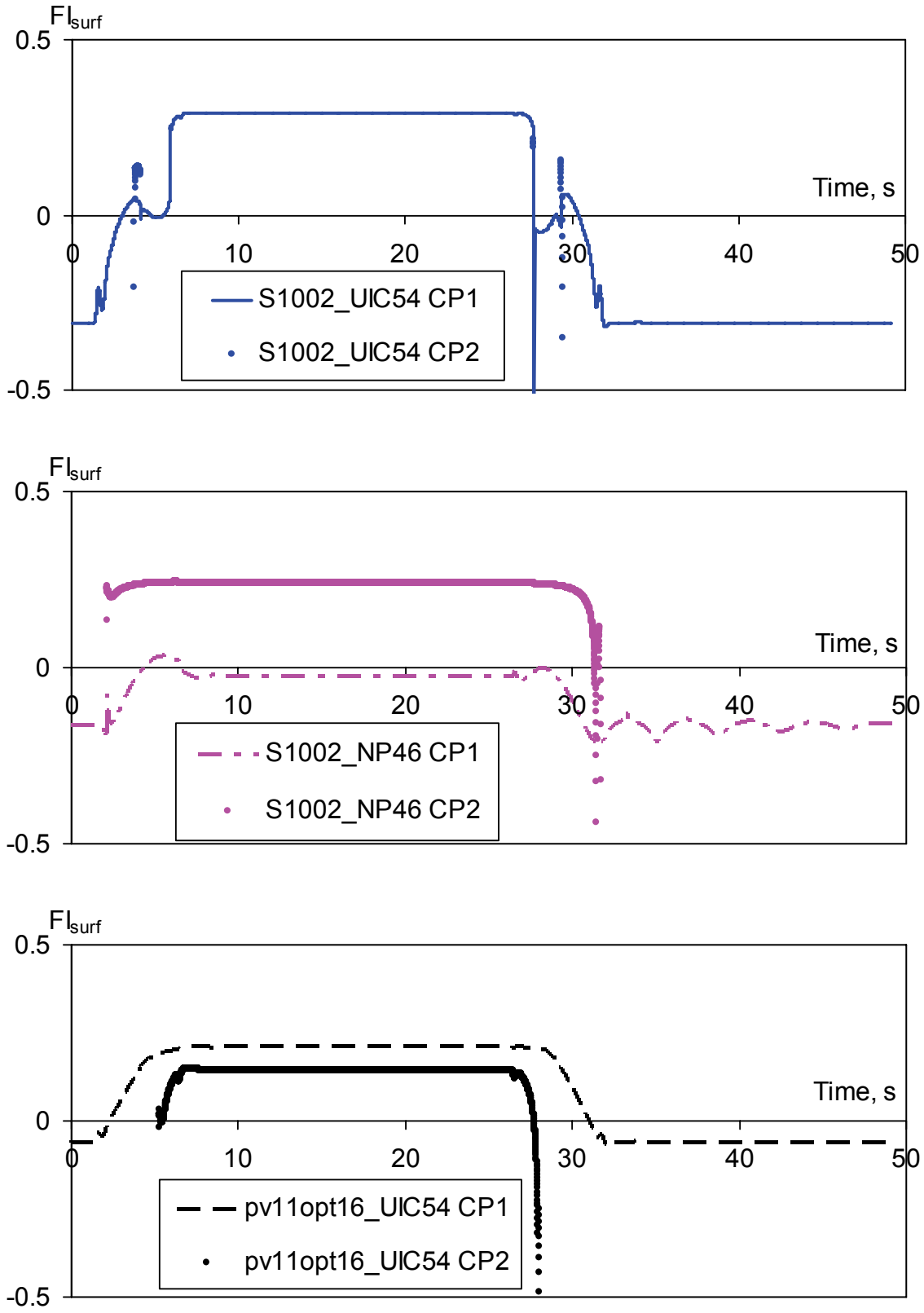

Figure 7.58: Surface fatigue index of the left front wheel vs. time S1002/UIC54, S1002/NP46 (1:20) and pv11opt16/UIC54 wheel/rail profiles. Curve radius is 1000 m. Running speed is 20 m/s.

After testing the designed wheel profile in curves, it must be checked for stability on a straight track. The critical velocities of the passenger coach with the S1002 and optimised wheel profiles on the UIC54 rail are evaluated. These are collected in Table 7.4. These velocities are obtained by performing a closed-loop stability analysis, and are confirmed by dynamic simulation of the coach running with different velocities on a straight track with lateral ramp. From this table, it is evident that, as a result of the modification of wheel profile, the critical velocity of the coach is slightly reduced, but in comparison with the absolute value, the difference is negligible. The critical velocity for the S1002 wheel on NP46 rail is much lower, which is explained by extremely low conicity of this wheel/rail profile combination.

It must be noted that the ERRI vehicle model is characterised by very stiff primary suspension in the horizontal direction, which results in high critical speed. The older types of rolling stock usually have softer suspensions and, consequently, lower critical speeds.

Table 7.4: Critical speed of a passenger coach for various wheel/rail profiles.

Wheel/rail profile	Critical speed from closed-loop stability analysis	Equivalent conicity (measured for 3 mm of lateral displacement of wheelset)
S1002/UIC54	97.0 m/s	0.187
S1002/NP46	30.0 m/s	0.0096
pv11opt16/UIC54	95.0 m/s	0.252

After calculation of the critical velocities using closed-loop stability analysis, the dynamic simulations of a train on a straight track are performed in order to analyse vehicle stability. The track has a length of 700 m, whereas at the distance of 50 m from the starting point of the track, a horizontal ramp (height: 5 mm, width: 0.1 m) is introduced. The ramp induces an initial disturbance to the wheelset, leading to oscillation of the bogie.

The lateral displacements of the first wheelset with different wheel profiles are shown in Figure 7.59. In this figure, the lateral displacements of the first wheelset with the optimised and S1002 wheel profiles on UIC54 and NP46 rails travelling with velocity 40 m/s are shown. S1002 and pv11opt16 wheel profiles on UIC54 rail are stable at this speed. From Figure 7.59, it is evident that the oscillations of the wheelset due to the lateral ramp are damping out quickly. However, on NP46 rail, profile S1002 wheel is unstable at this speed. The wheelset oscillations do not damp out, and the amplitude of these oscillations corresponds to flange-to-flange contact. Even more, the critical speed of S1002 wheel on NP46 rail profile is around 30 m/s. Such low critical speed is probably due to very low equivalent conicity of the S1002/NP46 wheel/rail profile combination (see Table 7.4), and the very stiff suspension of the ERRI vehicle model. However, rolling stock used on NP46 rails was less stiff, and consequently that rolling stock profits from the low conicity of the S1002/NP46 wheel/rail combination. NP46 rails are largely out of use today, therefore, stability problems on this rail type are not observed in practice.

Therefore, it can be concluded that the motion of the railway vehicle with optimised wheel profile is stable at the operational speed (up to 40 m/s).

Modification of contact properties of the wheel to reduce RCF in curves does not worsen the dynamic behaviour of the vehicle on a straight track.

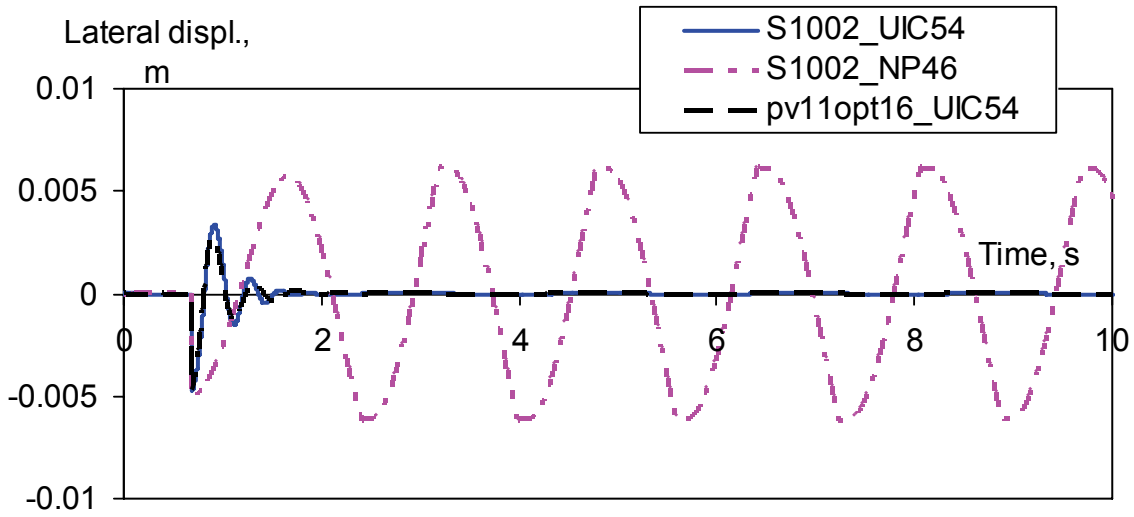

Figure 7.59: Lateral displacements of wheelset with S1002/UIC54, S1002/NP46 (1:20) and pv11opt16/UIC54 wheel/rail profiles, velocity 40 m/s. S1002 wheel profile on NP46 rail is unstable.

7.4.3.3 Results of field tests

Field tests have not been performed using the designed profile. Therefore, comparison of the results of simulations and field tests is not possible. It is known to the author that a wheel profile developed by NedTrain Consulting was successfully tested on the Dutch railway network. However, details of the wheel design are of commercial interest and are not available to TU Delft.

7.4.4 Conclusions

The presence of the RCF problem on the Dutch railway network is confirmed by the results of the numerical simulations. Results from the dynamic simulations show that the shape and combination of the wheel and rail profiles affect the occurrence of RCF damage.

Dynamic simulations, as well as field experience, show that double point contact leads to higher wear, however, it reduces risk of RCF due to lower contact stresses as well as the removal of crack initiation. Single point non-conformal contact at a rail gauge corner is the most damaging scenario for the rail, as high contact stresses occur under high creep conditions, resulting in RCF.

In this section, the procedure for wheel design is modified to take into account not only the dynamic behaviour of the wheelset and wheel/rail wear, but also RCF.

To define the shape of a wheel profile, a B-spline representation is used. The description of wheel profile with B-splines in a shape-optimal design problem is a powerful and rather general approach.

An optimised wheel profile is obtained using the design procedure. The results of the dynamic simulations show a small increase in the wear index and a reduction in surface fatigue index for the designed wheel profile. Using the optimised wheel profile, the RCF damage observed for the existing wheel/rail combination can been reduced.

An optimum wheel design is a compromise between stability, curving, wear, and RCF.

7.5 Discussion and conclusions

Three application cases of the wheel profile design procedure are described in this chapter. Three types of railway systems are considered, namely tram, metro, and passenger coach of a conventional railway. New wheel profiles are designed for each case, respectively solving the problems of flange wear, stability (as a result of excessive tread wear), and RCF. In the first two cases, wheel profiles are successfully implemented on each corresponding network.

Successful implementation of the design procedure has proven its usability and practicability. The procedure is flexible, and differing requirements with regard to optimal wheel profile can be included in the design procedure. For example, in the third application case the procedure is modified to take into account not only the dynamic behaviour of the wheelset and wheel/rail wear, but also RCF during the design of a wheel profile.

Various approaches to wheel profile modification are employed, namely variation of the vertical position of the node points, variation of arcs and lines describing profile, and variation of the position of the B-spline nodes. Each method has advantages and disadvantages, which are described in Section 6.2. Variation of the wheel profile using nodes of B-spline is the most advanced method, and is the most suitable for the solution of the numerical optimisation problem.

Dynamic simulation of railway vehicles using ADAMS/Rail allows testing and comparison of the properties of the designed wheel profiles with the currently existing wheel/rail profiles in a very fast and efficient way. Results from wear modelling in dynamic simulations show very good correlation with field experience; for example, see the dramatic decrease in wheel wear from replacement of conical HTM1 wheel by curvilinear HTM2 wheel, observed both in simulations and on-track.

The comparison of RRD functions for tram, metro, and trains made in Figure 6.16 confirms the idea that every railway system requires its own optimal RRD function.

Lower flange angle increases the possibility of derailment. On the other hand, lower flange angle can improve wheel/rail contact. Therefore, optimisation of wheel flange angle represents a tradeoff between improvement of safety and improvement of performance. It should be noted that the Nadal formula is known to be very conservative, and the real risk of derailment is lower than from that calculated from the Nadal formula. The Nadal formula is not conservative for independently rotating wheels.

Double point contact between wheel tread and rail produces high wear, and leads to hollow wear of wheels.

Worn wheels contribute highly to wheel/rail wear and vehicle instability. Closer attention to profiles and radii of the left and right wheels on one wheelset can reduce wear and hunting problems. Tread wear can be influenced by bogie design and/or wheelset maintenance. Decreased tolerance between left and right wheel diameters can reduce the hollow wear of wheels.

Dynamic simulations, as well as field experience, have shown that double point contact leads to higher wear, however, double point contact reduces the risk of RCF, due to lower contact stresses as well as to the removal of crack initiation. A single-point non-conformal contact at rail gauge corner is (probably) most damaging to the rail, as the highest contact stresses occur under high-creep conditions, resulting in RCF.

Introduction of new wheel and/or rail profiles requires thorough investigation of all involved aspects. It is highly advisable to perform monitoring of the behaviour of wheels and rails before and after introduction of new profiles. It must be understood that worn wheels and rails

can have significantly different profile shapes in comparison with unworn theoretical profiles. A transition program with intermediate (temporary) wheel or rail profiles might be required to introduce new wheel and rail profiles.

8 Conclusions and recommendations for further research

Design of an optimal wheel/rail profile combination is a complex interdisciplinary task combining geometric and physical contact of wheel and rail, vehicle–track dynamic interaction, profile design modelling, numerical optimisation methods, mathematical programming, and interactive computer graphics. Expertise in all these fields is necessary to achieve satisfactory results. Each problem is described in this thesis. Together, they are combined in a wheel (rail) profile design procedure.

The procedure of wheel (rail) profile design is developed, verified and presented in this thesis. The wheel (rail) profile design procedure uses optimality criteria based on the Rolling Radius Difference function, which to a large extent defines the contact properties of the wheel and rail. A new wheel profile is obtained by minimising the difference between target and current RRD. The MARS method is chosen as a general optimisation technique. The design procedure allows development new wheel profiles with *a priori* defined contact properties. The dynamic simulation program ADAMS/Rail is used to assess wheel/rail interaction and vehicle behaviour for the designed profiles.

Under the procedure described in this paper, wheel profile designs for an HTM tram, an RET metro train, and an NS passenger coach are improved. Target RRD functions are obtained through modification of the RRD function of existing wheel and rail profiles used on the respective networks. Using the proposed design procedure, new wheel profiles are obtained and tested for each respective vehicle.

The results from the optimisation show that the performance of a railway vehicle can be improved by improving the contact properties of the wheel and rail. Application of optimised wheel profiles results in improvement in wheel/rail interaction and railway vehicle dynamics, and wheel life is increased.

Successful implementation of the design procedure shows its usability and practicability. The procedure is flexible, and requirements on optimal wheel profile can be varied within the design procedure. For example, in the railway passenger coach application, the wheel profile design procedure is modified to take into account not only the dynamic behaviour of the wheelset and wheel/rail wear, but also RCF.

Improvement of bogie dynamic performance seems a promising way to reduce problems with wheel/rail wear and RCF. Many investigations show significant influence from bogie parameters and bogie imperfections on the dynamic performance of railway vehicles and, consequently, on wheel and rail wear and RCF behaviour.

The question of tolerances in wheel lathes and rail grinding machines frequently arises during the design of wheel and rail profiles. Designers must be certain that proposed changes to wheel and rail profiles can be implemented in practice by the available machinery. Otherwise, more precise machines must be utilized.

Freight rolling stock is not considered in the present research. There are several reasons for this exclusion. First, a major criterion for the freight vehicles is interoperability. For this reason, the wheel profile of freight wagons should be unified, unless the vehicle is operated on a closed line. Second, variety in freight vehicles is probably as great as that in passenger vehicles. Consequently, each type of vehicle requires its own optimal wheel profile. Third,

operating requirements for freight vehicles are significantly different than for passenger rolling stock (axle load is greater and travel speed is lower). Therefore, freight vehicles constitute a separate field of research, requiring separate investigation.

RCF is a problem that affects many railway systems around the world. Inspection of the rail surface to monitor crack growth and grinding of railheads is used to control RCF on many railway networks. Railhead grinding removes metal from the area most prone to RCF, the gauge root part of the contact surface. Although railhead grinding has proven effective, it is also rather costly and difficult to implement in practice. Changing the wheel profile is a promising way of reducing the possibility of RCF developing — primarily on rails, but also on wheels.

It should been mentioned that the simultaneous optimisation of both rail and wheel profiles is more effective than the optimisation of only one. However, experience shows that implementation of the optimisation of the wheel profile usually is faster and proceeds under better control conditions, and it requires less maintenance investment. Implementation of rail profile optimisation requires grinding of the entire network, which is costly and requires good planning, due to intervention on an active network. Furthermore, it usually requires a long time period to complete over an entire network.

The old approach of “one size fits all” cannot be applied if the railway system is to be optimised. Regarding wheel/rail profiles, this could mean that each type of rolling stock would require a custom wheel profile. Moreover, each type of railway track curve could be considered individually, resulting in the possibility that several rail profiles must be used on a network, depending on curve radii. Sometimes a political decision will be required, and additional measures will be necessary to prevent negative consequences. Rail profiles can be applied to reduce RCF or rolling noise, but not both, while RCF and squealing noise can both appear in one curve; therefore, a combined approach is required.

Although the impact of wheel and rail profiles is understood quite well, there is certainly no universal opinion on what are the best shapes for a given environment. Comprehensive models that combine vehicle dynamics, contact mechanics, and crack propagation models are developing as viable systems for assessing the impact of vehicle, track, metallurgical, and environmental parameters on wheel and rail life. The wide range in these properties assures that these models will require continuing development and validation for many years to come.

Some potential improvements for future research include but are not limited to:

1. Wheel (rail) profile design procedure could be extended to incorporate such uncertainties as wheelset and track gauge variation, and wheel profile tolerance, which are inherent in the real life.
2. Reduction in squealing noise could be included as a constraint in the design procedure.
3. Wheel/rail interaction is optimised only from the physical point of view. In future, wheel/rail profiles could be designed to optimise costs over the entire lifecycle. However, to achieve this, precise data (simulated or measured) on wheel/rail wear and RCF will be required.

References

ADAMS/Rail (2005) MSC.Software Corporation MSC.ADAMS®, http://www.mscsoftware.com, 2005.

Arnold M., Frischmuth K. (1998) Solving problems with unilateral constraints by DAE methods, Mathematics and Computers in Simulation, vol. 47, 1998, pp. 47-67.

Arrus P., Pater A.D. de and Meyers P. (2002) The Stationary Motion of a One-Axle Vehicle Along a Circular Curve with Real Rail and Wheel Profiles, Vehicle System Dynamics, 2002, Vol. 37, No. 1, pp. 29-58.

Augusta Neto M. and Ambrósio J. (2003) Stabilization methods for the integration of differential-algebraic equations in the presence of redundant constraints. Multibody Systems Dynamics, 2003, Vol. 10, No 1, pp. 81–105.

Barbosa R.S. (2004) A 3D Contact Force Safety Criterion for Flange Climb Derailment of a Railway Wheel, Vehicle System Dynamics, 2004, Vol. 42, No. 5, pp. 289–300.

Barthelemy J.-F.M. and Haftka R.T. (1993) Approximation Concept for Optimum Structural Design – a Review, Structural Optimization, vol. 5, 1993, pp. 129-144.

Beynon J.H., Kapoor A., and Tyfour W.R. (1996), Deterioration of rolling contact fatigue life of pearlitic rail steel due to dry-wet rolling-sliding line contact, Wear 197, pp. 255-265.

Bletzinger K.-U., Kimmich S. and Ramm E. (1991) Efficient modelling in shape optimal design, Computing Systems in Engineering, 1991, Vol. 2, iss. 5-6, pp. 483-495.

Böhm W., Farin G., Kahmann J. (1984) A Survey of Curve and Surface Methods in CAGD, Computer Aided Geometric Design, 1984, vol. 1, pp. 1-60.

Bolton P.J., Clayton P. (1984) Rolling-Sliding Wear Damage in Rail and Tyre Steels, Wear, Vol. 93, 1984, pp. 145-165.

Boocock D., Steady-state motion of railway vehicles on curved track, Journal Mechanical Engineering Science, 11, pp. 556–566, 1969.

Bower A. F. and Johnson K. L. (1991) Plastic flow and shakedown of the rail surface in repeated wheel-rail contact, Wear, 1991, vol. 144, iss. 1-2, pp. 1-18.

Braghin F., Bruni S. and Diana G. (2006), Experimental and numerical investigation on the derailment of a railway wheelset with solid axle, Vehicle System Dynamics, Vol. 44, No. 4, 2006, pp. 305–325.

Braibant V. and Fleury C. (1984) Shape Optimal Design Using B-Splines, Computer Methods in Applied Mechanics and Engineering, 1984, vol. 44, pp. 247-267.

Braibant V. and Fleury C. (1985) Shape Optimal Design: An Approach Matching CAD and Optimization Concepts, in "Optimization in Computer-Aided Design", edited by J. S. Gero, Elsevier Science Publishers, IFIP 1985.

Bushan B. (edt.) (2001) Modern Tribology Handbook Volume One, Principles of Tribology, CRC Press, Boca Raton, ISBN 0-8493-8403-6.

Carter F.W. (1926) On the action of a locomotive driving wheel. Proc. R. Soc. A 1125, pp. 151-157.

Casini C. and Tacci G. (1996) The geometrical construction of the FS DR wheel profile, Proceedings of the 2nd mini conference on Contact Mechanics and Wear of Rail/Wheel Systems, Budapest, Hungary, 29-31 July, 1996, pp. 235-242, ISBN 963-420-509-7.

Chelli F., Corradi R., Diana G., Facchinetti A. (2003) Wheel–rail contact phenomena and derailment conditions in light urban vehicles. Proceedings of the 6th International Conference On Contact Mechanics and Wear of Rail/Wheel Systems. Gothenburg, Sweden, June 10-13, 2003, pp. 461-468.

Cooperrider N.K., Law E.H., Hull R., Kadala P.S. and Tutaqn J.M. (1976) Analytical and Experimental Determination of Nonlinear Wheel/Rail Constraints, Proceedings ASME Symposium on Railroad Equipment Dynamics, April 1976.

Dang Van K., Cailletaud G., Flavenot J.F., Le Douaron A., Lieurade H.P., Criterion for High Cycle Fatigue Failure under Multiaxial Loading, in Brown M.W., Miller K.J., Editors, Biaxial And Multiaxial Fatigue, Mechanical Engineering Publications, London, 1989, pp. 459–478.

Dendy Marshall C. F. (1938) A History of British Railways down to the Year 1830, Oxford University Press, London, pp. 147 – 148, 1938.

Duffek W. (1982) Contact geometry in wheel rail vehicles. Proceedings International Symposium on Contact Mechanics and Wear of Rail/Wheel Systems, Vancouver, Canada, July 6-9, 1982, pp 161-181. ISBN 88898-043-4.

Dukkipati R.V. (2000), Vehicle Dynamics, Boca Raton: CRC Press, 2000, ISBN 0-8493-0976-X.

Ekberg A., Marais J., (1999) Effects Of Imperfections on Fatigue Initiation in Railway Wheels, Proceedings of the IMechE Part F, Journal of Rail and Rapid Transit, Vol. 214, 1999, pp. 45–54.

Ekberg A., Sotkovszki P. (2001) Anisotropy and Fatigue of Railway Wheels, International Journal Of Fatigue, Vol. 23, No. 1, 2001, pp. 29–43.

Ekberg A., Kabo E., Andersson H., (2002) An engineering model for prediction of rolling contact fatigue of railway wheels, Fatigue and Fracture of Engineering Materials and Structures, 2002, vol. 25 (10), pp. 899-909.

Elkins J.A. (1991) Prediction of wheel/rail interaction: The state of the art. In Sauvage, G. (Ed.), The Dynamics of Vehicles on Roads and on Tracks, Proc. 12th IAVSD Symposium, Lyon, France, August 1991, Vehicle System Dynamics, Supplement to Vol. 20, 1-27, Swets & Zeitlinger, Amsterdam/Lisse, 1992.

Enbolm R. and Berg M. (2005) Emerging Engineering Models for Wheel/Rail Wear Simulation, Proceedings of Railway Engineering, 2005.

Esping B.J.D. (1985) A CAD Approach to the Minimum Weight Design Problem, International Journal of Numerical Methods in Engineering, 1985, vol. 21, pp. 1049-1066.

Esveld C. (2001) Modern Railway Track, (Second Edition), Zaltbommel: MRT-Productions, 2001, ISBN 90-8004-324-3-3.

Esveld C., Markine V.L., Shevtsov I.Y. (2003) Optimization of Wheel Profile of a Tram for HTM (in assignment of HTM, The Hague), Report 7-03-220-3, ISSN 0169-9288, December 2003.

Esveld C., Markine V.L., Shevtsov I.Y. (2005) Optimization of Wheel Profile of a Tram for HTM (second stage) (in assignment of HTM, The Hague), Report 7-05-220-9, ISSN 0169-9288, January 2005.

Esveld C., Markine V.L., Shevtsov I.Y. (2006) Shape optimization of a railway wheel profile, European Railway Review, vol. 12 (2), 2006, pp. 81-86, ISSN 1351-1599.

Evans J., Iwnicki S. (2002) Vehicle Dynamics and the Wheel/Rail Interface, Wheels on Rails – An update, Understanding and managing the Wheel/Rail Interface, The Institution of Mechanical Engineers Seminar, London, April 2002.

Gilchrist A.O., Brickle B.V. (1976) A re-examination of the proneness to derailment of a railway wheelset, J. Mech. Eng. Sci., vol. 18, 1976, pp. 131–141.

Gilchrist A.O. (1998), The long road to solution of the railway hunting and curving problems, Proc. Instn. Mech. Engrs., 212 (Part F), 1998, pp. 219–226.

Grohmann H.-D., Schoech W., (2002) Contact geometry and surface fatigue—minimizing the risk of headcheck formation, Wear 253, Issue 1-2, 2002, Elsevier, pp 54-59.

Harris W., Eberson W., Lundgren J., Tourney H., Zakharov S., (2001) Guidelines to Best Practices for Heavy Haul Operations: Wheel and Rail Interface Issues, IHHA, Virginia Beach, USA, 2001, 508 p.

Heumann H. (1950) Grundzege der Fehrung der Schienenfahrzeuge, Elektrische Bahnen 21. Jahrg., Heft 4,5,7,11,12 1950.

Ishida M. and Abe N. (1997) Experimental Study on the Effect of Preventive Grinding for Shinkansen Rails, in Proc. 6th Int. Heavy Haul Conf., Cape Town, pp. 565-575.

Iwnicki S. (ed.) (1999) The Manchester Benchmarks for Rail Vehicle Simulation, Volume 31 of Supplement to Vehicle System Dynamics. Swets & Zeitlinger, Lisse, 1999.

Iwnicki S. (ed.), (2006) Handbook of railway vehicle dynamics, CRC Press, Taylor & Francis Group, 2006, ISBN-13: 978-0-8493-3321-7.

Jendel T. (2000) Prediction of wheel profile wear – methodology and verification. Licentiate thesis, Royal Institute of Technology, ISRN KTH/FKT/L-00/49-SE, Stockholm 2000, ISSN 1103-470X.

Jendel T. (2002) Prediction of wheel profile wear—comparisons with field measurements, Wear, Volume 253, Issues 1-2, 2002, pp. 89-99.

Johnson K.L. (1958a) The effect of spin upon the rolling motion of an elastic sphere upon a plane. Journal of Applied Mechanics 25, pp. 332-338.

Johnson K.L. (1958b) The effect of a tangential force upon the rolling motion of an elastic sphere upon a plane. Journal of Applied Mechanics 25, pp. 339-346.

Johnson K.L. (1985) Contact Mechanics, Cambridge University Press.

Johnson K.L. (1989) The Strength of Surfaces in Rolling Contact, Proceedings of the Institution of Mechanical Engineers, Vol. 203, 1989, pp. 151–163.

Kabo E., Ekberg A. (2002a) Fatigue Initiation in Railway Wheels – A Numerical Study of the Influenece of Defects, Wear, Vol. 253, No. 1-2, 2002, pp. 26-34.

Kabo E. (2002b) Material Defects in Rolling Contact Fatigue – Influence of Overloads and Defect Clusters, International Journal of Fatigue, Vol. 24, No. 8, 2002, pp. 887-894.

Kalker J.J. (1967) On the rolling contact of two elastic bodies in the presence of dry friction, Thesis, Delft.

Kalker J.J. (1979) Survey of wheel-rail rolling contact theory, Vehicle System Dynamics, Vol. 8, No. 4, pp.317–358.

Kalker J.J. (1982) A fast algorithm for the simplified theory of rolling contact, Vehicle System Dynamics, 11 (1982), pp. 1-13.

Kalker J.J. (1983) A simplified theory for non-Hertzian contact, Proc. 8th IAVSD Symposium The Dynamics of Vehicles on Roads and Tracks, Cambridge, Mass., August 1983, pp. 295-302, Swets and Zeitlinger Publishers, Lisse, 1984.

Kalker J.J. (1990) Three-Dimensional Elastic Bodies in Rolling Contact, Dordrecht: Kluwer Academic Publishers, 1990, ISBN 0-7923-0712-7.

Kalousek J.J. (2002) Keynote address: light to heavy, snail to rocket, Wear 253, Issue 1-2, 2002, Elsevier, pp. 1-8.

Kalousek J., Sroba P., and Hegelund C. (1989), Analysis of rail grinding tests and implication for corrective and preventive grinding, in Proc. 4th Int. Heavy Haul Conf., Brisbane, pp. 193-204.

Kik W., Knothe K. and Steinborn H. (1981) Theory and Numerical Results of a General Quasi-Static Curving Algorithm. In: A. Wickens (ed.): Proc. 7th IAVSD Symp. on The Dynamics of Vehicles on Roads and on Tracks, Cambridge, 1981, pp. 427-440.

Kik W. and Steinborn H. (1983) Wheel/Rail Connection Element for use in a Multi-Body Algorithm. In: J.K. Hedrick (ed.): Proc. 8th IAVSD Symp. on The Dynamics of Vehicles on Roads and on Tracks, Cambridge Mass, 1983, pp. 303-316.

Kik W. and Piotrowski J.P. (1996) A Fast, Approximate Method to Calculate Normal Load at Contact between Wheel and Rail and Creep Forces During Rolling, Proc. of 2nd Mini Conf. on Contact Mechanics and Wear of Rail/Wheel Systems. Ed. I. Zabory, TU Budapest, 1996.

Knothe K. L. and Grassie S. L. (1993) Modeling of railway track and vehicle/track interaction at high frequencies, Vehicle System Dynamics, vol. 22, 1993, pp. 209–262.

Knothe K., Bohm F. (1999) History of stability of railway and road vehicles. Vehicle System Dynamics, vol. 31, 1999, pp. 283–323.

Knothe K., Wille R. and Zastrau B.W. (2001) Advanced contact mechanics – road and rail. Vehicle System Dynamics, vol. 35, No 4–5, 2001, pp. 361–407.

Leary J.F., Handal S.N. and Rajkumar B. (1991) Development of freight car wheel profiles – a case study, Proceedings of the Third International Conference on Contact Mechanics and Wear of Rail/Wheel Systems, Cambridge, U.K., July 22-26, 1990, ISBN 0444-88774-1 also in Wear, vol. 144, 1991, pp 353-362.

Lewis R., Braghin F., Ward A., Bruni S., Dwyer-Joyce R.S., Bel Khani K., Bologna P., (2003) Integrating dynamics and wear modelling to predict railway wheel profile evolution, Proceedings of the 6th International Conference on Contact Mechanics and Wear of Rail/Wheel Systems (CM2003), Gothenburg, Sweden, June 10-13, 2003, pp 7-16, ISBN 91-631-3928-6.

Lewis R., Dwyer-Joyce R.S., Bruni S., Ekberg A., Cavalletti M., Bel Knani K., (2004 a) A New CAE Procedure for Railway Wheel Tribological Design, 14th International Wheelset Congress, 2004, 17-21 October, Orlando, USA

Lewis R., Dwyer-Joyce R.S., Olofsson U., Hallam R.I., (2004 b) Wheel Material Wear Mechanisms and Transitions, 14th International Wheelset Congress, 2004, 17-21 October, Orlando, USA.

Li Z., Kalker,J.J., Wiersma P.K., Snijders E.R., (1998) Non-Hertzian wheel-rail wear simulation in vehicle dynamical systems, Proceedings of 4th International Conference on Railway Bogies and Running Gears, Budapest, 21-23 September, 1998, pp. 187-196.

Li Z., (2002) Wheel-rail rolling contact and its application to wear simulation. Delft. DUP Science. ISBN 90-407-2281-1.

Magel E.E., (1999) Optimizing wheel, rail profiles, Railway track and structures, July 1999.

Magel E.E., Kalousek J., (2002) The application of contact mechanics to rail profile design and rail grinding, Wear 253, Issue 1-2, 2002, Elsevier, pp 308-316.

Magel, E., Roney, M., Kalousek, J., and Sroba, P., (2003) The blending of theory and practise in modern rail grinding, Fatigue Fract. Eng. Mater. and Struct., 2003, 26(10), pp. 921–929.

Magel E.E., Kalousek J., (2004) The Influence of Creep Forces on Rolling Contact Fatigue of Wheels, 14th International Wheelset Congress, 2004, 17-21 October, Orlando, USA.

Manchester benchmarks for rail vehicle simulation, Iwnicki S. (ed.), Vehicle System Dynamics, 30, 1998, pp. 295-313.

Markine V.L. (1999) Optimization of the Dynamic Behaviour of Mechanical Systems, PhD Thesis, TU Delft: Shaker Publishing BV, 1999, ISBN 90-423-0069-8.

Markine V.L. and Toropov V.V. (2002) Use of High- and Low-Fidelity Models In Approximations for Design Optimization. Proceedings of the 9th AIAA/USAF/NASA/ISSMO Symposium on Multidisciplinary Analysis and Optimization, Atlanta, Georgia,USA, 4th–6th September 2002 (CD Proceedings). AIAA Paper 2002-5651.

Markine V.L., Shevtsov I.Y., Esveld C. (2003) Optimalisatie Wielbandprofiel Bombardier Metrorijtuigen Beneluxlijn (in opdracht van RET), Report 7-03-220-2 ISSN 0169-9288, September 2003.

Markine V.L., Shevtsov I.Y., Esveld C., Markina M.V. (2004a), OPTIMISATION OF RAILWAY WHEEL PROFILE, 5th ASMO UK / ISSMO conference on Engineering Design Optimization, The Falcon Hotel, Stratford upon Avon, UK, July 12 –13, 2004.

Markine V.L., Shevtsov I.Y., Esveld C. (2004b) Shape Optimisation of Railway Wheel Profile. Proceedings of 21st International Congress of Theoretical and Applied Mechanics. August 15-21, 2004, Warsaw, Poland. (On CD-ROM) ISBN 83-89697-01-1.

Markine V.L., Shevtsov I.Y., Esveld C. (2006) (online) An Inverse Shape Design Method for Railway Wheel Profiles. Structural and Multidisciplinary Optimization, Vol. 33, no. 3, pp. 243-253, 2007, Springer Berlin / Heidelberg. ISSN 1615-147X (Print) 1615-1488 (Online) (online first http://www.springerlink.com/content/mq71704071h7471r/).

McEwen I. J. and Harvey R. F. (1986), Interpretation of Wheel/Rail Wear Numbers, TM VDY 004, July 1986, BR Research, Derby.

Nadal M. J. (1908), Locomotives a Vapeur, Collection Encyclopédie Scientifique, Bibliothèque de Mécanique Applique´ et Génie, Paris, 1908.

Newland D. E., Steering characteristics of bogies, Railway Gazette, 124 (19), 745–750, 1968.

Nikravesh P.E. (1988) Computer-Aided Analysis of Mechanical Systems (Englewood-Cliffs, New Jersey: Prentice-Hall).

Novales M., Orro A., Bugarín M.R. (2006) A New Approach for the Design of Wheel Profile Geometries, Proceedings of 7th World Congress on Railway Research, Montreal, Canada, June 4-8, 2006 (CD Proceedings).

Pater A.D. de (1962) On the reciprocial pressure Between two bodies, Proccedings of the Symposium Rolling Contact Phenomena, Ed.J.B. Bidwell, Elsevier, 1962, pp. 29-75.

Pater A.D. de (1988) The Geometrical Contact Between Track and Wheelset, Vehicle System Dynamics, vol. 1, 1988, pp. 127-140.

Pater A.D. de (1995a) The Motion of a Single Wheelset Along a Curved Track. Delft University of Technology, Laboratory for Engineering Mechanics, Report No. 1072, 1995, 145 pp.

Pater A.D. de (1995b) The Motion of a Single Wheelset Along a Tangent Track for Single and Double Point Contact. Delft University of Technology, Laboratory for Engineering Mechanics, Report No. 1096, 1995.

Pater A.D. de (1997) The equations of motion of a simplified railway vehicle moving along a curved track and the simulation of an uneven tangent railway track by means of a roller rig, Delft University of Technology, Laboratory for Engineering Mechanics, Report No. 1158, 109 pp.

Pater A.D. de (1999) The motion of a multi-axial railway vehicle along a curved track, Delft University of Technology, Laboratory for Engineering Mechanics, Report No. 1187, 63 pp.

Pearce T.G., Sherratt N.D., (1990) Prediction of wheel profile wear, Proceedings of the Third International Conference on Contact Mechanics and Wear of Rail/Wheel Systems, Cambridge, U.K., July 22-26, 1990, ISBN 0444-88774-1, also in Wear, Volume 144, 1991, pp. 343-351.

Persson I. and Iwnicki S.D. (2004) Optimisation of railway profiles using a genetic algorithm, Vehicle System Dynamics, Supplement to vol. 41, 2004, pp. 517-527. ISBN 90-265-1972-9.

Petzold L. (1994), Computational challenges in mechanical systems simulation. In: M. Pereira and J. Ambrósio (Eds.), Computer-Aided Analysis of Rigid and Flexible Mechanical Systems (Dordrecht, The Netherlands: Kluwer Academic Publishers), 1994, pp. 483–499.

Polach O. (1992) Solution of wheel–rail contact forces suitable for calculation of rail vehicle dynamics, in: Proceedings of the Second Int. Conference on Railway Bogies, Budapest, September 14–16, 1992, pp. 10–17.

Polach O. (1999) A fast wheel-rail forces calculation computer code, Proc. of the 16th IAVSD Symposium, Pretoria, August 1999, Vehicle System Dynamics Supplement, 33, 1999, pp. 728-739.

Polach O. (2006) On non-linear methods of bogie stability assessment using computer simulations, Proc. IMechE Vol. 220 Part F: J. Rail and Rapid Transit, 2006, pp. 13-27.

Rocard Y. (1935) La stabilité de route des locomotives, première partie, aÕec une note de M. R. Lévy. Hermann & Cie., Paris, 1935.

Sato Y. (1990) Design of rail head profiles with full use of grinding, Proceedings of the Third International Conference on Contact Mechanics and Wear of Rail/Wheel Systems, Cambridge, U.K., July 22-26, 1990, ISBN 0444-88774-1 also in Wear, Volume 144, 1991, pp 363-372.

Sato Y. (1996) Benefits of heavy rail on high-speed railways and design of 75G rail using coordinates, Wear, Volume 194, 1996, pp 163-167.

Sato Y. (2005) Historical study on designing Japanese rail profiles, Wear, vol. 258, 2005, pp. 1064-1070.

Sawley K. and Wu H. (2005) The formation of hollow-worn wheels and their effect on wheel/rail interaction, Proceedings of the 6th International Conference on Contact Mechanics

and Wear of Rail/Wheel Systems. Gothenburg, Sweden, June 10-13, 2003, pp. 469-477, also in Wear, vol. 258, 2005, pp. 1179-1186.

Schoech W. and Heyder R. (2003) Rail surface fatigue and grinding: exploring the interaction, Proceedings of the 6th International Conference on Contact Mechanics and Wear of Rail/Wheel Systems(CM2003), Gothenburg, Sweden, June 10-13, 2003, pp 133-138, ISBN 91-631-3928-6.

Schoech W., Heyder R.., Grohmann H.-D. (2006) Contact Geometry and Surface Fatigue – Guidelines for Appropriate Rail Maintenance, Proceedings of 7th International Conference on Contact Mechanics and Wear of Rail/Wheel Systems (CM2006), Brisbane, Australia, September 24-26, 2006, pp. 23-29, ISBN 1 876855 27 4.

Schupp G., Weidemann C., Mauer L., (2004) Modelling the contact between wheel and rail within multibody system simulation, Vehicle System Dynamics, Vol. 41, No. 5, 2004, pp. 349–364.

Seireg A.A., Rodriguez J. (1997) Optimizing the shape of mechanical elements and structures, Marcel Dekker, INC., USA, 1997, ISBN 0-8247-9555-5.

Seydel R. (1988) From Equilibrium to Chaos. Elsevier, 1988, 11+367 pp. (ISBN 0-444-1250-8).

Shen Z.Y., Hedrick J.K., Elkins J.A. (1983) A comparison of alternative creep force models for rail vehicle dynamic analysis, Proc. of the 8th IAVSD Symposium. Cambridge, MA, August 15-19, 1983, pp. 591-605.

Shen G., Ayasse J.B., Choller H., Pratt I. (2003) A unique design method for wheel profiles by considering the contact angle function, Proceedings of the Institution of Mechanical Engineers, Part F: Journal of Rail and Rapid Transit, vol. 217, 2003, pp. 25-30.

Shevtsov I.Y., Markine V.L., Esveld C. (2002a) One procedure for optimal design of wheel profile, Proceedings of the IQPC conference on Achieving Best Practice in Wheel/Rail Interface Management, Amsterdam, The Netherlands, January 31-February 1, 2002.

Shevtsov I.Y., Markine V.L., Esveld C. (2002b) Optimization of Railway Wheel Profile Using Mars Method. Proceedings of the 43rd AIAA/ASME/ASCE/AHS/ASC/ Structures, Structural Dynamics, and Material Conference, Denver, Colorado, USA, 22-25 April 2002. Paper AIAA 2002-732. ISBN 1-56347-560-X (On CD-ROM).

Shevtsov I.Y., Markine V.L., Esveld C. (2003) Optimal design of wheel profile for railway vehicles, Proceedings 6th International Conference on Contact Mechanics and Wear of Rail/Wheel Systems, Gothenburg, Sweden, June 10-13, 2003, pp. 231-236, ISBN 91-631-3928-6.

Shevtsov I.Y., Markine V.L., Esveld C. (2005) Optimal design of wheel profile for railway vehicles. Wear, vol. 258, 2005, pp. 1022–1030. ISSN 0043-1648.

Shevtsov I.Y., Markine V.L., Li Z., Esveld C. (2006) Design of railway wheel profile taking into account rolling contact fatigue and wear, Proceedings of 7th International Conference on Contact Mechanics and Wear of Rail/Wheel Systems (CM2006), Brisbane, Australia, September 24-26, 2006, pp. 667-674, ISBN 1 876855 27 4.

Shevtsov I.Y., Markine V.L., Esveld C. (2008) Design of railway wheel profile taking into account rolling contact fatigue and wear. Accepted for publication in Wear.

Smallwood R., Sinclair J. C. and Sawley K. J., (1990) An optimization technique to minimize rail contact stresses, Proceedings of the Third International Conference on Contact Mechanics

and Wear of Rail/Wheel Systems, Cambridge, U.K., July 22-26, 1990, ISBN 0444-88774-1 also in Wear, Volume 144, 1991, pp. 373-384.

Smith R.E., Kalousek J. (1991) A design methodology for wheel and rail profiles for use on steered railway vehicles, Proceedings of the Third International Conference on Contact Mechanics and Wear of Rail/Wheel Systems, Cambridge, U.K., July 22-26, 1990, ISBN 0444-88774-1 also in Wear, Vol. 144, 1991, pp. 329-342.

Smulders J. (2003) Management and rolling contact fatigue, Railway Gazette, July 2003.

Smulders J., Bontekoe T., Jong E. de, Hiensch M., Watson A. (2003) Management and research of rolling contact fatigue in the Netherlands, Proceedings of World Congress on Railway Research 2003, Edinburgh, Scotland, 2003.

Toropov V.V. (1989) Simulation Approach to Structural Optimization, Structural Optimization, vol. 1, 1989, pp. 37-46.

Toropov V.V., Filatov A.A. and Polynkin A.A. (1993) Multiparameter structural optimization using FEM and multipoint explicit approximations. Structural Optimization, vol. 6, 1993, pp. 7-14

Toropov V.V. and Markine V.L. (1996) The Use of Simplified Numerical Models as Mid-Range Approximations, Proceedings of the 6-th AIAA/USAF/NASA/ISSMO Symposium on Multidisciplinary Analysis and Optimization, Part 2, Bellevue WA, September 4-6, 1996, pp. 952-958, ISBN 1-56347-218-X.

Toropov V.V., Keulen F. van, Markine V.L., Alvarez L.F. (1999) Multipoint Approximations Based on Response Surface Fitting: a Summary of Recent Developments. In V.V. Toropov (Ed.) Proceedings of the 1st ASMO UK/ISSMO Conference on Engineering Design Optimization, Ilkley, West Yorkshire, UK, July 8-9, 1999, pp. 371-381. ISBN 0-86176-650-4.

True H. (1999) On the theory of nonlinear dynamics and its application in vehicle systems dynamics. Vehicle System Dynamics, 1999, vol. 31, pp. 393–421.

Tunna J., Sinclair J., Perez J. (2006) A Review of Wheel Wear and Rolling Contact Fatigue, Rail Safety & Standards Board, UK.

UIC Code 513: Guidelines for Evaluating Passenger Comfort in Relation to Vibration in Railway Vehicles, 1st ed., 1.7. 1994, International Union of Railways, Paris 1995.

UIC Code 518: Testing and Approval of Railway Vehicles from the Point of View of their Dynamic Behaviour – Safety – Track Fatigue – Ride Quality, International Union of Railways, 3rd ed., Paris, October 2005.

Ushkalov V.F. et al. (1998) STCU report.

Ushkalov V.F. (1999) Effect of the wheel profile on dynamics of rail vehicle and wear of the wheel/rail contact pair, in: Proceeding of IHHA'99 Conference, vol. 1, 1999.

Ushkalov V.F. and Zhechev M.M. (2002) Dynamic Analysis of the Bolster-Wedges-Sideframes Subsystem of a Truck, International Applied Mechanics, 2002, vol. 38, no. 11, pp. 1407-1413.

Vermeulen P.J., Johnson K.L. (1964) Contact of non spherical bodies transmitting tangential forces, Journal of Applied Mechanics, Vol. 31, 1964, pp. 338-340.

Wang K.W. (1984) The computation of wheel-rail contact locus and wheel-rail contact geometrical parameters (in Chinese), Journal of Southwest Jiaotong University, 1984, vol. 1, pp. 89-98.

Wang S., Sun Y. and Gallagher R.H., (1985) Sensitivity Analysis in Shape Optimization of Continuum Structures, Computers and Structures, 1985, vol. 20, no. 5, pp. 855-867.

Wickens A.H. (1965a), The Dynamic Stability of Railway Vehicle Wheelsets and Bogies Having Profiled Wheels, International Journal of Solids and Structures, vol. 1, issue 3, 1965, pp. 319-341.

Wickens A.H. (1965b), The Dynamic Stability of a Simplified Four-Wheeled Railway Vehicle Having Profiled Wheels, International Journal of Solids and Structures, vol. 1, issue 4, 1965, pp. 385-406.

Wickens A.H. (1998), The dynamics of railway vehicle — From Stephenson to Carter, Proc. Instn. Mech. Engrs., 212 (Part F), 209–217, 1998.

Wickens A.H. (2003), Fundamentals of Rail Vehicle Dynamics, Swets and Zeitlinger, 2003, ISBN 902651946X.

Wiersma P.K. (2000), Optimalisatie wielprofiel HTM (Optimisation of wheel profile HTM), NS Technisch Onderzoek, June 9, 2000.

Wu H., Shu X., Wilson N. (2005), TCRP Report 71, Track-Related Research Volume 5: Flange Climb Derailment Criteria and Wheel/Rail Profile Management and Maintenance Guidelines for Transit Operations, Transportation Technology Center Inc. (TTCI), Pueblo, Colorado, USA, ISBN 0-309-08830-5.

Yang G. (1993), Dynamic analysis of railway wheelsets and complete vehicle systems, Ph. D. Thesis, Delft University of Technology, 1993, 6 + 156 pp. ISBN 90-370-0080-0.

Zakharov S., Komarovsky I., Zharov I. (1998) Wheel flange / rail head wear simulation, Wear, Volume 215, 1998, pp. 18-24.

Zakharov S., Zharov I. (2000) Simulation of mutual wheel/rail wear, Proceedings of the 5th International Conference On Contact Mechanics And Wear Of Rail/Wheel Systems. Tokyo, Japan, 2000, pp. 125-130, also in Wear, Volume 253, Issues 1-2, 2002, pp 100-106.

Zakharov S.M., Goryacheva I.G. (2003) Rolling contact fatigue defects in freight car wheels , Proceedings 6th International Conference on Contact Mechanics and Wear of Rail/Wheel Systems, Gothenburg, Sweden, June 10-13, 2003: 231-236, also in Wear, vol. 258, 2005, pp. 1142-1147. ISSN 0043-1648.

Zakharov S., Bogdanov V., Goryachea I., Pogorelov D., Zharov I., Yasikov V., Torskaya E., Soshenkov S. (2006) Problems of Wheel and Rail Profiles Selection and Optimization, Proceedings of 7th International Conference on Contact Mechanics and Wear of Rail/Wheel Systems (CM2006), Brisbane, Australia, September 24-26, 2006, pp. 697-703, ISBN 1 876855 27 4.

Summary

"Wheel/Rail Interface Optimisation"

by I.Y. Shevtsov

Railway transport is the most cost effective method for moving passengers and freight between two locations connected by land. Steel on steel contact between wheel and rail produces low energy loss during motion while bearing large loads. In recent years, the problem of wheel/rail contact has become very important in railway transport. Increased axle load in heavy-haul freight cars, the presence of tight curves and light vehicles in tram and fast transit systems, and the high speeds of vehicles on high-speed lines, produces different wheel/rail interface requirements. But these differing requirements aim for the same goals – extension of durability, reduction of maintenance costs, and increased safety. To solve such complex problems, a combination of knowledge from different areas of the mechanical, mathematical and physical sciences is required.

In this thesis, wheel/rail interface optimisation, and particularly the problems of wheel and rail profile design are considered. The research task pursued by this thesis engenders investigation of a range of problems. First, geometric properties of contact between wheel and rail are investigated. Then, physical properties of rolling contact between wheel and rail are studied with the help of contact mechanics. Railway vehicle dynamics are then considered using ADAMS/Rail multibody dynamic simulation software. Finally, a numerical optimisation method is used for the design of the wheel profile. All these disciplines are combined in one wheel (rail) profile design procedure.

The wheel (rail) profile design procedure is developed with the idea that the rolling radius difference (RRD) function, to a large extent, describes the wheel/rail contact properties. Therefore, for a known optimal RRD function, a wheel profile that delivers the required contact properties defined by this RRD can be determined. Wheel profile design procedure comprises a number of steps. First, data are collected about wheelset and track geometric parameters, and type of railway system (tram, metro, train). Analysis of existing (new and worn) wheel/rail profiles, and their contact properties, is of vital importance as well. In the next step, the contact properties (RRD curve) for various wheel and rail combinations are analysed. After analysis of initial data from this procedure, the designer must determine constraints applied on wheel profile and create a target (optimal) RRD function. Wheel and rail profile measurements are used to analyse wheelset contact properties in order to design the target RRD function. Then, the problem of finding a wheel profile corresponding to the target RRD function is formulated as an optimisation problem. The problem is solved using the Multipoint Approximations based on the Response Surface fitting (MARS) optimisation method.

The result of the optimisation is then considered as the designed wheel profile. Since the dynamic behaviour of a vehicle is not directly controlled during the optimisation process, which serves to reduce the computational efforts of the optimisation, this behaviour is verified afterwards. During such verification, the designed wheel profile is tested for stability, wear, and dynamic contact stresses using the ADAMS/Rail computer package. If the dynamic performance of a vehicle with the obtained wheel profile does not satisfy the imposed requirements, the RRD function and/or constraints should be modified and the optimisation should be performed again. This process must be repeated iteratively until all requirements

have been satisfied. Finally, the obtained wheel profile is considered the optimum profile. This procedure is applied to various real-world wheel/rail interface optimisation problems.

In this research, three railway system types are considered – tram, metro, and conventional railway. Tram systems are characterised by the presence of many sharp curves, and comparatively low vehicle speed. Flange wear is the biggest concern of tram operators. Metro lines are characterised by larger radius curves and higher operating speeds in comparison with tram systems. Therefore, together with wear of the wheel profile, a problem of vehicle stability arises. Conventional railways are characterised by high speeds and large radius curves. Consequently, wear and the stability of vehicles have always been of great concern for railway engineers. However, with the development of new types of rolling stock and the introduction of curvilinear profiles, new problems arose. Recently, Rolling Contact Fatigue (RCF) has become the greatest problem for the railways. In summary, these three railway systems have different requirements with respect to wheel/rail contact, and require different wheel design solutions.

The trams of the Haagsche Tramweg Maatschappij N.V. company (HTM, The Hague, The Netherlands) suffered from high wear of the wheel flanges. This problem was solved by a new wheel profile design. The wear rate has been reduced by modification of the flange and flange root parts of the wheel profile, which has resulted in better distribution of contact points along the wheel and rail profiles.

The metro trains of the Rotterdamse Electrische Tram N.V. company (RET, Rotterdam, The Netherlands) had problems with excessive tread wear and, consequently, wheelset oscillation. Using the design procedure described in this thesis, a new wheel profile is obtained and applied to the RET metro trains. Results from dynamic simulation and field tests show that the performance of metro vehicles was significantly ameliorated by improving the contact properties of wheel and rail. Due to application of an optimised wheel profile, the instability of the metro trains has been eliminated, and the lifetime of the wheels has increased from 25,000 km to 120,000 km.

The rails of the large radius curves on the Dutch railway (Nederlandse Spoorwegen, NS) network are prone to RCF problems on the gauge root part of the outer rail in curves. An optimised wheel profile is obtained for an NS passenger coach. Results from dynamic simulation show a small increase in the wear index, and reduction in surface fatigue index for the designed wheel profile. Using the optimised wheel profile, RCF damage observed for the existing wheel/rail combination can been reduced.

Using the developed design procedure, new wheel profiles are designed for each above mentioned case, solving for, respectively, the problems of flange wear, stability (as a result of excessive tread wear), and RCF. In the first two cases, wheel profiles were successfully implemented on the respective networks.

There are several possibilities for effectively using the described design procedure:

- Obtaining wheel profiles for a new rail profile (e.g., upgrade of rail type due to track renewal), when previous wheel/rail profile combination was satisfactory. The RRD function of the previous wheel/rail couple must be used as the target RRD function. In this way, the new combination of wheel/rail profiles will have the same contact conditions as the previous one.
- When existing wheel and rail profiles mismatch each other, as clearly seen from their geometric wheel/rail contact. In this case, RRD function must be modified to remove unwanted contact behaviour thus improving wheel/rail contact.

- When current wheel/rail behaviour must be changed for new conditions, for example, vehicle must be used on a track with another rail inclination, operational speed must be increased, or sharper curves are introduced. In this case, current RRD function can be modified to satisfy new conditions, and consequently new wheel profiles can be designed.

Successful application of the design procedure to real-life problems has proven its usability and expediency. The procedure is flexible, and different requirements can be combined to obtain an optimal wheel profile. In future, with the appearance of new problems in wheel/rail contact, the design procedure could be easily extended to include new requirements for wheel/rail interface.

Samenvatting (Summary in Dutch)

"Wiel/Rail Interface Optimalisatie"

door I.Y. Shevtsov

Het spoorwegvervoer is één van de meest kosteffectieve methoden voor landgebonden transport van passagiers en goederen. Staal op staal contact tussen de wiel en rail zorgt voor laag energieverlies tijdens de voortbeweging van een voertuig waardoor relatief zwaarder ladingen vervoerd kunnen worden. In de afgelopen jaren zijn de problemen rond het wiel/rail contact aanzienlijk toegenomen. Hogere aslasten bij het goederen vervoer, krappe bogen in tram en 'light rail' systemen, alsmede de hoge snelheden op HSL lijnen stellen verschillende eisen aan de wiel/rail interface. Aan de andere kant streven de verschillende eisen naar dezelfde doelen, zoals verbeterde duurzaamheid, lagere onderhoudskosten en grotere veiligheid. Om zulke complexe problemen op te lossen is een combinatie van kennis van verschillende wetenschappen op het gebied van mechanica, wis- en natuurkunde vereist.

In dit proefschrift worden de problemen van optimalisatie van de wiel/rail interface beschouwd, toegespitst op de bepaling van het optimale ontwerp van wiel en rail profiel. Verschillende aspecten van de wiel-rail problematiek zijn binnen dit onderzoek aangepakt. In eerste instantie zijn de geometrische eigenschappen van het wiel-rail contact onderzocht. Fysische eigenschappen van wiel-rail contact werden met behulp van contact mechanica bestudeerd. De voertuigdynamica werd geanalyseerd met het pakket ADAMS/Rail, een multibody simulatiesoftware. Ten slotte werd een numerieke optimalisatie methode voor het ontwerp van het wielprofiel gebruikt. Al deze disciplines zijn geïntegreerd in de ontwerpprocedure optimale combinatie van wiel en rail profiel.

Deze ontwerpprocedure is ontwikkeld met als achtergrond dat het rolstraalverschil (rolling radius difference, RRD) grotendeels de eigenschappen van het wiel/rail interface bepaalt. Voor een gegeven (optimaal) RRD functie wordt geprobeerd een wielprofiel met de gewenste contacteigenschappen (bepaald door de gegeven RRD) te vinden. De die hier ontwikkelde ontwerpprocedure, bestaat uit een aantal stappen. Eerst worden de gegevens van het onderzochte voertuig-spoor systeem, zoals wielstel, spoorgeometrie enz. verzameld. De analyse van de bestaande (nieuwe en versleten) wiel/rail profielen is ook van groot belang. In de volgende stap worden de geometrische contacteigenschappen van verschillende wiel en rail combinaties geanalyseerd. Op basis van deze resultaten en eventuele systeemvoorwaarden kan de optimale (doel) rolstraalverschilfunctie berekend worden. Het bepalen van het wielprofiel dat voldoet aan deze rolstraalvershilfunctie wordt geformuleerd als een optimalisatie probleem. Om dit probleem op te lossen wordt gebruik gemaakt van een specifiek optimalisatie techniek (Multipoint Approximations based on the Response Surface fitting, MARS).

Omdat het dynamische gedrag van het voertuig met het ontworpen wielprofiel tijdens het optimalisatie proces niet wordt gecontroleerd (om de computerinspanningen van de optimalisatie te verminderen), wordt dit achteraf gedaan. In de voertuigdynamica analyse met ADAMS/Rail worden stabiliteit, wiel/rail slijtage en contactspanningen gecontroleerd. Indien het dynamische gedrag van het voertuig met het ontworpen wielprofiel niet voldoet aan de opgelegde eisen, moet de RRD functie worden aangepast en de optimalisatie opnieuw moeten worden verricht. Dit proces moet worden herhaald totdat het gevonden profiel aan alle eisen voldoet, en daarmee als het optimale profiel kan worden beschouwd.

Deze ontwerpprocedure is toegepast op drie verschillende spoorwegsystemen namelijk tram, metro en conventionele reizigerstrein. De kenmerken van tramsystemen zijn lage voertuigsnelheden en vele krappe bogen waardoor hoge slijtage aan de wielflenzen optreedt. Metrolijnen worden door wat grotere boogstralen en hogere voertuigsnelheden gekarakteriseerd. Daarom ontstaat bij metro's naast slijtage van het wielprofiel, een probleem met voertuigstabiliteit. Bij conventionele reizigerstreinen zijn snelheden en boogstralen nog groter, als gevolg waarvan wielslijtage en voertuigstabiliteit altijd een punt van zorg zijn geweest voor spoorwegingenieurs. In de laatste decennia hebben de ontwikkeling van nieuw typen railvoertuigen en de introductie van slijtageprofielen tot nieuwe problemen geleid. Rollende contact vermoeiing (Rolling Contact Fatigue, RCF) is thans wereldwijd een groot probleem voor de spoorwegen. Door de verschillende kenmerken worden verschillende eisen gesteld aan het wiel/rail contact in deze drie spoorwegsystemen. De optimale wielprofielen voor deze systemen verschillen dan ook.

De HTM (Haagsche Tramweg Maatschappij) had hoge slijtage van de wielflenzen. Door de wijziging van het wielprofiel, resulterend in betere distributie van contactpunten langs het wiel en railprofielen, werd de wielslijtage verminderd.

De RET metrotreinen (Rotterdamse Elektrische Tram) hadden grote problemen met loopvlakslijtage van de wielen waardoor instabiliteit (trillingen) van de wielstellen ontstond. Met behulp van de in dit proefschrift ontwikkelt procedure werd een nieuw wielprofiel ontworpen en toegepast. Resultaten van dynamische simulaties en praktijkproeven met het ontworpen wielprofiel hebben laten zien dat de prestatie van metrovoertuigen aanzienlijk konden worden verbeterd door de aanpassing van de wiel/rail contact interface. Als gevolg van het toepassen van het geoptimaliseerde wielprofiel kon de levensduur van de wielen worden vergroot van 25.000 km naar 120.000 km.

De bogen in het net van de Nederlandse Spoorwegen (NS) zijn gevoelig voor RCF problemen, welke doorgaans optreden aan de loopkant van de buitenste rail. Een geoptimaliseerd wielprofiel werd voor een NS passagiersvoertuig ontworpen. De resultaten van een numerieke simulatie met dit wielprofiel hebben laten zien dat de kans van RCF minder wordt (door vermindering van de vermoeiingsindex). Daarentegen bleek in de praktijk een kleine toename van de wielslijtage op te treden.

De ontwikkelde ontwerpprocedure werd voor alle drie systemen toegepast. In de eerste twee gevallen werden de geoptimaliseerde wielprofielen ook met succes in de praktijk geïmplementeerd.

Er zijn verschillende toepassingsmogelijkheden voor de beschreven ontwerpprocedure:

- Bepalen van een wielprofiel voor een nieuwe type rail profiel (bijvoorbeeld na aanpassing spoorstaafprofiel bij spoorvernieuwing), bij goede prestatie van de oude wiel/rail combinatie. De RRD functie van het vorige wiel/rail paar moet worden gebruikt als doelfunctie voor RRD. Op deze manier zal de nieuwe combinatie van wiel en rail profiel de zelfde contacteigenschappen hebben als de vorige.
- Wanneer bestaande wiel en rail profielen slecht combineren, op basis van hun geometrisch wiel/railcontact. In dit geval moet de RRD functie worden gewijzigd om ongewenst contactgedrag te vermijden dat dus het wiel/rail contact te verbeteren.
- Wanneer het huidige wiel/rail gedrag aan nieuwe voorwaarden moet worden aangepast, bijvoorbeeld wanneer een voertuig moet worden gebruikt op een spoor met een andere spoorstaafhelling, de rijsnelheid moet worden verhoogd of krappere bogen worden ingevoerd. In dit geval kan de huidig RRD functie worden gewijzigd om aan

de nieuwe voorwaarden te voldoen en bijgevolg nieuwe wielprofielen kunnen worden ontworpen.

De succesrijke toepassing van de ontwerpprocedure naar praktijkproblemen heeft zijn bruikbaarheid en geschiktheid bewezen. De procedure is flexibel en verschillende vereisten kunnen worden gecombineerd ter verkrijging van een optimaal wielprofiel. Wanneer in de toekomst zich nieuwe problemen aandienen in wiel/rail contact, kan de ontwerpprocedure gemakkelijk worden aangepast aan eventuele nieuwe eisen aan de wiel/rail interface.

Реферат (Summary in Russian)

“Оптимизация Взаимодействия Колеса и Рельса”

И.Е. Шевцов

Железнодорожный транспорт является одним из наиболее экономичных способов перевозки пассажиров и грузов по суше. Контакт сталь по стали между колесом и рельсом приводит к низкой потери энергии во время движения, в тоже время выдерживает большие нагрузки. В последние годы проблема контакта колеса и рельса стала очень важной для железнодорожного транспорта. Увеличение осевых нагрузок у тяжеловесных грузовых вагонов, наличие кривых малого радиуса и легких транспортных средств у трамваев и скоростных систем перевозок, а так же высокие скорости транспортных средств на высокоскоростных линиях, накладывают различные требования к взаимодействию колеса и рельса. Но эти отличающиеся требования преследуют одни и те же цели - увеличение долговечности, сокращение затрат на обслуживание и увеличение безопасности. Чтобы решить такие сложные проблемы, требуется комбинация знаний из различных областей механических, математических и физических наук.

В этой диссертации рассматриваются проблемы оптимизации взаимодействия колеса и рельса, и в особенности проблемы дизайна профилей колеса и рельса. Исследовательская задача, рассматриваемая в этой диссертации, определяет диапазон изученных проблем. Вначале, были исследованы геометрические свойства контакта между колесом и рельсом. Далее, с помощью контактной механики изучены физические свойства контакта между катящимся колесом и рельсом. Динамика железнодорожного транспортного средства рассматривается с помощью программного пакета ADAMS/Rail для динамического моделирования многомассовых систем. Кроме того, для создания профиля колеса используется числовой метод оптимизации. Все эти дисциплины объединены в одну процедуру дизайна профиля колеса (рельса).

Процедура дизайна профиля колеса (рельса) основана на идее, что функция разницы радиусов качения (РРК) в большой степени описывает свойства контакта колеса/рельса. Поэтому, для известной оптимальной функции РРК, может быть найден профиль колеса, который обеспечивает требуемые свойства контакта, определенные этой РРК функцией. Процедура дизайна профиля колеса включает множество шагов. Сначала, собираются данные о колесной паре и требуемые геометрические параметры, а так же тип железнодорожной системы (трамвай, метро, поезд). Проводится обязательный анализ существующих (нового и изношенных) профилей колеса и рельса, и их свойства контакта. В следующем шаге процедуры, анализируются свойства контакта (функция РРК) для различных комбинаций профилей колеса и рельса. После анализа начальных данных из этой процедуры, дизайнер должен определить ограничения, наложенные на профиль колеса, и создать целевую (оптимальную) функцию РРК. Измерения профилей колеса и рельса используются при анализе свойств контакта колесной пары, чтобы спроектировать целевую функцию РРК. Далее, проблема нахождения профиля колеса, соответствующего целевой функции РРК, формулируется как проблема оптимизации. Проблема решается с использованием метода оптимизации Многоточечных Приближений, основанных на Поверхности Отклика (Multipoint Approximations based on the Response Surface fitting, MARS).

В результате оптимизации получается новый профиль колеса. Динамическое поведение транспортного средства непосредственно не проверяется во время процесса оптимизации, что уменьшает вычислительные затраты оптимизации. Поэтому, динамика экипажа проверяется после оптимизации. Во время такой проверки, разработанный профиль колеса проверяется на стабильность, износ и динамические напряжения контакта, используя программный пакет ADAMS/Rail. Если динамическое поведение транспортного средства с разработанным профилем колеса не удовлетворяет наложенным требованиям, функция РРК и/или ограничения должны быть изменены и оптимизация должна быть выполнена ещё раз. Этот процесс должен быть повторен до тех пор, пока все требования не будут удовлетворены. Полученный профиль колеса принимают как оптимальный профиль. Эта процедура была применена к различным реальным проблемам оптимизации взаимодействия колеса и рельса.

В этом исследовании, были рассмотрены три типа железнодорожных систем - трамвай, метро и обычная железная дорога. Трамвайная система характеризуется наличием большого количества крутых кривых, и сравнительно низкой скоростью транспортного средства. Износ гребней колес является самым большим беспокойством трамвайных компаний. Линии метро характеризуются большими радиусами кривых и более высокими скоростями движения по сравнению с трамвайными системами. Поэтому, вместе с износом профиля колеса, возникает проблема устойчивости транспортного средства. Обычные железные дороги характеризуются высокими скоростями и большими радиусами кривых. Закономерно, износ колес и рельсов, и устойчивость транспортных средств имели всегда большой приоритет для железнодорожных инженеров. Однако, с развитием новых типов подвижного состава и введения криволинейных профилей, возникли новые проблемы. С недавних пор, усталость в контакте качения (Rolling Contact Fatigue, RCF) стала самой большой проблемой для железных дорог. Обобщая, эти три железнодорожных системы имеют различные требования относительно контакта колеса и рельса, и требуют различных решений при дизайне профиля колеса.

Трамваи компании HTM (г. Гаага, Нидерланды) испытывали высокий износ гребней колеса. Эта проблема была решена с помощью нового дизайна профиля колеса. Износ был уменьшен с помощью модификации гребня и выкружки профиля колеса, что привело к лучшему распределению точек контакта на профиле рельса и колеса.

Поезда метро компании RET (г. Роттердам, Нидерланды) имели проблемы с чрезмерным износом конической части профиля и, как следствие, колебания колесной пары. Используя процедуру дизайна, описанную в этой диссертации, был получен и применен на поездах метро новый профиль колеса. Результаты динамического моделирования и полевых испытаний показали, что поведение транспортных средств метро было значительно улучшено за счет модификации свойств контакта колеса и рельса. В результате применения оптимизированного профиля колеса, неустойчивость поездов метро была устранена, и продолжительность пробега колес увеличилась с 25000 км до 120000 км.

Рельсы в кривых большого радиуса на сети голландских железных дорог (Nederlandse Spoorwegen, NS) являются склонными к RCF проблемам на выкружках внешнего рельса в кривых. Оптимизированный профиль колеса получен для пассажирского вагона. Результаты динамического моделирования с разработанным профилем колеса показали небольшое увеличение показателя износа и уменьшение показателя усталости контактной поверхности колеса. Используя оптимизированный профиль колеса, RCF

повреждения, наблюдаемые у существующей комбинации профилей колеса и рельса, могут быть уменьшены.

Используя созданную процедуру, новые профили колеса разработаны для каждого вышеупомянутого случая. Соответственно, проблемы износа гребня колеса, устойчивости (в результате чрезмерного износа поверхности контакта) и RCF были решены. В первых двух случаях профили колеса были успешно применены на соответствующих транспортных системах.

Есть несколько возможностей для эффективного использования описанной процедуры дизайна:

- получение профиля колеса для нового профиля рельса (например, изменение профиля рельса в результате обновления пути), в случае если предыдущая комбинация профиля колеса и рельса была удовлетворительной. Функция РРК предыдущей пары колеса и рельса должна использоваться как целевая функция РРК. Таким образом, новая комбинация профилей колеса и рельса будет иметь те же самые свойства контакта как предыдущая комбинация.
- если существующие профили колеса и рельса не соответствуют друг другу, как явно видно из геометрического контакта колеса и рельса. В этом случае, функция РРК должна быть изменена, чтобы удалить нежелательные свойства контакта, таким образом улучшая контакт колеса и рельса.
- когда текущее поведение колеса и рельса должно быть изменено для новых условий, например, транспортное средство должно использоваться на пути с другой подуклонкой рельса, эксплуатационная скорость должна быть увеличена или введены более крутые кривые. В этом случае, функция РРК может быть изменена, чтобы удовлетворить новым условиям и, соответственно, могут быть разработаны новые профили колеса.

Успешное применение процедуры дизайна к реальным проблемам доказало её применимость и целесообразность. Процедура является гибкой, различные требования могут быть объединены для получения оптимального профиля колеса. В будущем, с появлением новых проблем в контакте колеса и рельса, процедура дизайна может быть легко расширена, чтобы включить новые требования к взаимодействию колеса и рельса.

About the author

Ivan Yevhenovich Shevtsov was born December 22, 1975 in Dnipropetrovsk, Ukraine. After finishing secondary school in 1992, he entered the Faculty of Applied Mathematics at Dnipropetrovsk State University and chose mechanical engineering as his specialization. During the final year of his studies at the university, he became interested in the dynamics of railway vehicles. At that time, he became acquainted with the mechanics of wheel/rail contact, and numerical simulations of the dynamics of railway vehicles. He obtained his degree, cum laude, in 1997. His thesis dealt with the wear of wheels and rails, and its influence on the dynamics of railway vehicles.

After graduation, Shevtsov worked as a research engineer and post-graduate (PhD student) at the Statistical Dynamics of Railway Vehicles department, Institute of Technical Mechanics of the National Academy of Sciences of Ukraine and the National Space Agency of Ukraine in Dnipropetrovsk.

From October 1998 to October 1999, Shevtsov worked under a Nuffic Research Fellowship at the Engineering Mechanics Group, Faculty of Mechanical Engineering and Marine Technology, Delft University of Technology, The Netherlands. After returning to Ukraine, he continued his work at the Statistical Dynamics of Railway Vehicles department at the Institute of Technical Mechanics in Dnipropetrovsk.

In June 2001, he became a researcher at the Railway Engineering group, Faculty of Civil Engineering and Geosciences, Delft University of Technology, The Netherlands, under the supervision of Professor Dr.Ir. Coenraad Esveld and Dr. Valeri Markine. At the Railway Engineering group, Shevtsov continued his work on wheel/rail contact and railway vehicle dynamics. In April 2003, he became a PhD student at the Railway Engineering group, where he continued his work on wheel/rail interface optimisation.

During his PhD research, Shevtsov developed procedures for the design of wheel and rail profiles. Based on this research, he presented numerous papers at both national and international conferences. He also published several articles on wheel/rail interface optimisation in international journals.

From October 2006 to February 2008, Shevtsov worked with Lloyd's Register Rail Europe B.V., as a consultant. He was involved in various wheel/rail interface and vehicle/track interaction projects for Dutch Railways and other European railway companies.

Since February 2008, Ivan Shevtsov has worked as a system specialist at ProRail, the infrastructure manager of the Dutch railway network. He works with a team of specialists responsible for all aspects of railway switches and crossings systems.

Propositions

accompanying the dissertation

Wheel/Rail Interface Optimisation

Ivan Shevtsov, June 3, 2008

1. A good engineer, like a good doctor, must cure the real illness of the system, rather than merely the symptoms.
2. Computer dynamic simulations should not be used as entire replacement of thorough field tests of railway vehicles.
3. Rolling radius difference has a strong influence on rolling contact fatigue occurrence in curves.
4. Independently rotating wheels solve some old railway problems associated with the classical wheelset with two wheels rigidly mounted on one axle; however, this gives rise to other phenomena that must yet be understood.
5. Catastrophes are almost never caused by a single factor; usually, they are triggered by a combination of several factors.
6. Some day, an optimisation tool should be developed allowing locomotive driver to drive a train in the most economical and efficient way.
7. Railway rolling stock equipped with a system measuring wheel/rail contact forces, and analysing them on-the-fly, would help to detect derailment risk and/or unsafe track conditions in an early stage to prevent catastrophic outcomes.
8. Good intentions can be spoiled through bad execution. Therefore, implementation of a new invention must be closely supervised by the inventor.
9. Inventors of new materials must be obliged to also devise a procedure for the recycling of that material.
10. Bogie dynamics is a second parameter, in addition to wheel/rail profiles, which influences wear and rolling contact fatigue. This is a very important parameter, but it should not be considered independently of the wheel/rail profiles.

These propositions are regarded as defendable, and have been approved as such by the supervisor prof.dr.ir. C. Esveld.

Stellingen

behorende bij het proefschrift

Wiel/Rail Interface Optimalisatie

Ivan Shevtsov, 3 juni 2008

1. Een goede ingenieur, zoals een goede dokter, moet de echte ziekte van het systeem genezen, in plaats van slechts de symptomen.
2. Dynamische computer simulaties kunnen praktijkproeven van spoorvoertuigen nooit volledig vervangen.
3. Het rolstraalverschil heeft een sterke invloed op de ontwikkeling van RCF in bogen.
4. Onafhankelijk roterende wielen lossen sommige oude spoorwegproblemen op, die geassocieerd zijn met een klassieke wielstel met twee wielen vast verbonden aan een as; nochtans leiden zij tot andere fenomenen die thans nog niet goed worden begrepen.
5. Catastrofen vinden zelden hun oorzaak in één enkele factor, maar zijn gewoonlijk terug te voeren op een combinatie van factoren.
6. In de toekomst zal een optimaliseringinstrument worden ontwikkeld dat het mogelijk maakt een treinbestuurder op de meest zuinige en efficiënte wijze te laten rijden.
7. Spoorwegmaterieel uitgerust met een systeem dat wiel-rail contactkrachten in real time meet en analyseert, zou helpen ontsporingsgevaar en/of een onveilige spoorconditie vroegtijdig te detecteren en daarmee rampzalige gevolgen te voorkomen.
8. Goede intenties kunnen door slechte uitvoering teniet worden gedaan. Daarom moet de implementatie van een nieuwe uitvinding, van begin tot eind, in overleg met de uitvinder worden gerealiseerd.
9. Uitvinders van nieuwe materialen moeten ook worden verplicht een procedure voor de recycling van dat materiaal uit te werken.
10. Draaistel dynamica is, naast de wiel-rail profielen, een tweede parameter die slijtage en RCF beïnvloedt. Het is een belangrijke parameter, welke echter niet onafhankelijk van de wiel-rail profielen kan worden beschouwd.

Deze stellingen worden verdedigbaar geacht en zijn als zodanig goedgekeurd door de promotor prof.dr.ir. C. Esveld.